

**ASSESSMENT OF INORGANIC POLLUTANTS, MIXING
PROCESS AND TRANSPORT OF WATER MASS USING
NATURALLY OCCURRING RADIUM ISOTOPES
IN MARINE ENVIRONMENT**

By

**VIRBAHADUR YADAV
(Enrolment No: CHEM01201104018)**

BHABHA ATOMIC RESEARCH CENTRE, MUMBAI

*A thesis submitted to the
Board of Studies in Chemical Sciences*

*In partial fulfillment of requirements
For the Degree of
DOCTOR OF PHILOSOPHY
of
HOMI BHABHA NATIONAL INSTITUTE*

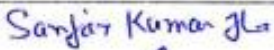
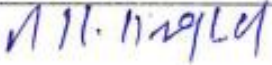


AUGUST, 2018

Homi Bhabha National Institute

Recommendations of the Viva Voce Committee

As members of the Viva Voce Committee, we certify that we have read the dissertation prepared by Shri VIRBAHADUR YADAV entitled "Assessment of inorganic pollutants, mixing process and transport of water mass using naturally occurring radium isotopes in marine environment" and recommend that it may be accepted as fulfilling the thesis requirement for the award of Degree of Doctor of Philosophy.

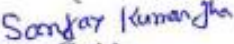
Chairman – Prof. R. M. Tripathi		Date: 21/8/2019
Guide & Convener – Prof. S. K. Jha		Date: 21-8-2019
Examiner - Prof. Onkar S. Chauhan		Date: 21/8/2019
Member 1- Prof. (Mrs.) G. G. Pandit		Date: 21/8/2019
Member 2- Prof. (Mrs.) Sangita D. Kumar		Date: 21.08.2019
Member 3- Prof. R. K. Singhal		Date: 21/8/2019

Final approval and acceptance of this thesis is contingent upon the candidate's submission of the final copies of the thesis to HBNI.

I/We hereby certify that I/we have read this thesis prepared under my/our direction and recommend that it may be accepted as fulfilling the thesis requirement.

Date: 21-08-2019

Place: Mumbai


Guide

STATEMENT BY AUTHOR

This dissertation has been submitted in partial fulfillment of requirements for an advanced degree at Homi Bhabha National Institute (HBNI) and is deposited in the Library to be made available to borrowers under rules of the HBNI.

Brief quotations from this dissertation are allowable without special permission, provided that accurate acknowledgement of source is made. Requests for permission for extended quotation from or reproduction of this manuscript in whole or in part may be granted by the Competent Authority of HBNI when in his or her judgment the proposed use of the material is in the interests of scholarship. In all other instances, however, permission must be obtained from the author.

Virbahadur Yadav
VIRBAHADUR YADAV

DECLARATION

I, hereby declare that the investigation presented in the thesis has been carried out by me. The work is original and has not been submitted earlier as a whole or in part for a degree / diploma at this or any other Institution / University.

Virbahadur Yadav
VIRBAHADUR YADAV

List of Publications arising from the thesis

International Journal

1. Estimation of Residence Time and flushing rate of water mass in the creek ecosystem of Mumbai Harbour Bay, **V. B. Yadav** and S. K. Jha; Journal of Regional Studies in Marine Science; Volume 31, September 2019, Article 100755; doi.org/10.1016/j.rsma.2019.100755
2. Estimation of Submarine Groundwater Discharge (SGD) in Mumbai Harbor Bay, India, using radium mass balance, **V. B. Yadav**, Vandana Pulhani, S. K. Jha and R. M. Tripathi J. Radioanal. Nucl. Chem. March 2019, Volume 319, Issue 3, pp 945–952
3. “Measurement of ^{224}Ra and ^{223}Ra activity using MnO_2 based in situ pre-concentration technique coupled with delayed coincidence counting in creek ecosystem of Mumbai Harbour Bay”, **V. B. Yadav**, S. J. Sartandel, S. K. Jha, and R. M. Tripathi Journal of Radioanalytical and Nuclear Chemistry; January 2017, Volume 311, Issue 1, pp 565–570
4. " Status of trace and toxic elements pollution in creek ecosystem using TXRF method ", **V. B. Yadav** and S. K. Jha, Journal of Radioanalytical and Nuclear Chemistry 03/2013; 295(3):1759-1762

Symposium Proceedings

1. Flux of trace and toxic elements from Mumbai Harbour Bay, **V. B. Yadav**, R. H. Pillay, S. S. Gothankar, S. K. Jha, Vandana Pulhani and R M Tripathi; Proceeding of NES 2018 page 62.

2. Study of longitudinal variation of short lived radium isotopes (^{224}Ra and ^{223}Ra) and underlying marine process in creek ecosystem of Mumbai Harbour Bay, Maharashtra, India, **V. B. Yadav**, S. Sartandel, S.K. Jha, R.M. Tripathi; Proceeding of ICRER 2017,; Page:465
3. Tracing water movement in Mumbai Harbor Bay using naturally occurring ^{224}Ra and ^{223}Ra as tracer. **V. B. Yadav**, S. J. Sartandel, S. K. Jha, R. M. Tripathi; Proceeding NUCAR 2017; Page: 542
4. "Feasibility of slurry method for TXRF analysis of estuarine core sample" **V. B. Yadav**, S. S. Gothankar, S. J. Sartandel, S. K. Jha and R. M. Tripathi; Proceeding NUCAR 2015; Page 337.
5. "Application of Total Reflection X-Ray Fluorescence Spectrometry for evaluation of Macronutrients & Micronutrients in Sea water ", **V. B. Yadav**, S. K. Jha, Proceeding of NUCAR-2013; Page 385

Virbahadur Yadav
VIRBAHADUR YADAV

DEDICATED
TO
MY FAMILY

ACKNOWLEDGEMENTS

It is indeed a great opportunity for me to express my deepest sense of gratitude and reverences to my mentor and guide **Dr. S. K. Jha** for introducing me to the present area of research. His valuable and meticulous guidance with lots of constructive criticisms has served as a vital source of inspiration for bringing the present work in the final shape.

I am extremely grateful to **Dr. R. M. Tripathi**, Chairman, Doctoral Committee, and members (**Dr. (Mrs.) G. G. Pandit, Dr. (Mrs.) Sangita D. Kumar, Dr. (Mrs.) D. Alamelu and Dr. R. K. Singhal**) for continuous encouragement, critical review, suggestions and help during the progress review, comprehensive review and pre-synopsis viva-voce.

I express my sincere thanks to **Dr. (Mrs.) Vandana Pulhani** for providing assistance, the motivation, the detailed technical attention and support. I am grateful to **Dr. (Mrs.) S. J. Sartandel** for her support in writing the paper and assistance during my experimental works. I express my sincere thanks to my other colleagues **Mrs. R. H. Pillay and Mrs. Sujata S. Gothankar** for their valuable help rendered by them during my experimental works. It would be incomplete if I do not acknowledge, **Shri G.L Teli, Shri A. K. Kazi and Shri S. N. Kisku** for giving me a helping hand during collection of samples and experimental works.

Further, I would like to thank the **Almighty**, without Him I could not do anything. I want to express my heartfelt gratitude to my mother **Smt. Abhiraji Yadav** and father **Shri Uday Raj Yadav** for their endless love and blessings. I would like to express my sincere thanks to my in-laws (**Smt. Indu Bala Yadav and Shri. Nandlal Yadav**) for their blessing and affection. I express my deepest sense of gratitude to my Teacher **Shri Chandrasen Singh** for his endless motivations at every stage of my study.

Finally, I would like to thanks my wife **Mrs. Leena Yadav** for her relentless support and affection. I am grateful to have her as my best friend for last seven years, without her help, patience and understanding; I would hardly be possible to come out of this thesis.

Table of Content

<u>SYNOPSIS</u>	ix
<u>List of Figures</u>	xviii
<u>List of Tables</u>	xxii

CHAPTER 1 INTRODUCTION

1.1. Radium.....	1
1.1.1. Radium in Seawater.....	3
1.1.2. Radium in Groundwater.....	4
1.1.2.1. Natural sources of Ra in groundwater	4
1.1.2.1.1. Weathering.....	4
1.1.2.1.2. Recoil.....	5
1.1.2.1.3. Decay of adsorbed and dissolved parent Th isotopes	5
1.1.2.2. Factors affecting groundwater radium concentrations.....	5
1.1.3. Radium in earth crust Soil, Freshwater, River Water and Air	6
1.2. Chemical Properties of Ra	8
1.2.1. Basic Characteristics:.....	8
1.2.2. Aqueous Characteristics:.....	8
1.2.3. Adsorption and desorption	9
1.3. Measurement of Radium isotopes:.....	10
1.3.1. Alpha Spectrometry	11
1.3.2. Gamma Spectrometry	12
1.3.3. Liquid Scintillation Counting (LSC)	13

1.3.4. Mass spectrometry	13
1.3.5. Method for ²²³ Ra and ²²⁴ Ra.....	14
1.4. Application of Radium:	15
1.5. Definitions and Drivers of SGD.....	15
1.6. Significance of SGD:.....	18
1.7. Methods Used to Measure SGD.....	20
1.7.1. Seepage Meter	21
1.7.2. Piezometer.....	22
1.7.3. Natural tracers	23
1.7.4. Infrared Imaging	25
1.7.5. Hydrologic Approach	26
1.7.6. Hydrograph separation techniques	27
1.7.7. Mathematical Models	27
1.8. History of SGD Research and Work Done.....	28
1.8.1. SGD in the Indian Costal Areas	32
1.8.1.1. Studies related to existance of SGD.....	32
1.8.1.2. Studies related to quantification of SGD	33
1.9. Scope of Present Work:	33

CHAPTER 2
ANALYTICAL TECHNIQUES AND EXPERIMENTAL METHODS

2.1. Introduction.....	35
2.1.1. Ra concentration in marine environment.....	35
2.1.2. Analytical Method for Ra Measurement.....	37

2.1.3. Coincidence and Delayed Coincidence Counting	38
2.2. Theory of Radium Delayed Coincidence Counter	42
2.2.1. Quantification of ^{223}Ra and ^{224}Ra Activity Concentration.....	44
2.2.2. Uncertainties in measurement of ^{223}Ra and ^{224}Ra	46
2.3. Standardization of method used in the present study	48
2.3.1. Evaluation of Ra extraction efficiency of MnO ₂ -fiber.....	50
2.3.2. Selection of Carrier gas.....	51
2.3.3. Flow rate of carrier gas (Helium)	52
2.3.4. Equilibrium	53
2.3.5. Build-up of ^{222}Rn	54
2.3.6. Sample Counting	54
2.3.7. Water-loss during the measurement	58
2.3.8. Checking for leaks in the system.....	59
2.3.9. Background and Minimum measurable activity	59
2.3.10. Measurement of uncertainty.....	60
2.4. The efficiency of the counting system for ^{224}Ra and ^{223}Ra measurement:	61
2.4.1. Probability of Rn decaying in the counting cell:.....	63
2.4.2. Loss resulting from the delay and window settings	64
2.4.3. Calculation of efficiency for 219 channels:	64
2.5. Validation of Method for Measurement of ^{224}Ra and ^{223}Ra by coincidence counting:.....	65
2.6. Total Reflection X-Ray Fluorescence (TXRF) Spectrometry	66
2.7. Component of TXRF	75

2.7.1. X-ray Source	75
2.7.1.1. X-ray tube sources	76
2.7.1.2. Radio-isotopic sources	78
2.7.1.3. Synchrotron sources.....	80
2.7.2. Collimator and Monochromator	81
2.7.3. Sample support	82
2.7.4. Energy Dispersive Detectors:.....	84
2.8. Fundamentals of total reflection of X-rays	87
2.9. TXRF System used in Present Study:	97

CHAPTER 3
STUDY AREA “MUMBAI HARBOUR BAY (MHB)” AND SAMPLING

3.1. Introduction.....	105
3.2. Mumbai Harbour Bay	108
3.2.1. Trans Thane Creek.....	109
3.2.2. Various discharges and water movement in the bay	110
3.2.3. Tidal flow patterns and dilution.....	111
3.3. Sample Collection from Study area.....	113
3.3.1. Collection of Surface seawater for Radium Analysis:.....	117
3.3.1.1. Preparation of MnO ₂ Coated acrylic fiber:	118
3.3.1.2. Adsorption of Ra on MnO ₂ fiber:	119
3.3.1.3. Pre-concentrated of Radium on MnO ₂ fiber from seawater in the laboratory:.....	121
3.3.1.4. Design and Fabrication of in-situ pre-concentration sampling assembly	121
3.3.1.5. Sampling Locations covered during different sampling trips	122

3.3.2. Collection of groundwater for Radium Analysis:	127
3.3.3. Collection of Surface Water for trace and toxic elements Analysis:.....	128
3.3.4. Collection of core sample for trace and toxic elements Analysis:	128
3.3.4.1. Gravity Corer.....	129
3.3.4.2. Collection of the sediment core sample	129
3.3.5. Collection of Bulk mass of Suspended sediment:	130
3.3.6. Measurement of physicochemical parameters of seawater:.....	130

CHAPTER 4
ESTIMATION OF APPARENT WATER AGE AND MIXING PROCESS IN THE
CREEK ECOSYSTEM OF MUMBAI HARBOUR BAY, INDIA

4.1. Introduction.....	133
4.1.1. Earlier Study in the present study area	136
4.1.2. Apparent Water Age of Creek Water using Radium Age Model.....	138
4.1.3. Apparent Water Age of Creek Water using Radium Balance Approach	139
4.1.4. Study of Flow and Mixing of Creek Water to the offshore:	140
4.2. Study Area and Sample Collection	140
4.3. Measurement of ²²⁴ Ra and ²²³ Ra:	141
4.4. Result	142
4.4.1. Sampling in April 2016 (Trip-1):	142
4.4.2. Sampling in March 2017 (Trip-2):	144
4.4.3. Sampling in May 2017 (Trip-3):	146
4.4.4. Sampling in December 2017 (Trip-4):.....	147
4.4.5. Physico-Chemical Parameter	148

4.5. Discussion.....	150
4.5.1. Apparent Age by Radium Age Model:.....	150
4.5.2. Apparent Age by Radium Balance Approach:.....	151
4.5.3. Tracing of Water Movement in Creek:.....	152
4.5.4. Estimation of Flushing Rate of Creek Water.....	153
4.5.5. Estimation of Horizontal Dispersion Coefficient (K_h).....	155
4.6. Conclusion.....	159

CHAPTER 5
ESTIMATION OF SUBMARINE GROUNDWATER DISCHARGE IN MUMBAI
HARBOUR BAY

5.1. Introduction.....	160
5.2. Study Area and Sampling.....	162
5.3. Mass Balance in Mumbai Harbour Bay.....	164
5.3.1. Loss of Ra-fluxes from the bay.....	166
5.3.1.1. Radioactive Decay.....	166
5.3.1.2. Ra export during exchange of bay water with Arabian Sea water.....	167
5.3.2. Input of Ra-fluxes into bay.....	167
5.3.2.1. Arabian Sea Exchange.....	167
5.3.2.2. Input from Rivers.....	168
5.3.2.3. Input from Wastewater Discharge.....	169
5.3.2.4. Diffusion of Ra from bottom sediments.....	170
5.3.2.5. Input from suspended particles.....	171
5.3.3. Estimation of SGD.....	172

5.4. Conclusion	174
-----------------------	-----

CHAPTER 6
STATUS OF TRACE AND TOXIC ELEMENTS IN CREEK ECOSYSTEM USING
TXRF METHOD

6.1. Introduction.....	175
6.2. Standardization of method for a simultaneous multi-element determination from seawater by TXRF	176
6.2.1. Preparation and Purification of Chemicals	177
6.2.2. Pre-concentration Procedure	178
6.2.3. Sample Preparation and Measurement	179
6.2.4. Validation of method	179
6.3. Development of method for removal of chloride by vapour phase decomposition from seawater sample for TXRF measurement:	181
6.4. Development of method metals detections in solid samples using TXRF coupled with slurry sampling.....	186
6.4.1. Slurry Sedimentation:	187
6.4.2. Critical mass on the sample support.....	189
6.4.3. Validation of method:	189
6.5. Status of trace and toxic elements in creek ecosystem of MHB.....	190
6.5.1. Direct measurement of seawater by TXRF.....	190
6.5.2. Pre-concentration of elements and TXRF analysis	191
6.5.3. Results.....	191
6.6. Flux of trace and toxic elements toward the open sea.....	193

6.7. Analysis of core sample collected from the Thane Creek:	195
6.7.1. Sample Preparation and Measurement	195
6.7.2. Results.....	196
6.8. Conclusion	198

CHAPTER 7
SUMMARY, CONCLUSION AND FUTURE PROSPECTS 199

Bibliography	208
--------------------	-----

SYNOPSIS

River and streams and submarine groundwater discharge (SGD) are considered as important pathways for material transport to the marine environment from land. SGD is considered as any flow of water from the seabed to the coastal ocean, regardless of fluid composition or driving force. The inflow of the freshwater and desorption from freshwater particle enrich coastal water with various pollutants and radionuclides. The SGD has a smaller water flow rate compared to surface water flow rate but the associated chemical fluxes are comparable to surface chemical fluxes. Groundwater seepage is patchy, diffuse, temporally variable, slow, persistence through sediments and may involve multiple aquifers. SGD can occur at almost all coastal zones where an aquifer with a positive head relative to sea level is hydraulically connected to a surface water body. The SGD into the near-shore marine ecosystem may have a significant impact, as groundwater in many areas is contaminated with a variety of substances like nutrients, heavy metals, radionuclides and organic compounds. The input of different pollutants in the coastal marine ecosystem is leading to eutrophication, harmful algal bloom and alarming level of contamination in coastal water.

Rapid urbanization, large-scale industrialization and uncontrolled sprawling settlements around many coastal and harbour cities of the world brought an alarming level of pollution to the surrounding aquatic ecosystem due to various anthropogenic discharges. It becomes all the more critical in case of creek/bay ecosystem due to its landlocked and relatively stagnant nature. The distributions of the naturally occurring radionuclide, nutrients, trace and toxic elements are subjected to chemical differences between coastal and offshore water. The distributions of pollutants also depend on how fast the sea water in the creek is transported to open sea. The removal or circulation of creek water can provide insights into mobility of contaminants in the

creek. The flushing rate, residence time and apparent age of water are used to describe how long the water remains in an ecosystem.

Mumbai city is one of the heavily populated and industrialized cities of India. The creek known as Thane creek is part of Mumbai Harbour bay that separate mainland from Mumbai city. The Thane Creek industrial area houses a number of majors, medium and small scale industrial units largely involved in the manufacture, storage and use of chemicals, petrochemicals, pharmaceuticals and fine chemical products, pesticide formulation, etc. Thane Creek is the ultimate recipient of all the liquid discharges from these industries. Therefore understanding and monitoring of water quality in the Thane Creek is important for an accurate and systematic environmental assessment. There is various literature on the release of pollutants through surface but the input of pollutants via submarine groundwater discharge is not studied for the Mumbai Harbour Bay. This was one of the motives/reason to choose this study area for the present study.

Scope of Present Work:

The objective of the present study was;

1. Development and standardization of method for the estimation of short-lived radium isotopes (^{224}Ra and ^{223}Ra) in water samples using delayed coincidence counting.
2. Application of radium isotopes as a geochemical tracer to study the apparent water age, flushing rate and mixing process of water in the present study area.
3. Application of radium balance Model for the quantification of submarine groundwater discharge in the present study area.
4. Development and standardization of method for the estimation of trace and toxic elements in seawater and sediment using TXRF.
5. Study of status and fate of inorganic pollutants in the present study area.

Briefly, thesis describes the estimation of different inorganic pollutants in the study area using TXRF and study of transport and mixing using short-lived radium isotopes as geochemical tracer. The thesis is divided into seven chapters as described below;

CHAPTER 1: INTRODUCTION

The chapter discusses the various pathways for the input of pollutants in the marine ecosystem like surface discharge and influx through the land. The basic details about submarine groundwater discharges (SGD), significance and the method (viz. seepage meter, piezometer, natural tracers, infrared imaging, hydrologic approach, hydrograph separation techniques and mathematical models) used for the measurement of SGD is discussed. The published literature pertaining also summarised in this chapter. The four naturally occurring radium isotopes (^{223}Ra , $T_{1/2} = 11.4$ days; ^{224}Ra , $T_{1/2} = 3.6$ days; ^{226}Ra , $T_{1/2} = 1,600$ years and ^{228}Ra , $T_{1/2} = 5.75$ years) are used as geochemical tracers for variety of environmental processes; like groundwater discharge, residence time, flushing rate and coastal water circulation pattern etc. The abundance, behaviour of radium in different environments and methods for measurement of radium are discussed briefly. The chapter also discusses the importance of study in present study area and objective of the work.

CHAPTER 2:

Analytical Techniques and Experimental Methods

The chapter discusses the different methods and techniques developed and used during present work. The chapter is categorized in the two parts.

The first part of the chapter discusses the details of delayed coincidence counting technique, its standardization and calibration. The technique is an alpha scintillation counter that

distinguishes decay events of short-lived radium daughter products based on their contrasting half-lives using a delayed coincidence counter and mainly used for measurement of ^{223}Ra and ^{224}Ra in the water sample. The chapter describes the optimization of the flow rate of carrier gas, selection of better carrier gas, estimation of efficiency and other parameter required for the quantification. The chapter also describes the use of delayed coincidence counter for the estimation of ^{226}Ra and ^{228}Ra in the water samples.

The second part of the chapter gives the theory, principle and instrumentation involved in TXRF spectrometry. Since the discovery in the year 1895, X-rays have played a very crucial role in the field of analytical sciences for material characterization. In past few years, TXRF (based on the principle of total reflection of X-rays) has become one of the well-known methods of spectrochemical analysis. In TXRF sample in thin film form on the support is excited with primary X-ray at glancing angle. The secondary (characteristic) X-ray emitted from the element present in the sample is detected using energy dispersive detector and quantification is done using internal standard. In this part of the chapter the details of instrument GNR Slr. TXRF instrument (TX-2000) is also discussed.

CHAPTER 3:

Study Area “Mumbai Harbour Bay (MHB)” and Sampling

The chapter describes an overview of the study area including, water movement, tidal flow patterns, industrial and domestic discharges etc. The present study carried out in Mumbai Harbour bay which separates the mainland from Mumbai city. Mumbai Harbor Bay (MHB) is located on the west coast of India. The funnel-shaped bay is a land-locked mass of water broad at the southern end and receives tidal waters from the Arabian Sea. The bay opens to the Arabian Sea to the south and influenced by dominant semi-diurnal tides with a period of 12 hrs 40 min.

The study area, extensively exploited for multifarious activities and recipient of industrial discharges. The bay is characterized by abundant mudflats and exhibits good coverage of mangroves. The average area of water surface of the bay is about 215 km² at high tide level and about 160 km² at low tide level. The total volume of water at mean sea-level as calculated from surrounding area is 9.1×10^{11} litres. The average tidal volume is 4.8×10^{11} litres. Bay receives water from rivers (Ulhas and Panvel) discharges and tidal input. Of these rivers contribute a small fraction towards the movement of water in the bay as compared to the factor caused by the volume of tidal water moving in or out of the bay. Discharges during the monsoon do not affect the tidal curves, as these are small compared to the tidal volume. The study focused mainly on creek known as Thane creek which is part of Mumbai Harbour bay. The Thane Creek waterway lies between the city of Thane and the Arabian Sea at Trombay before the Gharapuri islands. The creek receives effluents from various industries containing trace and toxic elements and acts as sinks for most of the pollutants. The chapter also discusses the details of sampling in the study area for the measurement of radium isotopes and other pollutants.

CHAPTER 4:

Estimation of Apparent Water Age and Mixing Process in the Creek Ecosystem of Mumbai harbour Bay, India

The chapter IV covers application of short-lived radium isotope for the study of the apparent water age and mixing process in the creek ecosystem of Mumbai Bay. The chapter comprised of three parts.

The first part discusses the application of Radium Age Model for the estimation of apparent water age for different sampling trips (April 2016, March 2017 and December 2017) in the creek and water age was found to be 3.65 ± 1.22 days, 3.75 ± 1.10 days and 4.51 ± 1.51 days

respectively. The overall range varied from 1.56 to 7.53 days with an average of 4.06 ± 1.20 days from the three sampling trips. Result of sampling at various time intervals showed steady state in study area with respect to radium. To support the result by Radium Age Model in the study system, Radium Balance Approach was also used to estimate the apparent age of creek water which gives water age as 6.51 ± 1.27 days. It was observed that in our study area both the model gives a similar result. The previous study in the Mumbai harbour bay shown that for 90% of renewal of bay water, 6 tidal-cycles are required. Thus the present study give higher value (4.1 days and 6.5 days) compare to previous study (3.2 days) which may be attributed to return flow factor, not considered in the previous study.

In second part longitudinal variation of the radium isotopes in middle of the creek against the distance was discussed to find the net movement of water towards the open sea. Also, the flushing rate of water within the creek was estimated using the variation of the apparent age of water at the middle of the creek with distance. The net flow of water was found toward open sea and the flushing rate of water within the creek was estimated to be 9.09 km.d^{-1} .

The third part of the chapter describes mixing and flushing rate of the creek water to the Arabian Sea, as one of the objectives of the study was to understand, how a pollutant will be mixed to open seawater and flush out of creek if released from shore. The average activity concentration in the creek was taken as source value and apparent age at the different location in the open mouth of the bay and open sea was calculated. Variation of apparent age with distance resulted flushing rate to be $6.67 \pm 0.89 \text{ km.d}^{-1}$. The present study system was in steady state and variation of ^{223}Ra with distance showed dispersion is dominant process for mixing. Therefore, using 1-dimensional advection-dispersion model, the horizontal dispersion coefficient was estimated to be $800 \pm 107 \text{ m}^2 \cdot \text{s}^{-1}$

CHAPTER 5:

Estimation of Submarine Groundwater discharge using radium mass balance in the Mumbai Harbour Bay

The chapter describes different pathways of radium input sources (viz. input from the ocean during the high tide, river, sediment and wastewater discharge), losses (viz. mixing and radioactive decay) and estimation of SGD in the Mumbai Harbour Bay. The total flux of ^{223}Ra and ^{224}Ra in the bay was estimated to be $6.4 \times 10^9 \text{ dpm.d}^{-1}$ and $106.1 \times 10^9 \text{ dpm.d}^{-1}$ respectively. The contribution of radium flux was negligible (about 0.01% of total radium flux in the bay) from each river. The contribution from surface sediment through diffusion was found about 1.7 % and 2.7 % for ^{223}Ra and ^{224}Ra respectively. The suspended sediment contribution was found about 0.7 % and 0.4 % for ^{223}Ra and ^{224}Ra respectively. The contribution from wastewater discharge was found about 0.1 % and 0.4 % for ^{223}Ra and ^{224}Ra respectively. The tidal input for ^{223}Ra and ^{224}Ra was found as 44.1 % and 25.2 % of total radium flux respectively. Total fluxes out of the system via ocean exchange and decay was found to be $7.3 \times 10^9 \text{ dpm.d}^{-1}$ and $268.5 \times 10^9 \text{ dpm.d}^{-1}$ for ^{223}Ra and ^{224}Ra respectively. The SGD in the bay was estimated based on the imbalance between input and losses contribution of radium. The volume of SGD based on ^{223}Ra and ^{224}Ra mass balance was found to be $33.4 \times 10^9 \text{ L.d}^{-1}$ and $64.9 \times 10^9 \text{ L.d}^{-1}$ respectively. The SGD contribution of ^{223}Ra and ^{224}Ra flux in the bay was found as 53.4 % and 71.7 % respectively.

CHAPTER 6:

Status of Trace and Toxic Elements in Creek Ecosystem using TXRF method

The first part of the chapter describes the study carried out in the creek ecosystem of Mumbai to understand the current status of trace and ultra-trace elements and also to check the

effect of effluents from industrial and urban settlements. The chapter describes a method for seawater analysis using Total Reflection X-Ray Fluorescence Spectrometry (TXRF) and online removal of Chloride from seawater samples. It was found that the concentration of P, Ca, Mn, Fe, Co, Cu, Zn, Pb and As was found higher in the industrial side of the creek whereas V, Cr and Ni concentration were found higher in the samples collected from the side receiving city effluent.

The second part of the chapter deals with the simultaneous determination of trace metals in seawater using dithiocarbamate pre-concentration and Total Reflection X-Ray Fluorescence Spectrometry. Briefly, the procedure involve a double extraction of acidified seawater using chloroform and combined ammonium tetramethylene dithiocarbamate (APDC)-diethylammonium diethyldithiocarbamate (DDDC) followed by back-extraction of the metal carbamates into nitric acid and analysis using TXRF. Using this procedure seawater samples were analysed for the trace elements Cr, Mn, Fe, Co, Ni, Cu, Zn and Pb. The result was found similar to previously reported value.

The third part of chapter deals with the standardization of method for the measurement of trace elements in sediment samples using TXRF technique associated with slurry sample preparation method. 1% Triton X-100 aqueous solution associated with ultra-sonication was used for the preparation of the slurry. Average relative error in the measurement of reference material (IAEA-Soil-7) was found to be 13%. Core sediment samples collected from Mumbai Harbour Bay were processed and analysed for K, Ca, Ti, Cr, Mn, Fe, Ni, Cu, Zn, Pb, Rb and Sr. Calculation of Pollution Load Index (PLI) shows that there is also a significant anthropogenic contribution to the surface sediment sample.

The fourth part of chapter describes the result of Fe Ca, Mn, K, Ti, V, Cr, Ni, Cu, Zn, Pb, Rb, Sr, Al and Si in suspended sediment collected from Mumbai harbour bay. The chapter

also describes estimation of trace element flushing out, once we have suspended sediment load and flushing rate of the water.

CHAPTER 7:

Conclusions and future prospects

This chapter summarises the main results from the thesis and proposed future work that can be carried out. The thesis describes the method for the analysis of trace and toxic element in seawater and sediment using TXRF technique. The TXRF technique is used for analysis of seawater and sediment samples from the study area to study the status of trace and toxic elements. The thesis discuss the method for the measurement of short-lived radium isotopes and their application for the estimation of apparent water age, flushing rate, dispersion coefficient and submarine groundwater discharge in the Mumbai Harbour Bay.

The method can be used to study input of different nutrients and pollutants via groundwater discharge in the MHB as we have estimate of SGD. This technique and approach can be applied to study the apparent water age, flushing rate, dispersion coefficient and submarine groundwater discharge in the other coastal area. The information obtained could be used to help the developing management strategies for controlling the supply of terrestrial nutrients and contaminants to offshore areas and protect the environment in the study area.

List of Figures

Figure 1.1: ^{238}U , ^{235}U and ^{232}Th Decay series	2
Figure 1.2: Description of different pathways of SGD.....	16
Figure 2.1: Block diagram of the electronic component of the electronic circuit	39
Figure 2.2: Schematic diagram of ^{223}Ra and ^{224}Ra measurement system.....	42
Figure 2.3: Schematic diagram of the ^{224}Ra and ^{223}Ra decay & delayed coincidence circuit	43
Figure 2.4: The Radium Delayed Coincidence Counter used in the study	49
Figure 2.5: Sampling assembly for efficiency measurement	50
Figure 2.6: Variation of efficiency for different carrier gases at the flow rate of 4lpm	52
Figure 2.7: Variation in ^{224}Ra efficiency vs. He Flow Rate	53
Figure 2.8: First and second counting of the sample. Row No. 2 represents the first count and Row number 4 shows second counting	56
Figure 2.9: Third counting of two representative samples after a delay of 38.86 days.....	57
Figure 2.10: Apparent activity of ^{224}Ra and emanation efficiency vs. water content of the standards	58
Figure 2.11: (a): $\ln ^{224}\text{Ra}$ (dpm) vs. decay time and (b): $\ln ^{223}\text{Ra}$ (dpm) vs. decay time	65
Figure 2.12: Survey of techniques available for analysis of the environmental samples	68
Figure 2.13: Moseley's Law plot of energy versus the atomic number.....	71
Figure 2.14: Production of Fluorescence Photon	71
Figure 2.15: Schematic diagram of the basic difference between WDXRF and EDXRF	72
Figure 2.16: Schematic Representation Total Reflection X-ray Fluorescence (TXRF)	74
Figure 2.17: Comparison of the geometrical difference of conventional EDXRF and TXRF	74
Figure 2.18: Schematic diagram of an X-ray tube of Coolidge type.....	77

Figure 2.19: Spectrum generated from Rh target X-ray tube	78
Figure 2.20: Schematic representation of a synchrotron source facility	81
Figure 2.21: Liquid sample on a clean quartz sample support which leaves a dry residue after evaporation	83
Figure 2.22: A cross-sectional view of a Si(Li) detector crystal	86
Figure 2.23: Reflection and refraction of the incident ray on glass surface.....	88
Figure 2.24: Total reflection of incident ray	89
Figure 2.25: Variation of reflectivity and transmittivity of incidence beam (MoK α) on quartz surface against incidence angle	91
Figure 2.26: Penetration depth vs. angle of incidence	92
Figure 2.27: Schematic diagram for double excitation of the sample in TXRF	94
Figure 2.28: Critical thickness and critical mass for different matrices in TXRF analysis	94
Figure 2.29: Detection limit vs. matrix content (% NaCl)	95
Figure 2.30: TX2000 TXRF instrument used in the present study.....	99
Figure 2.31: Front view: Multi-Sample Holder.....	99
Figure 2.32: High-Resolution SDD Detector	100
Figure 2.33: Back view: Step motors plus optical encoders assure a high angular accuracy	100
Figure 2.34: Sample processing in TXRF analysis.....	101
Figure 2.35: Preparation of sample for TXRF measurement	102
Figure 2.36: TXRF Spectrum of multi-element standards (ICP-IV) excited by MoK α beam...	102
Figure 2.37: TXRF Spectrum of multi-element standards (ICP-IV) excited by WL β beam.....	103
Figure 2.38: Comparison of expected and observed conc. in the multi-element standard	104
Figure 3.1: Mumbai and Mumbai Harbour Bay (MHB).....	108

Figure 3.2: General direction of ebb current in MHB [219]	112
Figure 3.3: Small motor boat used for sampling	114
Figure 3.4: Boat (with small dinghy) used for the sampling	115
Figure 3.5: Heating bath assembly for preparation of MnO ₂ coated fiber	119
Figure 3.6: Radium Pre-concentration on MnO ₂ fiber system in the Laboratory	121
Figure 3.7: Schematic diagram of the in-situ pre-concentration assembly	122
Figure 3.8: MnO ₂ fiber, Sample holder, Pre-filter and sampling assembly	123
Figure 3.9: Sampling location covered during different sampling Tips (1-4).....	126
Figure 3.10: Piezometer groundwater sampler and groundwater sampling.....	127
Figure 3.11: Collection of core sample using gravity corer	131
Figure 3.12: Deployment of suspended sediment sampler and collection.....	132
Figure 3.13: Multi-parameter kit (EUTECH Instrument PC650).....	132
Figure 4.1: Variation of ln(Ra activity Concentration) as a function of distance in the creek for the sampling trip-1	144
Figure 4.2: Variation of ln(Ra activity concentration) as a function of distance in the creek for the sampling trip-2	146
Figure 4.3: Variation of ln(Ra activity concentration) as a function of distance in the creek for the sampling trip-4.....	148
Figure 4.4: Variation of apparent water age the distance within the creek.....	153
Figure 4.5: Variation of the apparent age of water mass in the open mouth of the bay and offshore location	154
Figure 4.6: Variation of ²²³ Ra activity concentration with distance	156
Figure 4.7: Variation of ln ²²⁴ Ra with distance against distance	156

Figure 4.8: Variation of $\ln^{223}\text{Ra}$ with distance against distance	157
Figure 5.1: Study area (Mumbai Harbour Bay) and sampling locations.	163
Figure 5.2: Different sources of input and loss of Ra in the Mumbai Harbour Bay.....	166
Figure 5.3: Variation of ^{223}Ra vs. ^{224}Ra (a) Activity Conc. and (b) $\ln(\text{Activity Conc.})$	173
Figure 6.1: TXRF spectra of liquid phase after separation of trace elements from NAAS-6	180
Figure 6.2: Setup for removal of chlorine from the seawater samples	182
Figure 6.3: TXRF Spectrum of untreated seawater	183
Figure 6.4: TXRF Spectrum of seawater treated for 8 minutes with HNO_3 vapour	183
Figure 6.5: TXRF Spectrum of seawater treated for 16 minutes with HNO_3 vapour	184
Figure 6.6: TXRF Spectrum of seawater treated for 24 minutes with HNO_3 vapour.....	185
Figure 6.7: TXRF Spectrum of seawater treated for 32 minutes with HNO_3 vapours	186
Figure 6.8: Settling velocity of quartz (SiO_2) and goethite ($\alpha\text{-FeOOH}$) in H_2O and NMP	188
Figure 6.9: Concentration Ratio of Elements	193
Figure 6.10 a, b and c: Depth profile of elements	197

List of Tables

Table 1.1: Radium isotopes and their mode of decay	2
Table 1.2: Global studies on contribution of SGD.....	31
Table 2.1: Molar ratio daughter and parent radionuclide in decay series	36
Table 2.2: Counts rate (cpm) 220 channels for both cartridges and background	50
Table 2.3: X-ray techniques and their applications.....	69
Table 2.4: List of commonly used radioisotope sources for X-ray radiation.....	80
Table 2.5: Characteristics of different sample support materials	85
Table 3.1: Quantum of a pollutant into the coastal ecosystem of India.....	106
Table 3.2: GPS value of sampling locations in the study area	116
Table 3.3: Details of sampling trips and samples collected	124
Table 4.1: Activity concentration of ^{224}Ra and ^{223}Ra (dpm/100L), AR and apparent age of water at different locations for sampling trip-1(April-2016)	143
Table 4.2: Activity concentration of ^{224}Ra and ^{223}Ra (dpm/100L), AR and apparent age of water at different locations for sampling trip-2 (March-2017).....	145
Table 4.3: Activity concentration of ^{224}Ra and ^{223}Ra (dpm/100L) in seawater samples collected from the open end of the bay and the Arabian Sea for sampling trip-3.....	147
Table 4.4: Activity concentration of ^{224}Ra and ^{223}Ra (dpm/100L), AR and apparent age of water at different locations for sampling trip-4 (December-2017).....	148
Table 4.5: Physico-Chemical Parameter in Mumbai Harbour Bay	149
Table 4.6: Physico-Chemical Parameter in Arabian Sea	150
Table 4.7: Comparison of Apparent Water Age from other Ecosystem of the World	152
Table 4.8: Comparison of Flushing Rate (km.day ⁻¹) in the different ecosystem of the world..	155

Table 4.9: Comparison of horizontal mixing constant (dispersion constant) from other ecosystems of the world.....	158
Table 5.1: The parameters and values used for calculation of Ra fluxes.....	165
Table 5.2: Estimate of different process and sources involved in the mass balance of the Ra flux in Mumbai Harbour Bay	168
Table 5.3: Activity conc. of ²²⁴ Ra and ²²³ Ra in bay, porewater and groundwater samples	172
Table 6.1: Result of analysis of seawater reference material (NAAS-6).....	180
Table 6.2: Result of certified reference material IAEA-Soil-7 by the slurry method.....	190
Table 6.3: Results of seawater analyzed by TXRF	192
Table 6.4: Suspended sediment load (mg/l) at sampling locations.....	194
Table 6.5: Concentration and flux of elements (µg/l) from suspended sediment.....	195

CHAPTER 1

INTRODUCTION

Coastal water includes estuaries, coastal wetlands, seagrass, coral reef, intertidal zones, mangrove, coastal ocean and upwelling areas. Estuaries are bodies of water that receive fresh-water and sediment influx from rivers and tidal influx from ocean, providing transition zones between the fresh water of a river and the saline environment of the sea. Coastal processes become relatively more significant than open-ocean processes because mankind is most closely associated with coastal environments, through fishing, recreational pursuits, transportation routing, mineral extraction, oil & gas production, and dumping of wastes.

1.1. Radium

Radium, linked to the discovery of radioactivity, in form of radium chloride, was discovered by Marie and Pierre Curie in 1898. They extracted the radium compound from uraninite. There are four Ra isotopes naturally present in the environment; ^{223}Ra ($T_{1/2} = 11.4$ days), ^{224}Ra ($T_{1/2} = 3.6$ days), ^{226}Ra ($T_{1/2} = 1600$ years) and ^{228}Ra , ($T_{1/2} = 5.75$ years). ^{226}Ra is a part of the ^{238}U decay series, ^{228}Ra and ^{224}Ra are a part of the ^{232}Th decay series and ^{223}Ra is a part of the ^{235}U decay series Figure 1.1. Each Ra isotope produces a chain of daughters that are short lived and contributes to the terrestrial radiation exposure. The daughter isotopes of ^{223}Ra and ^{224}Ra , are very short half-lived, and will quickly attain secular equilibrium with the parent. For ^{226}Ra , the immediate decay product is the noble gas ^{222}Rn , which may readily escape prior to decay from non-retentive materials.

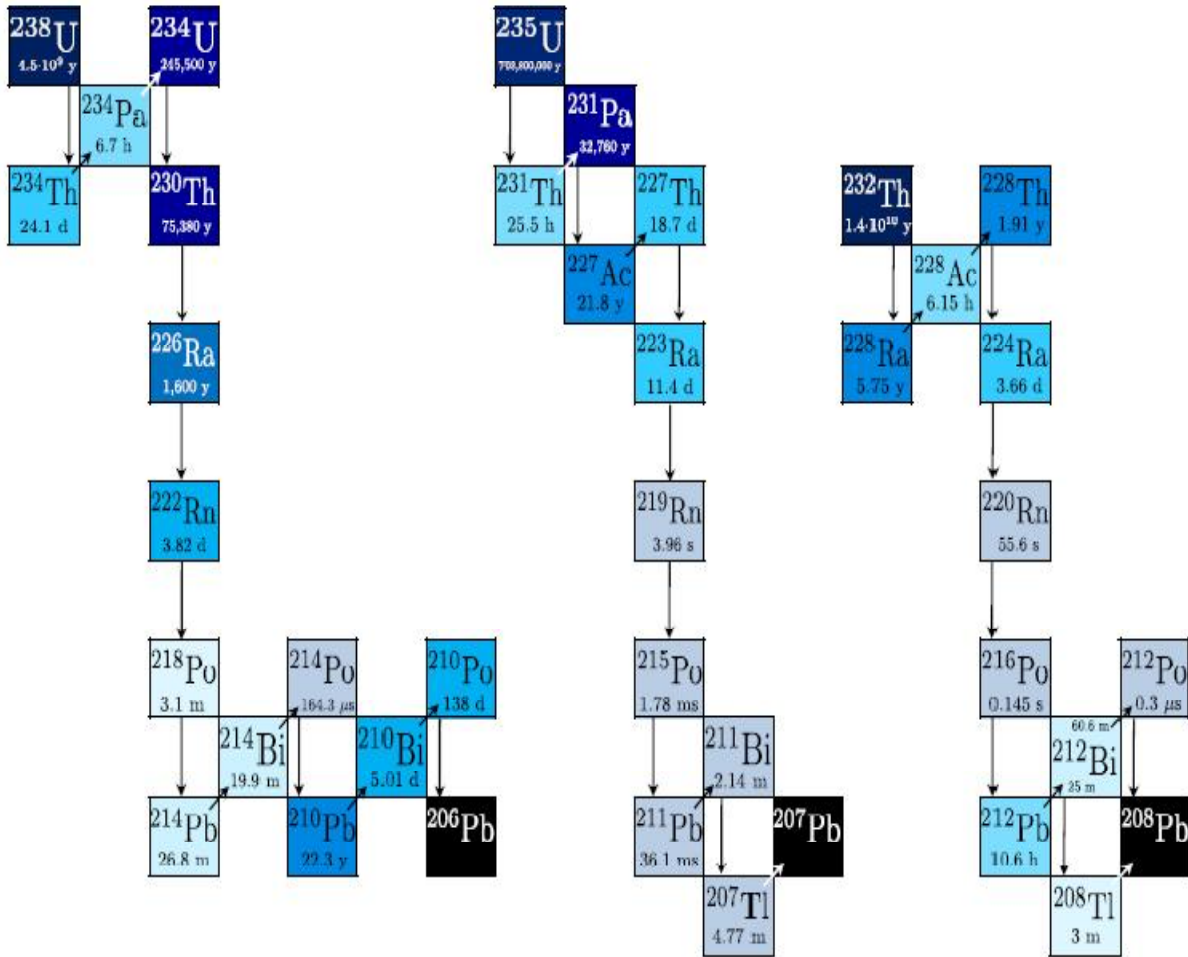


Figure 1.1: ^{238}U , ^{235}U and ^{232}Th Decay series

Table 1.1: Radium isotopes and their mode of decay

Isotope	Half-life	Parent Series	Decay mode	Specific activity
^{223}Ra	11.43 d	^{235}U	α	1.89×10^{15}
^{224}Ra	3.63 d	^{232}Th	α	5.92×10^{15}
^{226}Ra	1600 y	^{238}U	α	3.66
^{228}Ra	5.75y	^{232}Th	β	1.0×10^{13}

However, in minerals or large organisms, the ^{222}Rn may not escape and secular equilibrium can be attained with daughter radionuclides. ^{228}Ra , in ^{232}Th decay series generally found to be in secular equilibrium with its immediate daughter ^{228}Ac . Table 1.1 shows the mode of decay of the different isotopes of Ra with their specific activity.

Among the four naturally occurring Ra isotopes, ^{226}Ra and ^{228}Ra have relatively long half-lives (1600 and 5.75 years, respectively), and the majority of the published work confine to these two isotopes. However, both ^{223}Ra and ^{224}Ra , which have half-lives of few days, have several applications, particularly as environmental tracers in coastal area. All Ra isotopes exhibit similar behaviour in the environment may provide useful information on the coastal process.

1.1.1. Radium in Seawater

Radium concentration in seawater governed by, Th content of sediments, rocks in contact with marine waters, Bioturbation and physical mixing. Uranium present in seawater (3ppb) produces Th which is scavenged and transported to deep sea by sediment particles. ^{226}Ra decay product of terrigenous ^{230}Th gets mixed throughout water column. This U-Th-Ra dis-equilibrium was applied in earlier study of marine bioturbation and mixing process [1]. Minor sources of ^{226}Ra include hydrothermal fluids, rivers, dust deposition and fine grained continental margin sediments. ^{226}Ra is distributed throughout the water column as its half life is on the order of the mixing time of the ocean circulation pattern. But its variation within the ocean may be found due to particle scavenging superimposed on the mixing pattern of the world ocean [2].

The inventories of ^{228}Ra are controlled by the decay of ^{232}Th in deep-sea sediments and processes that mix the sediments. Because of shorter half life compare to vertical ocean mixing time ^{228}Ra derived from continents is only spread throughout the surface ocean and near bottom water. The source of short lived ^{223}Ra and ^{224}Ra to coastal water are SGD, fine grained sediments

and surface discharges (rivers and streams). Their fluxes generally exceed those of their parents as these isotopes are recoil products. Because of their (^{223}Ra and ^{224}Ra) short half-lives they are not able to penetrate into ocean.

Ra input in the estuaries and coastal waters can be due to rivers, sediments and submarine groundwater discharge (SGD). Apart from these sources, phosphate industry may also add significant Ra to coastal water in form of phosphogypsum that contains nearly all of the ^{226}Ra , ^{210}Pb and ^{210}Po present in the ore and smaller quantities of U and Th isotopes [3]. Generally Ra in estuaries is enriched by over an order of magnitude relative to the surface ocean.

1.1.2. Radium in Groundwater

Radium in groundwater can arise from natural sources, resulting from the interaction of groundwater with Ra bearing materials such as rocks, soil, ore bodies and other source materials. Radium concentration in groundwater depends on availability and solubility of the nuclides in the rocks, ionic strength, the acidity of the medium, etc. All of these parameters are highly variable and explain variation of ^{226}Ra and ^{238}U concentrations in groundwater by three to five orders of magnitude [4]. Geothermal springs and geothermal energy production are another source of ^{226}Ra to groundwater [4]. The most abundant Ra isotope reported in groundwater is ^{226}Ra . Concentrations of ^{226}Ra in groundwater vary widely. Groundwater generally have Ra concentrations that broadly correlate with salinity or total dissolved solids (TDS) [5].

1.1.2.1. Natural sources of Ra in groundwater

1.1.2.1.1. Weathering

Breakdown of minerals (Weathering) containing Ra can provide a continuing subsurface supply throughout an aquifer. Primary minerals containing U and Th have Ra isotopes in secular

equilibrium with the decay series parents. ^{238}U and ^{235}U will be similarly distributed within aquifer phases along with their daughters ^{226}Ra and ^{223}Ra whereas ^{232}Th may be in different phases along with its daughter ^{224}Ra and ^{228}Ra . Depending upon physico-chemical parameter Ra isotopes in the different decay chains may be released at different rates.

1.1.2.1.2. Recoil

Another important source for U/Th series nuclides in aquifers is alpha Recoil [6]. Each alpha decay occurs with sufficient energy to propelled daughter radionuclides in a random direction for a distance of ~ 20 nm in most U/Th bearing minerals. The recoil radionuclide can migrate to water phase from damaged lattice through mineral water interface. This is a purely physical process, unaffected by groundwater chemistry.

1.1.2.1.3. Decay of adsorbed and dissolved parent Th isotopes

Decay of parent Th isotopes that are in solution will supply Ra directly to groundwater. Th is highly particle reactive it is highly depleted in groundwater and is largely adsorbed onto aquifer surfaces. Decay of adsorbed Th will recoil Ra directly into the surrounding water or into the underlying mineral, from which it is likely to be readily leached.

1.1.2.2. Factors affecting groundwater radium concentrations

Barite co-precipitates radium from groundwater and commonly controls the groundwater Ra concentrations [7]. Adsorption onto aquifer surfaces is also a dominant controlling factor for Ra behaviour in many groundwater. Fe and Mn oxyhydroxide and clays are the most important phases for Ra adsorption. Time scale for Ra adsorption and desorption very rapidly, over timescales of seconds to hours [8, 9], Colloids and suspended particulates that have strong affinity for Ra also affect the radium in groundwater.

Radium is not directly affected by changes in aquifer redox state as it is present in only one (Ra^{2+}) oxidation state. However, other species (e.g. Sulphate ions, Fe oxyhydroxide etc.) can have an impact on Ra behaviour. Kraemer [10, 11] has observed that saline waters are highly enriched in radium which is due to negligible scavenging process of Ra rather than to increased supply of Ra. The behaviour of Ra in saline waters has generally been explained by sorption processes in secondary mineral phases [12] due to:

- Competition by other, more abundant cations for adsorption sites [11,13].
- Dissolution of Fe and Mn phases in anoxic brines, thereby decreasing the availability of adsorption sites[14] .
- Increases in mineral surface charge [15] due to decreases in pH
- Increases in stabilities of inorganic complexes such as chloride complexes [14]
- Increased solubility of sulphate minerals [16] releasing recently incorporated Ra or limiting removal by precipitation
- The presence of strong dissolved organic complexes [17]

Gonnea et al. [18] observed that adsorption decreased with increased salinity within an aquifer where saltwater intrusion occurs, although it was not possible to separate the effects of ion exchange from those due to Mn and Fe cycling due to redox changes.

1.1.3. Radium in earth crust Soil, Freshwater, River Water and Air

Isotopes of Ra are progeny of the U and Th natural radioactive decay series of radioactive elements and are therefore widely distributed in the Earth's crust. The estimated average ^{238}U concentration in the continental crust is 32.9 Bq/kg [19] and, assuming radioactive equilibrium with ^{238}U , the crustal ^{226}Ra activity is expected to be of same order. Although it can be

anticipated that in most igneous rocks Ra isotopes are present in equilibrium concentrations with their precursors, the impact of some environmental factors, such as weathering, can change ratios between ^{226}Ra or ^{228}Ra and their precursors

In soil radium concentration depends to a large extent on the parent rock. Change in environmental condition such as temperature, water, flora and fauna etc. causes weathering of rocks. Migration of Ra in soil is similar to Ba due to its similar ionic radii. Radium dissolved in groundwater (or surface water) is transferred with the water flow until it becomes adsorbed in the soil [4]. The average worldwide population weighted value for ^{226}Ra concentration in soil of 32 Bq/kg, ranging 3.7 to 126 Bq/kg was reported in UNSCEAR[20].

Radium in freshwater can arise from natural sources such as groundwater inflow, sediment re-suspension, re-solubilisation of sediment bound radionuclides and from air through precipitation and particle deposition. While ^{226}Ra and ^{228}Ra activity concentrations have a wide range in groundwater, depending upon the source characteristics and the ionic strength of the groundwater, ^{226}Ra and ^{228}Ra activities in surface water are low and lie within a relatively narrow range of concentrations [4, 21–27].

Radium in river water generally ranges between 0.5 and 20 mBq/L for ^{226}Ra , though enhanced concentrations (about 300mBq/L) have been reported [4]. For ^{228}Ra , data are scarce but the range is similar to that for ^{226}Ra [28]. For other surface areas, such as lakes, ^{226}Ra concentrations are also within a narrow range (0.5–15 mBq/L), similar to that observed for river water [28].

Radium in air is contributed by re-suspended soil particles, coal ash and fly ash. Considering dust concentration in $50\mu\text{g}/\text{m}^3$ assumed for inhalation and the worldwide concentration of 32 Bq/kg for ^{226}Ra in soil, the concentrations in air was estimated to be 1.5

$\mu\text{Bq}/\text{m}^3$. In particular, UNSCEAR 2000 [29] reported, representative values of $0.6 \mu\text{Bq}/\text{m}^3$, 1.2–3.3 and 0.8–32 $\mu\text{Bq}/\text{m}^3$ for the United States of America, Germany and Poland, respectively. However, these values are presented only for temperate environments, and ^{226}Ra concentrations in air can vary according to climate and to location within a given climate. For example, ^{226}Ra concentration can be substantially higher in areas with a dry climate, and concentrations of Ra in sea air may be an order of magnitude lower at coastal locations than in continental or industrialized areas [30].

1.2. Chemical Properties of Ra

1.2.1. Basic Characteristics:

Radium is an alkaline earth metal, present in nature in the +2 oxidation state. The behaviour of Ra is similar to that of Ba due to the similarity of their ionic radii. Radium can be readily separated through chemical processes from its parent. Thorium is highly insoluble in natural waters, and strongly adsorbs onto mineral surfaces. Due to strong affinity to humic acids and other organic ligands, it can concentrate in organic deposits or transported in organic colloids [31]. In contrast, U is highly soluble under oxidizing conditions. It is readily adsorbed onto mineral surfaces, though to a lesser degree than Th and Ra, and can be complexed by organic ligands.

1.2.2. Aqueous Characteristics:

The aqueous speciation of Ra reviewed in detail by Dickson [4]. In low salinity solutions, Ra can be as un-complexed Ra^{2+} . The thermodynamic data for Ra complexes was calculated from data of other alkaline earth metals [17, 32]. In waters with high sulphate concentrations, a significant fraction of Ra^{2+} would be in the sulphate form; for a sulphate

concentration of 70 mg L^{-1} , half of the Ra would be found as RaSO_4 . In the water with high chloride and salinity only 10% would be in the form RaCl^- . A significant fraction of Ra would be complexed as RaCO_3 only at high pH (>10.25) and high carbonate concentrations ($>60 \text{ mg/L}$) [32].

In waters with high carbonate concentrations, the alkali earths can be precipitated as carbonates. Due to the very low molar concentrations of Ra in the environment, precipitation of Ra phases is rarely important. Ra removal from waters can occur by co-precipitation of phases in which it forms a solid solution. Barium is typically present in natural waters [33] and in groundwater [34] 108 times greater molar concentrations than Ra. In the presence of sulphate the Ba concentrations may be controlled by the precipitation of barite (BaSO_4), as typical Ba concentrations are generally near saturation levels. Barite can incorporate Ra in solid solution as $(\text{Ba,Ra})\text{SO}_4$.

1.2.3. Adsorption and desorption

The mobility of Ra in the environment is controlled by interaction with solid phase by adsorption through ion exchange. This is commonly described by a partition coefficient (K_d), which is defined as:

$$K_d = \frac{\text{Concentration in solid phase}}{\text{Concentration in solution}}$$

The concentration in the solid phase is expressed as the amount of adsorbent in a total mass of solid (in e.g. moles/kg), while the concentration in solution is expressed in moles L^{-1} . Data on K_d values for Ra are limited compared to many other contaminants. The studies indicated, Ra is readily adsorbed to clays and mineral oxides present in soils, especially at near neutral and alkaline pH conditions. Sorption studies generally confirm the adsorption behaviour

expected for Ra^{2+} as a function of pH, with negligible adsorption at very acidic pH values and increasing adsorption with increasing pH. The pH range at which adsorption of cations begins to increase on mineral surfaces depends on the values of the point of zero charge (PZC) i.e. when the electrical charge density on a surface is zero [35]. At pH values greater than the PZC, the surface strongly adsorbs dissolved cations. Radium competes with other alkaline earth cations for sorption sites. In comparison to other alkaline earth elements, the relative affinity of this group of elements for ion exchange is in order: $\text{Ra}^{2+} > \text{Ba}^{2+} > \text{Sr}^{2+} > \text{Ca}^{2+} > \text{Mg}^{2+}$ [36]. The adsorption of Ra depends on ionic strength and other competing ions.

Manganese oxide has strongly scavenging properties for Ra and used for pre-concentrating from bulk water samples. Manganese oxides commonly occur in sediments as coatings and fine aggregates with large surface areas and controlling Ra behaviour. Although many Mn minerals are known, its oxides are typically fine-grained and poorly crystalline and often remain uncharacterized [37]. Koulouris have [38] investigated the sorption of Ra on MnO_2 is independent of initial Ra concentrations, chemical species and pH at values greater than 3.5.

1.3. Measurement of Radium isotopes:

There are several methods reported for the estimation of Ra via its decay products using alpha, beta and gamma spectrometry. Alpha spectrometry is performed using radium-barium co-precipitate. For beta spectrometry liquid scintillation counting is performed. Gamma spectrometry is performed for active samples using gamma peaks of daughter products. Gross counting of the Ra carried out by co-precipitation after appropriate chemical separation procedure. Most widely used procedure for ^{226}Ra estimation is Emanometry, which is based on the emanation and isolation of the activity of the radon ingrown from radium in solution and measurement of radon and its decay products.

The concentration of Ra in environmental water samples is extremely low, thus before measurement using any suitable technique, the radium from water sample must be concentrated by:

- Evaporation
- Sorption of Ra on cationic exchange resin
- Manganese-oxide impregnated acrylic fibers
- Co-precipitation followed by dissolution

Manganese dioxide (MnO_2) effectively removes a variety of radionuclides (including Ra, Th, U, Po, Ac and Pb) which are assumed to be in dissolved phase [39]. Mn fibres can be used to pre-concentrate Ra isotopes from high volume up to 1000 L of seawater [40, 41]. The MnO_2 resin consists of an inert macro porous carrier substrate on which the manganese dioxide is precipitated in finely divided form by reduction.

1.3.1. Alpha Spectrometry

The Ra isotopes ^{226}Ra , ^{223}Ra and ^{224}Ra are alpha particle emitters and can be directly measured by alpha spectrometry using radiochemical separation. The beta emitting Ra isotope ^{228}Ra can be indirectly measured by alpha spectrometry via its progeny ^{228}Th or ^{224}Ra . Due to long half-life of ^{228}Th ($T_{1/2} = 1.9$ y) the equilibrium period ranges between 3 and 18 months (depending on the ^{228}Ra activity and required sensitivity). For routine analysis of ^{228}Ra alpha spectrometry is not considered as practical measurement method. A prime disadvantage of alpha spectrometry is the necessity for time consuming chemical dissolution and Ra separations for preparation of the thin source.

Alpha emitting radionuclides other than Ra can be present in the sample; can interfere in the alpha spectrometric determination, if not separated completely. For example, interferences with the alpha energy of ^{226}Ra could be caused by ^{230}Th , ^{229}Th , ^{231}Pa and ^{234}U . Interferences with the alpha energies of ^{223}Ra and ^{224}Ra can occur by $^{243+244}\text{Cm}$, ^{241}Am , ^{238}Pu , ^{228}Th , ^{227}Th , ^{225}Ac , ^{222}Rn , ^{218}Po , ^{213}Bi and ^{210}Po . Involving radiochemical separations, the number of radionuclides possibly emerging at the measurement is rather limited, and such interferences are minimized. A more common difficulty arises from the separation of the contributions due to the other alpha emitters.

1.3.2. Gamma Spectrometry

An attractive feature of gamma spectrometry is its ability to use bulk samples without any radiochemical separation. For solid materials including soils and sediments, the sample can be placed directly into the sample holder or container. In gamma spectrometry basic preparation e.g. drying, ashing, sieving and homogenization required. Another advantage of gamma spectrometry is the ability to determine ^{224}Ra and also ^{228}Ra by measurement of the gamma rays of its progeny (^{228}Ac). Sample matrix effects (including self-attenuation) and paired coincidence decays need to be considered in quantification by gamma spectrometry [42]. There are two basic approaches to the determination of ^{226}Ra by gamma spectrometry [43]. The first is by measurement of the ^{226}Ra peak at 186.2 keV. However, the emission probability of this gamma photo peak is quite weak (3.6%), and associated with interference from the primary gamma emission of ^{235}U (at 185.7 keV), with emission probability of 57%. Hence, this approach requires an independent estimate of ^{235}U to estimate interference [44]. A more sensitive approach to estimate ^{226}Ra based on strong gamma lines of the ^{222}Rn progeny ^{214}Pb (295 and 352 keV) and ^{214}Bi (609 keV). The

application of this approach requires an ingrowth period (generally of approximately 3–4 weeks) for ^{222}Rn equilibrium with its progeny.

1.3.3. Liquid Scintillation Counting (LSC)

Ra determination using LSC can be divided into two general groups:

- Where no sample preparation is required
- Where radiochemical methods may be used prior to measurement.

Measurements in the first category are performed directly either without a cocktail (Cerenkov counting), with a water immiscible cocktail (as a two phase sample). Such methods can only be used for samples with relatively high activity; otherwise the counting time needs to be rather long. The second method can be applied not only for the determination of ^{222}Rn but also for the determination of ^{226}Ra in water samples. In this method, radon is extracted from the water phase into an organic phase (containing the scintillation cocktail, leaving Ra and other interfering radionuclides in the aqueous phase). A method of direct Ra determination is a simple mixing of the water sample with a water miscible cocktail. In this method, the cocktail forms a homogeneous mixture with the sample [45]. The interference of other radionuclides is, however, a limiting factor for the determination of Ra isotopes. Co-precipitation with a Ba carrier is the most popular technique for reduction of sample volume and removal of the interfering radionuclides for LSC applications.

1.3.4. Mass spectrometry

Mass spectrometry is a more sensitive method for the determination of ^{226}Ra and ^{228}Ra and their isotope ratio. Three types of mass spectrometry have been used for the determination of ^{226}Ra and ^{228}Ra : thermal ionization mass spectrometry (TIMS), inductively coupled plasma mass

spectrometry (ICP-MS) and accelerator mass spectrometry (AMS). TIMS is one of the most sensitive and most accurate mass spectrometric techniques. The major disadvantage is the complicated radiochemical separation procedure necessary to; concentrate the Ra in the small source volume, separation of the matrix components, removal of possible interferences and preparation of source on the filament. The detection limit for ^{226}Ra is about 40 μBq [46], better than the sensitivity of alpha spectrometry. The detection limit of 12 mBq for ^{228}Ra is comparable to that of beta counting. ICP-MS is the most frequently used mass spectrometric technique for the determination of ^{226}Ra concentration and the $^{228}\text{Ra}/^{226}\text{Ra}$ isotope ratio. The detection limit of ICP-MS varies from 10^{-15} g to 10^{-18} g, and the precision varies between 0.1 and 0.5 %. Better precision of isotope ratio measurements can be achieved by using multi-ion collector devices in sector field ICP-MS [47]. AMS is an expensive technique known for its sensitivity towards elements that form negative ions. Many of the interferences are suppressed or eliminated during the combined ionization, acceleration and mass analysis steps. A detection limit of 0.1 mBq for ^{226}Ra and 40 mBq for ^{228}Ra has been reported[48]. This sensitivity is comparable to the alpha spectrometric method for ^{226}Ra and to LSC and beta counting methods for ^{228}Ra . The major advantage of AMS for Ra measurements is its ability to measure both isotopes within a short time.

1.3.5. Method for ^{223}Ra and ^{224}Ra

The short half life and very low concentration (in environment) of ^{223}Ra and ^{224}Ra restrict the applicability of various methods for their estimation. Generally, low level Gamma spectrometry and delayed coincidence counting method are used for the measurement of these short-lived isotopes. In present study, estimation of ^{224}Ra and ^{223}Ra in seawater was carried out by pre-concentration of Ra from seawater on MnO_2 -fiber. The gaseous daughter product (Rn) of

Ra adsorbed on MnO₂-fiber, were flushed and re-circulated into scintillation cell by carrier gas. The alpha particle from decay of corresponding Rn and Po isotopes is recorded by photomultiplier tube.

1.4. Application of Radium:

Ra has four naturally occurring isotopes with half-lives ranging from 3.7 d to 1600 y, having applicability as a powerful tracer of environmental processes. ²²⁶Ra and ²²⁸Ra have long half-lives (1600 and 5.75 years, respectively), and the majority of the published literature on Ra as tracer in marine process relates to these two isotopes. However, both ²²³Ra and ²²⁴Ra, with a half-life of few days, have several applications, particularly as environmental tracer in coastal areas. The signature pattern arises due to distributions of Ra isotopes reveal important information about the environment. Ra is known for radiological significance and also as tool for solving marine issues. The four naturally occurring radium isotopes (²²³Ra, T_{1/2} = 11.4 days; ²²⁴Ra, T_{1/2} = 3.6 days; ²²⁶Ra, T_{1/2} = 1,600 years and ²²⁸Ra, T_{1/2} = 5.75 years) can be used as tracers of a variety of environmental processes; like groundwater discharge and coastal water circulation pattern.

1.5. Definitions and Drivers of SGD

There are various pathways for water discharge from land to ocean viz. Surface water (River and streams) and groundwater flow. These water discharges are important pathway for material transport to the marine environment from land. The surface water discharge, an input source for material discharge to the ocean is well documented. Groundwater discharge has a smaller water flow rate compared to surface flow rate but the associated chemical fluxes are comparable to river chemical fluxes [49].

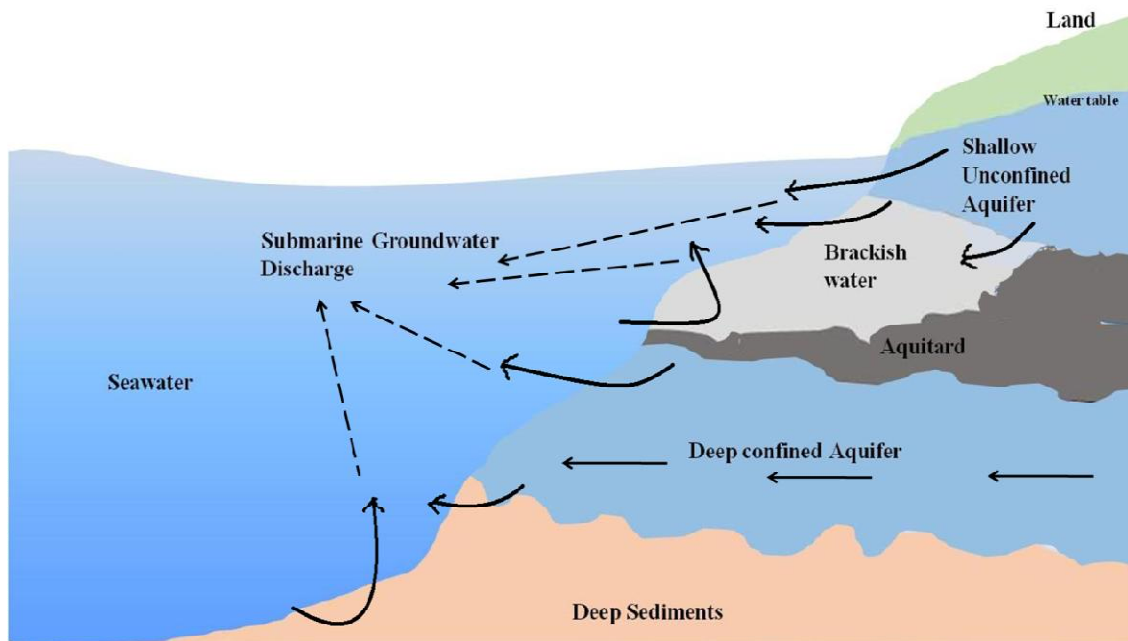


Figure 1.2: Description of different pathways of SGD [51].

The groundwater discharge associated with nutrients, heavy metals, radionuclides and organic compounds have significant impact in the near-shore marine ecosystem [50]. Usually coastal aquifers consist of complicated confined, semi-confined and unconfined system as shown in Figure 1.2. Groundwater located in the shallow, unconfined aquifer can discharge directly to the coastal water or can mix with seawater. Freshwater flows through an aquifer driven by hydraulic head and intrudes seawater. Seawater percolates through the seabed driven by a variety of forces. The zone of intermediate salinity extended between fresh water and seawater is called subterranean estuary.

There are various driving forces for groundwater flow to the coastal ecosystem and a number of them including terrestrial and marine forces [49]. The hydraulic gradient is the primary terrestrial driving force of fluid flow through coastal aquifers. Groundwater from the upland region of a watershed flows to unconfined or semi-confined aquifers on the coast and can

mix with salty pore water that has infiltrated from the ocean [51]. The main driving forces influencing the SGD are; water level differences across a permeable barrier, tidal pumping, wave setup [52–54] mars-storms, current induced pressure gradients in the coastal zone; upland recharge causing seasonal inflow and outflow of seawater into the aquifer [55] and geothermal heating.

Some reported literature consider only the discharge of terrestrial groundwater and refer groundwater as rainwater which has infiltrated and percolated to the water table [51]. Others consider SGD as “any flow of water from seabed to the coastal ocean, regardless of fluid composition or driving force”[53] and include fresh SGD, saline SGD and brackish SGD. The latter being a mixture of groundwater and seawater end-members.

Water flow (SGD) occurring on the continental shelf (coming from deeper aquifers), driven by buoyancy and pressure gradients, called as deep pore water upwelling (DPU) [49, 56]. Also the flow of water driven by an inland hydraulic head through highly permeable aquifers or by large-scale cyclic movement of water caused by thermal heating, called as offshore submarine springs [49]. In sandy coastal areas ripples created by seafloor currents also drive the pore water exchange when waves generate pressure gradient. The water percolates through the sediments in ripples and flows on a curved path towards crests and released as SGD.

The most general and cited definition of groundwater is “water residing within the saturated zone of geologic material” [49, 51]. Therefore pore water filling space among sediments grains and making sediments saturated like submerged, porous materials, is synonymous with groundwater [49]. There is some doubt for groundwater discharge definition, as it occurs as a slow diffuse flow or seepage through sediment and characterized by substantial temporal and spatial variability [51]. We thus consider “submarine groundwater discharge” to be

any flow of water out across the sea floor. The advantage of defining groundwater discharge as a flow of water from the seabed to the marine environment (including fresh, saline and brackish SGD) takes into account discharges of both: terrestrial groundwater and re-circulated seawater. It is obvious that in the coastal ecosystem the seawater intrusion into the sediment is a common process [54].

1.6. Significance of SGD:

Submarine groundwater discharges recognised as an important pathway of dissolved chemical substances to the coastal ecosystems that is deteriorating coastal environment. SGD makes a larger contribution to the flux of dissolved chemical compounds than river run-off due to contamination of groundwater in many areas with various chemical substances like nutrients, metals, organic compounds etc. Groundwater seepage is patchy, diffuse, temporally variable, slow, persistence seepage through sediments and may involve multiple aquifers. Groundwater seepage can occur at almost all coastal zones where an aquifer with a positive head relative to sea level is hydraulically connected to a surface water body [61–66].

The subterranean non-point or groundwater discharge is very important pathways of material transport in coastal areas and in some areas even of greater ecological significance than surface runoff [63]. The studies [64–66] has specific examples of the ecological impact of groundwater flow into coastal zones and concluded that groundwater inputs of nitrogen are critical to the overall nutrient economy of salt marshes. The groundwater nutrient inputs were found to be approximately equal to nutrient inputs via surface freshwater runoff in eastern Florida Bay [67, 68]. Studies [69, 70] showed that groundwater discharge accounts for greater than 20% of the freshwater input into the Great South Bay, New York. Capone and Bautista (1985) and Capone and Slater (1990) latter found that groundwater is a significant source

(~50%) of nitrate to the Great South Bay. Study [71] concluded that higher flux of nutrients than that derived from all South Carolina Rivers, is supplied from SGD to salt marshes on the South Carolina coast. Significant groundwater inputs of nitrogen and dissolved organic phosphorus to canals and surface waters in the Florida Keys may be a major factor for initiating the phytoplankton blooms observed in that area [72]. It was studied that Harmful Algal Blooms (HABs) in some areas were also related to nutrient supply via SGD [50, 73, 74]. It was studied that, a large nutrient flux via SGD is the reason for not only to eutrophication but also to the occurrence of red tides in Masan Bay, Korea [75].

Various studies indicated that SGD is generally a significant source for fluxes of trace elements and metals to the marine environment. Jeong et al. (2012) determined fluxes of some trace elements viz. aluminium, manganese, iron, cobalt, nickel and via SGD and concluded that SGD was the source for unusually higher concentrations of some trace elements in coastal seawater of the volcanic island Jeju during summer. Similar to radium, barium and strontium also have higher abundance in coastal seawater. Fluxes of barium via SGD were found equal or higher than that of via river [76–78] Strontium fluxes via SGD were found to be comparable to its river flux [79].

Various studies [63, 80, 81] concluded that some metal behaves non-conservatively in groundwater upon mixing with seawater. For example Beck et al. [80] showed that dissolved cobalt and nickel behaves non-conservatively as oppose to the conservative behaviour of salinity upon the mixing of groundwater and seawater end-members [80].

Mineralization of organic matter, manganese oxidation-reduction cycle, forming or dissolution of colloids and organo-metallic complexes are the some of the process affecting conservative behaviour of the selected metal [82, 83]. On the other hand dissolved copper, lead,

silver, aluminium and manganese, did not show clear dependences in relation to salinity changes. Several studies have been carried out for the estimation of mercury concentrations in groundwater and mercury flux associated with SGD [84–89]. The studies indicate that mercury flux via SGD is one order of magnitude greater than its atmospheric flux in the Waquoit Bay [85].

Various studies also concluded that SGD is an important source of both dissolved organic carbon (DOC) and dissolved inorganic carbon (DIC) to the marine environment [78, 90–93]. Using multiple measurement technique (thermal infrared aerial remote sensing, geophysical and geological data, geochemical characterization and radium isotopes), the role of groundwater for dissolved nutrients, carbon, and trace gases source in Okatee River estuary, South Carolina, was studied. The higher ^{226}Ra activity correlated to higher concentrations of organics dissolved inorganic carbon, nutrients, and trace gases to the Okatee system.

1.7. Methods Used to Measure SGD

Determination of groundwater discharge is a difficult task considering temporal and spatial variability of groundwater flow, hydrogeological conditions, weather parameters shifts and human management of the coastal ecosystem [75]. Zektser have [94] showed that submarine groundwater discharge is a part of a complex hydrological and hydrogeological problem of water exchange between land and sea. There are two inter-related processes involved in subsurface water exchange between land and ocean involves: (1) submarine discharge into seas and oceans (2) seawater intrusion into the shore.

Groundwater discharge to the coastal ecosystem can be estimated by a number of methods. However, each technique has certain limitations because of generalized assumptions and natural variability. The most popular methods used to quantify SGD are: hydrodynamic

method for calculating lateral groundwater flow [94]; methods based on investigation of the coastal drainage area [95]); methods based on investigation of the sea [95]; modeling [49, 51]; direct measurements [49, 51] and tracer techniques [49, 51]. A brief description of important technique used for measurement of SGD is given below:

1.7.1. Seepage Meter

Groundwater seepage rates can be directly measured using manual “seepage meter”. Israelsen and Reeve [96] had developed first seepage meter to measure water loss from irrigation canals. Lee in 1977 [97] designed a seepage meter that consist a 55-gallon (208 L) steel drum, fitted with a sample port and plastic collection bag. The open end of chamber shaped drum is inserted down into the sediment. Groundwater seeping through the sediment displaces water trapped in the chamber and forces it up through the port into the plastic bag. The actual volume of groundwater can be calculated using the end-member approach [51, 98]. The change in volume of water in the plastic bag over a measured time interval is used to find flux of SGD [51, 99]. There are several requirement and precaution to be taken while using the seepage meter method.

- In order to estimate the average groundwater seepage rate installation of several seepage meters is necessary because of temporal and spatial variability [100, 101]. The resistance of the tube and bag have to be minimized to prevent artifacts [102–104].
- In order to decrease the effects of surface water movements due to waves, currents or other activities the plastic bag may be covered [105].
- To determine the positive and negative seepage measured volume of water can be filled initially in the bag.

- Artifacts occasionally exist from pressure gradients developed by uni-directional currents passing over the meter [106].

Many types of automated seepage meters using different methods of water sensing were constructed [107] as seepage meters measurement are very labour intensive and time consuming. Boyle [108] installed remote device from the surface of various water bodies. Others used: hydrothermal vents [109] ultrasonic measurements [110], heat-pulse devices [111, 112], continuous heat type automated seepage meters based dye-dilution seepage meters [113] for measurement of SGD.

A serious limitation of seepage meters is the requirement of their deployed in a relatively calm environment. Breaking waves and strong currents induce flow through the seabed dislodge seepage meter [114].

1.7.2. Piezometer

The principle of the method is based on measurements of hydraulic conductivity and gradient of pore water combined with the Darcy's Law. Piezometer (usually multi-level piezometer nest) is inserted into the sediment and groundwater potential can be measured at several depths [115, 116]. Using observations or estimates of the aquifer hydraulic conductivity, the groundwater discharge rate into the ocean can be calculated using a one-dimensional form of Darcy's Law:

$$q = -K(dh/dL)$$

Where q: Darcian flux (groundwater discharge volume per unit area per unit time)

K: Hydraulic conductivity (here assumed constant)

dh/dL: Hydraulic gradient in which h is hydraulic head and L is distance.

The limitation of the method is the natural variability in seepage rates due to heterogeneity in the local geology. Because of that obtaining the representative hydraulic conductivity is difficult which often varies over several orders of magnitude within an aquifer. The piezometer nests combined with seepage meters were used to estimate the hydraulic conductivity from observed seepage rates and the hydraulic gradient [117, 118]

1.7.3. Natural tracers

The naturally occurring geochemical tracers have been used for local to regional-scale estimation of groundwater inputs into the ocean. The use of naturally occurring geochemical tracers have advantageous over seepage meters or piezometers as they present an integrated signal since they enter the marine water column via various pathways in the aquifer. Thus small spatial scale variations, a serious drawback for the use of seepage meters or piezometers, tend to be smoothed out over time and space in the case of tracer methods-

There are two ways to evaluate groundwater discharge rates into the ocean using natural geochemical tracers. First is the use of enriched geochemical tracers in the groundwater relative to the seawater [40, 119–121] and second the use of vertical profiles of the geochemical compositions in sediment pore waters [122, 123]. The second approach, applicable to homogeneous media is based on the assumption that natural tracer's distribution can be described by a vertical, one dimensional advection–diffusion model.

In order to use geochemical tracer for SGD determination, several criteria must be defined, including concentrations of the tracer, conservative behaviour of tracer, boundary conditions (i.e., area, volume), water and tracer sources and sinks and residence times of the surface water body. Sources may include groundwater, river water, ocean water, precipitation, in situ production, horizontal water column transport and sediment re-suspension, or sediment

diffusion. Sinks may include horizontal or vertical eddy diffusivity, horizontal water column transport, in situ decay or consumption and atmospheric evasion. After defining the conditions, simple mass balances or box models for the system can be constructed for the determination of SGD.

Thus an ideal tracer to provide a detectable signal, should be greatly enriched in the discharging groundwater relative to coastal marine waters, behave conservative and easy to measure. Since past few years several researchers have used radium isotopes (^{223}Ra , ^{224}Ra , ^{226}Ra , ^{228}Ra) and ^{222}Rn to estimate groundwater discharge into the ocean as they are highly enriched in coastal water and shown conservative mixing [53, 61, 126–135, 62, 67, 68, 71, 119, 120, 124, 125]

Luo et al. (2014) [136] have used ^{224}Ra and ^{223}Ra to qualify submarine groundwater discharge (SGD) in Tolo Harbour, a highly urbanized embayment in Hong Kong. SGD was estimated to be $1.2\text{--}3.0\text{ cm d}^{-1}$, lateral SGD was $5.7\text{--}7.9\text{ cm d}^{-1}$ and bottom SGD was $0.3\text{--}2.0\text{ cm d}^{-1}$. Fresh SGD was estimated to be $(2.1\text{--}5.5) \times 10^5\text{ m}^3\text{ d}^{-1}$ in the study area. The results showed that total SGD in this area represents about 1–2.4 % of the total sea water in the harbour and that fresh groundwater discharge is about 1.5–4 times larger than the total river discharge in the area.

Hawang et al. [74] have developed a geochemical model for local-scale estimation of SGD for system under steady state. In steady state addition of radium fluxes from sediment, river, and groundwater are balance by losses due to mixing and, in the case of ^{223}Ra and ^{224}Ra , radioactive decay. A steady-state mass balance approach may also be used for ^{222}Rn with the exception that atmospheric evasion must also be taken into account [137].

The method based on radon and radium isotopes have some limitations. Radium isotopes, for example, may not be enriched in freshwater discharges such as from submarine springs. Also ^{222}Rn may exchange with the atmosphere which may be difficult to model under some circumstances (e.g., sudden large changes in wind speeds, waves breaking along a shoreline). The combination of tracers can be used to avoid these limitations.

There are several other tracer like Methane (CH_4), natural radioactive isotopes (^3H , ^{14}C , U) and stable isotopes (^2H , ^3He , ^4He , ^{13}C , ^{15}N) that have also been used as geochemical tracers for estimation of SGD [49]. Cable in 1996 [119] has showed that SGD can be an important source of CH_4 to coastal waters and showed that ^{222}Rn and CH_4 concentrations not only have positive correlation with seepage meters measurements but are also inversely related with salinity. Basu et al. in 2001 [79] studied Sr and $^{87}\text{Sr}/^{86}\text{Sr}$ in the Bengal basin and concluded SGD as an important source of strontium to global oceans. Using Sr, $^{87}\text{Sr}/^{86}\text{Sr}$ and an inverse model Rahaman and Singh (2012) [138] characterised SGD (combined freshwater and recycled seawater) in estuaries of western India.

Salinity anomalies are also used for estimation of freshwater fluxes in SGD. However isotopes have an added advantage over chemical techniques where the estimation of brackish and saline fluxes (have more impact on the coastal environment) is required. Combination of stable, long-lived, and short-lived isotopes along with other complementary techniques can be used for the studying the detailed aspects of coastal hydrology.

1.7.4. Infrared Imaging

The groundwater temperature can also be used as a tracer to detect the location and spatial variability of groundwater discharge rates. There are two basic methods used: (1) Temperature–depth profiles assuming conservative heat conduction–advection transport [139];

(2) temperature differences in the groundwater and surface water system [140–142]. The groundwater temperature can be measured using techniques such as infrared sensors or other remote sensing methods like satellite images.

1.7.5. Hydrologic Approach

The hydrologic approach can be used for determining SGD by mass balance method [95, 107] and the Darcy's law calculation. Simple water balance approach has been also used to determine the fresh SGD in some basin and described as;

$$P = E_T + D_S + D_G + dS$$

Where P is precipitation, E_T is evapotranspiration, D_S is surface discharge, D_G is fresh groundwater discharge, and dS is the change in water storage. dS is usually considered over extended period (i.e. years) to be negligible. Therefore, accurate quantification of D_G by this approach requires precise measurement of the precipitation, evapotranspiration and surface runoff. There are certain things to be considered before using the method; (1) precise measurement of precipitation, evapotranspiration, surface discharge, and the change in water storage; (2) the aquifer should be isolated by impermeable layers and discharging directly to the sea [95]; (3) This method is only applicable to formations, where the value of deep infiltration exceeds the accuracy of other components of the water balance equation [143]. Moore in 2010 have [49] concluded that water balance method is suitable to estimate the fresh groundwater discharge. Several studies using water balance method have been performed in many places for basin-scale determinations of fresh SGD [144–146].

1.7.6. Hydrograph separation techniques

This technique is based on the assumption that the fresh groundwater component entering streams can be estimated via a hydrograph separation and the result may be extrapolated to the coastal zone. The method used by various authors for global-scale estimation of fresh SGD for the Pacific Ocean rim [147], eastern Russia [148] and in the local coastal plain stream in South Carolina [143].

Two different approaches were used to separate the hydrograph for estimating the fresh groundwater flow component. The first approach is to assign a base flow due to the shape of the hydrograph. The baseline changes depending on time, space, and prevailing hydrological is the limitation of this method. This technique is applicable to only coastal areas with well-developed stream networks and to zones of relatively shallow, mainly freshwater aquifers. The second approach of hydrograph separation uses geochemical end-member concentrations. The water and geochemical mass balances in a river can be represented as follows;

$$D_T = D_S + D_G$$

$$C_T D_T = C_S D_S + C_G D_G$$

Where D and C are the discharge rate and geochemical concentration respectively, the subscripts T, S and G represent the total, surface water and groundwater components. Using above two equations, measured D_T , C_T , C_S , and C_G , one can calculate for the D_S and D_G values.

1.7.7. Mathematical Models

Over the past few years various kinds of model have been developed for understanding subsurface flow in coastal aquifers [60, 75]. The mathematical and numerical simulations represent a form of differential equation for both: the flux and the transport phenomena.

Analytical solution of these equations can be implemented where aquifers are both homogenous and isotropic and boundary conditions are simple. Whereas numerical models can be used in heterogeneous and anisotropic aquifers [95]. These numerical models allow simplifying key features in aquifer systems for the analysis of groundwater and saltwater movement under varying conditions (pre-pumping, pumping, future) which are not possible to estimate by other methods. These models must be validated periodically by other independent methods as they are limited by the availability of data (e.g. groundwater pumping, hydraulic head, hydrostratigraphic, and transmissivity). Several study have been reported using mathematical model in literature e.g. [51, 54]

1.8. History of SGD Research and Work Done

The undersea discharge of fresh groundwater was known for many centuries. According to the Roman geographer, Strabo, who lived from 63 BC to AD 21, mentioned a submarine spring (fresh groundwater) 2.5 miles offshore from Latakia, Syria (Mediterranean), near the island of Aradus [149]. Water from this spring was collected from a boat, utilizing a lead funnel and leather tube, and transported to the city as a source of fresh water. Other historical accounts tell of water vendors in Bahrain collecting potable water from offshore submarine springs for shipboard and land use [150], Etruscan citizens using coastal springs for ‘hot baths’ (Pausanius, ca 2nd century AD), and submarine ‘springs bubbling fresh water as if from pipes’ along the Black Sea (Pliny the Elder, ca 1st century AD). Offshore discharge of fresh water has been used in a number of cases for water resource purposes. One particularly spectacular example of such use involved the construction of dams in the sea near the southeastern coast of Greece. The resulting ‘fence’ allowed the formation of a fresh water lake in the sea, which was then used for irrigation on the adjacent coastal lands [151].

The existence of submarine springs has been known for many years, but no scientific information was available. SGD has been neglected scientifically because of the difficulty in assessment and wide spread perception that the process is not significant. Therefore, direct discharge of the groundwater into the ocean has not been quantified in terms of the global water and material cycle on the Earth.

Later in 1980 it was recognition that in some cases, groundwater discharge into the sea may be both volumetrically and chemically important [57, 152]. Considering the importance of and increased interest in the field, the Scientific Committee on Oceanic Research (SCOR) formed two working groups to study

- Magnitude of Submarine Groundwater Discharge and its Influence on Coastal Oceanographic Processes
- Transport and Reaction in Permeable Marine Sediments

Global estimates of SGD vary widely (approximately 0.2–10% of river flow; [153, 154]. Studies on SGD have been reviewed upto 1970 [143]. study [40] suggested that SGD could contribute roughly 40% of the water supplied by rivers to the coastal ocean between Cape Fear, NC and Savannah, GA. Many studies of SGD in near shore coastal ocean environments have been conducted.

Taniguchi [52] have reviewed all available studies up to 2002 and indicated that SGD in the area studied was significant. This compilation was limited to literature citations of discharge estimates using seepage meters, piezometers, and/or geochemical/geophysical tracers.

Many independent studies have been performed on the east coast of the United States, Europe, Japan, and Oceania [52] for the estimation of SGD. Fewer studies carried out on the west coast of the US, South America, and Hawaii. Till the year 2002, no information is available

on SGD quantitative data from India though indications of groundwater discharge have been reported for Bangladesh [76] and Kenya [155]. Various estimates about role of SGD in the global water balance were carried out and estimated contribution range was about three orders of magnitude (approximately 0.01 to 10% of total river flow) as shown in Table 1.2.

International Atomic Energy Agency (IAEA) and UNESCO in 2000 has initiated and Coordinated Research Project (CRP) on Nuclear and Isotopic Techniques for the Characterization of Submarine Groundwater Discharge (SGD) in Coastal Zones". CRP carried out jointly by IAEA's Isotope Hydrology Section in Vienna and the Marine Environment Laboratory in Monaco, together with nine laboratories from eight countries. They have used several methods of SGD assessment and carried out a series of five inter-comparison experiments in different hydrogeologic environments (coastal plain, karst, glacial till, fractured crystalline rock, and volcanic terrains). It was concluded that while the process is essentially ubiquitous in coastal areas, the assessment of SGD magnitude at any one location is subject to enough variability. The study also pointed that measurements should be made by a variety of techniques and over large enough spatial and temporal scales to capture the majority of these changing conditions.

McCoy in 2009 [75] has reviewed the highlighted findings from SGD studies on three hydro geologically different continental margins (Onslow Bay, NC, southern Florida, and the Louisiana margin), provided the background on the common methods of assessing SGD, and suggests a regional management plan for coastal groundwater resources that should be incorporated in the development of new monitoring networks. A radium-based approach for estimating SGD to the marsh yielded a summer average of $3900 \text{ m}^3 \text{ day}^{-1}$ [162]. Valiela [163] reported a SGD range of $600\text{--}23,000 \text{ m}^3 \text{ day}^{-1}$ using Darcy's Law. Lee [164] using the same

approach, estimated SGD at $2800 \text{ m}^3 \text{ day}^{-1}$. Two independent field-based approaches yielded similar SGD values for Sippewissett Marsh: $13,000 \text{ m}^3 \text{ day}^{-1}$ [64] and $9000 \text{ m}^3 \text{ day}^{-1}$ [165]. Charette [162] used a radium-based approach for estimating SGD to the marsh yielded a summer average of $3900 \text{ m}^3 \text{ day}^{-1}$ in Great Sippewissett Marsh, West Falmouth, MA.

Table 1.2: Global studies on contribution of SGD

Amount of SGD	Study Area	Method	Reference
3% of total water flux	Great Sippewissett Marsh, MA, USA	Chemical budget	[64]
6% of the total water flux	Global estimates	Hydrograph separation	[156]
31% of the total water flux	Global estimates	Water balance	[157]
20% of total water flux	Great South Bay, NY, USA	Seepage meter	[158]
10% of total water flux	Chesapeake Bay, Virginia, USA	Rn, Ra	[61]
29% of total water flux	Adriatic Sea	Water balance	[159]
87% of total water flux	Buttermilk Bay, MA, USA	Nutrient balance	[160]
0.01–10% of surface runoff	Global estimates	Literature	[161]
0.3% of surface runoff	Global estimates	Hydrological assumptions	[154]
10% of surface runoff	Global estimates	Water balance	[153]
10% of surface runoff	Global estimates	Water balance	[143]

1.8.1. SGD in the Indian Coastal Areas

In last few decades, SGD has been known as a important source of water and nutrient discharge on the coastal region. India has a coastline of 7517 km and groundwater discharge is continuously taking place along the coast and within the coastal zone hydrological system. It was reported that more than 50% of the discharge were in the bay of bengal. It has been reported that in Indian hydrological system more than 50% of the annually hydrological input (>4000 billion m³) are losing due to various unaccounted process, including escape flow path by SGD to ocean [166]. Therefore, it very important to understand the various pathways of SGD along with its environmental impact.

In indian conntext there is a lack of available literature on coastal hydrology and the interaction of groundwater discharge with seawater. Most of the studies and published literatures focus on degradation of groundwater qualites by seawater intrusion, its geochemical aspect and management. There are very few SGD studies or related studies that have been reported in the indian coastsal areas. The notable studies in the Indian Coastal areas are mentioned discused below:

1.8.1.1. Studies related to existance of SGD

Among the notable studies, Mukharjee et al. have reported enhancement of SGD intrusion in the most of the coastal aquifiers in the south west bengal [167]. Chidambaram and Ramanathan carried out for coastal water management pupose in Cuddalore, India [168]. Jacobe et al. have used ²²²Rn monitoring to study the existance of SGD in the coastal area of Vizhinjam Tiruvananthapuram, India [169]. Chawla et al. [170] have reported the distribution of short lived radium isotope to study the presence of SGD in the Cuddalore coast, Tamil Nadu, location in the East Coast of India.

1.8.1.2. Studies related to quantification of SGD

Debnath et al. [171] have used high resolution thermal mapping and chemical profiling of porewater to identify the zones of SGD in Bay of Bengal (BOB). The total SGD to BOB was reported to be $1.16 \times 10^7 \text{ m}^3 \text{ m}^{-1} \text{ year}^{-1}$. Debnath and Mukherjee [172] have reported the quantity and seasonal variation of SGD towards BOB through high resolution spatiotemporal lunar-tidal cycle scale seepage meter experiment and total annual SGD to the BOB was estimated as $8.98 \times 10^8 \text{ m}^3 \text{ year}^{-1}$. Ravindran and Ramanujam [173] has used in-situ electrical resistivity imaging study to coastal zone at Manapad, Tuticorin, India for the Detection of submarine groundwater discharge. Variation in the resistivity values were used to demarcates the freshwater discharge in the subsurface condition in the coastal zone. Krishan et al. [174], using in-situ ^{222}Rn and electrical conductivity (EC) monitoring, showed that there is considerable submarine groundwater discharge on the coast of West Bengal, India. Rengarajan et al. [175] used multiple tracers: salinity, Si, ^{223}Ra , ^{224}Ra , ^{228}Ra and ^{226}Ra to estimate the submarine groundwater discharge to the coastal zone of the Godavari estuary, India. The SGD fluxes in Gautami Godavari estuary, Vasishta Godavari estuary and Kakinada bay was estimated to be $5 \times 10^6 \text{ m}^3 \text{ day}^{-1}$, $20\text{-}43 \times 10^6 \text{ m}^3 \text{ day}^{-1}$ and about $300 \times 10^6 \text{ m}^3 \text{ day}^{-1}$ respectively. Prakash et al. [176] have used mass balance of Radon (^{222}Rn) isotope to quantify SGD in Coleroon river estuary, India. The Radon mass balance quantifies SGD flux ranges between 7.47, 4.56 and 2.37 m days^{-1} .

1.9. Scope of Present Work:

Discharges of water from land to ocean viz. surface water (river and streams) and submarine groundwater discharge (SGD) are important pathways for material transport to the marine environment from land. These discharges enrich the coastal area with variety of nutrients, radionuclides, trace and heavy metals etc. The SGD has lower flow rate but the associated fluxes

with SGD are comparable to that of surface discharge since the ground water is heavily polluted in many areas. The impact of these elements in marine system also depends on their residence time along with their concentration level and physico-chemical properties. The impact of these elements in creek or bay system is more because these systems are land locked and relatively stagnant in nature. The concentration level, input flux and the time spend in the system is required to study the impact of discharged elements in any system.

In the present study the seawater and sediment is taken as indicator for the concentration level of the pollutants. The SGD was estimated to understand the input of elements from land. The apparent water age, flushing rate and mixing was estimated to understand the time spend by the discharged elements in the system. The objective of the present study is given below:

- Development and standardization of method for the estimation of short-lived radium isotopes (^{224}Ra and ^{223}Ra) in water samples using delayed coincidence counting.
- Study of temporal and longitudinal variation of ^{224}Ra and ^{223}Ra .
- Application of radium isotopes as a geochemical tracer to study the apparent water age, flushing rate and horizontal mixing (dispersion constant).
- Measurement of Submarine Groundwater Discharge (SGD) in Mumbai Harbour Bay using radium mass balance.
- Development and standardization of method for the estimation of trace and toxic elements in seawater and sediment using TXRF.
- The study of trace and toxic elements status in the creek ecosystem of Mumbai Harbour Bay using TXRF.
- Estimation of flux of trace and heavy metals elements from MHB.

CHAPTER 2

ANALYTICAL TECHNIQUES AND EXPERIMENTAL METHODS

2.1. Introduction

2.1.1. Ra concentration in marine environment

The four naturally occurring Ra isotopes ^{223}Ra ($T_{1/2} = 11.4$ days), ^{224}Ra ($T_{1/2} = 3.6$ days), ^{226}Ra ($T_{1/2} = 1600$ years) and ^{228}Ra , ($T_{1/2} = 5.75$ years) in the environment has been used as tracer to study various environmental process (e.g. SGD, residence time, flushing rate etc.) due to their conservative behaviour in the saline water. Their conservative behaviour also helps in understanding the fate and behaviour of pollutants from source to sink. The different decay series includes a number of isotopes with wide range of half-lives and number of elements with different characteristics. ^{226}Ra is a part of the ^{238}U decay series, ^{228}Ra and ^{224}Ra are a part of the ^{232}Th decay series and ^{223}Ra is a part of the ^{235}U decay series Figure 1.1. The concentration of each isotope is controlled by that of the parent and the amount of time since fractionation between the isotope and its parent has occurred. For a decay series in radioactive (secular) equilibrium the activity of each isotope (the decay rate) is the same as that of its parent. For ^{232}Th series:

$$(^{232}\text{Th}) = (^{228}\text{Ra}) = (^{228}\text{Th}) = (^{224}\text{Ra}) = \dots\dots\dots \quad (2.1)$$

Where, isotopes in parenthesis denote the activity of that isotope. In the secular equilibrium the activity of each daughter product is controlled by the long lived parent isotope.

The activities of all daughters are equal but the molar abundances are directly proportional to half-life (inversely proportional to the decay constants), therefore the

concentrations of short lived nuclides are low compare to long lived nuclides. In ^{232}Th series, the molar ratio at secular equilibrium is:

$$\frac{{}^{228}\text{Ra}}{{}^{232}\text{Th}} = \frac{\lambda_{232\text{Th}}}{\lambda_{228\text{Ra}}} = \frac{{}^{228}\text{Ra}_{t1/2}}{{}^{232}\text{Th}_{t1/2}} = 4.0 \times 10^{-9} \quad (2.2)$$

Table 2.1: Molar ratio daughter and parent radionuclide in decay series

Sr. No.	Description	Molar Ratio
1	$^{228}\text{Ra}/^{232}\text{Th}$, in ^{232}Th decay series	4.0×10^{-9}
2	$^{224}\text{Ra}/^{232}\text{Th}$, in ^{232}Th decay series	7.1×10^{-13}
3	$^{226}\text{Ra}/^{238}\text{U}$, in ^{238}U decay series	3.6×10^{-7}
4	$^{223}\text{Ra}/^{235}\text{U}$, in ^{235}U decay series	3.1×10^{-8}
5	$^{238}\text{U}/^{235}\text{U}$, in natural uranium	137.5
6	Th/U, in continental crust	3.8

Table 2.1 gives the molar ratio of the different Ra isotopes with their respective initial parent in the decay series. Thorium produced from U present in seawater (15nM in seawater) is scavenged by sediment particles and the Ra isotopes are produced from respective Th parents. For all natural uranium, moral ratio [$^{238}\text{U}/^{235}\text{U}$] and activity ratio [$(^{238}\text{U}) / (^{235}\text{U})$] is 137.5 and 21.8 respectively. Similarly for Th/U moral ratio and activity ratio is 3.8 and 1.2 for continental crust. Therefore, Ra isotopes have extremely low molar concentrations, even where U and Th are strongly enriched. In natural samples ^{226}Ra is predominantly present, even activity concentrations due to ^{224}Ra and ^{228}Ra are comparable. ^{223}Ra is a minor constituent, present in the natural samples. In the costal water average activity of ^{224}Ra reported is about 30 dpm/100L(5 mBq/l). Using the specific activity, 5.92×10^{15} Bq/g of ^{224}Ra , corresponding concentration of

^{224}Ra in coastal water is about 8.5×10^{-19} g/l. Similarly 3 dpm/100L (0.5 mBq/l) activity concentration of ^{223}Ra (Specific activity: 1.89×10^{15} Bq/g) correspond to concentration as 2.6×10^{-19} g/l. Thus estimation of extremely low concentration of Ra, present in the marine environment, requires the pre-concentration from seawater and technique with extremely low detection limit.

2.1.2. Analytical Method for Ra Measurement

There are several methods reported for the estimation of Ra via its decay products using alpha, beta and gamma spectrometry. Alpha spectrometry is performed using radium-barium co-precipitate. For beta spectrometry liquid scintillation counting is performed. Gamma spectrometry is performed for active samples using gamma peaks of daughter products. Gross counting of the Ra is done by co-precipitation after appropriate chemical separation procedure. Most widely used procedure for ^{226}Ra estimation is emanometry, which is based on the deemanation and isolation of the activity of the radon ingrown from radium in solution in known time, and measurement of the activity of radon and its short-lived decay products.

The concentration of Ra in environmental water samples is extremely low, thus before measurement using any suitable technique, the radium from water sample must be concentrated by:

- Evaporation
- Sorption of Ra on cationic exchange resin
- Manganese-oxide impregnated acrylic fibers
- Co-precipitation followed by dissolution

In present study Ra from seawater was pre-concentration on MnO₂-fiber. The gaseous daughter product (Rn) of Ra adsorbed on MnO₂-fiber, were flushed and re-circulated into scintillation cell by carrier gas. The alpha particle from decay of corresponding Rn and Po isotopes is recorded by photomultiplier tube. The alpha scintillation counter coupled with delayed coincidence circuit distinguishes decay events of short-lived radium daughter products based on their contrasting half-lives.

2.1.3. Coincidence and Delayed Coincidence Counting

Coincidence and anti-coincidence are detection modes (or techniques) used to produce a simplified spectrum from certain types of detector systems. These systems consist of two (or more) detectors, a segmented detector, or a combination of these produces separate signals. The use of coincidence or anti-coincidence counting improves the signal to noise ratio in the detection system. In anti-coincidence, the signals produced simultaneously in at least two of the detectors or segments cancel or veto each other, leaving the non-coincident signals to be counted. Generally, in coincidence, only those signals produced simultaneously in at least two of the detectors or segments are counted. The coincidence counting can also be done when two or more events occur within a short interval of time. This type of counting is called delayed coincidence counting. Thus delayed coincidence counting is the detection of two or more event/particles at separate detectors within a short interval of time.

The degree of inequilibrium in the decay series of ²³⁸U and ²³⁵U has been used to estimate the age of geological material with great sensitivity and accuracy. The age was estimated using ratio ²³¹Pa to ²³⁵U, ²³⁰Th to ²³⁸U and ²³¹Pa to ²³⁰Th [177–180]. In 1963 Giffin et al. [181] described a very sensitive technique for the determination of ²³¹Pa in geological materials which

simplified and improved compared previous studies [178, 179]. The same system could also be used for the estimation of ^{228}Th using one of its daughter ^{220}Rn ($t_{1/2}= 55$ sec).

Giffin et al. [181] used a closed circulation system to sweep radon gas from an acid solution containing the radioactive parents into a scintillation cell where the alpha particle activity was monitored. The gaseous product ^{219}Rn (actinon, the daughter product of ^{231}Pa) and ^{220}Rn (thoron, daughter product of ^{232}Th) were swept into scintillation cell and alpha particle from both the ^{219}Rn - ^{215}Po and ^{220}Rn - ^{216}Po pair counted and the electronic signal was produced from PMT for actinon and thoron respectively. The electronic signals from PMT were routed to three channels, total counter (b.c. recording before coincidence), one recording actinon after coincidence (referred as a.c._A) and one recording thoron after coincidence (referred as a.c._T) as shown in the Figure 2.1.

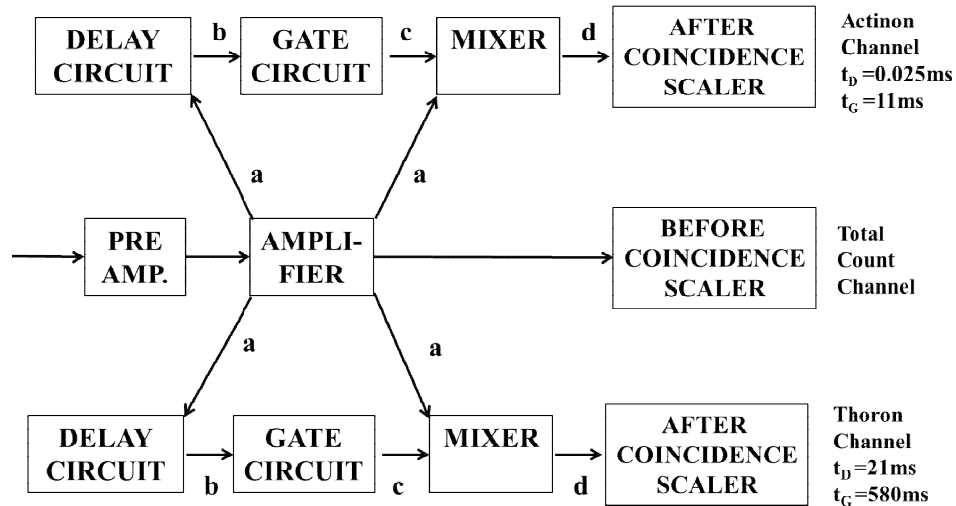


Figure 2.1: Block diagram of the electronic component of the electronic circuit [181]

The electronic signal activates a gate circuit turning on the a.c. register for a predetermined gate time (t_G). The initiating pulse itself is eliminated by delaying the opening of the a.c. circuit for a delay time (t_D). Thus any pulse; in the gate time, i.e. between t_D and ($t_D + t_G$), passing the mixer circuit is registered in the a.c. register. Any single count would open the gate in the a.c.

channel but, unless a second count was recorded within t_G , the gate would remain closed and no event would be recorded in this channel. For the ^{219}Rn channel t_D and t_G was 0.025 ms and 11 ms (6 times of ^{215}Po half-life) respectively. For ^{220}Rn channel the delay time was taken 21 ms (12 times the half-life of ^{215}Po), allowing all ^{215}Po from ^{219}Rn to decay, before the opening of the gate of the ^{210}Rn channel. During this t_D about 9% of thoron is not recorded but the actinon is totally decayed thus elimination the chances of contribution in thoron channel from actinon decay.

The short time of gate opening, the background in the ^{219}Rn and ^{220}Rn channel was found as 0.01 cpm and 0.15 cpm respectively in the 2-L scintillation chamber. The total background was found as 3.5 cpm. Based on total count rate and gate time, the expression for the chance coincidence events that can occur in each channel was derived as described below;

If x is count rate of random single pulses recorded in the “before-coincidence” (b.c. or Total) register and y is the count rate of chance coincidence events, i.e. events that occur within the time constant (t_G) of the circuit and record in the “after-coincidence” (a.c.) register, then

$$x - y = \text{rate at which the window opens}$$

Since a.c. events do not open the window.

$$(x - y) * t_G = \text{fraction of “on” time.}$$

This is equal to the fraction of window openings that result in a pulse recording in the a.c. register. y/x will be a fraction of random single pulses that record in the a.c. register. This must equal the fraction of “on” time i.e.

$$(x - y) * t_G = y/x \tag{2.3}$$

Solving for y we get;

$$y = \frac{x^2 t_G}{1 + x t_G} \tag{2.4}$$

There is also the probability of the chance coincidence resulting from the samples pulses apart from the background from the scintillation cell. The number of random pulses;

$$x = [(b.c.) - (a.c.) - y] \quad (2.5)$$

$$x - y = b.c. - a.c. \quad (2.6)$$

From equation (2.3)

$$y/x = (b.c. - a.c.) t_G \quad (2.7)$$

$$y = [(b.c. - a.c.) t_G] * x \quad (2.8)$$

$$y = [(b.c. - a.c.) t_G] * [(b.c.) - (a.c.) - y] \quad (2.9)$$

$$y = \frac{((b.c.) - (a.c.))^2 t_G}{1 - [(b.c.) - (a.c.)] t_G} \quad (2.10)$$

To verify the theoretical expression, Giffin et al. [181] added small activities of ^{222}Rn ($t_{1/2} = 3.8$ days) to the chamber. Because ^{222}Rn decay to ^{218}Po ($t_{1/2} = 3$ min) no coincidence events with time constants in the range of the electronics are produced. Thus ^{222}Rn should only increase the total and chance coincidence count rates. The system yielded the expected chance coincidence response from the addition of ^{222}Rn . A constant difference from the theoretical curve was attributed to a slight contamination of Th in the system. As Bubbling the gas through samples dissolved in strong acids produced variable results; no data from natural samples were ever published with this elegant technique. Also, the advent of alpha spectrometry promised to be an even more sensitive and specific technique for measuring ^{231}Pa and ^{228}Th . In the study radium delayed coincidence counter was used to estimate the activity concentration of ^{223}Ra and ^{224}Ra in water samples collected from different locations of study area.

2.2. Theory of Radium Delayed Coincidence Counter

Using the basic and detailed technique of Giffin et al., [181] the technique for the measurement of ^{223}Ra and ^{224}Ra in coastal water samples was developed [182]. The radium was extracted from seawater onto a column of MnO_2 coated fiber and partially dried fiber sample was placed in circulation system Figure 2.2. Helium gas is circulated over the sample through scintillation cell where alpha particles from Rn-Po pair were recorded.

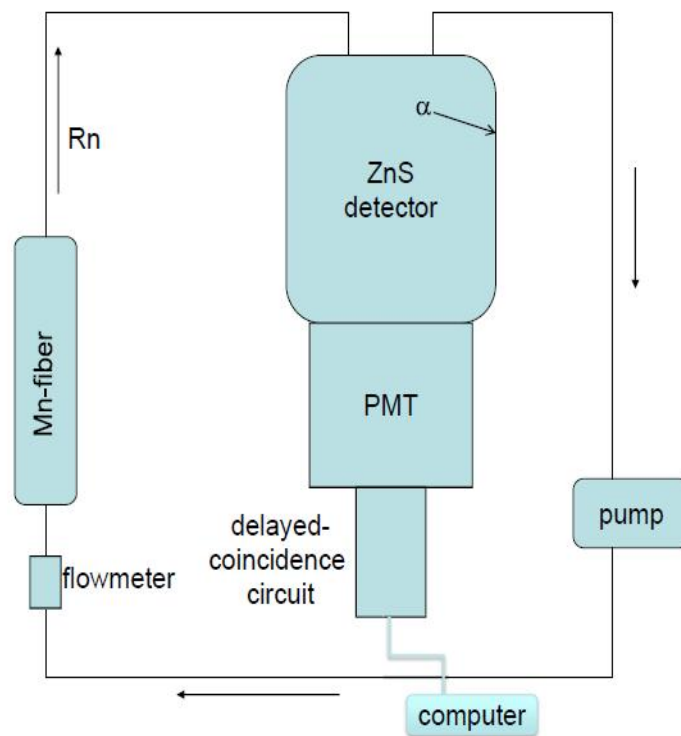


Figure 2.2: Schematic diagram of ^{223}Ra and ^{224}Ra measurement system

The scintillation cells are mostly of Lucas type with silver activated ZnS cell, mounted on photomultiplier tube (PMT) and bottom of the cell is transparent serving optical contact with PMT. The volume of Lucas cell used in the present study was 1.15L. A small diaphragm pump was used to circulate He gas through sample column and counting cell. If an atom of radon decays in the counting cell and the alpha particle strikes the wall, it will produce a flash of light.

This light is picked up by the photomultiplier tube, converted to an electrical signal, and passed to the chance coincidence circuit. This signal is recorded in the total counts window (Total). After this signal is delayed for 10 ms in the 220 circuit and 0.01 ms in the 219 circuit, it opens a gate in each circuit, and then the signal dies.

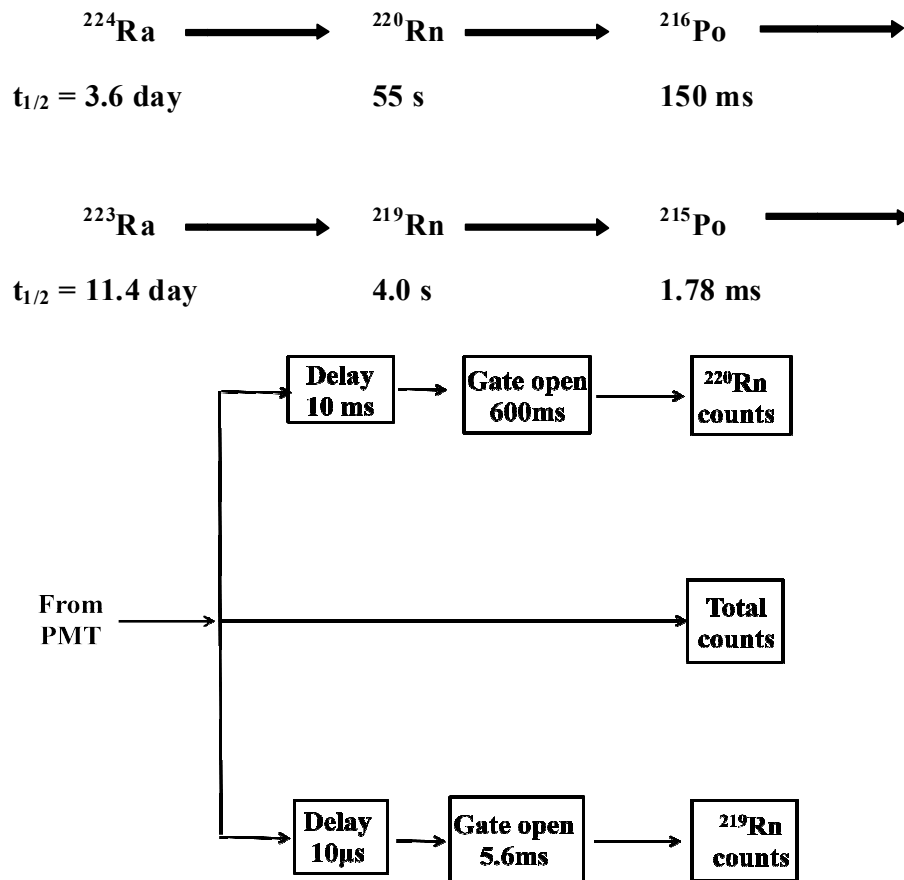


Figure 2.3: Schematic diagram of the ^{224}Ra and ^{223}Ra decay & delayed coincidence circuit [182]

The delay of 0.01 ms in the 219 channel, allow stabilizing the circuit. The signal then opens a gate which remains open for 5.6 ms (three half-lives of ^{215}Po). Any second count detected in this time interval is recorded in the 219 channel which is most likely due to ^{215}Po decay. The count would not have been recorded if a decay of ^{219}Rn had not opened the gate within the prior 5.6 ms. All signals are also fed to the 220 circuit with delayed of 10 ms and gate

remains open for 600 ms (four half-lives of ^{216}Po). If a signal occurs while this gate is open, it is recorded in the 220 channel.

Because all signals passed to the 220 circuit are delayed for 10 ms, any signal due to ^{215}Po will die before it can pass through the 220 window. Cross-talk between the channels is minimal. The delay on the 220 circuit effectively prevents the signal from $^{219}\text{Rn} - ^{215}\text{Po}$ from registering in this circuit. Some events due to $^{220}\text{Rn} - ^{216}\text{Po}$ fall into the 219 circuit because the 5.6 ms time constant is long enough for 2.5% of the $^{220}\text{Rn} - ^{216}\text{Po}$ decay to occur in this window. These are subtracted along with chance coincidence counts.

2.2.1. Quantification of ^{223}Ra and ^{224}Ra Activity Concentration

Quantification of activity concentration by chance coincidence counter involves following steps:

- Estimation of Chance Coincidence and correction to get corrected cpm
- Correction of cross contribution (i.e. contribution in 220 channel from 219 and vice versa) to get final cpm
- Efficiency (conversion from cpm to dpm)
- Decay correction to get initial activity on fiber sample
- Conversion of activity to activity concentration

The chance coincidence events occurring in the 220 channels (cc220) is expressed as:

$$cc220 = \frac{[(cpmtotal - cpm220 - cpm219)^2 \times 0.01]}{[1 - \{(cpmtotal - cpm220 - cpm219) \times 0.01\}]} \quad (2.11)$$

Where cpm_{total} , cpm_{220} and cpm_{219} are the counts per minute registered in the total, 220 and 219 circuits respectively. The chance coincidence contribution (cc_{220}) is subtracted from the cpm_{220} to obtain the chance coincidence corrected count rate in 220 circuits ($corr_{220}$) as:

$$corr_{220} = cpm_{220} - cc_{220} \quad (2.12)$$

Similarly chance coincidence events occurring in the 219 channels (cc_{219}) and chance coincidence corrected count rate in 219 circuits ($corr_{219}$) is expressed as:

$$cc_{219} = \frac{[(cpm_{total} - corr_{220} - cpm_{219})^2 \times 0.000093]}{[1 - \{(cpm_{total} - corr_{220} - cpm_{219}) \times 0.000093\}]} \quad (2.13)$$

$$corr_{219} = cpm_{219} - cc_{219} \quad (2.14)$$

Moore and Arnold [182] initially used cpm_{220} instead of $corr_{220}$ in Eq. (2.13). However, a posterior revision of the equations led to consider $corr_{220}$ as the most appropriate term to calculate cc_{219} [183].

The final adjustment to the 220 data is made which accounts for the ^{219}Rn and its daughter decays. If two ^{219}Rn decays occur while the 220 window is open, the second ^{219}Rn decay and the decay of ^{215}Po will be recorded in the 220 channel. The second order correction was made using ^{219}Rn activity and efficiency of the detector as;

$$final_{220} = corr_{220} - \frac{[(1.6 \times corr_{219})^2 \times 0.01]}{[1 - \{(1.6 \times corr_{219}) \times 0.01\}]} \quad (2.15)$$

Where, $final_{220}$ is the final count rate in the 220 circuit. Since this is a second-order correction, small differences in efficiency are not substantially important. On the other hand, the time constant of the 219 gate is long enough for 2.55% of the ^{220}Rn - ^{216}Po decays to occur in this window. Then, the final 219 (cpm) is calculated as:

$$final_{219} = corr_{219} - (corr_{220} \times 0.0255) \quad (2.16)$$

Where, final219 is the final count rate in the 219 circuit. The Once the final 219 and 220 cpm are calculated, they are converted to activity (decay per minute, dpm) by dividing them by the efficiencies of each channel as;

$$dpm219 = \frac{final\ 219}{E219} \quad (2.17)$$

$$dpm220 = \frac{final\ 220}{E220} \quad (2.18)$$

Where, dpm220 and dpm219 are the activity (disintegration per minute) of the ^{220}Rn and ^{219}Rn respectively, at the time of measurement. The decay of ^{223}Ra and ^{224}Ra occurred in the time interval (t) between the sample collected and counting thus decay correction is considered to find out the initial activity as;

$$(dpm220)_i = \frac{dpm220}{e^{-\lambda_{224}t}} \quad (2.19)$$

$$(dpm219)_i = \frac{dpm219}{e^{-\lambda_{223}t}} \quad (2.20)$$

Where, $(dpm220)_i$ and $(dpm219)_i$ represent the total activity (disintegration per minute) of the ^{223}Ra and ^{224}Ra respectively initial activity absorbed on fiber. Lastly, the activity concentration of ^{223}Ra and ^{224}Ra (dpm.L^{-1}) is calculated by dividing $(dpm219)_i$ and $(dpm220)_i$ by samples volume as;

$$^{224}\text{Ra}(\text{dpm.L}^{-1}) = \frac{(dpm220)_i}{Volume} \quad (2.21)$$

$$^{223}\text{Ra}(\text{dpm.L}^{-1}) = \frac{(dpm219)_i}{Volume} \quad (2.22)$$

2.2.2. Uncertainties in measurement of ^{223}Ra and ^{224}Ra

The uncertainty of a given function (f) with n uncorrelated variables (x_1, x_2, \dots, x_n) is given as

$$\delta f = \sqrt{\left(\frac{\partial f}{\partial x_1} \delta x_1\right)^2 + \left(\frac{\partial f}{\partial x_2} \delta x_2\right)^2 + \dots + \left(\frac{\partial f}{\partial x_n} \delta x_n\right)^2} \quad (2.23)$$

Where $\delta x_1, \delta x_2, \dots, \delta x_n$ are the uncertainties associated with the different variables. The uncertainties in the measurement ^{223}Ra and ^{224}Ra are estimated from uncertainty associated in each step (Eq. 2.11- Eq. 2.22) using error propagation law as:

$$\begin{aligned} \delta_{cc220} &= \sqrt{\delta_{cpm\text{total}}^2 + \delta_{cpm220}^2 + \delta_{cpm219}^2} \\ &\times \left[\frac{\left[(2 \times 0.01 \times (cpm\text{total} - cpm220 - cpm219)) - (0.01 \times (cpm\text{total} - cpm220 - cpm219))^2 \right]}{(1 - 0.01 \times (cpm\text{total} - cpm220 - cpm219))^2} \right] \end{aligned} \quad (2.24)$$

$$\delta_{corr220} = \sqrt{\delta_{cpm220}^2 + \delta_{cc220}^2} \quad (2.25)$$

$$\begin{aligned} \delta_{cc219} &= \sqrt{\delta_{cpm\text{total}}^2 + \delta_{corr220}^2 + \delta_{cpm219}^2} \\ &\times \left[\frac{\left[(2 \times 0.000093 \times (cpm\text{total} - corr220 - cpm219)) - (0.000093 \times (cpm\text{total} - corr220 - cpm219))^2 \right]}{(1 - 0.000093 \times (cpm\text{total} - corr220 - cpm219))^2} \right] \end{aligned} \quad (2.26)$$

$$\delta_{corr219} = \sqrt{\delta_{cpm219}^2 + \delta_{cc219}^2} \quad (2.27)$$

$$\delta_{final220} = \sqrt{\delta_{corr220}^2 + \left[\frac{[(2 \times 1.6)^2 \times 0.01 \times corr219 - (1.6^3 \times 0.01^2 \times corr219^2)]}{[1 - (1.6 \times 0.01 \times corr219)]^2} \times \delta_{corr219} \right]^2} \quad (2.28)$$

$$\delta_{final219} = \sqrt{\delta_{corr219}^2 + (0.0255 \times \delta_{corr220})^2} \quad (2.29)$$

$$\delta dpm219 = \sqrt{\left(\frac{\delta final219}{E219}\right)^2 + \left(\frac{final219 \times \delta E219}{E219^2}\right)^2} \quad (2.30)$$

$$\delta dpm220 = \sqrt{\left(\frac{\delta final220}{E220}\right)^2 + \left(\frac{final220 \times \delta E220}{E220^2}\right)^2} \quad (2.31)$$

$$\delta (dpm219)_i = \sqrt{\left(\frac{\delta final219}{e^{-\lambda_{Ra-223}t} \times E219}\right)^2 + \left(\frac{final219 \times e^{-\lambda_{Ra-223}t} \delta E219}{(E219 \times e^{-\lambda_{Ra-223}t})^2}\right)^2} \quad (2.32)$$

$$\delta (dpm220)_i = \sqrt{\left(\frac{\delta final220}{e^{-\lambda_{Ra-224}t} \times E220}\right)^2 + \left(\frac{final220 \times e^{-\lambda_{Ra-224}t} \delta E220}{(E220 \times e^{-\lambda_{Ra-224}t})^2}\right)^2} \quad (2.33)$$

Where, $\delta E220$ and $\delta E219$ are the uncertainty associated with counting efficiency of ^{224}Ra and ^{223}Ra and measured from the standard of the efficiencies measured using standard Mn-fiber.

$$\delta^{224}\text{Ra}(dpm L^{-1}) = \sqrt{\left(\frac{\delta (dpm220)_i}{volume}\right)^2 + \left(\frac{(dpm220)_i \times \delta volume}{volume^2}\right)^2} \quad (2.34)$$

$$\delta^{223}\text{Ra}(dpm L^{-1}) = \sqrt{\left(\frac{\delta (dpm219)_i}{volume}\right)^2 + \left(\frac{(dpm219)_i \times \delta volume}{volume^2}\right)^2} \quad (2.35)$$

2.3. Standardization of method used in the present study

The radium delayed coincidence counter used in the present study is shown in the Figure 2.4. The measurement of ^{223}Ra and ^{224}Ra from water samples using delayed coincidence counting involve the following steps:

1. The pre-concentration of Ra from water/seawater
2. Sample processing to achieve the desired fiber/water weight ratio
3. Delayed coincidence counting and calculation



Figure 2.4: The Radium Delayed Coincidence Counter used in the study

Considering the above steps involved in the measurement of ^{223}Ra and ^{224}Ra the following parameters should be studied and taken in account:

- 2.3.1. Evaluation of Ra extraction efficiency of MnO_2 -fiber
- 2.3.2. Selection of Carrier gas
- 2.3.3. The flow rate of carrier gas (Helium used in the present study)
- 2.3.4. Equilibrium
- 2.3.5. Build-up of ^{222}Rn
- 2.3.6. Sample Counting
- 2.3.7. Water-loss during the measurement
- 2.3.8. Checking for leaks
- 2.3.9. Background and Minimum measurable activity
- 2.3.10. Uncertainty (Error) in measurement

2.3.1. Evaluation of Ra extraction efficiency of MnO₂-fiber

Measurement of MnO₂-fiber efficiency was determined by keeping two sample holders in series, having an equal amount of MnO₂-fiber and passing seawater at flow rate ~0.8 litres per minute (lpm). The schematic diagram of the sampling assembly is shown in the Figure 2.5. The adsorption efficiency (ϵ) of cartridge place in series is calculated as;

$$\epsilon = 1 - \frac{C_B}{C_A} \quad (2.36)$$

Where; C_A and C_B are activity/concentration of radium retained in A and B cartridge respectively.

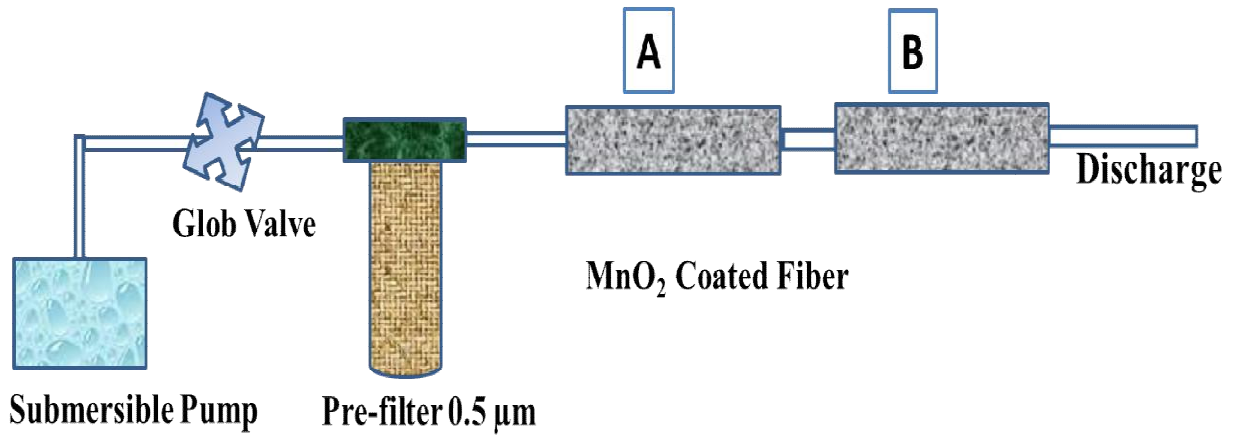


Figure 2.5: Sampling assembly for efficiency measurement

Table 2.2: Counts rate (cpm) in 220 channels for both cartridges and background

Sr. No.	Item/Sample	Count Rate (CPM)
		220 Channel
1	Cartridge A	3.845
2	Cartridge B	0.06
3	Background	0.04-0.06

After passing the seawater both the cartridges were equally partially dried and counted for under similar condition. Observed count rate for both the cartridges A, cartridge B and the background is given in Table 2.2. The activity on cartridge B is in the range of background. Observation indicates 100% adsorption efficiency of MnO₂-fiber for radium which is in accordance to Moore and Reid [184].

2.3.2. Selection of Carrier gas

Standard fiber (Mn-fiber coated with ²³²Th activity: 30.06 DPM) was kept in the sample holder and purge with different carrier gases viz. He, Air and Ar, at the flow rate of 4 lpm. Figure 2.6 shows variation of % efficiency for ²²⁴Ra vs. carrier gases at the flow rate of 4 lpm. Three repetitive measurements done for each gas and average value has been taken for comparison. It was found that efficiency is greatest for He and lowest for air as a carrier gas. The higher efficiency of He than air and Ar is because the range of alpha particles in He is much longer than in air and Ar.

Running the sample with helium offers another advantage over running with air. Because the mass of helium is smaller, a given flow rate of helium will appear to be less than the same flow rate of air. It was found that the flow meter response to helium was only 0.56 the response to air. Thus, if the system is filled with helium at the beginning of the run and with time air leaks into the system; the flow rate indicated by the flow meter will increase.

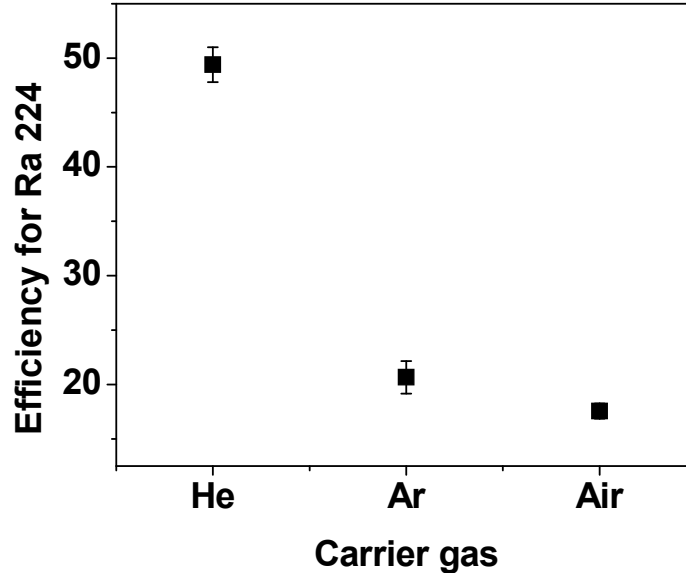


Figure 2.6: Variation of efficiency for different carrier gases at the flow rate of 4lpm

2.3.3. Flow rate of carrier gas (Helium)

To find the optimum flow rate for carrier gas, efficiencies at a different flow rate of He gas was estimated. He was flushed and re-circulated at a different flow rate (2, 3, 4, 5 and 6 lpm) in the system. At least three repetitive measurements were made at each flow rate and the average value was taken. Figure 2.7 shows the efficiency of the system for the measurement of ^{224}Ra at a different flow rate of He as a carrier gas. It was observed that efficiency for measurement is higher in 4-5 lpm flow rate. As ^{219}Rn and ^{220}Rn are released from the source, they are rapidly pumped through the system. Any Rn that decays outside the counting cell will reduce the efficiency of the system. At lower flow rate probability of ^{219}Rn and ^{220}Rn decay outside the counting cell will be higher. At higher flow rate ^{219}Rn and ^{220}Rn have a lower residence time in the cell which causes lower efficiency. Thus, the higher efficiency in 4-5lpm flow rate may be explained as an optimum condition for higher residence time in counting cell and lower probability of outside decay of Rn.

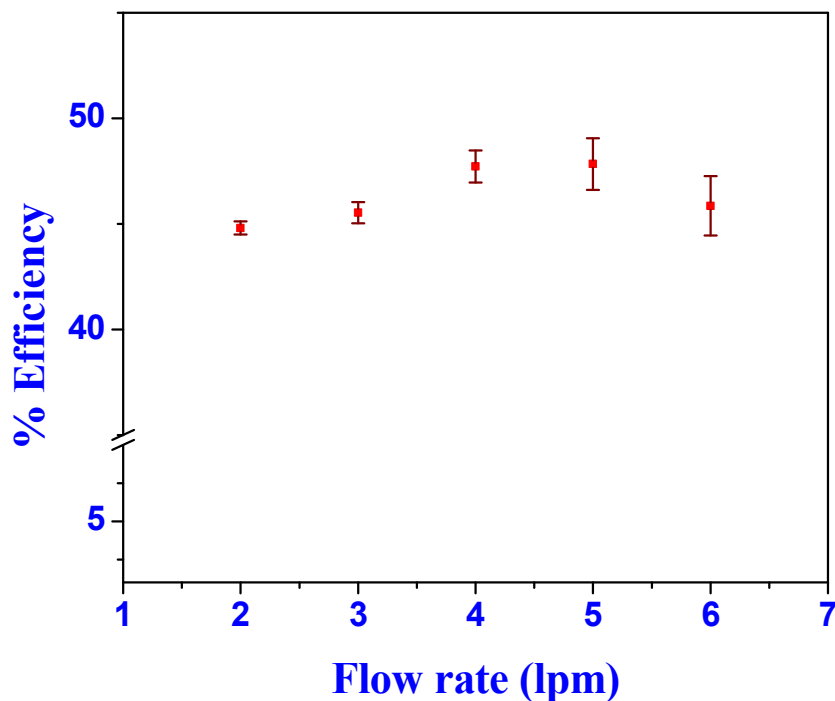


Figure 2.7: Variation in ^{224}Ra efficiency vs. He Flow Rate

2.3.4. Equilibrium

After flushing the sample column with He has to remove the air present in the system, the system kept in the recirculation loop for the carrier gas. The initial counts recorded do not represent the correct estimates as the ^{224}Ra - ^{220}Rn pair reaches in secular equilibrium within about 5 min. At this time the ^{220}Rn activity should be the same throughout the system. This is not the case for the ^{223}Ra - ^{219}Rn pair. The 4 s half-life of ^{219}Rn is too short to allow complete mixing. Here it is important to flush the ^{219}Rn into the counting chamber as quickly as possible. The efficiency of measuring ^{223}Ra should be lower than the efficiency for ^{224}Ra because some of the ^{219}Rn will decay in the sample column before reaching the detector. Higher efficiencies for ^{223}Ra was observed as flow rate was increased from 5.2 to 13 $\text{L}\cdot\text{min}^{-1}$; the ^{224}Ra efficiency was affected less and was not consistent with the flow rate [185].

2.3.5. Build-up of ^{222}Rn

The decay of ^{226}Ra present on the fiber to ^{222}Rn increases total count rate during the run. The linear chance coincidence correction does not properly correct for these events, as build-up follows exponential growth. Therefore, the system should be flushed at an appropriate time interval stopping the counts, to reduce the build-up of ^{222}Rn by looking at the data file. The samples with low ^{224}Ra , but high in ^{226}Ra activity needs to be purged frequently. The timing of the purge intervals depends on the activity on the fiber sample which needs to be determined on a case-by-case basis.

2.3.6. Sample Counting

Each sample is usually counted three times in a 1-month period after sampling. The first measurement (^{224}Ra count) is usually carried out within 1–3 days after sampling in order to avoid significant ^{224}Ra decay. Since the natural initial ^{224}Ra activity is usually approximately 10 to 20 times the ^{223}Ra activity [129, 186], the initial interference of $^{220}\text{Rn} - ^{216}\text{Po}$ decays falling into the 219 channel (a 2.55% of the total) can represent a high value compared to the ^{215}Po decays in this channel. Thus, only ^{224}Ra activity is quantified from the first measurement. In typical natural samples counting can be done up to 3 h without significant decay of ^{226}Ra or ^{222}Rn in-growth [187]. In the present case of study around 60-100 litres of seawater was sampled and first counting time was about 1-2 hours.

The second counting generally performed after typically 7 to 12 days for the measurement of ^{223}Ra . In this time period, much of the ^{224}Ra has decayed thus the interference of ^{216}Po in the 219 channel is reduced significantly. The second measurement requires longer counting times

(usually 3-4 hours in the present study) to obtain good statistics for the less abundant ^{223}Ra isotope. Even though a long measurement can result in an excessive background building up, it mostly affects the 220 and total channels.

After the second counting Mn-fiber samples are kept for about 4 weeks to allow the supported ^{224}Ra to equilibrate with its parent ^{228}Th adsorbed onto the Mn-fiber and initially adsorbed ^{224}Ra to decay. The measured ^{228}Th (i.e. supported ^{224}Ra) is subtracted from the total ^{224}Ra to obtain excess ^{224}Ra activities. This third measurement is carried out for a period of several hours to obtain good counting statistics. The average activity of ^{228}Th adsorbed on the Mn-fiber in our study was estimated to be 0.91 dpm/100L.

After 80 days the ^{223}Ra activity will be <1% of the initial activity and ^{223}Ra is essentially supported by ^{227}Ac in the sample. Thus, another count at this time will measure ^{227}Ac . Because ^{227}Ac is extremely low in the surface water, this 4th count is rarely required. Figure 2.8 describes estimation of different parameter in the excel sheet for the first and second counting. Figure 2.9 represents the third counting of two different samples at a delay of 38.36 days.

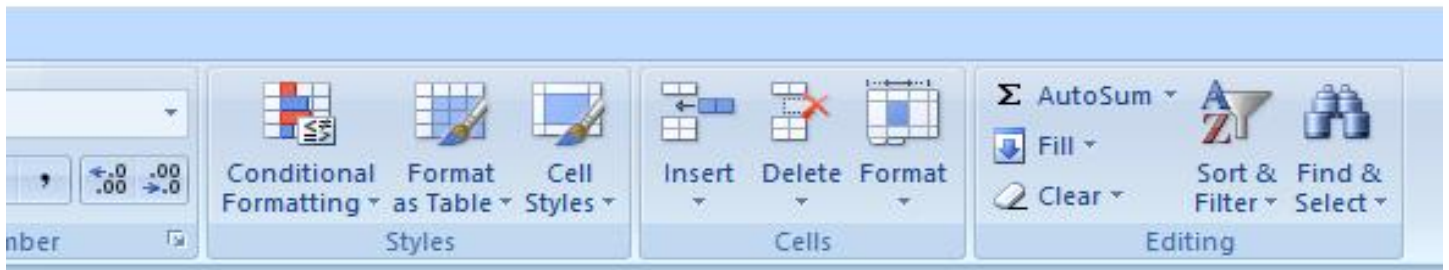
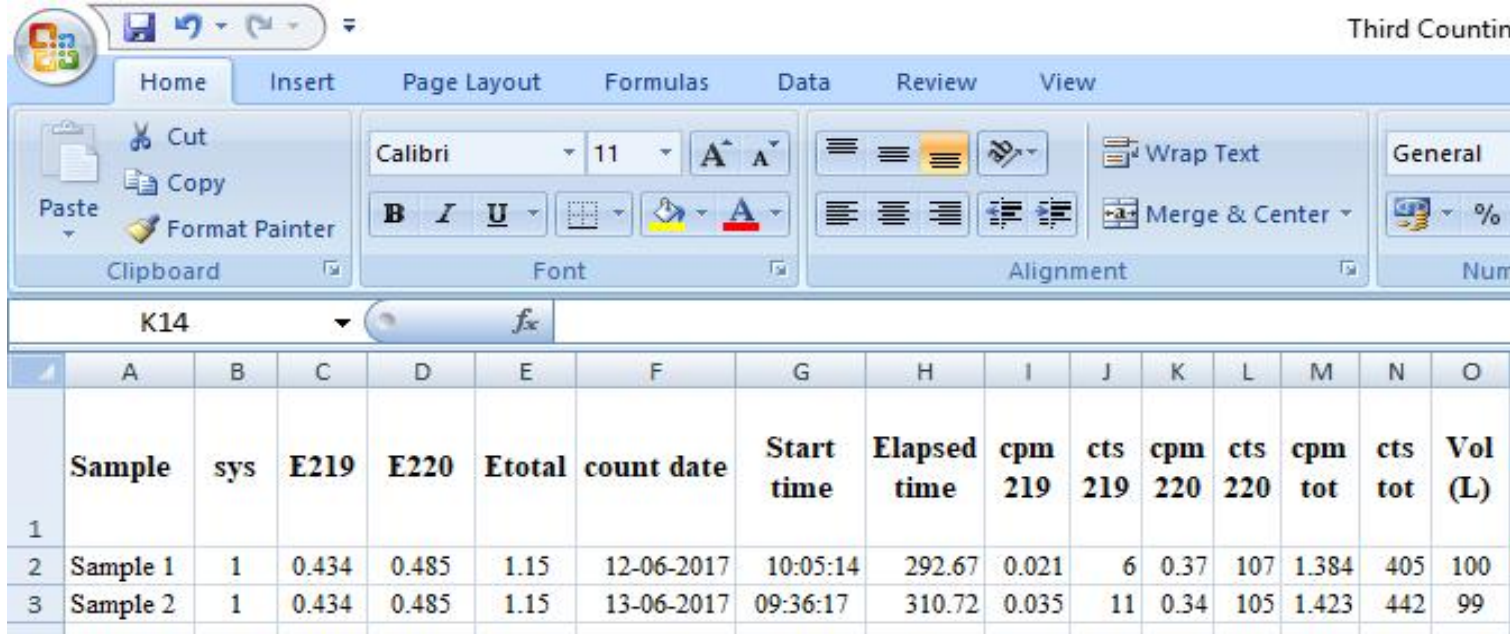
First and Second Counting - Microsoft Excel

	A	B	C	D	E	F	G	H	I	J	K	L	M	N	O	P	Q
1	Sample	sys	E219	E220	Ettotal	count date	Start time	Elapsed time	cpm 219	cts 219	cpm 220	cts 220	cpm tot	cts tot	Vol (L)	Samp date	Samp time
2	Sample 3	2	0.450	0.490	1.16	28-04-2016	14:04:08	76.03	0.18	14	3.6	277	8.14	619	56	25-04-2016	16:30:00
3																	
4	Sample 3	1	0.434	0.485	1.15	02-05-2016	09:54:13	172.88	0.17	30	1.6	268	4.43	766	56	25-04-2016	16:30:00

First and Second Counting - Microsoft Excel

	R	S	T	U	V	W	X	Y	Z	AA	AB	AC	AD	AE
1	Tot cpm bkg	220 CC	corr 220	219 CC	corr 219	final 220	Final 219	dpm 220	dpm 219	Delay (d)	Act 224 (dpm)	Act 223 (dpm)	Act 224 dpm per 100L	Act 223 dpm per 100L
2	0.378	0.194	3.449	0.0019	0.182	3.448	0.094	7.04	0.21	2.90	12.29	0.25	21.88	0.44
3														
4	0.378	0.075	1.475	0.0007	0.173	1.474	0.136	3.04	0.31	6.73	11.10	0.47	19.74	0.84

Figure 2.8: First and second counting of the sample. Row No. 2 represents the first count (delay: 2.9 days) and Row number 4 shows second counting (delay: 6.73 days)



P	Q	R	S	T	U	V	W	X	Y	Z	AA
Samp date	Samp time	Tot cpm bkgn	220 CC	corr 220	219 CC	corr 219	final 220	Final 219	dpm 220	dpm 219	Delay (d)
04-05-2017	13:30:00	0.542	0.010	0.356	0.00009	0.021	0.356	0.012	0.73	0.03	38.86
05-05-2017	12:30:00	0.542	0.011	0.327	0.0001	0.035	0.327	0.027	0.67	0.06	38.88

Figure 2.9: Third counting of two representative samples after a delay of 38.86 days

2.3.7. Water-loss during the measurement

The measurement efficiency of Rn is affected by Mn-fiber surface conditions and water content. It found that water/fiber weight ratio in 1.0-0.3 range is required for a maximum fraction of the produced radon to enter the circulating gas stream Figure 2.10 [188]. To check the amount of water loss in each measurement a blank fiber with water/fiber weight ratio 1.0 was taken and measurement is done.

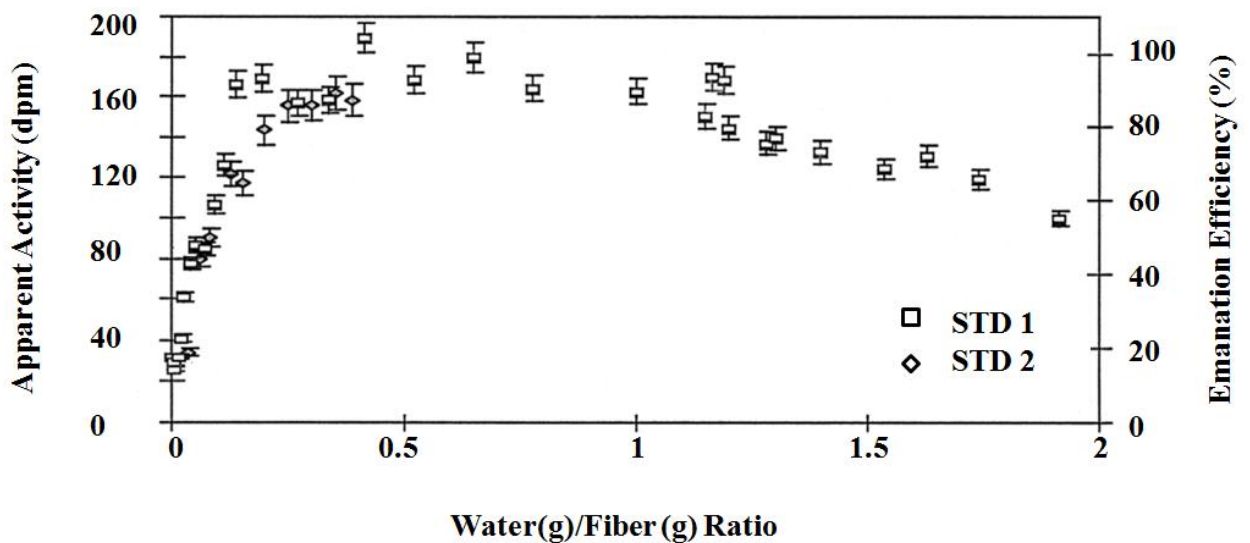


Figure 2.10: Apparent activity of ^{224}Ra and emanation efficiency vs. water content of the standards [188].

After each measurement total weight was measured to find the amount of was lost. The sample is stored in a self-sealing polythene bag after measurement. As measurement precedes some fraction of water content from fiber is lost in each measurement so water/fiber weight ratio starts decreasing from 1.0. After seven measurements on different days, it was found that amount of water loss in one measurement varies from 437.30 mg to 797.7 mg with an average of 703.48 mg. Sample collected from location 9 has also monitored for long time run and delay period and

it was found after 49 days decay and total 13 hrs of counting at various time interval water/fiber ratio changes from 1.0 to 0.77.

2.3.8. Checking for leaks in the system

If there is any leak in the system during run slowly He will decrease and air may enter into a system which will affect the efficiency of the counting. As the helium is lighter than air, the flow rate indicated by the flow meter will increase. Thus the increase of flow rate during measurement is indicative of a leak in the system.

2.3.9. Background and Minimum measurable activity

Low background count in the 220 and 219 windows in the delayed coincidence system is its main advantage. For a system having a nominal total background of 1 count per minute (cpm), the total background of the 220 channel will be of the order of 0.01 cpm and the 219 channel will typically have a total background of <1 count per day [182]. When these total backgrounds in the 220 and 219 channels are corrected for chance coincidence events, i.e. two random events occurring within the time constant of the window [181], the net backgrounds usually reduce to numbers that are not distinguishable from zero [182]. The background is reduced using an aged cylinder of He or nitrogen and isolating the circulation system from the ^{222}Rn present in outside air. Extremely low background and high efficiency of delayed coincidence system result a very low detection limit. Even a few counts per hour of ^{224}Ra or few counts per day of ^{223}Ra will be above the background and hence constitute a detectable activity.

In the present system the background counts after chance coincidence correction in 220 and 219 window was about 0.01cpm and 0.001 cpm respectively. Considering the counting time

to be 2 hrs and 4 hrs, efficiency 48.5% and 43.4% for ^{224}Ra and ^{223}Ra respectively and sample volume 100L, detection limit (DL) can be calculated as:

$$DL = 3 \times \frac{\sqrt{\text{Counts}}}{\text{time} \times \text{efficiency} \times \text{volume}} \quad (2.37)$$

Detection limit for estimation of ^{224}Ra and ^{223}Ra was estimated to be 5.6×10^{-4} dpm 100L^{-1} and 1.4×10^{-4} dpm 100L^{-1} respectively. DL is about 4 order of magnitude lower compared to activity concentration of ^{224}Ra and ^{223}Ra in the study area.

In delayed coincidence counting a good index is the measurement limit for a 2 sigma counting uncertainty of $\pm 20\%$ (i.e. 100 net counts) [189]. With 20% of relative error, Smith [189] reported measurements in the range 0.5 dpm/ m^3 for ^{224}Ra . So one m^3 of the sample with 0.25 cpm (0.5 dpm) will give 100 counts in 400 min. the 0.5 dpm/ m^3 activity is equivalent to about 3 atoms per liter ($N = \text{dpm}/\lambda = 0.5\text{dpm}/1.3 \times 10^{-4} \text{ min} = 3846 \text{ atoms}/\text{m}^3$). The limit for measurable ^{224}Ra activity is kept somewhat higher considering the contribution from dissolved ^{228}Th in waters and chance coincidence events from ^{222}Rn . For standard delayed coincidence counting system Moore [187] has considered ^{223}Ra activity of 0.2dpm/ m^3 , close to the measurement limit. Sample (1 M^3) with this activity (0.2 dpm) will give count rate 0.08-0.1 cpm and required overnight counting to get 100 counts. This will be equivalent to a concentration of 5 atoms/L ($0.2 \text{ dpm}/4.2 \times 10^{-5} \text{ min}^{-1} = 4700 \text{ atoms}/\text{m}^3$). Since the chance coincidence correction for ^{223}Ra is much less than for ^{224}Ra , such low-level measurements of ^{223}Ra are not affected significantly by a build-up of ^{222}Rn .

2.3.10. Measurement of uncertainty

Every analytical measurement is always associated with some degree of uncertainty or error, so does this technique. The major errors result from statistical variations in the decay of a

limited number of atoms, the calibration of the instrument, and failure to obtain a representative sample. The statistical variations are based on the number of events, recorded in a given time period so their estimation is easy. The relative error is given as

$$\% \text{ error} = \frac{\text{Standard deviation } (\sigma)}{\text{Measured value}} \times 100 \quad (2.38)$$

The delayed counting data generally reported at a confidence interval of 95% (2σ) so the percentage error in terms of relative percentage error. Thus statistical error at confidence interval of 95%

$$\% \text{ error (95 percentile)} = [1.96 \times (\text{square root } N)/N] \times 100 \quad (2.39)$$

For 100 net counts a good index (2 sigma counting uncertainty) gives 20% of relative error. Apart for counting uncertainty, there are other parameters contributing to uncertainty in the estimation as discussed in the **Section 2.2.3**. The uncertainty associated with measurement in the present study was calculated using steps involved using the Eq. 2.26 to Eq. 2.35 and average error found to be about 7% and 12% for ^{224}Ra and ^{223}Ra respectively.

2.4. The efficiency of the counting system for ^{224}Ra and ^{223}Ra measurement:

Total cell efficiency (CE) is the probability of recording a count from an alpha decay within the counting cell. Total System efficiency (SE) is the probability of recording a count from an alpha decay within the system (cell, column, tubing and pump). The fraction of decay occurred outside the cell depends on the ratio of the cell volume to the total system volume. If the ratio of the cell volume to the total system volume is 0.8 and the cell efficiency is 0.85, the total system efficiency will be 0.68. There are two alpha particle released for each radon decay. The Apparent System Efficiency is the probability of detecting either of these alpha particles. A system with an SE of 0.68 will have an apparent efficiency in the Total channel of 1.36.

The efficiency of the 220 channel (SE200) is the probability of recording a count in the 220 channel from ^{224}Ra decay on the fiber. The probability of detecting the ^{220}Rn - ^{216}Po coincident event is the square of the cell efficiency times the ratio of the cell volume to the total system volume. The efficiency of the 220 channel with cell efficiency 0.85 and ratio of the cell volume to the total system volume as 0.80 would be $0.85 \times 0.85 \times 0.80 = 0.58$. In the present study SE220 was estimated using ^{232}Th with daughters in equilibrium (Standard Mn-fiber coated with ^{232}Th activity: 30.06 DPM) and the average value was found to be 48.5%.

The efficiency of the 219 system (SE219) should be slightly less than SE200 because of the 4 sec half-life of ^{219}Rn results in some decays taking place before the gas moves from the fiber column to the cell. During the first pass through the counting cell decay of ^{219}Rn and ^{220}Rn is about 50% and 5% respectively. Thus the dead volume in the system between the counting cell and the Mn-fiber will only dilute the ^{219}Rn by 50% but will dilute ^{220}Rn by 95%.

It is impractical to obtain a true standard for a short-lived isotope. To calibrate a system for measurement of short-lived isotopes, standards containing long-lived parents are used. For ^{224}Ra , we use ^{232}Th with daughters in equilibrium (Mn-fiber coated with ^{232}Th activity: 30.06 DPM). For ^{223}Ra efficiency calibration ^{227}Ac with daughters in equilibrium can be used, but well-calibrated ^{227}Ac solutions are difficult to obtain. Secondly, the activity of ^{223}Ra in standards prepared from ^{227}Ac decreases with time [190]. Moore and Cai [191] have estimated the efficiency of ^{223}Ra from the ^{224}Ra efficiency, calculated from the ^{232}Th standards as:

The factors affecting the system efficiencies can be expressed by the following equations;

$$SE_{220} = CE_{220} \times P_{220} \times (1 - L_{220}) \quad (2.40)$$

$$SE_{219} = CE_{219} \times P_{219} \times (1 - L_{219}) \quad (2.41)$$

SE: system efficiency

CE: Apparent cell efficiency

P: Probability of Rn decaying in the counting cell

L: Loss resulting from the delay and window settings

The efficiency for the measuring ^{222}Rn and its daughters in Lucas cell with a cell volume of 96 ml (Original Lucas Cell by Lucas [192]), 98 ml [193] and 2 litres [181] was found as 0.86, 0.88 and 0.87 respectively using He as transfer gas. Thus for He as carrier gas efficiency for the measuring ^{222}Rn and its daughters remains almost equal. Semkow et al. [194] found that ^{222}Rn and ^{218}Po had similar efficiencies in spite of slightly higher decay energy for ^{218}Po and concluded that energy has very little effect if He is used as carrier gas. Thus the cell efficiencies for detecting $^{220}\text{Rn} - ^{216}\text{Po}$ and $^{219}\text{Rn} - ^{215}\text{Po}$ are the same i.e.

$$CE_{219} = CE_{220}$$

$$SE_{219} = \frac{SE_{220}}{P_{220} \times (1 - L_{220})} \times P_{219} \times (1 - L_{219}) \quad (2.42)$$

2.4.1. Probability of Rn decaying in the counting cell:

The carrier gas rapidly sweeps the Rn into counting cell part of Rn that decays outside the counting cell will reduce the efficiency of the system. The probability (P) of Rn decaying within the counting cell is given by the following equation;

$$P = \exp - \left[\lambda \frac{V_d}{F} \right] \times \left[\frac{1 - \exp - \left[\lambda \frac{V_c}{F} \right]}{1 - \exp - \left[\lambda \frac{V_s}{F} \right]} \right] \quad (2.43)$$

Where, V_d : dead volume between the source and the counting cell, V_c : Volume of the counting cell, V_s : volume of the entire system, F: flow rate and λ : is the decay constant of Rn. For standard radium delayed coincidence counter the probabilities of ^{220}Rn (i.e. P_{220}) and ^{219}Rn (i.e. P_{219}) decaying in the counting cell was found as 0.847 and 0.801 [191].

2.4.2. Loss resulting from the delay and window settings

The electronics of delay coincidence system have delay and window time constants that are set to minimize background and maximize counting efficiency. Following is the coincidence lost due to window constant:

^{216}Po coincidence events loss during the delay in the channel,

$$1 - \exp - [(0.693/150)*5.6 \text{ ms}] = 0.026$$

^{215}Po coincidence events loss during the delay in the channel,

$$1 - \exp - [(0.693/0.01)*1.78 \text{ ms}] = 0.004$$

The 600 ms window in the 220 channel captures 94.3% of the expected ^{216}Po decays

$$1 - \exp - [(0.693/150)*600 \text{ ms}] = 0.943$$

The 5.6 ms window in the 219 channel captures 88.7% of the expected ^{216}Po decays

$$1 - \exp - [(0.693/0.01)*5.6 \text{ ms}] = 0.887$$

The net fractional loss for the 220 channel: $(1 - 0.974 \times 0.943) = 0.082$;

The net fractional loss for the 219 channel: $(1 - 0.996 \times 0.887) = 0.117$.

2.4.3. Calculation of efficiency for 219 channels:

In the present study SE_{220} was estimated with the standards Mn-fiber coated with ^{232}Th (activity: 30.06 DPM) and was found 0.485

$$\text{SE}_{219} = \frac{0.485}{0.847 \times (1 - 0.082)} \times 0.801 \times (1 - 0.117)$$

$$\text{SE}_{219} = 0.434$$

2.5. Validation of Method for Measurement of ^{224}Ra and ^{223}Ra by coincidence counting:

The activity of the sample collected was measured at different decay time and logarithmic of ^{224}Ra activity is plotted against decay time. Figure 2.11a, shows linear fit gives R^2 value as 0.99808 and slope as -0.18625 ± 0.0049 which gives half-life of ^{224}Ra as 3.72 ± 0.09 days. Measured half-life is within 2.5% of the reported value of ^{224}Ra half-life (^{224}Ra $T_{1/2}$: 3.66 days)

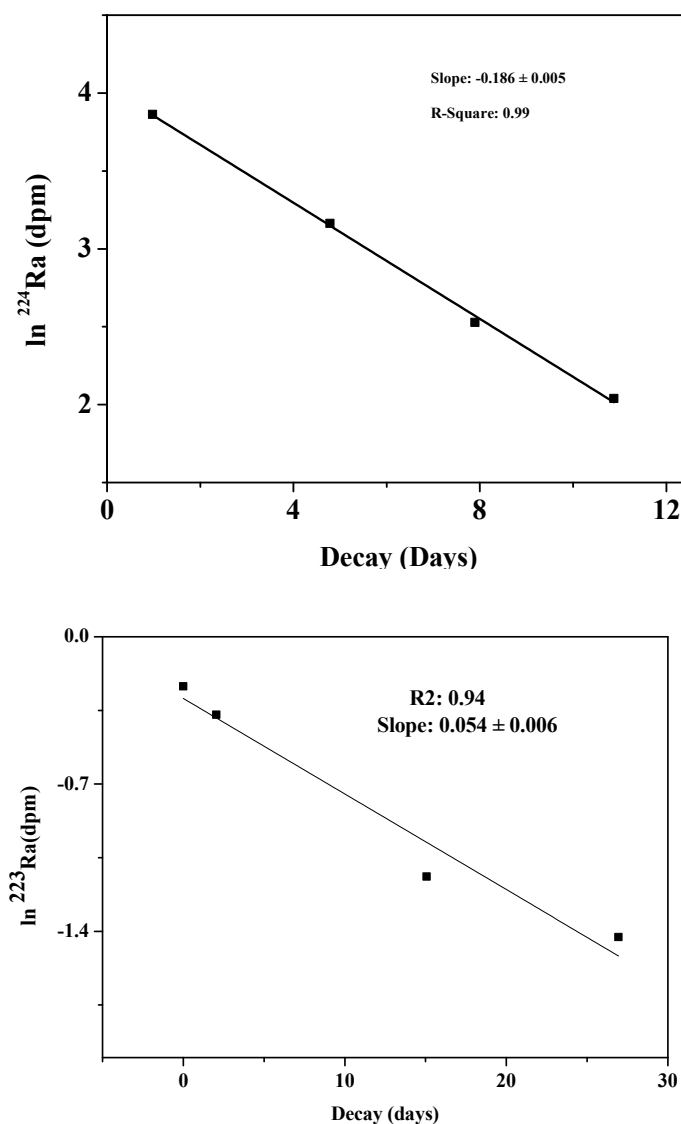


Figure 2.11: (a): $\ln ^{224}\text{Ra}$ (dpm) vs. decay time and (b): $\ln ^{223}\text{Ra}$ (dpm) vs. decay time

The linear fit ($R^2=94$) of $\ln^{223}\text{Ra}$ (dpm) vs. decay time plot results slope as 0.54 ± 0.006 (Figure 2.11b). Using the slope the half of ^{223}Ra was estimated and found to be 12.83 days with an uncertainty of 12.6%. The measurement validates the method for the measurement of a short-lived isotope of Ra by delayed coincidence counting in water samples.

2.6. Total Reflection X-Ray Fluorescence (TXRF) Spectrometry

The elemental quantification of environmental samples is quite difficult due to the unknown constituents, low concentrations and interferences due to different chemical species present. The concentration of some of the elements in environmental samples varies from low, ranging from ppb (even some elements in sub-ppb) to percentage range. The lower ends of concentrations are near the detection limits of most of the conventional techniques even below the detection limit of techniques. The higher end concentration may cause matrix effect for the analysis of the other elements using a technique where the matrix is important in analysis.

Therefore for the elemental quantification of environmental samples, analytical methods should be selected based on the following criteria;

1. High linear dynamic range
2. Simultaneous multi-elemental capability
3. High sensitivity at low concentrations
4. Independent of matrix effects and chemical interference
5. Minimum contamination problem
6. High selectivity
7. Good precision and accuracy
8. Simple to operate and maintain
9. Large sample throughput

Besides the above criteria the speed of the method, a number of samples that can be analysed, nature of the sample, cost per analysis and availability of the instrumentation and methodology are also to be considered. Being idealistic, no analytical method currently in use for environmental analysis satisfies all the above criteria. Analysis of a sample can be made using multiple instrumental techniques and hence thorough knowledge of these techniques is required, as no single technique can produce all the information. The different techniques used depend on the nature of the material and the type of information required.

Analytical chemistry can be split into two main types, qualitative and quantitative. Most of the modern analytical chemistry is quantitative. Quantitative analysis can be further split into different areas of study. There are many techniques for the analysis of materials on the basis of spectroscopic, electrochemical, mass, thermal and separation parameters. Some of the most common techniques used in the environmental analysis are given in Figure 2.12.

Wilhelm Conrad Roentgen discovered X-rays in 1895 [195] and since then it has played a vital role in the field of material characterization and elemental determination. X-rays are electromagnetic radiations having wavelengths in the range from 10^{-5} to 100 \AA [196]. The similar light they possess corpuscular and wave character also shows the properties like polarization, diffraction, reflection and refraction. Most of the X-ray methods are based on the scatter, emission and absorption properties of X-rays [196].

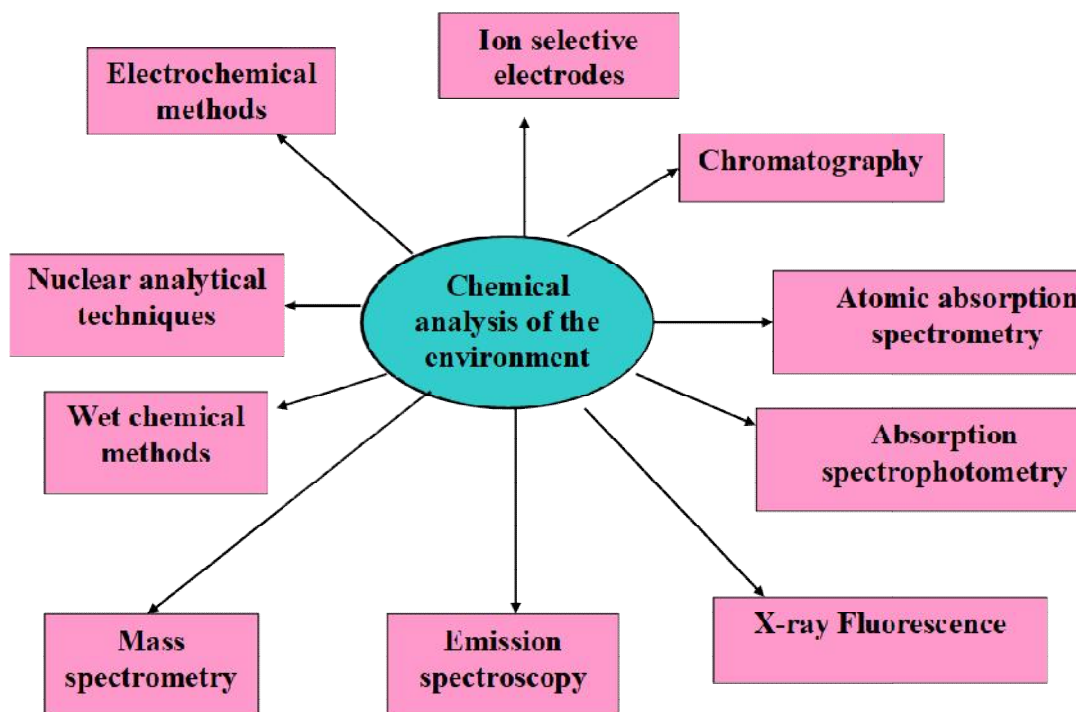


Figure 2.12: Survey of techniques available for chemical analysis of the environmental samples

The most common of them are X-Ray Diffraction (XRD), X-Ray Fluorescence (XRF) and X-Ray Absorption Spectroscopy (XAS). Table 2.3 gives a brief description of various X-ray techniques and the type of information given by these techniques. These techniques are very strong analytical tools for material characterization [197, 198].

X-ray Secondary Emission Spectrometry popularly known as X-Ray Fluorescence (XRF) spectrometry is a powerful method for the compositional characterization of materials. It is based on the principle of measurement of the energies or wavelengths of the X-ray spectral lines emitted from the sample, which are the characteristic or signature of the elements present in the sample. Moseley established the basis of x-ray spectral analysis by relating the wavelength to an atomic number of the elements in 1913.

Table 2.3: X-ray techniques and their applications

S. No.	Technique*	Type of information
1.	XRD	Phase identification, Bond type, Crystal structure, Crystal defects, Local structure, Crystallite size, Strain
2.	XRF: EDXRF, TXRF, WDXRF	Elemental concentration, Chemical environment, Oxidation state
3.	XPS	Elemental composition, Chemical state, Electronic state, Density of states
4.	XAS : XANES, EXAFS	Local coordination, Oxidation state, Inter-atomic distances, Coordination number
5.	XRR	Thickness and density of thin films, Interface roughness and multi-layers
6.	SAXS	Particle sizes, Size distributions, Shape and orientation distributions in liquid, powders and bulk samples

***Acronyms:** XRD: X-Ray Diffraction, XRF: X-Ray Fluorescence, XPS: X-Ray Photoelectron Spectroscopy, XAS: X-Ray Absorption Spectroscopy, XRR: X-Ray Reflectivity, SAXS: Small Angle X-ray Scattering

Moseley Law states that the reciprocal of wavelength ($1/\lambda$) or frequencies (ν) of characteristic X-rays are proportional to the atomic number (Z) of the element emitting the characteristic X-rays. Because X-ray spectra originate from the inner orbital, which is not

affected substantially by the valence of the atom, normally the emitted X-ray lines are independent of the chemical state of the atom. However, in the case of low and medium atomic number elements, the energy of the characteristic X-rays depends on oxidation state. This phenomenon is observed in case of high Z elements also, for the lines originating due to electron transfers from the outer orbital. Moseley's law is represented as:

$$\sqrt{\nu} = \sqrt{\frac{c}{\lambda}} = k_1(Z - k_2) \quad (2.44)$$

Where c is the velocity of light, k_1 and k_2 are constants different for each line and depend on the atomic number. Figure 2.13 shows the relationship of the energy of the X-ray photon with atomic number. As Moseley's law is not very stringent, the exact positions of the characteristic X-rays deviate from this law.

In XRF, the primary beam from an X-ray source irradiates the specimen thereby exciting each chemical element. These elements, in turn, emit secondary X-ray spectral lines having their characteristic energies or wavelengths in the X-ray region of the electromagnetic spectrum. In brief, incident photon knocks out an electron (photoelectron) from inner shell target element to create a hole which is filled by an electron from the higher energy level. In this process, a photon (Fluorescence Photon) is emitted having energy equal to the difference between the energy of two energy level i.e. $\Delta E = E_2 - E_1$ where E_1 and E_2 are the energy of inner and higher electronic level Figure 2.14. The intensities of these emitted characteristic X-rays are proportional to the corresponding elemental concentrations.

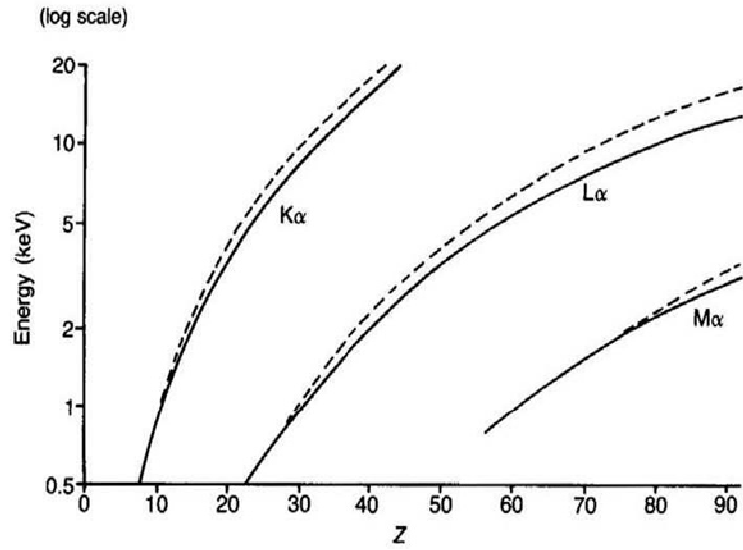


Figure 2.13: Moseley's Law plot of energy versus the atomic number

(----- Dashed line shows the deviation of Moseley Law at the higher atomic number)

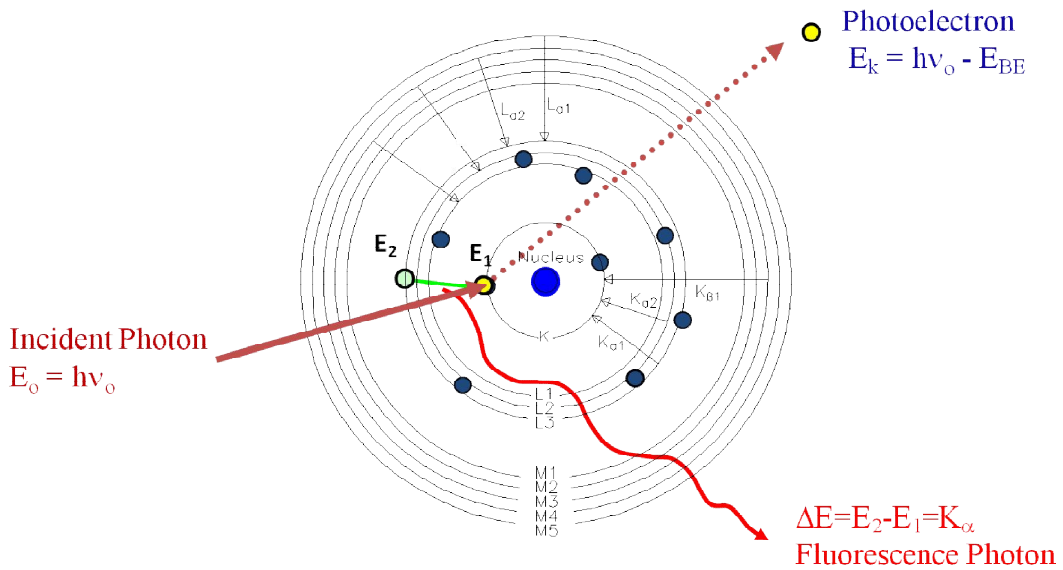


Figure 2.14: Production of Fluorescence Photon

There are two major modes of analysis in X-ray spectrometry: Wavelength Dispersive X-Ray Fluorescence (WDXRF) and Energy Dispersive X-Ray Fluorescence (EDXRF)

Spectrometry. The difference between these two modes of analysis lies in the detection component Figure 2.15. In EDXRF, the detectors directly measure the energy of the X-rays with the help of multichannel analyzer, whereas in WDXRF, the X-rays emitted from the samples are dispersed spatially using a dispersion crystal and wavelength of the each emitted X-rays is determined by the detector sequentially. The first commercial XRF instrument available was WDXRF, in the year 1940.

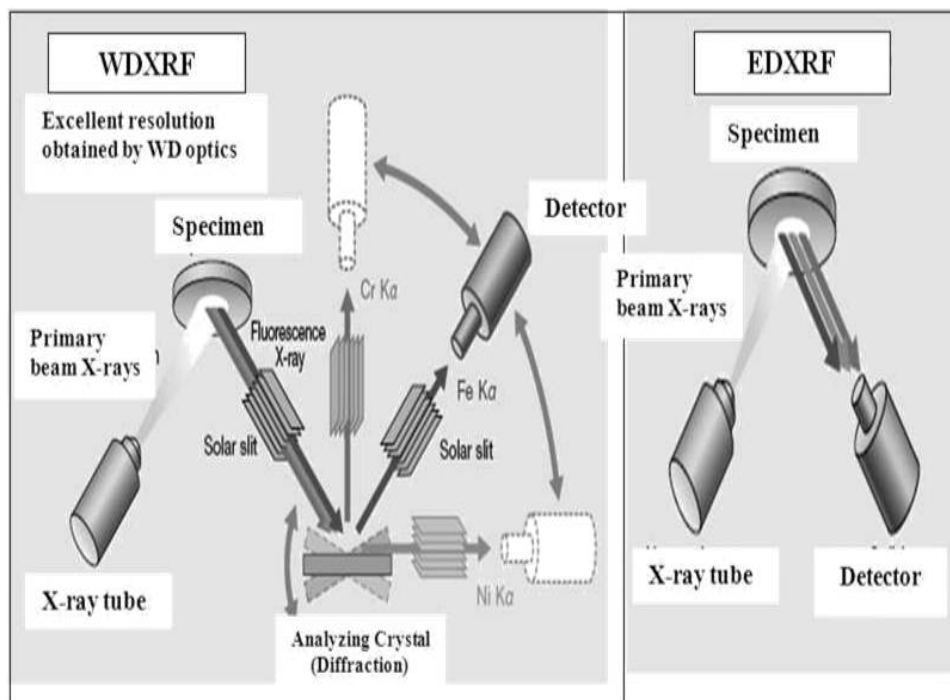


Figure 2.15: Schematic diagram of the basic difference between WDXRF and EDXRF

XRF method has a large dynamic range, sensitive up to microgram per gram level and is considerably precise and accurate. For these reasons, XRF has become a well-established method of spectrochemical analysis. It has got a variety of applications in industries of material production, quality control laboratories, scientific research centres, environmental monitoring, medical, geological and forensic laboratories [199–202]. This technique has also got sample versatility as a sample in the form of solid, liquids, slurry, powder, etc. can be

analysed with little or no sample preparation. In most cases, XRF is a non-destructive/non-consumptive technique. Along with various advantages, conventional XRF technique is associated with systematic errors caused by the matrix.

Arthur H. Compton [203] in 1923 described for the first time total reflection of X-rays under grazing incidence of the primary beam. Y. Yoneda and T. Horiuchi in 1971 [204] suggested that with appropriate specimen preparation the background could be reduced by total reflection of the exciting beam at an optically flat sample support and simultaneously detected absolute amounts of the elements Cr, Fe, Ni, and Zn with a detection limit in ng range. This variant of EDXRF is now considered a separate X-ray spectrometric technique is known as Total Reflection X-Ray fluorescence (TXRF) Spectrometry Figure 2.16. In late 70s Knoth and Schwenke [205] developed a compact, stable and easily adjustable total reflection module which was a decisive step towards the introduction of the method into analytical practice and for commercialization of the Total Reflection X-ray Fluorescence (TXRF).

In Classical EDXRF, the X-ray beam from an X-ray source falls on the sample at an angle of about 45° and the X-rays emitted from the samples are detected at an angle of 45° . This leads to penetration of X-rays inside the sample to a thickness of about a few 100 microns, thereby resulting in a lot of scattering of the X-rays by the sample and increasing the background drastically. Because of this, EDXRF has relatively poor detection limits and low signal to noise ratio. In TXRF, the exciting beam from the X-ray source falls on the sample support at an angle slightly less than the critical angle of the support so that the beam gets totally reflected. The emitted fluorescence intensity from the sample is detected by the detector mounted at an angle of 90° with respect to the sample support as shown in Figure

2.17. This leads to virtually no interaction of the exciting radiation with the sample support, resulting in a drastic decrease of the scattered radiation and hence negligible background. TXRF, due to very low background and better detection limits, is primarily used for trace and micro-elemental analysis.

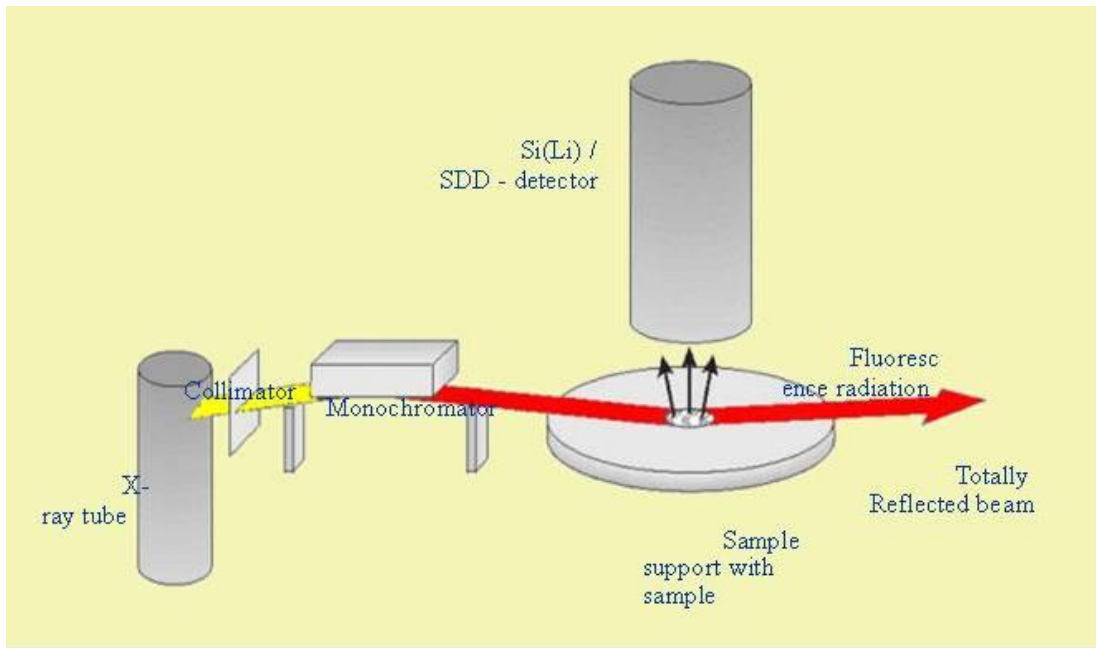


Figure 2.16: Schematic Representation Total Reflection X-ray Fluorescence (TXRF)

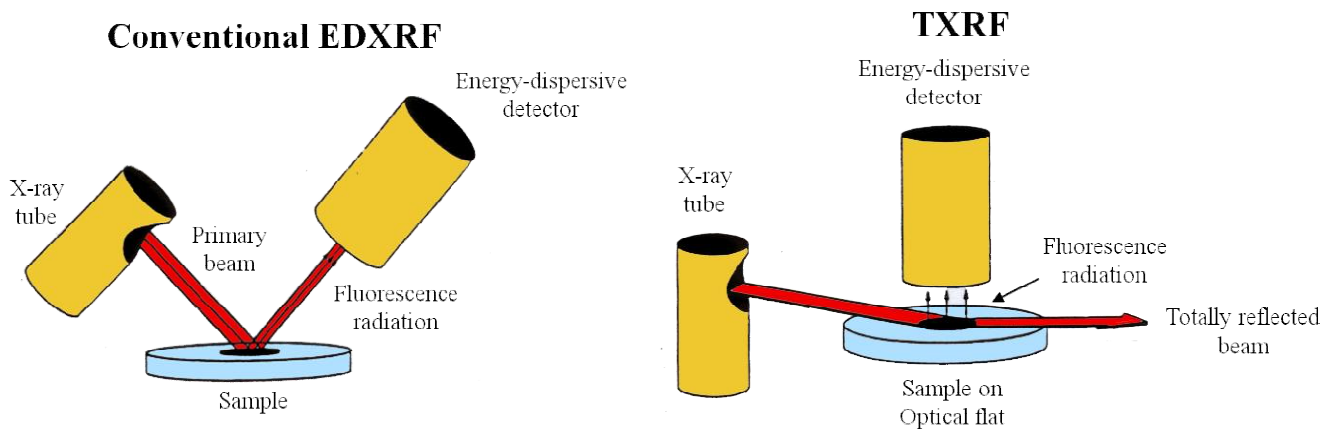


Figure 2.17: Comparison of the geometrical difference between conventional EDXRF and TXRF

Another severe drawback in EDXRF is the effect of matrix composition on the analyte line intensity. This is known as matrix inter-element or absorption enhancement effect. Such effect arises due to the following phenomena:

- The matrix may have larger or smaller absorption coefficient for the primary X-rays than the analyte
- The matrix may absorb the analyte line which will lead to a decrease in the analyte intensity than expected and
- The matrix may emit secondary X-rays which may excite the analyte line very efficiently, leading to increase in the analyte line intensity than expected.

As the amount of sample loaded in TXRF analysis is very small and the X-ray penetrates only a few nm, matrix effect is almost absent. In TXRF, elements with $Z > 13$ can be analysed in ambient air. Helium purging is used to suppress the argon peak and for analysis of low Z elements below $Z = 13$, vacuum chamber TXRF spectrometer is used.

2.7. Component of TXRF

As shown in Figure 2.16 TXRF system consists of mainly different component

1. X-ray source
2. Collimator and Monochromator
3. Sample support
4. Energy-dispersive detector

2.7.1. X-ray Source

The three primary sources of X-ray production used in XRF are X-ray tubes, radioisotopes and synchrotron [206, 207]. X-ray tubes are the most common source of

sample excitation used in laboratories. In spectrochemical analysis like XRF, the characteristic X-rays generated may be classified as primary or secondary depending on whether excitation of the target, used to produce X-rays, is by particles (electrons or ions) or by photons, respectively. In primary excitation, the characteristic line spectrum of the target is superimposed on a continuum, which is generated simultaneously, and in secondary excitation, only characteristic X-ray spectra of the target are emitted.

2.7.1.1. X-ray tube sources

The X-ray tube is the most commonly used source of excitation in XRF technique. Production of X-ray in the tube is based on two principles. The first acceleration or deceleration of charged particle through the Coulomb field of the nucleus of the target produces radiation called 'Bremsstrahlung' or 'continuous X-ray'. This spectrum contains energies from zero to short wavelength limit λ_{\min} , corresponding to the maximum energy of the particles. In addition to this, if an inner orbital electron of the atom is knocked out by radiation or accelerated charged particles, the atom becomes unstable. In order to come to the ground state, the atom emits X-rays of specific energies, characteristic to the atom. An X-ray tube consists of a tungsten cathode filament, an anode target, thin beryllium window, focusing cup, a glass envelope that retains the vacuum, high voltage and water connection. W. D. Coolidge in the year 1913 introduced the basic design of the modern X-ray tubes [208]. Figure 2.18 shows the X-ray tube of the Coolidge type. The tungsten filament serves as the hot cathode. Electrons emitted from this filament, by thermionic emission, are accelerated by an applied high voltage in the direction of the anode. The high energy electron bombardment of the target produces X-rays that emerge out of this tube through the beryllium window, which is highly transparent to X-rays. However, only about 0.1% of the

electric power is converted into radiation and most is dissipated as heat. Due to this reason, cooling of the tube target by water is required. The beam emerging from a tube consists of two types of radiation as stated above: Continuous and Characteristic.

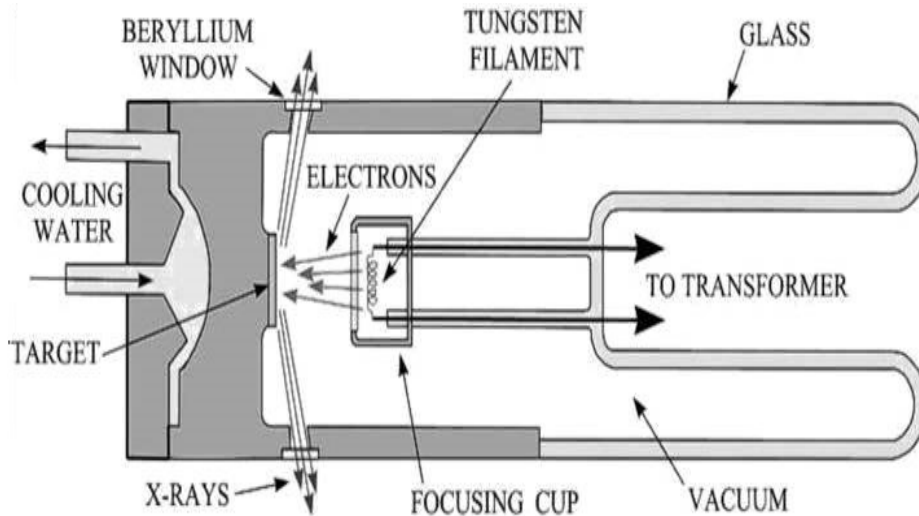


Figure 2.18: Schematic diagram of an X-ray tube of Coolidge type

The intensity of the continuum emitted from the target depends on the excitation parameters and is related as [209]:

$$I_{\text{int}} = (1.4 \times 10^{-9}) i Z V^2 \quad (2.45)$$

where I_{int} is the integrated intensity of the continuum, i and V are X-ray tube current and potential, respectively and Z is the atomic number of the X-ray tube target element.

The characteristic or the principal target line intensity, emitted along with the continuum, for example of K-line (I_k), is governed by the equation;

$$I_k \propto i(V - V_k)^{-1.7} \quad (2.46)$$

Where i is the tube current, V is the applied potential and V_k is the excitation potential. Figure 2.19 represents the spectrum generated from an X-ray tube consists of characteristic peaks of the target superimposed on high background produced by the continuum. The target element is chosen in such a way that the characteristic X-ray of the target is just above the

absorption edge of the analyte in the sample. The tube voltage should be 1.5 - 2 times the absorption edge of an element of interest. Most commonly used target elements are tungsten, molybdenum, rhodium and silver. Low Z elements like chromium and aluminium are used as targets for the excitation of K lines of low Z elements like magnesium, sodium, etc. Secondary target and filters are used to achieve better detection limit. Depending on the geometry and designs used, X-ray tubes can be classified as side – window, end- window and transmission target. Dual target X-ray tube for both high and low energy, Rotating anode X-ray tubes for high power rating up to 18 kW and Windowless X-ray tubes for low Z element are also used depending on requirement.

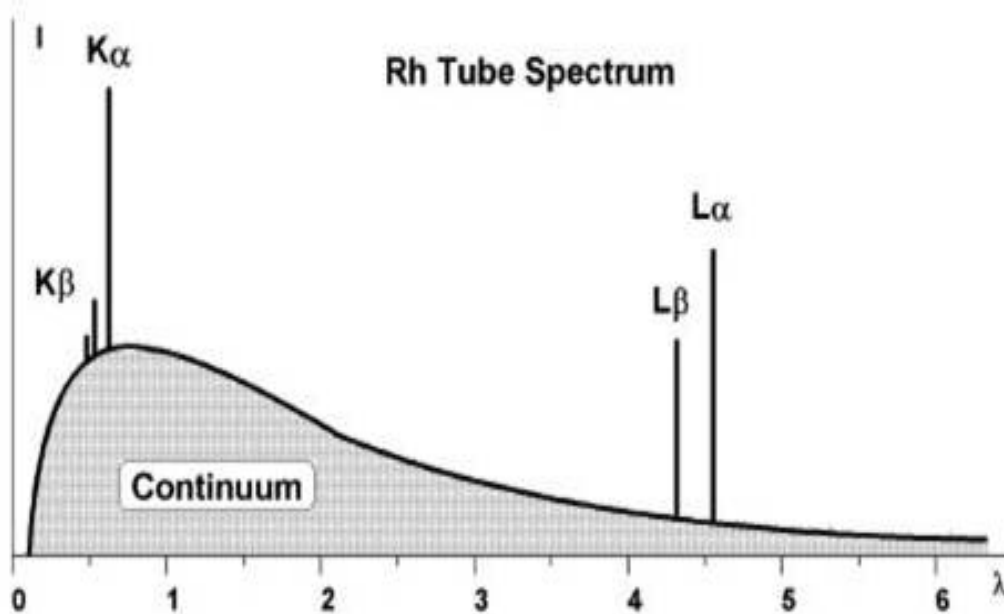
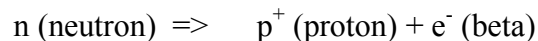


Figure 2.19: Spectrum generated from Rh target X-ray tube

2.7.1.2. Radio-isotopic sources

The radio-isotopic source of X-ray is commonly used in EDXRF spectrometers. Radioactive isotopes that decay by γ emission may undergo internal conversion during which γ photon is absorbed within the atom and its energy is used to expel an orbital electron. This

electron is known as internal conversion electron. Once the vacancy is created, the electronic rearrangement takes place with the emission of characteristic X-rays. Internal γ conversion is regarded as secondary excitation in which the ionizing photon originates within the atom. The two other modes of decay in radioactive isotopes are β emission and orbital electron capture. In internal β conversion, the β particle emitted from a radioactive nuclei occurring due to the process,



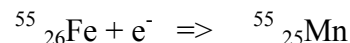
loses a part of its energy in ejecting an orbital electron. The internal conversion results in the emission of X-rays characteristic of the element, $Z+1$. Thus ^{129}I source emits Xe X-rays.



In orbital electron capture (EC), K or L electron is captured by the nucleus, thereby producing an electron vacancy and a neutron by the process,



decreasing the atomic number to $Z-1$. Here the characteristic X-rays of the atom having the atomic number one lower than the parent atom are emitted.



A Radioisotope source contains a specified amount of a specific radioisotope encapsulated to avoid contamination. These sources are characterized by

1. Radioactive decay process
2. Energy of the emitted radiation
3. Activity of the source
4. The half-life of a radioactive isotope

Table 2.4 lists these properties for some of the commonly used radioisotope sources. These sources are considerably less expensive, compact size, reliable and less expensive, radioisotope excitation is monoenergetic but the X-ray photon output is relatively lower than other sources and reduces with the time.

2.7.1.3. Synchrotron sources

Synchrotron radiations are produced when charged particles travelling at relativistic energies are constrained to follow a curved trajectory under the influence of a magnetic field.

Table 2.4: List of commonly used radioisotope sources for X-ray radiation

Radioisotope source	Decay process	Half-life	Useful radiation	Energy (keV)
$^{129}_{53}\text{I}$	β	60d	Xe $K\alpha$	29.8
$^{55}_{26}\text{Fe}$	EC	2.7y	Mn $K\alpha$	5.9
$^{57}_{27}\text{Co}$	EC	270d	Fe $K\alpha$	6.4
$^{109}_{48}\text{Cd}$	EC	1.3y	Ag $K\alpha$	22.2
$^{210}_{82}\text{Pb}$	β	22y	Bi $L\alpha$	10.8

The total emitted intensity (I) of the radiation is proportional to

$$I \propto E_p / mc^2 \quad (2.47)$$

Where E_p and m are the energy and mass of the particle and c is the velocity of light.

The above equation (2.47) shows that for certain energy, the highest intensity will be emitted by electrons and positron. The schematic presentation of the basic mode of operation of a synchrotron radiation source is shown in Figure 2.20. They have high photon flux with continuous energy distribution and mono-energetic beams can be tuned over a wide range.

This improves the excitation efficiency and detection limits by several orders of magnitude. They have low divergence (natural collimation), high intensity and brightness about 3-4 orders of magnitude greater than those of laboratory sources. The beam is polarized either linearly or circularly, which is extremely important for background reduction.

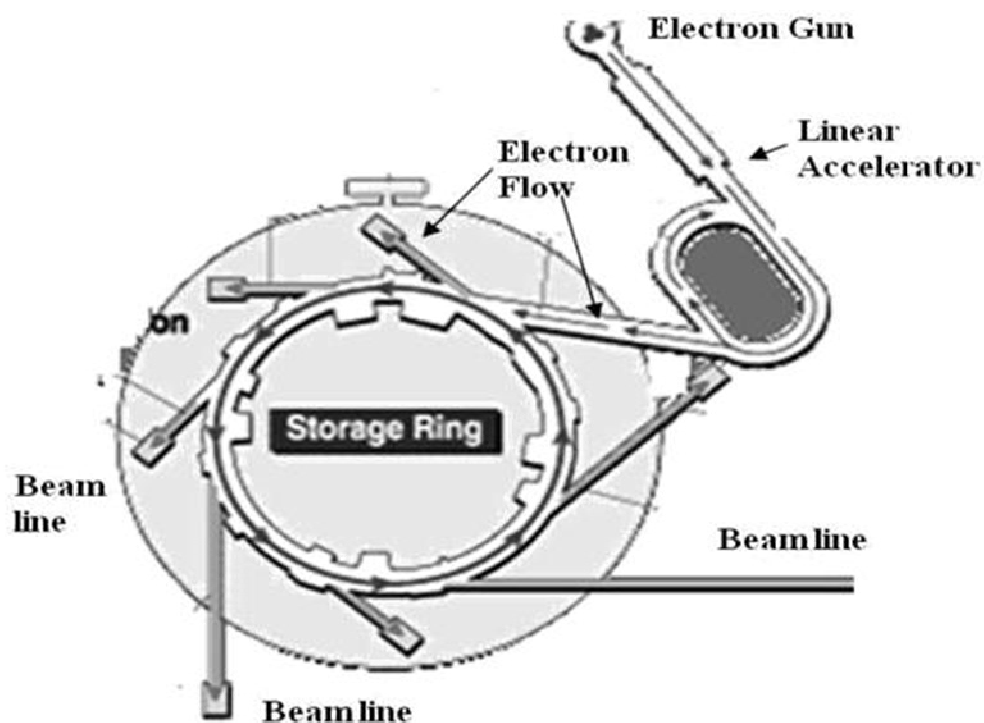


Figure 2.20: Schematic representation of a synchrotron source facility

2.7.2. Collimator and Monochromator

TXRF method is based on total external reflection of the primary beam from the sample carrier surface so the alignment of the instrument is very critical. The glancing angle of the incident primary beam must be less than the critical angle of the support used. The critical angle for sample support used is in order of few minutes of arc (e.g. quartz support has a critical angle of 5.9 min of arc). The primary beam is generated by an X-ray tube and is

shaped like a strip of paper realized by an X-ray tube with a line focus. The primary beam filter, consisting of thin metal foils, is placed in the path of the beam to alter the tube spectrum by increasing certain peaks in relation to the spectral continuum. By means of a pair of precisely aligned diaphragms or slits, the beam is shaped like a strip of paper. The primary polychromatic beam consisting of the continuum and the characteristic peaks of the anode material can be altered using simple quartz reflector block acting as low pass filter. It cuts the high energy part of the continuum and the low energy part is used for sample excitation. But sometimes it is required to use a considerably pure spectral line for excitation, which is achieved by using monochromator like natural crystal or multilayer. Both these monochromator work on the principle of Bragg's law with definite energy band selected at a particular angle of reflection. Unlike natural crystals, multilayer consists of stack bilayer, each being isotropic and homogenous. The bilayers are arranged in such a way that, alternately lower and higher refractive indices n_1 and n_2 , respectively are put one above the other. The total thickness (d) is the sum of both the layers $d = d_1 + d_2$. The first layer having lower refractive index is called reflector and the other is called spacer. Natural crystals like LiF or graphite have very small energy bandwidth but very poor reflectivity but multilayer have very high reflectivity but energy bandwidth is large.

2.7.3. Sample support

TXRF sample supports are an essential part of the TXRF analytical technique. Most of the carriers are circular disks of diameter 30 mm and thickness 2-3 mm (Fig.2.21). Usually, a droplet of 2-100 μL is pipette out on a support with a diameter of 3 cm which leaves a dry residue after evaporation under IR lamp or on a hotplate. Samples support works as reflecting mirror for liquid samples. For such analysis, the mean roughness of the sample

support should be in the order of a few nm and the overall flatness should be typically $\lambda/20$ ($\lambda = 589$ nm, the mean of visible light wavelength). Many sample carriers have been investigated for their use in TXRF [205, 210–212].

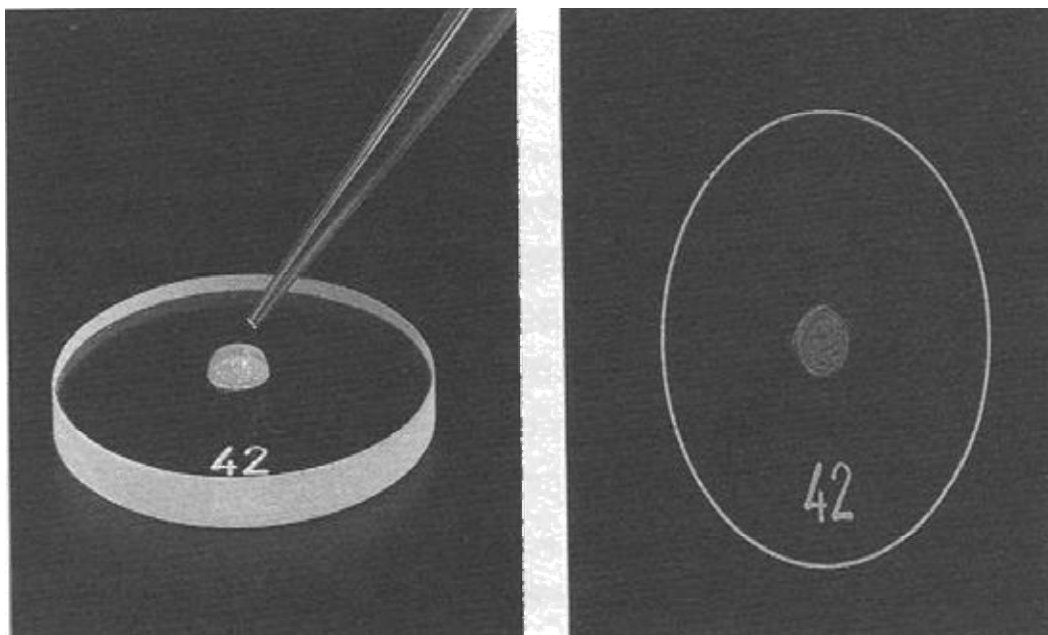


Figure 2.21: Liquid sample on a clean quartz sample support which leaves a dry residue after evaporation

Following the general requirement must be satisfied by sample support for TXRF analysis:

1. The surface should be dense and even
2. The material should be resistant to energy transfer through the interface under the operating condition
3. A high reflectivity and optically flat surface
4. Chemically inert material
5. Free from trace impurities
6. No fluorescence peak interference from the sample carrier at the region of interest
7. Easy to clean and economical

Some of the commonly used samples supports with important characteristics are given in Table 2.5 [205]. Quartz gives rise to silicon peak and hence silicon cannot be determined using a quartz carrier. Boron nitride is the most resistant material suitable for the analysis of strong acid. Glassy carbon is preferentially used for electrochemical applications and Plexiglas is extremely cheap, once use, sample carrier. In general, quartz and Plexiglas carriers are mostly used for micro and trace analysis. Cleanliness of the sample supports is very important so acid cleaning is done and the spectrum of cleaned sample support is taken to ensure proper cleaning.

2.7.4. Energy Dispersive Detectors:

The detector for TXRF is a transducer (solid state detector) for converting X-ray photon energy into voltage pulses. Normally lithium drifted semiconductor detectors like Si(Li) or Ge(Li) commonly used in TXRF, which basically consist of Si or Ge crystal doped with lithium. In Si(Li) detectors, lithium is added to neutralize the boron impurity which is the most common element present in silicon and modifies silicon to the p-type semiconductor. As it is possible to produce high purity germanium, Ge(Li) detectors are replaced by high purity germanium detectors (HPGe).

Lithium diffuses into the silicon crystal at elevated temperatures and drifts under the influence of the electric field. In this way, a crystal with high intrinsic resistivity is produced with a thin p-type and n-type layer at the end plane and large intrinsic region in between. The detector requires to be cooled to liquid nitrogen temperature (77 K) for two reasons: i) reducing the thermal leakage current and ii) to prevent the reverse diffusion of the Li ions.

Table 2.5: Characteristics of different sample support materials

Features	Quartz	Plexiglass	Glassy carbon	Boron nitride
	With Mo Kα excitation			
Reflectivity (R)	0.994	0.998	0.998	0.999
Critical angle (α_{crit})	0.10	0.08	0.08	0.10
Purity	Very Good	Zn	Fe, Cu, Zn	Zn
Surface Quality	Very Good	Good	Satisfactory	Good
Fluorescence Peak	Si	None	None	None
Cleaning	Easy	Impossible	Difficult	Easy

X-ray photons interact with the detector crystal and raising the valence band electrons to the conduction band of the crystal lattice thereby creating an electron-hole pair. These electron-hole pair moves to the respective electrode under the applied high voltage and produces charge pulse for a single photon counting. The number of electron-hole pairs produced is directly proportional to the energy of the detected photon and magnitude of the charge pulse is proportional to the photon energy. A schematic diagram of the Si(Li) detector crystal is given in Figure 2.22.

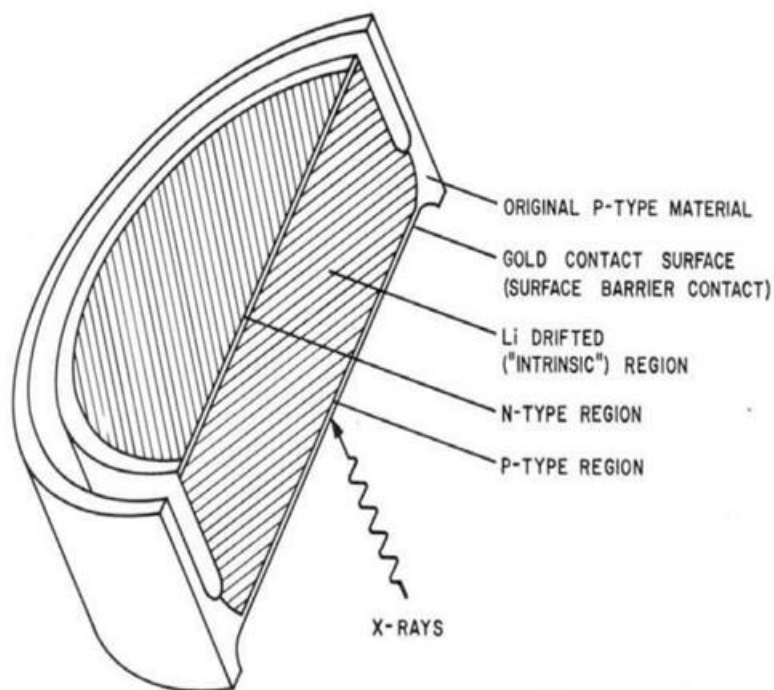


Figure 2.22: A cross-sectional view of a Si(Li) detector crystal

The efficiency (ϵ) of a semiconductor detector is defined as the percentage of detected photons with respect to the incident photons. A Si(Li) detector, having 3mm thick intrinsic region, has an efficiency of nearly 100% for photon energies between 6 to 11 keV. Semiconductor detectors have better spectral resolution than gas-filled proportional and scintillation detectors. Like high purity germanium now very high purity Si is availability leads to room temperature operated Peltier cooled detectors. Si-PIN photodiode detectors are such detectors which are made of very pure Si, called intrinsic material. Since nothing is doped into them, a simple electrical Peltier cooling at approximately -30°C is good enough for reducing the leakage current. Though these electronically cooled detectors have relatively poor energy resolution compared to that of liquid nitrogen cooled detectors, such detectors are widely used nowadays in EDXRF and TXRF spectrometers and are much suited for field

applications because of their compact size and no requirement of liquid nitrogen for cooling [213].

Silicon Drift Detectors (SDD) is another type of photodiode detector similar to Si-PIN detectors but having better energy resolution. The resolution of these detectors is comparable to Si(Li). Si-PIN detectors are used where resolution is not critical but detection efficiency is important. SDD detectors are more complicated as well as more expensive [214].

2.8. Fundamentals of total reflection of X-rays

When any electromagnetic radiation travels from one medium to another, it gets partly reflected into the first medium and partly refracted into the second medium. According to the laws of reflection, the incident angle is equal to the angle of reflection and the incident, normal and reflected rays are coplanar. The glancing angle of the incident and reflected beams are also equal and refraction follow the Snell's law which states that

$$\frac{\sin \theta_1}{\sin \theta_2} = \frac{n_2}{n_1} = \frac{v_1}{v_2} \quad (2.48)$$

Where n_1 : refractive index of medium 1, n_2 : refractive index of medium 2, v_1 : velocity of light in medium 1, v_2 : velocity of light in medium 2, θ_1 is the incident angle (Angle of the incident), θ_1' is the angle of reflection and θ_2 is the angle of refraction Figure 2.23.

It is clear from the equation 2.48, if the radiation travels from a denser medium to rarer medium, the refracted beam will be deflected towards the interface boundary. For X-rays, any medium is optically thinner than air or vacuum so when it travels from air (optically denser) to solid medium (optically less dense) the refracted beam gets deflected towards the boundary plane.

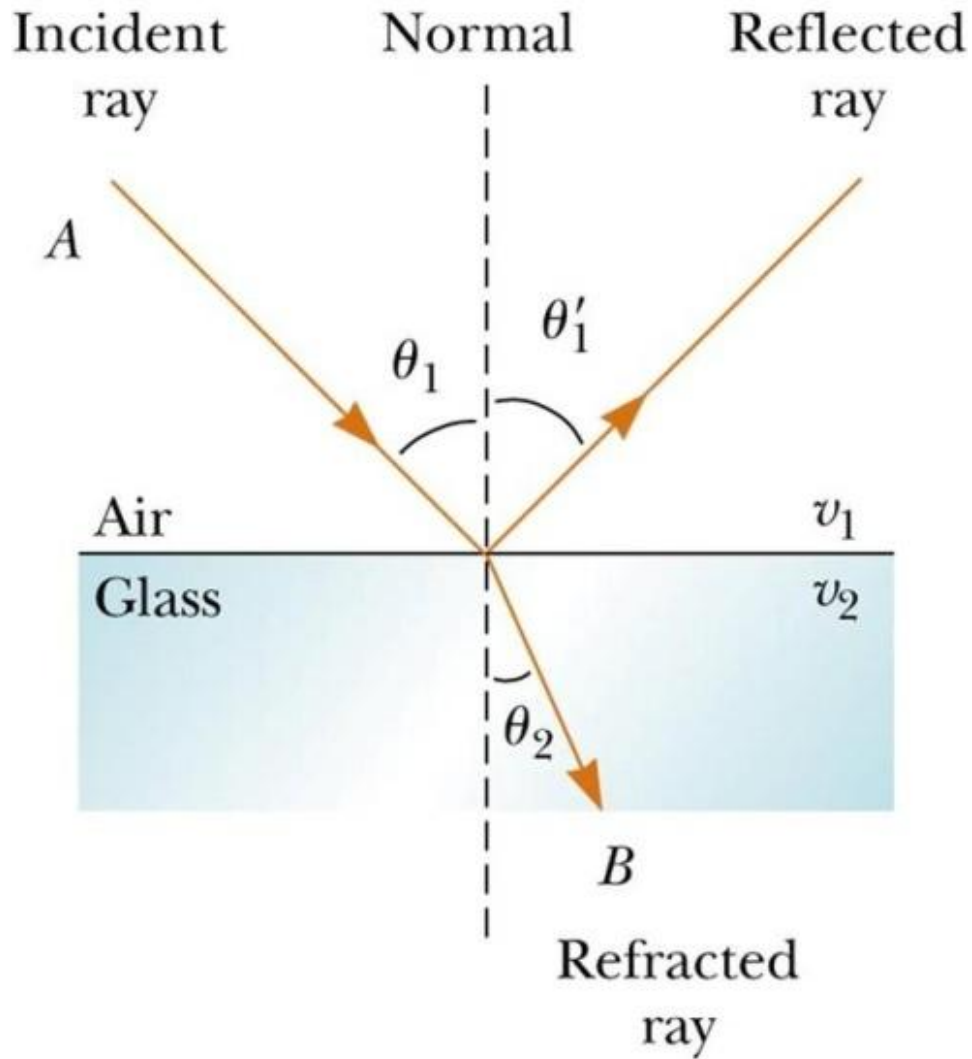


Figure 2.23: Reflection and refraction of the incident ray on glass surface

Increasing the angle of incident results increase in the angle of refraction and at a particular incident angle the refracted beam will be parallel to boundary plane. This glancing angle is called critical angle (θ_c) for the particular beam and medium. A beam incident with glancing angle lower than the critical angle will be totally reflected in the same medium Figure 2.24.

TOTAL INTERNAL REFLECTION OF LIGHT

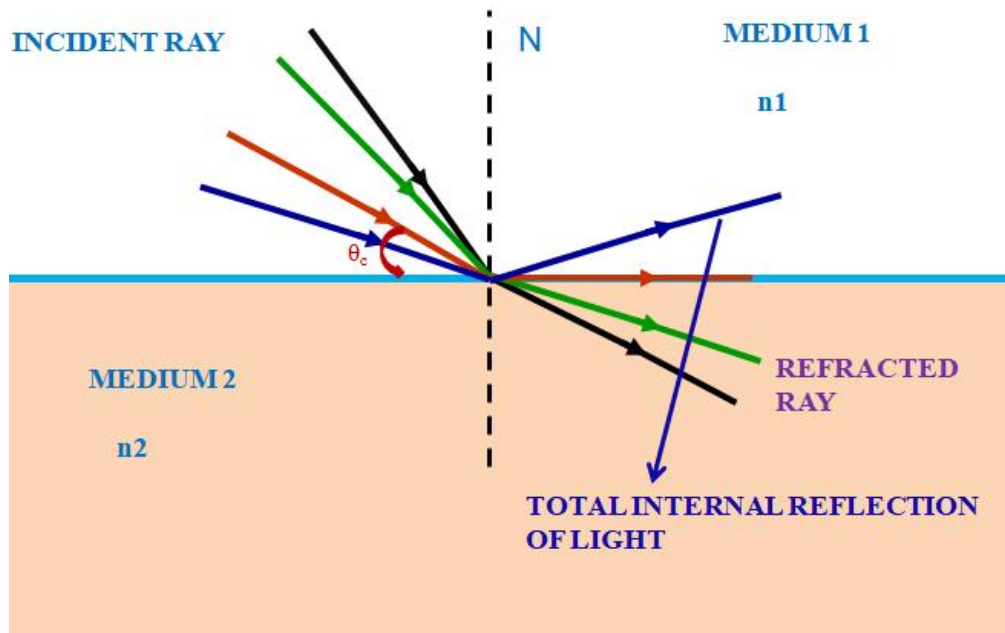


Figure 2.24: Total reflection of incident ray

At critical angle $\theta_2 = 90^\circ$ so;

$$\sin \theta_1 = \frac{n_2}{n_1}$$

For vacuum and air $n=1$ i.e. $n_1 = 1$, so at critical incidence

$$\cos \theta_c = n_2$$

X-rays, like other electromagnetic waves, exhibit total reflection for a particular angle of incidence when passing from a material with a higher refractive index to a material with lower refractive index. This is fulfilled for X-rays when they pass from e.g. vacuum (or air) to any other material. In particular, for X-rays, any medium has a smaller refractive index than air so that total reflection is generally possible although the glancing angles might be small. For absorptive media the refractive index is given by a complex quantity as

$$n = 1 - \delta + i\beta \quad (2.49)$$

δ called the decrement is a measure of the dispersion and is given by

$$\delta = \frac{N_A}{2\pi} r_0 \lambda^2 \frac{Z}{A} \rho \quad (2.50)$$

N_A : Avogadro's number, r_0 : the classical electron radius, λ : the wavelength of the primary radiation, Z : atomic number, A : atomic mass and ρ : density of the matrix. The imaginary component β is a measure of the absorption and given by

$$\beta = \frac{1}{4\pi} \mu \lambda \quad (2.51)$$

μ : linear mass absorption coefficient and λ : wavelength of the primary radiation. Since β and $\theta_c \ll 1$ so from Snell's Law at the critical angle,

$$\begin{aligned} \cos \theta_c &\approx 1 - \frac{\theta_c^2}{2} = n \approx 1 - \delta \\ \theta_c &= \sqrt{2\delta} \end{aligned} \quad (2.52)$$

From Eq. 2.50 and Eq. 2.52:

$$\theta_c = \frac{1.65}{E} \sqrt{\frac{Z}{A} \rho} \quad (2.53)$$

Where E is the energy of the x-ray, for Mo-K α X-rays passing from vacuum to quartz glass; $\delta = 1.5 \times 10^{-6}$ and $\beta = 4.6 \times 10^{-9}$ which results in $\theta_c = 0.00173$ rad or 5.9min of the arc.

Reflectivity (R) is defined as the intensity ratio of the reflected beam and the incident beam. During total reflection, since the entire beam gets completely reflected back the reflectivity increases to approximately 1. At higher glancing angles the reflectivity is less (less than 0.1%) and increases very steeply to about 100 % when the glancing angle reaches below the critical angle (Figure 2.25).

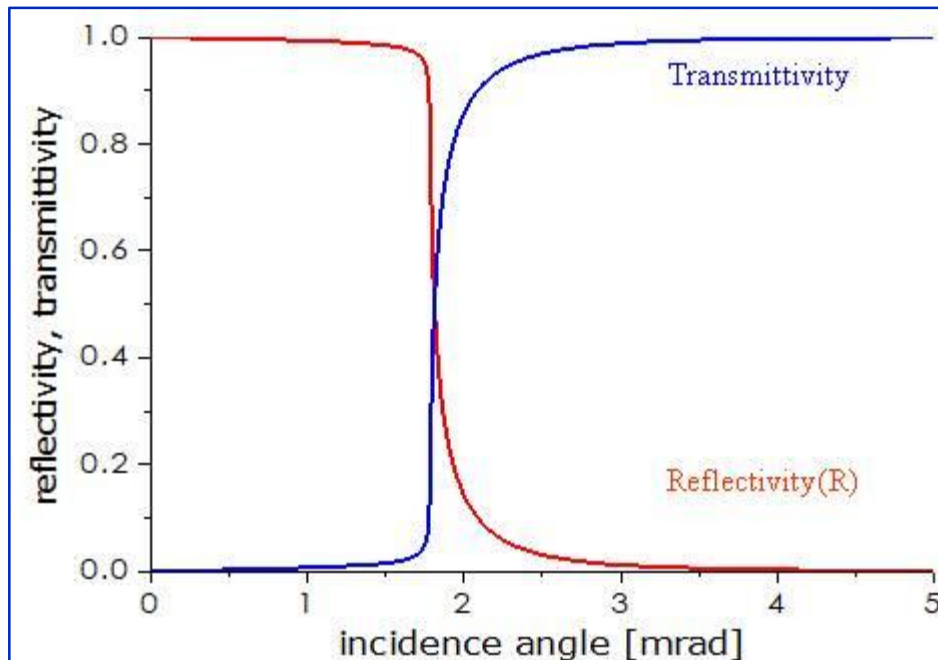


Figure 2.25: Variation of reflectivity and transmittivity of incidence beam (MoK α) on quartz surface against incidence angle

The intensity of fluorescence line (I_L) is proportional to reflectivity as $I_L \propto (1+R)$ and intensity of background (I_B) is related as $I_B \propto (1-R) \sin\phi$ so below the critical angle in the total reflection region the signal to noise ratio increases dramatically.

Penetration depth is another critical factor in the total reflection mode of operation. It is defined by the depth of a homogeneous medium to which a beam can penetrate while its intensity is reduced to $1/e$ or 37% of its initial value. The penetration depth at angles greater than the critical angle is of the order of a few micrometres but under total reflection condition, the penetration depth is drastically reduced to a few nanometers. After that, it is nearly constant as that of the reflectivity curve. Figure 2.26 penetration depth of the primary radiation for glassy carbon and quartz carrier for an incidence energy of 17.5 keV (Mo-excitation)

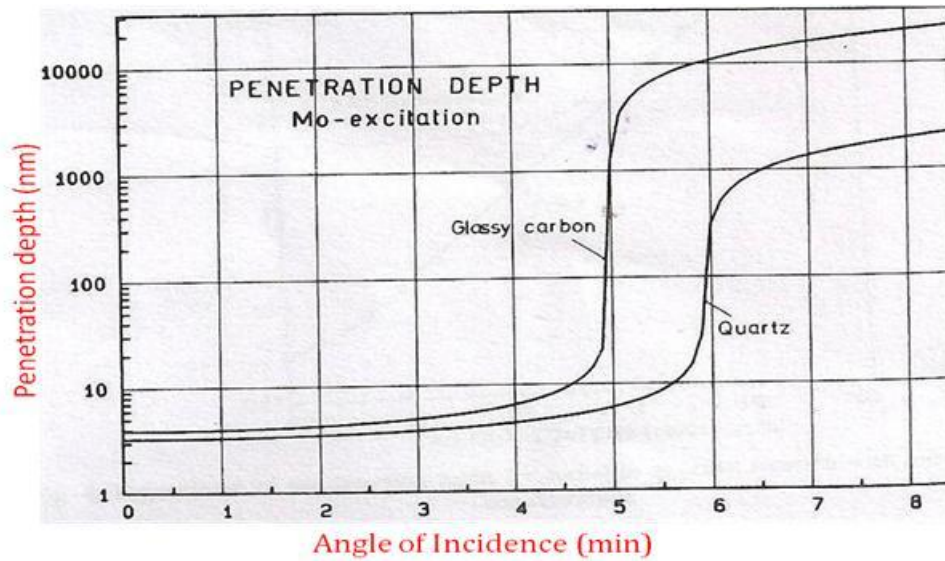


Figure 2.26: Penetration depth vs. angle of incidence

Fluorescence intensity of a spectral line given by Sharman Equation

$$I_j = C_j K_j \frac{1 - \exp(-(\mu/\rho)\rho t)}{(\mu/\rho)\rho} I_0 \quad (2.54)$$

I_j : Net intensity of the spectral line of the element j

C_j : mass fraction or concentration of the analyte j

K_j : proportionality constant for the analyte line

(μ/ρ) : mass absorption coefficient of the entire specimen

ρ : density of the specimen

t: thickness of the sample

I_0 : intensity of the incident monochromatic primary beam

At first glance it seems from above equation intensity is linearly related to the concentration of analyte but Mass absorption coefficient of the entire specimen is related to the mass absorption coefficient of the different elements as below;

$$(\mu/\rho) = C_i [(\mu/\rho)_{i,\lambda_0} * \csc \phi + (\mu/\rho)_{i,\lambda_i} * \csc \varphi] \quad (2.55)$$

C_i : mass fraction of the element i in the matrix

$(\mu/\rho)_i$: mass absorption coefficient of the different element

ϕ : incident angle of the primary beam

ϕ : take-off angle of the fluorescent beam

λ_0 : wavelength of the primary beam

λ_i : wavelength of analyte line

As in TXRF analysis we use a very thin layer of the sample on sample support and if the thickness is very less then we can use thin layer approximation as;

$$\lim_{t \rightarrow 0} \frac{1 - \exp(-(\mu/\rho)\rho t)}{(\mu/\rho)\rho} = t \quad (2.56)$$

In this case

$$I_j = C_j K_j t I_0 \quad (2.57)$$

From the above equation, it is clear that the intensity of the spectral line of a particular element is independent of the concentration of other elements present in the matrix. So if have a very thin layer of the sample, matrix effect is not there in TXRF analysis which is the main drawback in conventional EDXRF technique. A criterion for a film to be infinitely thin so that matrix effects disappear can be derived if the exponent (μ/ρ) of the equation 2.56 is confined to a small value.

$$t \leq \frac{0.1}{(\mu/\rho)\rho} \quad (2.58)$$

The sample thickness satisfying the above condition of the thickness gives results within 5% of error [215]. The above results are based on assumption that primary is monochromatic and penetrate the sample only in forward direction. In practical the primary beam passes twice through matrix once while incident and second while after reflecting from sample support as shown in Figure 2.27 below;

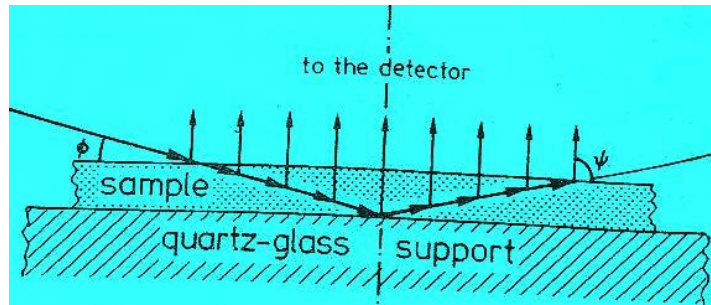


Figure 2.27: Schematic diagram for double excitation of the sample in TXRF

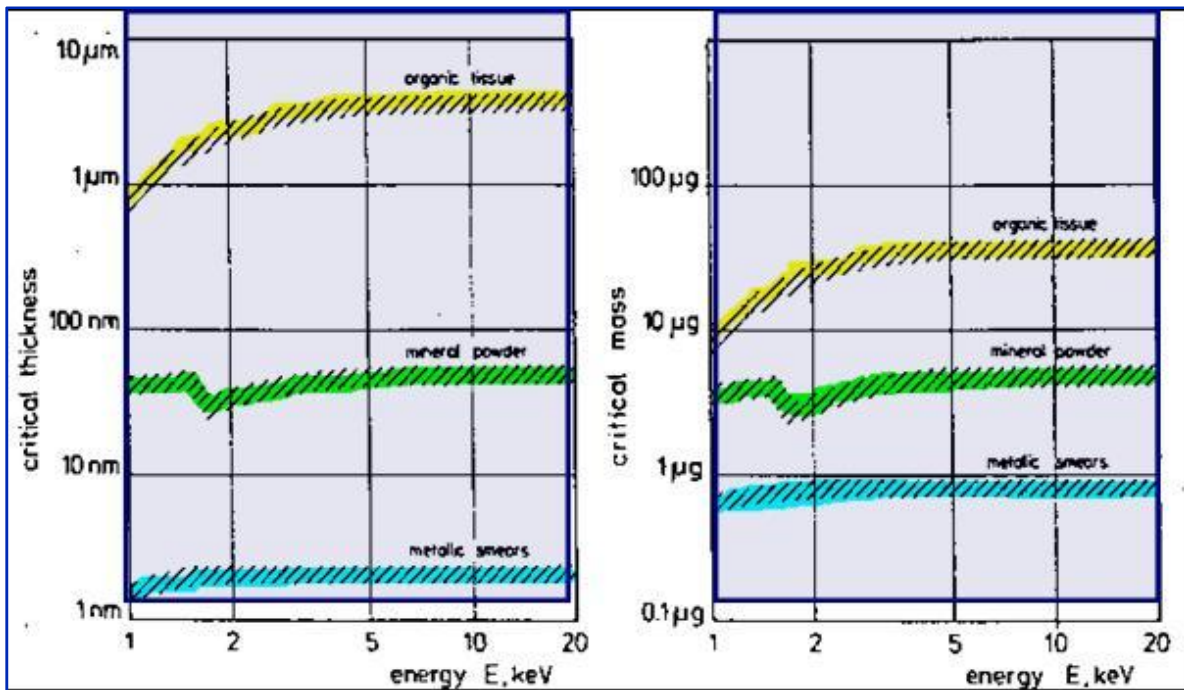


Figure 2.28: Critical thickness and critical mass for different matrices in TXRF analysis

Considering the twice excitation of the sample by primary incident radiation thickness should be as;

$$t \leq \frac{0.05}{(\mu/\rho)\rho} \quad (2.59)$$

The thickness is called critical thickness for TXRF analysis as a sample with thickness would not show the matrix effect and result will be good agreement with true value. Considering the above criterion and area of the thin layer as 40 mm² critical thicknesses and critical mass for different matrices is calculated [215]. Figure 2.28 the value of critical mass and critical thickness for different matrices.

Effect of the matrix on the detection limit was studied by [216] and it was found that at higher matrix content TXRF also works similar to conventional XRF as shown in the figure below;

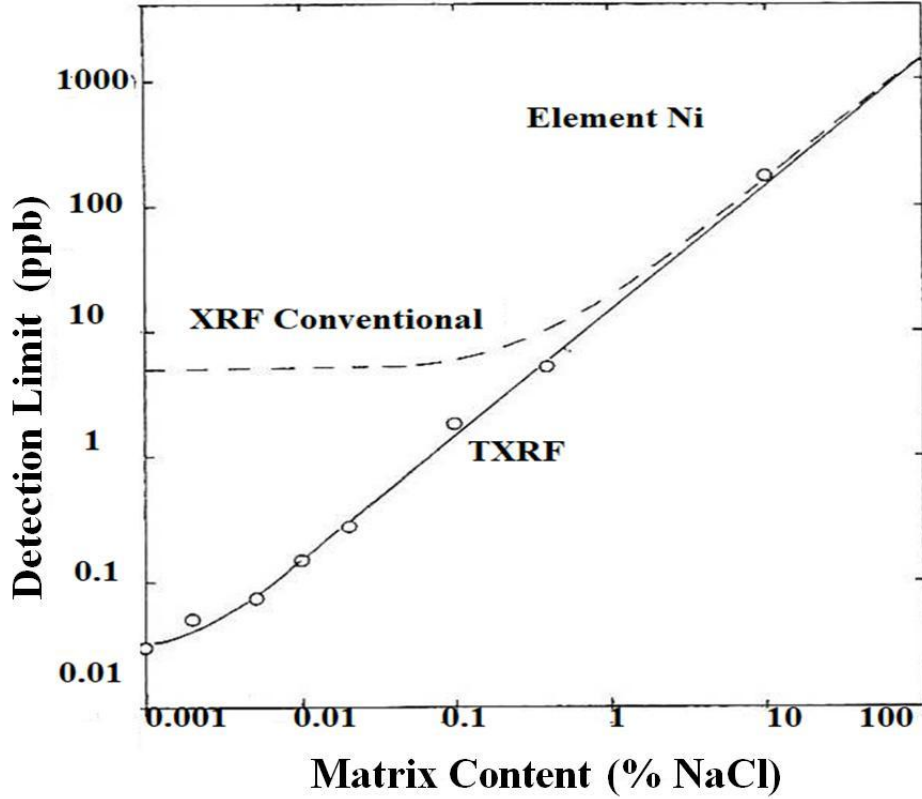


Figure 2.29: Detection limit vs. matrix content (% NaCl)

The sensitivity of any analyte line is given by the following equation

$$S_i = \frac{I_i}{C_i} \quad (2.60)$$

For TXRF analysis taking double excitation and Sharman Equation may be written as

$$I_j = 2C_j K_j t I_o \quad S_j = 2K_j t I_o \quad (2.61)$$

Where K is proportionality constant and given by

$$K_j = g_L w_j \frac{r_j^{-1}}{r_j} (\mu/\rho)_{j \lambda_o} \rho \cos \phi \frac{\Omega}{4\pi} \quad (2.62)$$

Where:

g_L = Relative transition probability for the particular analyte line in its series

w_j = Fluorescence yield of the analyte line

r_j = Jump ratio at the absorption

$(\mu/\rho)_{\lambda_0}$ = mass-absorption coefficient (photoelectric part)

of the element j for the primary beam

ρ = Density of the specimen

ϕ = Incident angle of the primary beam

Ω = Solid angle of the effective aperture of the detector

ω_j , r_j and $(\mu/\rho)_j$: can be taken from literature and g_L : set equal to 1, which requires that all analysis line within a series are integrated. $2\rho\cos\phi$ ($\Omega/4\pi$) I_0 are chosen arbitrarily as only relative sensitivities were needed for the method of Internal Standardization. The sensitivity of the internal standard can be given as;

$$S_{IS} = \frac{I_{IS}}{C_{IS}} \quad (2.63)$$

From above equations sensitivity of an element is related to the sensitivity of internal standard as

$$S_i = \frac{I_i}{I_{IS}} * \frac{C_{IS}}{C_i} * S_{IS} \quad (2.64)$$

As in TXRF analysis, we use relative sensitivity for the quantification of the concentration of different elements present in the sample. For determination of relative sensitivities, standard solutions (Merck, Aldrich, etc.) of multi-elements or single elements are chosen and relative sensitivity is calculated as

$$RS_i = \frac{S_i}{S_{IS}} = \frac{I_i}{I_{IS}} * \frac{C_{IS}}{C_i} \quad (2.65)$$

Experimental as well as theoretical investigation proved the absence of matrix effects if “Infinitely Thin” sample were analysed. Internal standardization by a single standard element which is added to the sample in known concentration C_{IS} . All unknown concentration C_i of the other analyte can be calculated by:

$$C_i = \frac{I_i}{I_{IS}} * \frac{S_{IS}}{S_i} * C_{IS} = \frac{I_i}{I_{IS}} * \frac{1}{RS_i} * C_{IS} \quad (2.66)$$

Thus procedure for elemental quantification is also very simple in TXRF. It is done by adding a single internal standard to the sample. The pre-requisite for the element to be added as an internal standard is that it should not be present in the sample. For quantification, the net intensities of the analyte and internal standard peak need to be determined. Besides this, the relative sensitivity has to be pre-calculated for each element with respect to the added internal standard. The mode of excitation along with applied voltage, current, Monochromator as well as geometry has to be fixed for a fixed set of relative sensitivity values and any alteration requires a new calibration. As the relative sensitivity values remain constant for a particular set of instrumental parameters, these values can be used for quantification of elements in samples irrespective of their matrices. Internal standardization based method for TXRF quantification is very simple and reliable. Generally, rare elements which are not usually present as contaminants are chosen as internal standards.

2.9. TXRF System used in Present Study:

In the present studies, a GNR makes TXRF spectrometer TX-2000 (Figure 2.30- 2.33) was used for the analysis. It can be operated in total reflection as well as conventional XRF i.e. 45°/45° geometry. The spectrometer is equipped to use single (Mo) or dual (Mo-W) target X-ray tubes for excitation (Figure 2.33). The dual target tubes can be tuned to allow Mo-K α , W L α and

W L_{β} beam to fall on the sample for excitation without changing the X-ray tube. Mo-K α can efficiently excite medium and high atomic number elements K and L lines and W L_{β} can excite K lines of low Z elements. Automatic switching of primary beam (MoK α , WL α /L β) is done using double anode Mo/W X-ray tube, based on innovative software. Required energy is selected using a high reflectivity of 80% (MoK α , WL α /L β) multilayer (Figure 2.33). These high power X-ray tubes are cooled using a water chiller. The spectrometer is usually operated at a voltage and current of 40 kV and 30 mA, respectively. The sample chamber consists of twelve sample positions (Figure 2.31). So twelve samples can be loaded simultaneously and measured sequentially. The characteristic X-rays emitted from the sample were detected with a Peltier-cooled Silicon Drift Detector with an energy resolution of 124eV FWHM @ Mn K α with shaping time 1 μ s (Figure 2.32). Distance between the sample and the detector (mounted to the axis normal plane of the sample) is minimal. In this position the detector is also completely out of the primary beam, as the angle between the incident and the reflected beams is so large. The spectrometer is fully automated and you can control different total reflection conditions for different energies from the PC, using stepping-motors moving monochromator and tube shield and MS Windows software.

The X-ray spectra were acquired and processed by computer programs TXRFACQ-32 and EDXRF-32, respectively, provided with the instrument. EDXRF32 is an XRF spectra evaluation and quantitative analysis program for both total reflection and traditional XRF geometry. The program EDXRF32 analyses the TXRF spectra by nonlinear least-squares fitting based on the Marquardt algorithm. The elements are determined by means of the total areas of their characteristic X-ray lines and the instrumental calibration by means of standard solutions with known certified elemental concentrations.



Figure 2.30: TX2000 TXRF instrument used in the present study

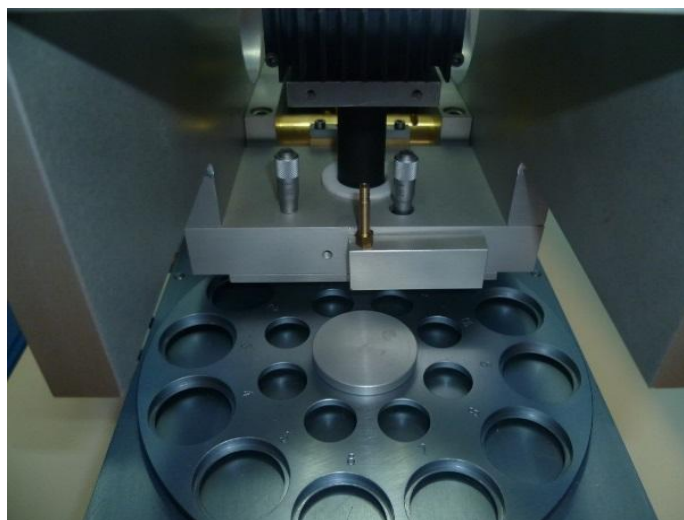


Figure 2.31: Front view: Multi-Sample Holder

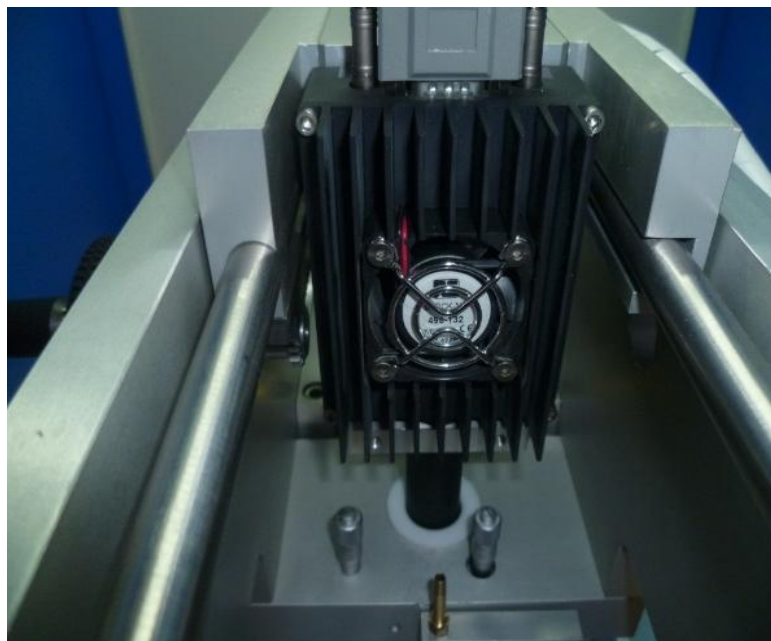


Figure 2.32: High-Resolution SDD Detector

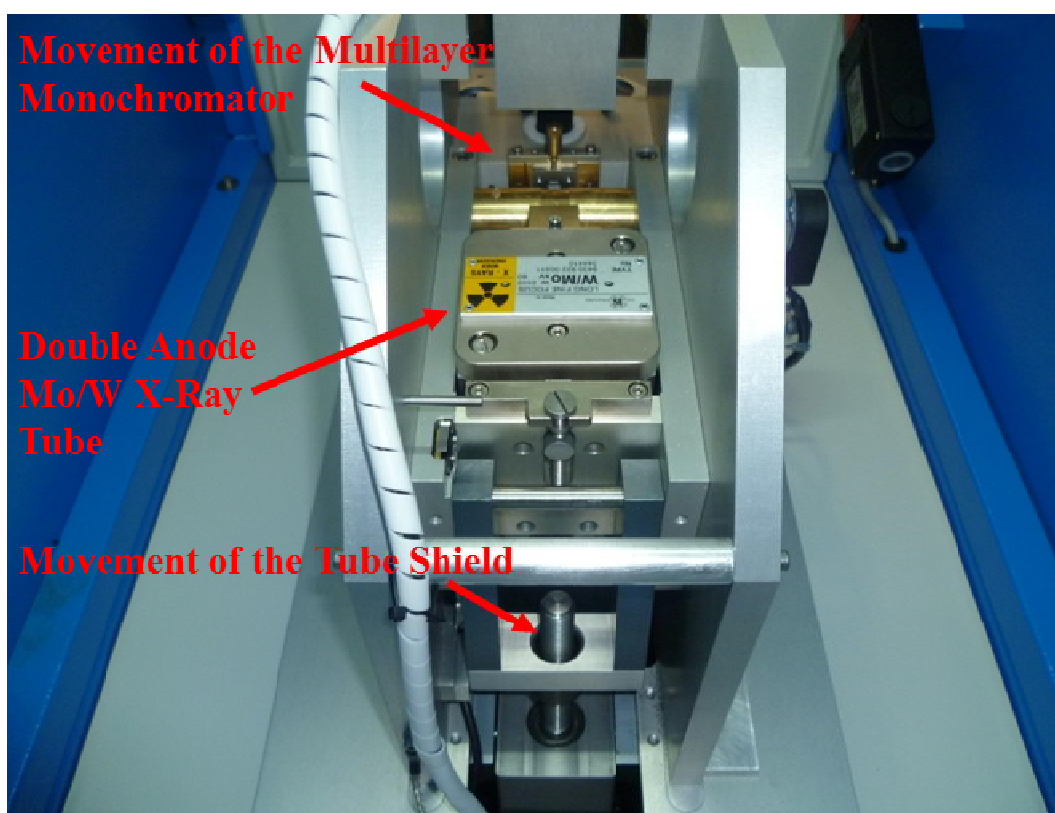


Figure 2.33: Back view: Step motors plus optical encoders assure a high angular accuracy

As in TXRF analysis sample is required liquid form so in case of the solid sample it needs to be taken in liquid form. Below (Figure 2.34) is the different step in the preparation of the sample for TXRF measurement;

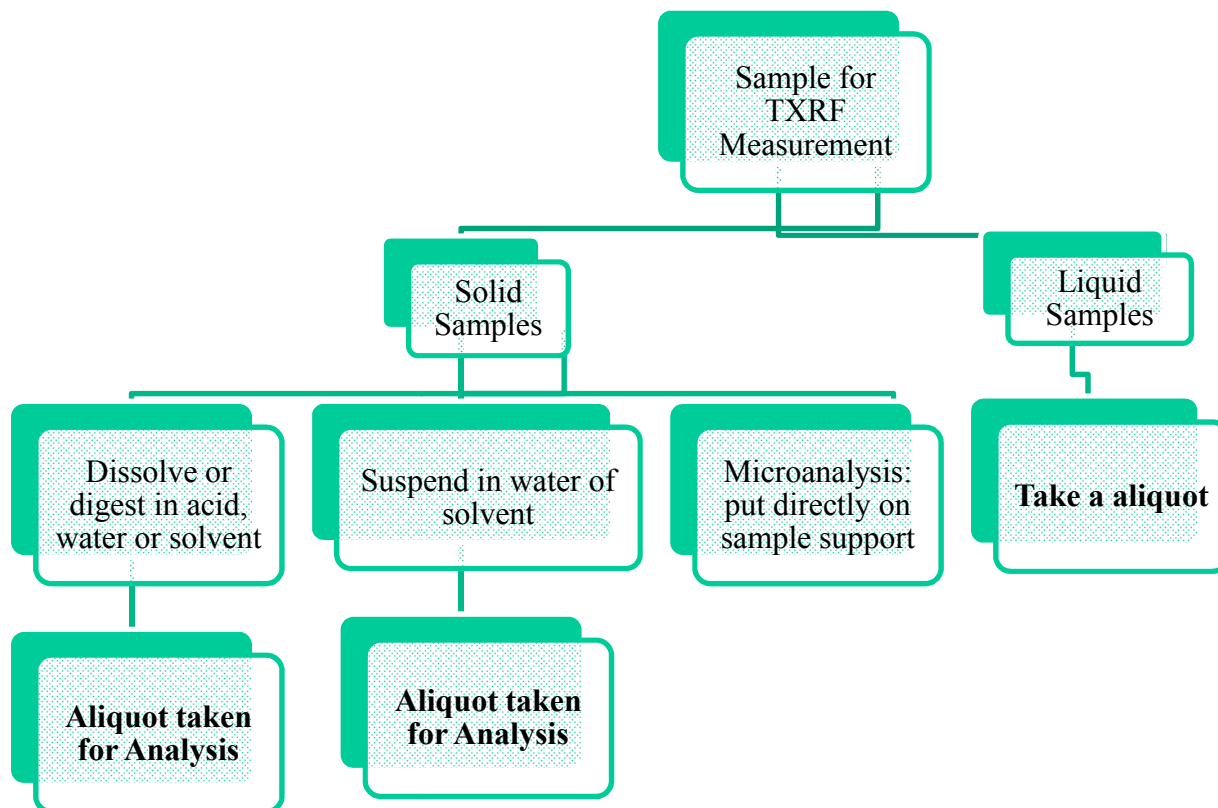


Figure 2.34: Sample processing in TXRF analysis

The internal standard is added to aliquot and the solution was homogenised on a shaker. A 2-10 ul of sample is pipette out on sample carrier and after drying under IR lamp kept for analysis (Fig 2.35)

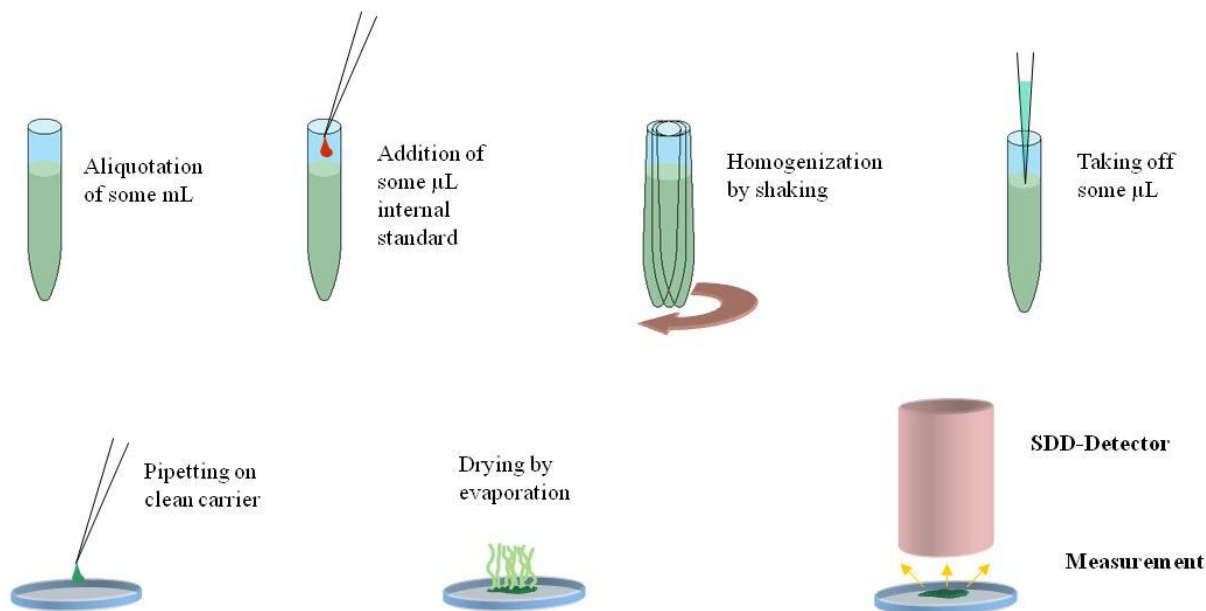


Figure 2.35: Preparation of sample for TXRF measurement

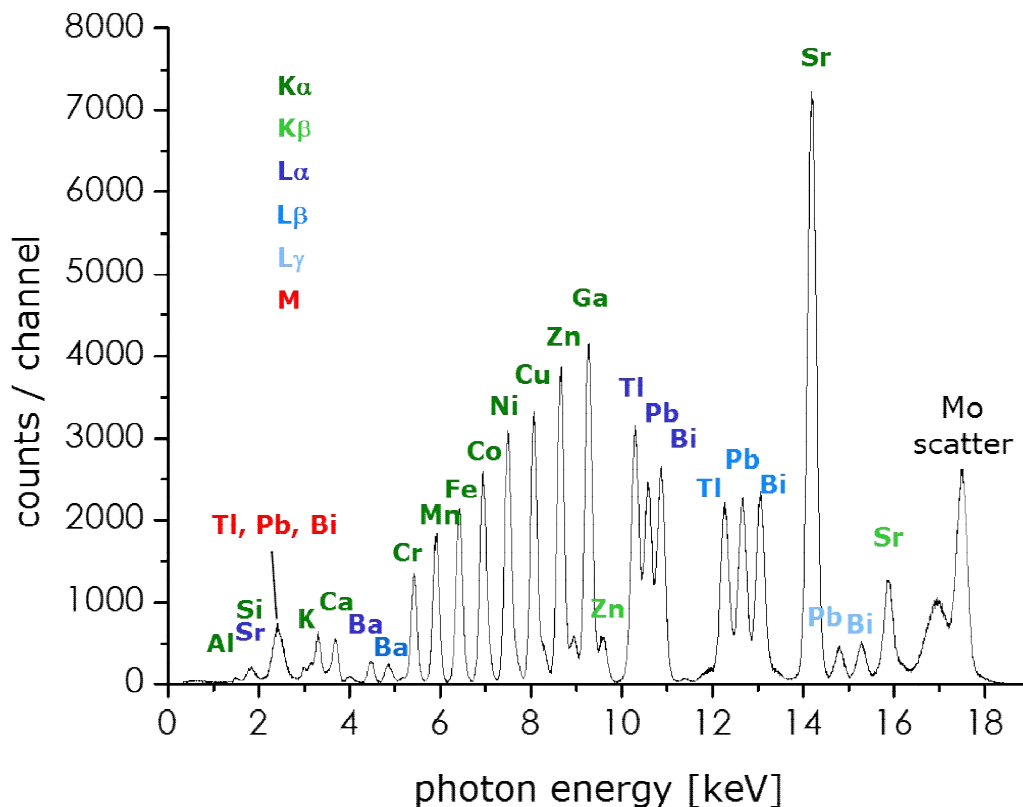


Figure 2.36: TXRF Spectrum of multi-element standards (ICP-IV) excited by MoK α beam

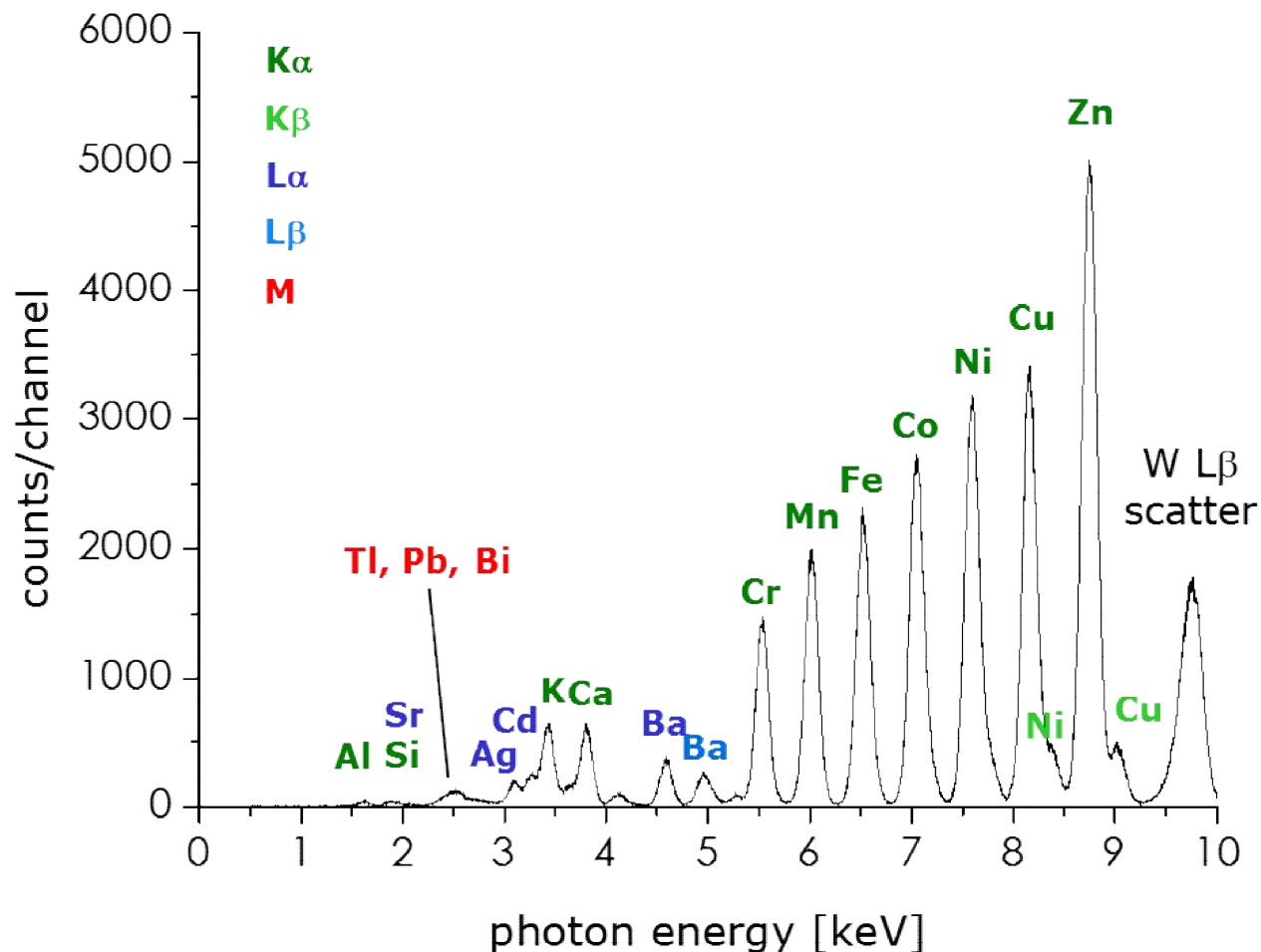


Figure 2.37: TXRF Spectrum of multi-element standards (ICP-IV) excited by $W L_{\beta}$ beam

Figure 2.36 and Figure 2.37 above showed the TXRF Spectrum of multi-element standards with 50 ppm concentration excited by $Mo K_{\alpha}$ and $W L_{\beta}$ beam respectively. The standard was prepared by dilution of Merck ICP-IV reference standard. The spectrum was recorded for 300 seconds and considering Ga as the internal standard concentration of remaining element was estimated. The figure showed the comparison of expected concentration with an observed concentration of different elements.

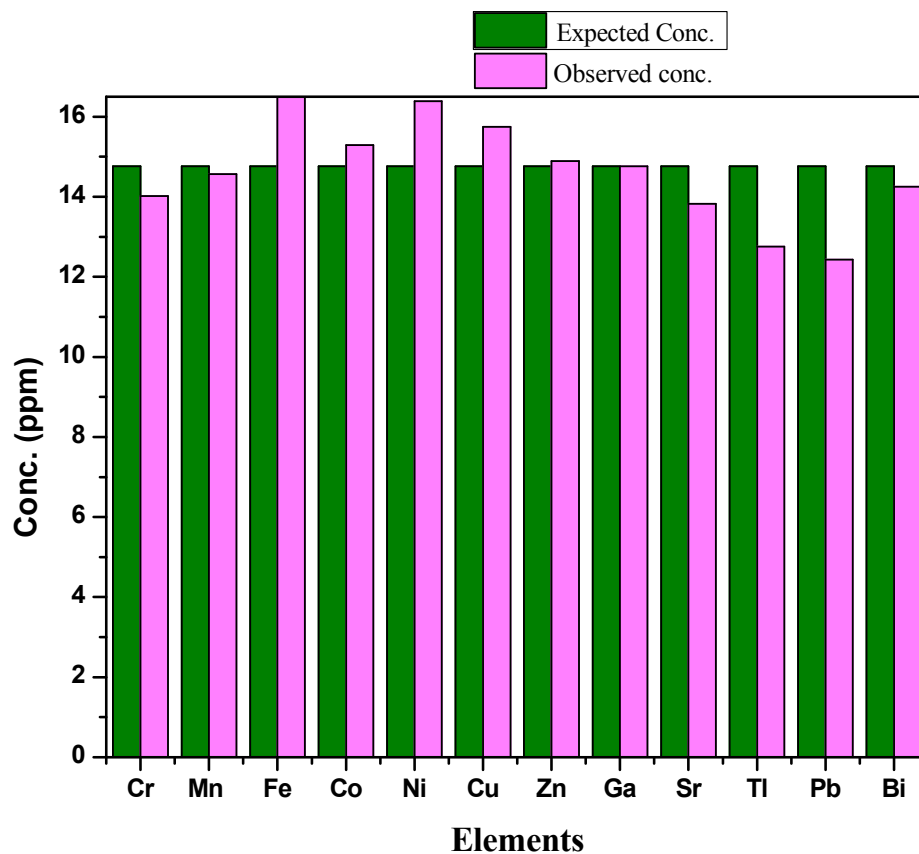


Figure 2.38: Comparison of expected and observed concentration in the multi-element standard

The concentration of elements present in the standard is evaluated using calibration and sensitivity provided with the instrument and the results were found to be within 10% of the relative error. The precision of the measurement of the concentration of each element was calculated as a relative standard deviation and found within 5%. The observed concentrations of elements which are present in the environment as aerosol and water contaminants e.g. Fe, Co, Ni, Cu and Zn were found in comparatively larger concentrations. The determination of elements in part per billion (ppb) concentration range with the precision and accuracy required clean room conditions.

CHAPTER 3

STUDY AREA “MUMBAI HARBOUR BAY (MHB)” AND SAMPLING

3.1. Introduction

The coastal zone represents that part of the land affected by its proximity to the sea and that part of the ocean affected by its proximity to the land. The coastal zone, extending from the coastal planes to the outer edge of the continental shelves, matches the approximately the region that has been alternately flooded and exposed during the sea level fluctuations of the late Quaternary period. The coastal region houses 60% of the human population throughout the world occupies 18% of the surface of the globe. This region also houses two-thirds of the world cities with a population of 1.6 million people are located. It also supplies approximately 90 % of world fish catch and 75% to 90 % of global sink of suspended river load and its associates.

Pollution in India in different aquatic environment arises from land-based sources, industrial and domestic waste, agricultural runoff and associated shipbuilding, breaking and port activities are becoming increasingly significant. The crops of recently started, coastally located industries use seawater as a source and coastal domain as a sink of altered seawater (e.g. composition, temperature and density). These pose newer, more direct threats to sensitive eco-areas. The first compilation of the type and quantum of a pollutant into the coastal ecosystem of India [217] are given in Table 3.1 (below):

Table 3.1: Quantum of a pollutant into the coastal ecosystem of India

Sr. No.	Input/pollutant	Quantum – Annual
1	Sediment	1600 million ton
2	Industrial effluents	$50 \times 10^6 \text{ m}^3$
3	Sewage largely untreated	$0.41 \times 10^9 \text{ m}^3$
4	Garbage and other solids	$34 \times 10^6 \text{ ton}$
5	Fertilizer residue	5×10^6
6	Synthetic detergents residue	1,30,000 ton
7	Petroleum hydrocarbon (Tar bull residue)	3,500 ton
8	Mining rejects, dredged spoils and sand extractions	$0.2 \times 10^6 \text{ ton}$

These have brought alarming levels of contaminants surrounding the many coastal and harbour cities of the world aquatic regions due to various anthropogenic discharges. In the case of the creek ecosystem, it became more critical due to its landlocked and relatively stagnant nature. The trace and toxic elements such as Cu, Fe, Pb, and Zn etc. are brought into the coastal zone in the form of dissolved and particulate fluxes from industrial effluents, sewerage discharge from the city and due to chemical weathering. Though it has been established that surface water is the most obvious medium of pollution assessment, pollutant concentration in sediments provides a more stable means of obtaining an indication of the state of associated water. Sediments can also serve as sorbents or concentrators for various

inorganic and organic chemicals. The evaluation of the possible interactions of various anthropogenic pollutants in creek sediment, therefore, assumes significant importance.

Apart from the abovementioned sources, the Submarine Groundwater Discharge (SGD) is generally a significant source of fluxes of trace elements and metals to the marine environment [78, 79]. SGD is the direct discharge of groundwater into the sea and includes re-circulated sea water. It is the pathways for the freshwater and dissolved solutes from land to marine system. Globally it is estimated that 15-20% of nutrient in sea discharged through SGD. The SGD is important for the marine geochemical cycles of elements and can lead to environmental deterioration of coastal zones. The assessment of SGD and its impact is much more difficult compared to a river discharge as there is no single gauge to these fluxes to the sea. Therefore a reliable and refined method is required to measure these fluxes.

Mumbai (latitude $18^{\circ} 53'$ to $19^{\circ} 04'$ N; longitude $72^{\circ} 48'$ to $72^{\circ} 53'$ E) is heavily populated industrial island city on the West coast of India (Fig. 3.1). Mumbai is surrounded by coastal marine environment comprising of the Arabian Sea to the west and a number of tidal inlets around it such as the Thane creek, Back Bay, Mahim creek, Versova creek, Ulhas estuary and the Bassein creek.

This city has a high humid climate with an annual average relative humidity of more than 60% [218]. The climate of Mumbai is highly influenced by the Arabian Sea. Generally, May is the hottest month of the year and the average temperature ranges between 32°C and 40°C . January is the coldest month and the average temperature is about 18°C . The sediment samples have highest percentage of particle size $<63\mu\text{m}$, followed by fraction belonging to $>63\mu\text{m}$. The average percentage composition of size fractions $<63\mu\text{m}$ and $>63\mu\text{m}$ are 71.83% and 28.17% respectively, indicating clay-silt texture of the sediment. The underlying rock of

the region is composed of black deccan basalt. The present study carried out in a bay near Mumbai, known as Mumbai Harbour Bay (MHB) which separate mainland from the city.

3.2. Mumbai Harbour Bay

Mumbai Harbour Bay (MHB) is located on the west coast of India (Figure 3.1). The bay is a triangular mass of brackish water which opens to the Arabian Sea in the South and the narrow end is fed by freshwater Ulhas River in the north. The Panvel River flows into the bay from the eastern mainland [219–221].

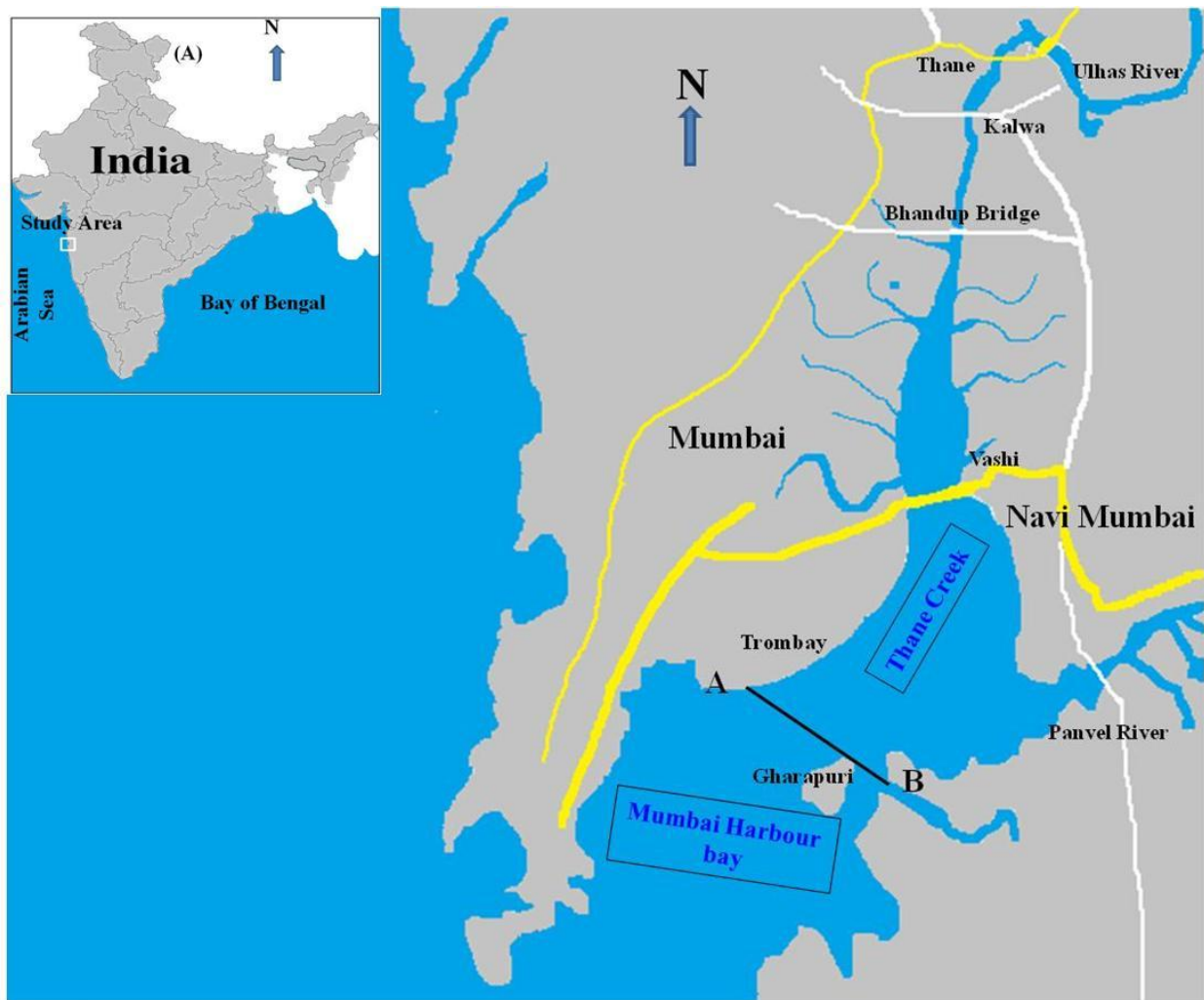


Figure 3.1: Mumbai and Mumbai Harbour Bay (MHB)

The average area of water surface of the bay is about 215 km² at high tide level and about 160 Km² at low tide level. The total volume of water at mean sea-level as calculated from the surrounding area is 9.1×10^{11} litres [219, 220]. The average tidal volume is 4.8×10^{11} litres [219]. The bay is subjected to wave actions and semi-diurnal tides.

3.2.1. Trans Thane Creek

The narrower, northern part of the bay is called Thane Creek lies between the city of Thane and the Arabian Sea at Trombay before (north to line AB) the Gharapuri islands. The creek (Fig 3.1.) is a triangular mass of brackish waters and widens out in the south. The creek has extensive mudflats along the intertidal zone on both banks. Lack of vegetation and extensive development, which includes surface quarrying for the construction materials, provides a large amount of lithogenic flux into the Thane creek. The creek area is rich in benthic organisms which are frequently harvested and consumed by locals. The bay has abundant mudflats and good coverage of mangroves; however, in recent years the mangrove areas are being intensively targeted for dumping garbage, disposal of sewage and also overexploited by salt industries, fishing, navigation and recreational activities.

Industrial complexes, including the textile mills of south and central Mumbai, the petrochemical, fertilizer and thermal plants at North Mumbai, the pharmaceutical and chemical complexes of Mulund, the engineering and metallurgical units at Thane and newly developed industrial belt of Thane-Belapur region which is about 20 km long and 2 km wide with an average area of 2650 hectares surrounds the creek.

3.2.2. Various discharges and water movement in the bay

Along the east and west sides of the bay, many industrial units like textile mills of South and Central Mumbai, the petrochemical, fertilizer, thermal plants, the pharmaceutical and chemical industries. MHB also houses ports thus witnesses the intense movement of cargo ships and often various mishaps have taken place resulted in released contaminants in water. In the past, the only source of wastewater to the bay was from domestic discharge. But in recent years, development of nearby areas for residential purposes and industrial complexes has resulted in increasing level of pollution in the bay. The creek ecosystem of bay known as Thane Creek, houses a number of major, medium and small scale industrial units largely involved in the manufacture, storage and use of chemicals, petrochemicals, pharmaceuticals and fine chemical products, pesticide formulation, etc. Of the 1800 odd industries registered in the area, nearly 50 could be termed as major and the rest classified as small and medium scale. The effluent discharges both treated and untreated are let into the creek. The discharges from the western side of the city are dominated by the sewerage and industrial effluents. Industrial complexes, including the textile mills of South and Central Mumbai, the petrochemical, fertilizer and thermal plants at Chembur, the pharmaceutical and chemical complexes at Vikroli, Bhandup and Mulund, the engineering and metallurgical units of Thane-Belapur region surround the creek and discharge their toxic effluents into it. The Mumbai harbour in the west and the new Navy Seaport in the east, handling more than 30 million tones yr^{-1} , additionally contribute to the pollutants to the creek by way of leakage and spill. Being landlocked with very few freshwater inlets and a large amount of sewerage and industrial effluent discharges, the creek is relatively stagnant.

Apart from these industrial and domestic discharges in the bay following sources also contributes to the total discharge and responsible for water movement in the bay is caused by the following factors:

1. Tidal water
2. Riverine input
3. Freshwater input during Monsoon
4. Input from submarine groundwater discharge (SGD)

Of these four, rivers contribute a small fraction towards the movement of water in the bay as compared to the factor caused by the volume of tidal water (4.8×10^{11} litres). SGD was not studied till date in the present study area. As far as rain on land is concerned, Mumbai receives annual rainfall from 1800 mm to 2400 mm with an average value of 2170 mm. More than 95% of the annual rainfall occurs during the four months period of June to September due to southwest monsoon winds. Discharges during the monsoon do not affect the tidal curves, as these are small compared to the tidal volume. However, the flow into the bay by the first two factors during the monsoon causes a considerable renewal of water in the bay.

3.2.3. Tidal flow patterns and dilution

Three major streams (Figure 3.2) are noticeable during both high and low tides:

1. Stream flowing near the Trombay shore
2. Stream flowing near the Elephanta shore (middle stream)
3. Stream flowing between Elephanta and Nhava Island

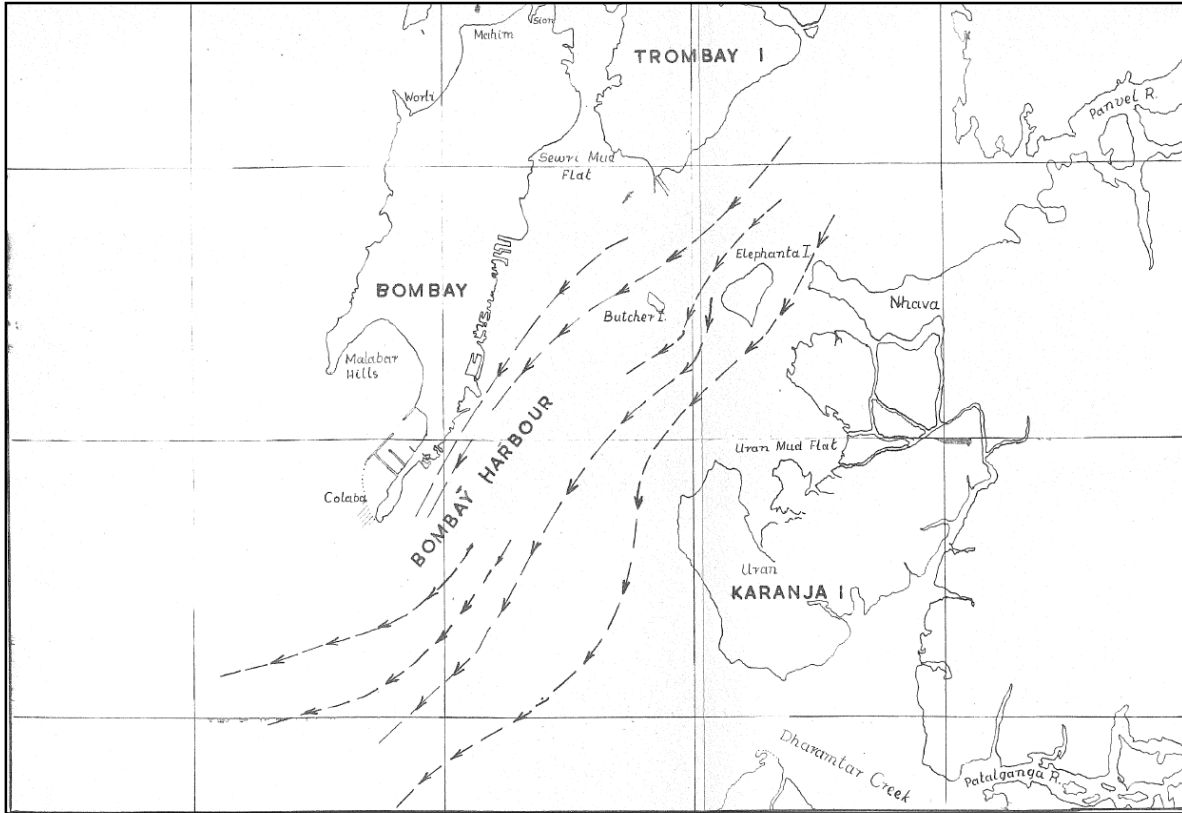


Figure 3.2: General direction of ebb current in MHB [219]

During high tides, water flowing near Trombay shore and near Elephanta and Nhava moves mainly into the creeks to the east of the bay. The pattern of water movement and dilution availability in the bay was determined in 1959 with a tracer discharge. A total of 4Ci of ^{24}Na were dissolved in 180000 L of seawater and discharged through a pipeline at the peak of high tide for about 30 hrs. The movement of radioactivity was traced with underwater probes and dilution was measured in water samples collected at various intervals. The observations were:

- a. Discharged radioactivity returned to the outfall on the reversal of the tide,
- b. There was an immediate dilution by factors of 10^4 - 10^5 for a 0.3 L/s
- c. Discharge Patches of radioactivity remained close to the shore

In a second experiment conducted, 20Ci ^{42}K dissolved in 810000 L of seawater were released in 3 hrs through the outfalls (700 L.s^{-1}) at low tide. Observations confirmed the earlier pattern of dilution and tidal oscillations. Most of the earlier studies carried out in this region have focused more on the main channel of the estuary (Ulhas) or larger creeks (Thane), especially near major industrial units [222–225].

3.3. Sample Collection from Study area

In the proposed study requirement was to carry out marine sampling in MHB using hired motorboat. It was ensured that boat was suitable to carry out activities in the field related to sampling, storing, providing sample support system and transportation for various matrices of the environment. Initially, the sampling in MHB was carried out in the using a small boat powered by engine motors (Figure 3.3). The boat was not suitable for deep-sea sampling.

Thus, we hired a sampling vessel with approximately 7.0 m monohull (Figure 3.4) powered by twin 125HP, 2 stroke outboard engines with trailer and tow vehicle (4WD) and a maximum speed is 28 knots. The boat was registered with Maharashtra Maritime Board, Mercantile Marine Department, Govt. of India or competent authority for operation as a safe commercial workplace. The vessel was certified for operations up to 15 nautical miles offshore enabling access to the edge of the continental shelf off Mumbai coast and can carry a maximum of 6 persons. The boat had additional dinghy of approx. 3 meters powered by a 30hp 2 stroke outboard motor. The boat was equipped with safety equipment including life jackets, flares, V-sheet, whistle, torch, horn, life buoys, radio, charts, bucket & lanyard, compass, anchor, fire extinguisher, ice slabs, small refrigerator, ice box, etc.



Figure 3.3: Small motor boat used for sampling

In the coastal zone, the sea floor type can change greatly over small distances. A precise and reproducible positioning of the sampling location was insured which was adequate for scientific studies. Samples must be collected and analyzed replicate cores at key stations to establish the extent of variability over small spatial scales. The aim was to observe the variability primarily due to real field variability and not to variations in ship navigation. The ship's

navigator had the knowledge to record the precise latitude and longitude of the sampling site and be able to reposition at the desired sampling site



Figure 3.4: Boat (with small dinghy) used for the sampling

The different environmental samples (surface seawater, groundwater, suspended sediment and sediment core) were collected from a different location from Mumbai Harbour Bay (MHB) and some part of Arabian Sea as shown in Figure 3.2. The surface water was collected to estimate the activity concentration of ^{223}Ra and ^{224}Ra and different trace and toxic elements. Similarly, the groundwater was collected to estimate the activity concentration of ^{223}Ra and ^{224}Ra which was used for the estimation of submarine groundwater discharge. Table 3.2 gives the GPS value of the different sampling locations in the present study area.

Table 3.2: GPS value of sampling locations in the study area

Location No.	Latitude	Longitude
1	19°11'46.01"N	72°59'07.46"E
2	19° 09'01.23"N	72°58'45.85"E
3	19°08'59.90"N	72°58'49.00"E
4	19° 08'58.18"N	72°58'54.39"E
5	19° 07'34.67"N	72°58'12.86"E
6	19° 06'36.90"N	72°58'22.20"E
7	19° 05'33.34"N	72°57'38.01"E
8	19°05'11.10"N	72°58'13.20"E
9	19° 04'09.19"N	72°58'45.56"E
10	19° 03'58.14"N	72°58'14.79"E
11	19° 04'01.80"N	72°57'21.72"E
12	19°04'03.20"N	72°57'27.00"E
13	19°03'22.32"N	72°57'49.78"E
14	19° 01'28.78"N	72°57'29.55"E
15	19° 01'10.46"N	72°58'15.53"E
16	19° 00'51.61"N	72°59'02.90"E
17	18°59'54.71"N	73° 01'46.38"E
18	18°59'37.40"N	72°57'27.30"E
19	18°59'54.50"N	72°55'21.79"E
20	18°57'43.82"N	72°57'27.02"E
21	18°59'13.05"N	72°52'58.15"E
22	18°57'31.20"N	72°55'22.20"E

23	18°56'21.25"N	72°55'15.90"E
24	18°54'59.92"N	72°52'17.61"E
25	18°56'11.70"N	72°52'19.37"E
26	18°57'29.43"N	72°53'7.04"E
27	18°50'34.30"N	72°49'27.7"E
28	18°50'10.00"N	72°48'24.1"E
29	18°49'45.60"N	72°47'20.8"E
30	18°49'21.20"N	72°46'17.5"E
31	18°48'56.70"N	72°45'13.6"E

3.3.1. Collection of Surface seawater for Radium Analysis:

In MHB the surface water (1 m deep from the surface) was collected onboard the ship using submersible pumps. Initially, water was run for a few minutes before collecting. The delayed coincidence counting method has extremely low background 0.03 dpm and .0003 dpm for ^{224}Ra and ^{223}Ra respectively. The limit of quantification for a counting system is estimated as:

$$LoQ = 10 \frac{\sqrt{Counts}}{time \times efficiency}$$

Considering counting time 2 hrs the limit of quantification for ^{224}Ra is 0.3 dpm. Thus considering only counting uncertainty (error), samples with 0.3 dpm activity can be measured with delayed coincidence counter. But, the uncertainty propagation in the estimation involves all the parameters e.g. counting time, decay time, counts in the each channel etc. as discussed in Chapter 2. Taking all the parameters, Garcia et al. [183] has shown that the uncertainty in estimation decreases exponentially with sample volume and it is not impossible to achieve uncertainty better than 4%. The limit is due to the propagation of uncertainties from other

parameters like efficiency, background and others. The activity range of ^{224}Ra in Mumbai Harbour Bay) was in the range of 15-50 dpm.100L⁻¹ and in Arabian Sea was 7-20 dpm.100L⁻¹. Considering activity concentrations range in the study area and error about 10%, about 60 liters and 100 liters from bay and Arabian Sea was collected. Representative Sampling reflects releases, distribution and concentration of radionuclides. Techniques involve passage of water through filters to remove particulate matter followed by pre-concentration on MnO₂ coated acrylic fiber as described below.

3.3.1.1. Preparation of MnO₂ Coated acrylic fiber:

A heating bath attached with a temperature controller unit and an (Resistance Temperature Detector) RTD Pt 100 temperature sensor is assembled (Figure 3.5) for the preparation of MnO₂ coated acrylic fiber. The system was tested for leakage and heating of water at desired temperature for a time period of 4 days. The acrylic fiber was allowed to soak in a water bath overnight. The fiber was rinsed with distilled water for 20 minutes. The fiber was then allowed to soak in 0.1 M NaOH and 1M HCl solution sequentially, for half an hour and then rinsed with distilled water. A saturated solution of KMnO₄ was prepared and the fiber was allowed to soak in the solution at about 60 °C for 3 days. KMnO₄ was converted to MnO₂ as per following reaction equation:



The MnO₂ formed in-situ is attached to the acrylic fiber. The filters were rinsed with distilled water until the Mn stops running off the fibers (until rinsing water is clear). The MnO₂ coated fibers were dried and kept in zip lock plastic bags, ready for use.

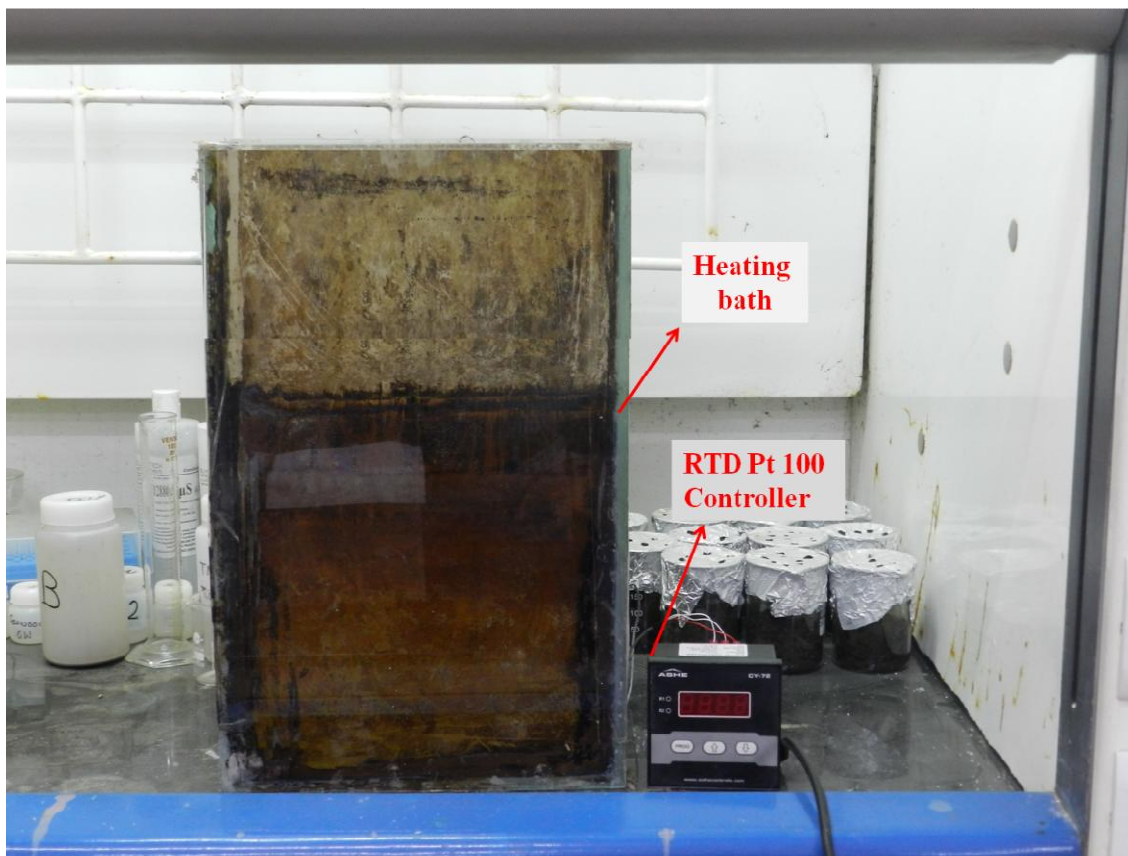


Figure 3.5: Heating bath assembly for preparation of MnO₂ coated fiber

3.3.1.2. Adsorption of Ra on MnO₂ fiber:

Surface molecules of solid complexes are subjected to imbalances of their chemical forces or surface energy. This dispersed solid phase tends to lower its surface energy by reducing its surface area or by adsorbing adjacent molecules and ions dispersed in the liquid phase [226]. Those solids having as their sole constituents one or more metallic cations combined with the elements of water, hydrogen and oxygen, known as hydrous metal oxides. This group includes metal oxide, metal hydroxide and metal oxy-hydroxides that are at least partially hydrated. Hydrous metal oxides have been found to exhibit rapid adsorption of cations ([227]. In recent years, many researchers have applied metal oxides for the adsorption of heavy metals from water systems [228–230]. Hydrous manganese oxide belongs to those metal oxides thought as natural

scavengers of heavy metals in water systems. Manganese oxide has the large surface area, microporous structure, and OH functional groups capable of reacting with metals and other specifically sorbing ions, thus hydrous manganese oxide can strongly interact with a number of chemical species, and hence it is a good adsorbent in aqueous environments [231].

The point of zero charge value of hydrous manganese oxide is about 1.5 – 4.5, thus it is a kind of surface acidic oxides and the charge of the hydrous oxide depends on the pH of the medium. Normally, manganese oxide is used as an adsorbent to remove heavy metals from wastewater as the surface charge of is generally negative [232]. The fine particle size of pure hydrous manganese oxide is very difficult to separate from the water phase or to infiltrate through. Therefore, pure hydrous manganese oxide is not favourable as a filter media. However, coating manganese oxide on some media surface improves the solid-liquid separation and thus provides a good adsorbent for heavy metals from wastewater.

The minerals typically occur as thin layers of fine-grained and poorly crystalline mixtures. It has been concluded that for manganese oxides, the predominant minerals are manganese (IV) related to the terrestrial minerals todorokite, birnessite and nsutite. Disordered phases showing only short-range crystallographic order include δ -MnO₂ and hydrated ferric oxyhydroxide polymer (incipient goethite) [233]. The manganese oxides have more variable mineralogy compared to other oxides such as aluminium or iron oxides, since it may contain Mn³⁺ and Mn²⁺ besides Mn⁴⁺ and for the charge balancing foreign ions as Li, Na, K, Ca, Ba, Al and Fe are easily accommodated in the structure. Thus, manganese oxides are normally non-stoichiometric compounds [234]. The radium is present as Ra²⁺ in the saline water which has high affinity to MnO₂. Thus passing the seawater through MnO₂-fiber at flow rate less than 1 liter per minute Ra got adsorbed quantitatively.

3.3.1.3. Pre-concentrated of Radium on MnO₂ fiber from seawater in the laboratory:

Initially, we used to bring about 60 litres of seawater to the laboratory and radium from seawater were pre-concentrated as shown in Figure 3.6. Seawater was pumped from 1st bucket through two pre-filter to 2nd bucket. Then filtered seawater was passed through MnO₂ fiber using the peristaltic pump.



Figure 3.6: Radium Pre-concentration on MnO₂ fiber system in the Laboratory

3.3.1.4. Design and Fabrication of in-situ pre-concentration sampling assembly:

The above process required transportation of seawater from field to lab which needs lots of manpower. A small sampling assembly was designed and fabricated to have in-situ pre-concentration of radium from seawater. Figure 3.7 shows the schematic diagram of the sampling assembly used in the present study. The seawater was allowed to pass initially through pre-filter (0.5 μm) with help of submersible pump to remove suspended particles and silt load. Filtered seawater then passes through a column containing manganese impregnated acrylic fiber (~25 g dry weight) at the flow rate less than 1 lpm (~ 0.8 lpm). This flow rate allows the

quantitative adsorption of Ra onto the MnO_2 -fiber [184]. Figure 3.8 gives the picture of MnO_2 fiber, Sample holder, Pre-filter and sampling assembly during their use during sampling.

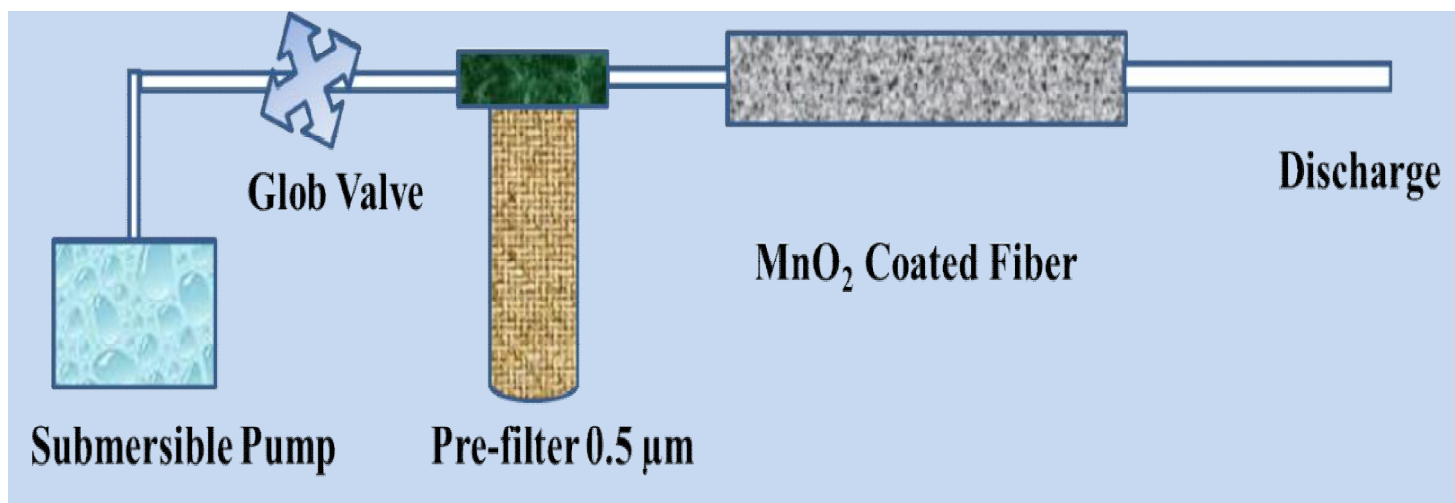


Figure 3.7: Schematic diagram of the in-situ pre-concentration assembly

3.3.1.5. Sampling Locations covered during different sampling trips

Most recent and detailed nautical charts available for the region of interest were taken into account for the design of field trips. Due consideration was given to likely sources of sediments and contaminants, such as rivers, municipal sewage or industrial outfalls, etc. The Table 3.3 gives the area covered during the sampling trips.

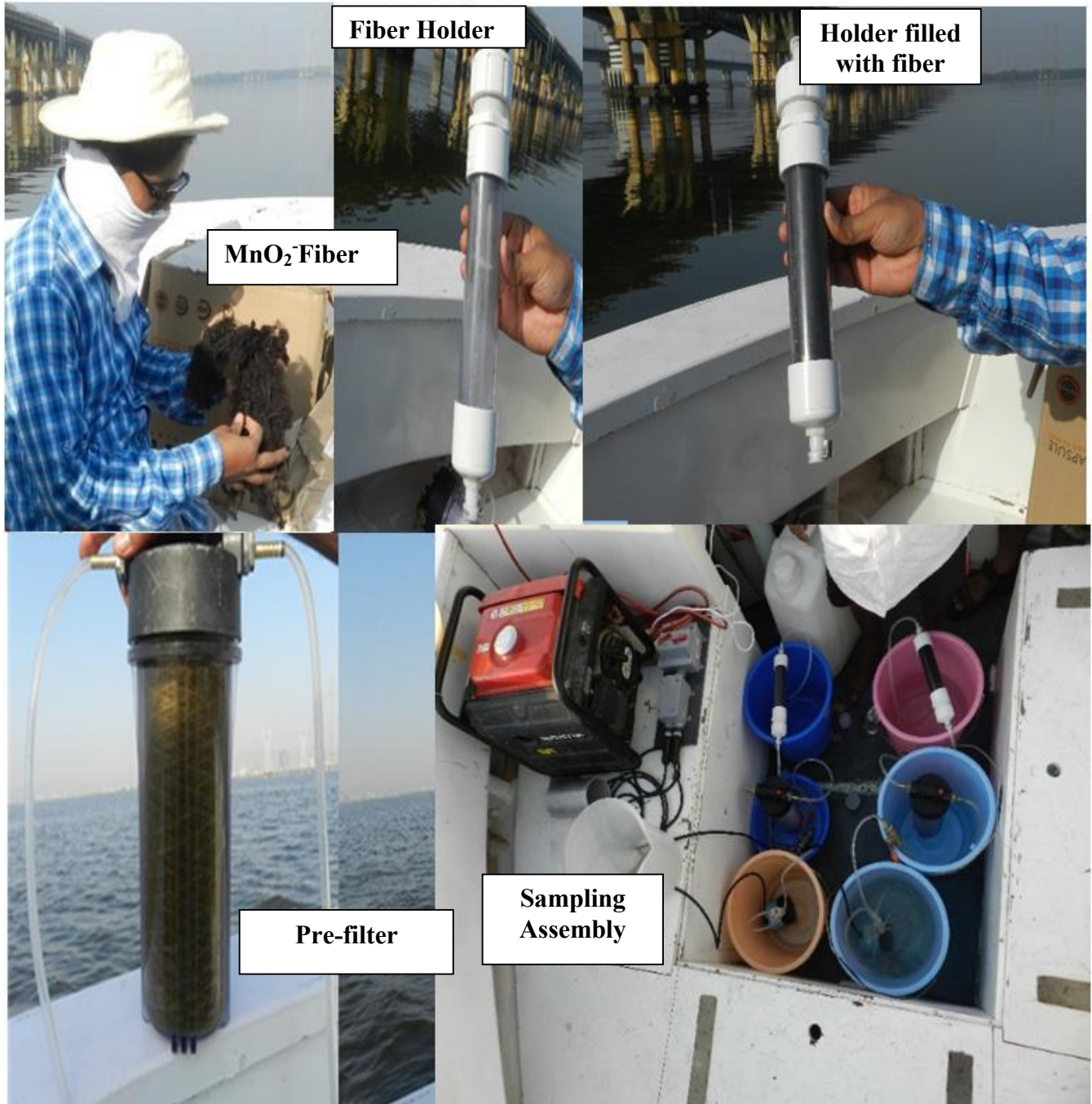


Figure 3.8: MnO₂ fiber, Sample holder, Pre-filter and sampling assembly

Table 3.3: Details of sampling trips and samples collected

Sr. No.	Trip	Time	Collection of samples
1	Trip-1	April 2016	Surface water from entire bay
2	Trip-2	March 2017	Surface water from entire bay
3	Trip-3	May 2017	Surface water from Arabian Sea
4	Trip-4	December 2017	Surface water from middle of the creek and groundwater

Seawater samples were collected from different locations of the bay at the different time April 2016 (trip-1), March 2017(trip-2), May 2017(trip-3) and December 2017(trip-4) as shown in Figure 3.9(A-D). Due to the influx of water during high tide, the radium enriched creek water can be diluted in comparison to low tide condition. Maximum samples were collected during the mid-tide condition as mid-tide scenario represents average mixing rates [235]. The samples from the open end of Bay and the Arabian Sea at equidistance of 2 km towards open sea were collected during the sampling trip-3(Fig. 3.9C). During the sampling trip-4 (Fig. 3.9C), surface seawater was collected only from the middle of the creek.

Fig. 3.9A:
Trip- 1

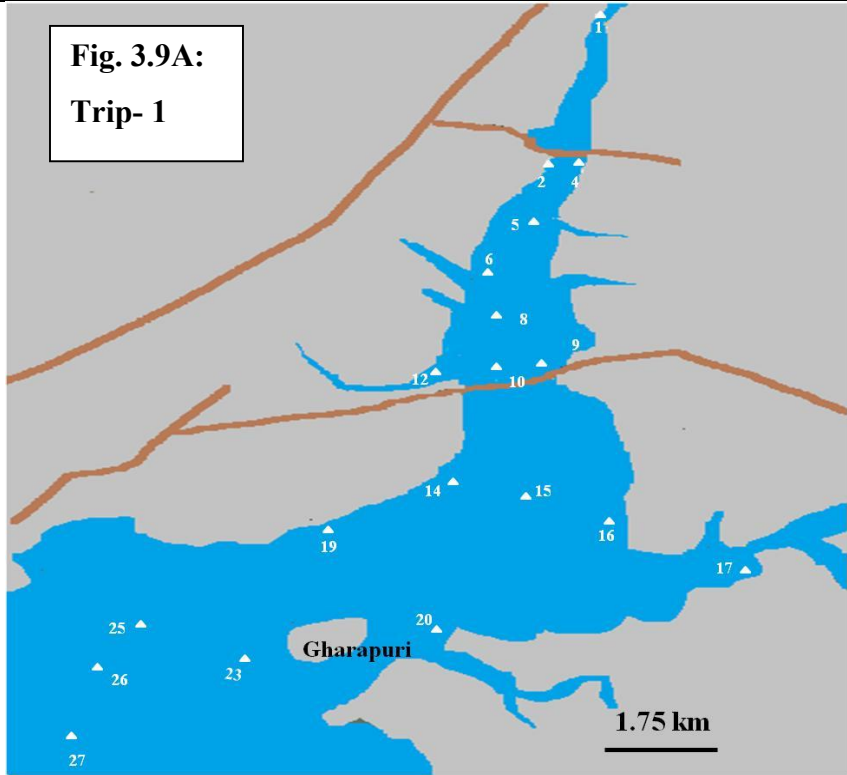
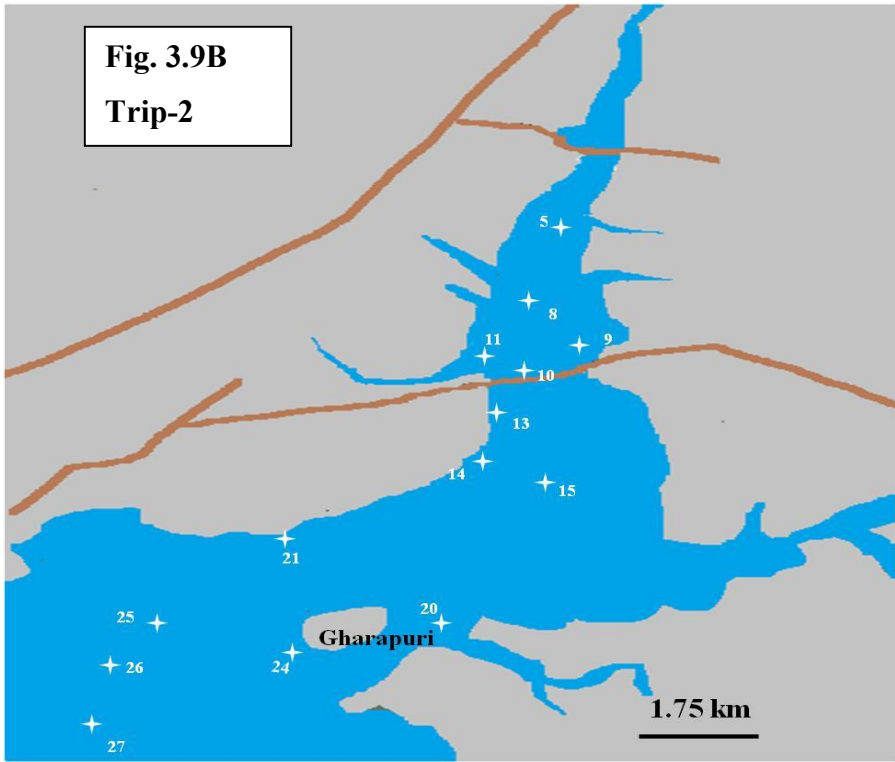


Fig. 3.9B
Trip-2



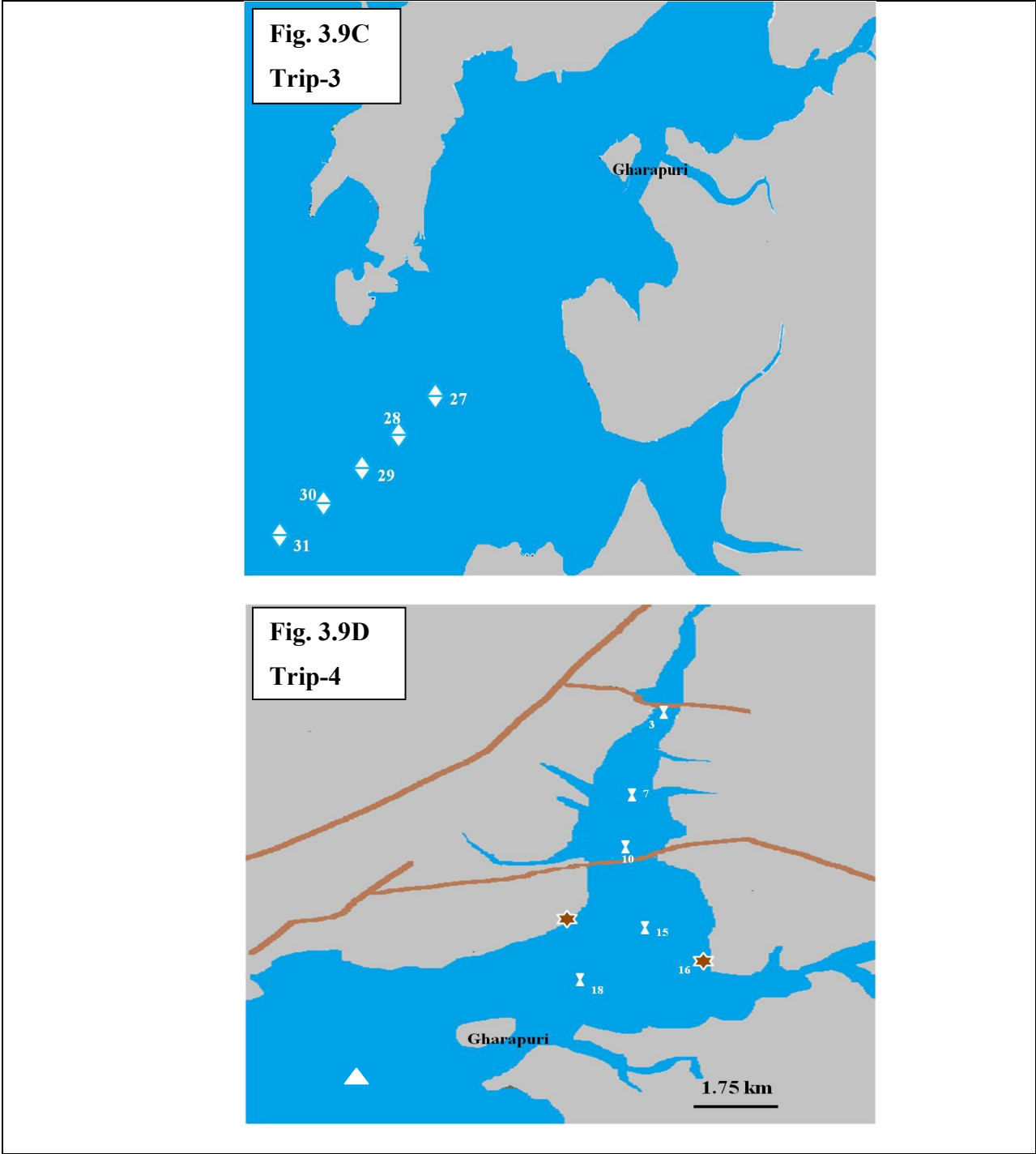


Figure 3.9: Sampling location covered during different sampling Ttips (1-4). Sampling locations (**▲**) covered during sampling trip-1, Locations covered (**★**) covered during sampling trip-2, Sampling locations; (**⌘**): for surface water and **★** : for groundwater during sampling trip-3 and Sampling locations (**◆**) covered during sampling trip-4

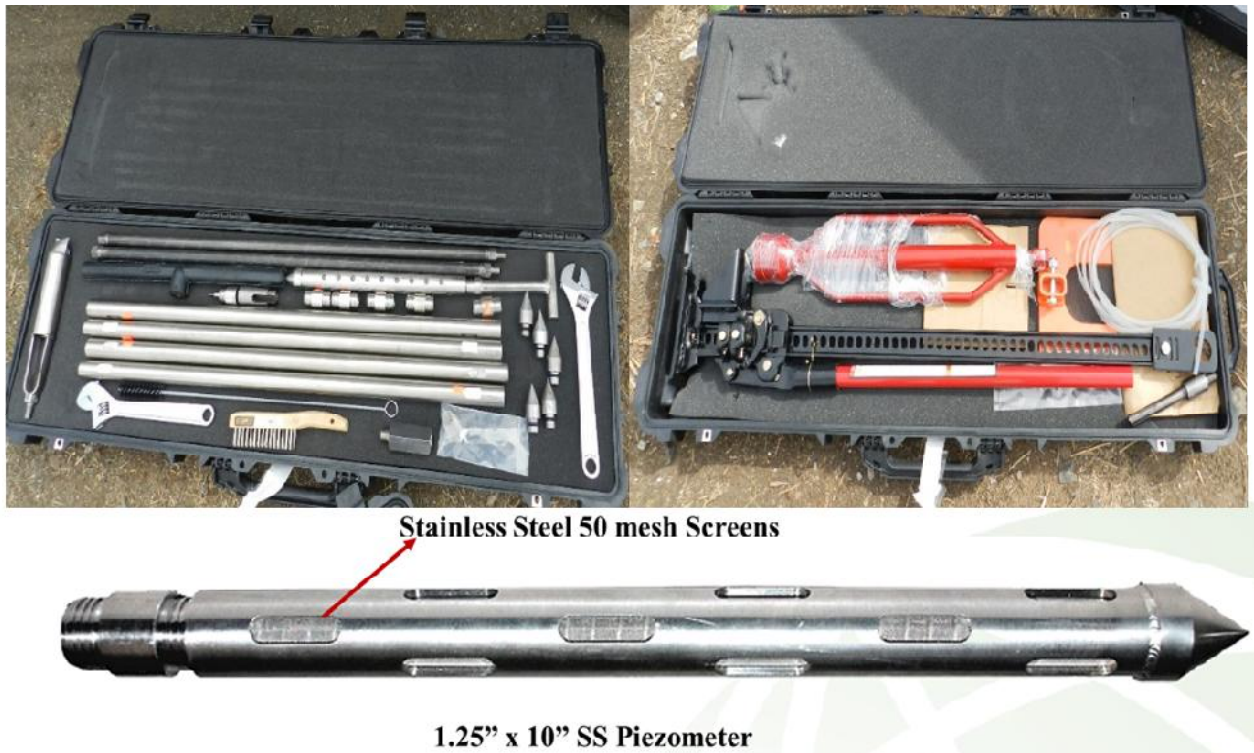


Figure 3.10: Piezometer groundwater sampler and groundwater sampling

3.3.2. Collection of groundwater for Radium Analysis:

The groundwater samples were collected during low tide near the locations 14 and 16 on nearshore (Fig. 3.3D) to find out the initial activity concentration ratio ($^{224}\text{Ra}/^{223}\text{Ra}$) during

sampling trip-4. The sampling end (Piezometer having SS mesh) of the device is inserted into the sediment to the desired depth (1.5-2.0 meter as per international recommendation for groundwater) with an available extension rod. The groundwater, seeped into piezometer through the mesh was collected using a peristaltic pump in the pre-cleaned plastic bottle (Figure 3.10).

3.3.3. Collection of Surface Water for trace and toxic elements Analysis:

To study the status of trace and toxic elements in the creek ecosystem (Thane Creek) of MHB, seawater from the city effluent discharge side of the creek (Location 11), mid-stream (Location 10) and Industrial side of the creek (Location 9) was collected, during the receding period of high tide. Water samples were collected in pretreated high-density polyethylene bottles and stored in the refrigerator as per APHA guidelines [236].

3.3.4. Collection of core sample for trace and toxic elements Analysis:

Bottom sediments consist of particles that have been transported by water, air or glaciers from the sites of their origin in a terrestrial environment and have been deposited on the floor of a river, lake, or ocean. In addition to these particles, bottom sediments will contain materials precipitated from chemical and biological processes. Natural processes responsible for the formation of bottom sediments can be altered by anthropogenic activities. Many man-made materials have entered bodies of water through atmospheric deposition, runoff from land, or direct discharge into the water. Most hydrophobic organic contaminants, metal compounds, and nutrients, which enter the water, become associated with particulate matter. This particulate matter then settles and accumulates in the bottom sediments. Under certain conditions, the contaminants in the bottom sediments may be released back into the water or enter the food chain. Consequently, bottom sediments are a sink as well as a source of contaminants in the

aquatic environment. These contaminants may pose a high risk to the environment on a large scale and hence need to be monitored at regular intervals. To understand the status of different trace and toxic elements, a sediment core sample was collected from Airoli, Vashi and Elephanta locations of the creek using gravity corer.

3.3.4.1. Gravity Corer

These devices are plastic tubes inside metal pipes 4-8 cm in diameter which is driven into sediments by weights atop the pipe. The gravity types are cheap and fairly easy to deploy & recover, but must be kept upright during retrieval to avoid disturbing the water-rich surface layers. They collect longer sediment sections than "grabs" up to 1-2 meters for gravity types and 10-20 meters for largest piston types. However, they are too narrow to sample benthic organisms reliably and they may not have enough sediment in 1-2 cm thick layers for all desired chemical analyses. They do not penetrate well in sandy sediments, and because they are top-heavy with the weight, they often tend to fall over instead of entering the sediment. The friction of sediment against the tube walls and the 'catcher' device placed inside the tube to prevent sediment from falling out during retrieval cause disturbances & smearing & shortening of sediment layers.

3.3.4.2. Collection of the sediment core sample

The gravity coring unit was lowered as slowly as possible into the sediments to prevent lateral motion of the pressure wave created by the descent of the corer. The collected cores were extruded vertically and sliced at 6.5 cm intervals. Care was taken during coring to ensure minimum disturbance of the sediment-water interface. Sediment core samples were collected in sealed polyethylene bags, numbered and taken to the laboratory for further processing and analysis. Figure 3.10 shows the collection of core sample using gravity corer in the study area.

3.3.5. Collection of Bulk mass of Suspended sediment:

The capacity of the suspended sediment to concentrate elements is higher compared to surface sediment which makes them better indicators for detecting sources of pollution in the marine ecosystem. The trace elements on suspended sediments show an important role in understanding of biological and geochemical cycle in marine ecosystem. A cylindrical time-integrated suspended sediment sampler (Figure 3.12) was used to collect the bulk mass of suspended sediments from the locations (5, 10, 19 and 23) as discussed by Pillai et al. [237]

3.3.6. Measurement of physicochemical parameters of seawater:

The fate and transport of many anthropogenic pollutants are determined by not only hydrological cycles but also physicochemical processes. Thus to understand the fate and transport of anthropogenic pollutants and the impact of human activities on natural waters, it is important to implement to have an understanding of the physicochemical parameters of the water system. In the present study the following water quality parameters were monitored, using **EUTECH** Instrument PC650 (Figure 3.13), at each sampling locations:

- pH
- Electrical Conductivity
- Total Dissolved Solid and Salinity



Figure 3.11: Collection of core sample using gravity corer



Figure 3.12: Deployment of suspended sediment sampler and collection



Figure 3.13: Multi-parameter kit (EUTECH Instrument PC650)

CHAPTER 4

ESTIMATION OF APPARENT WATER AGE AND MIXING PROCESS IN THE CREEK ECOSYSTEM OF MUMBAI HARBOUR BAY, INDIA

4.1. Introduction

The inflow of fresh water and desorption from freshwater particles, enrich coastal water in some of the radionuclides and high levels of various pollutant. Rapid urbanization, large-scale industrialization and uncontrolled sprawling settlements around many coastal and harbour cities of the world brought an alarming level of pollution to the surrounding marine ecosystem. It becomes all the more critical in case of creek ecosystem due to its landlocked and relatively stagnant nature. The evaluation of possible interaction and behaviour of various anthropogenic pollutants in any creek system have significant importance. The distributions of the naturally occurring radionuclide, nutrients, trace and toxic elements are subjected to chemical differences between coastal and offshore water. The distributions also depend on how fast the sea water in the creek is transported to open sea. The removal or circulation of the creek can provide insights into mobility of contaminants in the creek. The flushing rate, residence time and apparent age of water are used to describe how long the water remains in an ecosystem. The apparent age is defined as the time a water parcel has spent in the water body after entering the system through one of its boundaries. The word apparent age denotes estimation of age based on radioactive decay of radium isotopes introduced to water mass; these are not direct measurements of the age

of the water mass itself. This type of analysis is useful for information concerning the history of dissolved components in the water masses sampled. The residence time is defined as “the time required for a water parcel to leave a given water body through its outlet to the sea. Both the residence time and apparent water age would have almost similar value for a steady state ecosystem(Moore et al., 2006). The apparent water age and resident time are controlled by many factors including tides, basin size and geometry, prevailing winds, and inputs from terrestrial and subsurface water.

Radium isotopes supply from the seabed, removal by radioactive decay and particle scavenging are major process affecting the distribution in the coastal marine environment. Desorption of Ra from suspended particles, as they pass into the salty estuarine water, is the primary factor controlling the riverine input of Ra to the bay since increasing the ionic strength of the water in contact with sediments reduces K_d and releases Ra into solution [239]. Increasing the mean particle size of the sediment reduced both the exchangeable Ra concentration and the ratio of the exchange equilibrium constants of the sodium and Ra[240]. Also, only a portion of the total Ra associated with the sediments was in ion exchangeable form, the rest being retained within the mineral lattice. Sediments containing abundant organic matter had lower K_d than the same sediments after the organic matter had been removed by gentle oxidation [125].

Because of its mean life is of the order of mixing of the ocean ^{226}Ra is distributed throughout the water column. The process involving particle scavenging have a more dominant role in the distribution of Radium. Since the mean life of ^{228}Ra is much shorter than the vertical ocean mixing time, its distribution is restricted to regions near its source of input, namely surface and near-bottom waters in contact with sediments in the ocean. In addition to the long-lived isotopes, short-lived ^{223}Ra and ^{224}Ra enter grained sediments and rivers. Because these isotopes

are recoil products, their fluxes often exceed those parents. However, their short half-lives restrict their penetration into the ocean and restricted in coastal area. The development of a technique (Discussed in chapter 2) to rapidly measure the low activity of ^{223}Ra and ^{224}Ra in seawater has opened its application to understand various processes in the coastal marine environment.

The four naturally occurring radium isotopes (^{223}Ra , $T_{1/2} = 11.4$ days; ^{224}Ra , $T_{1/2} = 3.6$ days; ^{226}Ra , $T_{1/2} = 1,600$ years and ^{228}Ra , $T_{1/2} = 5.75$ years) can be used as geochemical tracers for variety of environmental processes; like groundwater discharge, residence time, flushing rate and coastal water circulation pattern etc. Radium isotopes are produced by the decay of Th parent isotopes contained on terrigenous materials. In freshwater radium is highly particle reactive and supported by parent thorium. Mixing saltwater results in ion exchange transformation that causes rapid desorption of radium from particle surfaces into solution. The input of continual flux of radium in the creek from any location can result in a unique and constant isotopic composition providing a fingerprint of the source term. Activity concentration of radium isotopes, introduced into a marine ecosystem, influenced by both decay and mixing provides a timescale for estuarine mixing [241]. Moore and Jackson [238] have reported the apparent age of Okatee estuary, South Carolina using radium isotopes. Radium isotopic approach was also used for estimating apparent water age and residence times in other estuaries such as the Apalachicola Bay estuary in Florida [242], the Chao Phraya estuary in Thailand [243], as well as other coastal systems (Kelly & Moran, 2002; Moore, 2000c).

The present study carried out in a creek near Mumbai city, one of the heavily populated and industrialized cities of India. The creek known as Thane creek is part of Mumbai Harbour Bay (MHB) and separate mainland from Mumbai city. MHB houses a large number of industry

and ports which releases various pollutants. Apart from industrial and domestic release, the bay witnesses the intense movement of cargo ships and often various mishaps have taken place resulted in released contaminants in water e.g. collision of ships (Times of India, Aug 9, 2010).

4.1.1. Earlier Study in the present study area

The previous study carried in the MHB by Pillai et al. [219] to estimate the renewal rate (residence time). The study was based on the release of tracer (4 Ci ^{24}Na and 20 Ci ^{42}K in separate experiments) at a particular location at low tide and assumed that it was thoroughly mixed in bay water. The concentration of tracer in the bay (C_n) after mixing with the first tidal water may be given as:

$$C_1 = \frac{V_1 C}{V_1 + V_t} = k \cdot C; \text{ where } k = \frac{V_1}{V_1 + V_t} \quad \text{Eq. 4.1}$$

Where k is constant and represents the ratio of average volume at mean sea level to the volume at high tide. V_1 is the total volume of water at mean sea level in the bay at low tide level, V_t is the volume of tidal water in the bay, C is the concentration of an indicator in the bay at low tide level and C_n is the concentration of the indicator after n tide cycles. As $V_t = 4.8 \times 10^{11}$ litres and $V_1 = 9.1 \times 10^{11}$ litres

$$k = \frac{9.1}{4.8 + 9.1} = 0.65$$

The water renewal per tidal cycle $1-k = 0.35$ or 35%. Thus 35% of the old water gets out of the bay after a complete cycle of the high and low tide.

Similarly;

$$C_2 = kC_1 = k^2 C \quad \text{Eq. 4.2}$$

$$C_n = k^n C = (0.65)^n \quad \text{Eq. 4.3}$$

For reducing the concentration to 10% of the initial value, the number of tidal cycles n , will be given as:

$$0.1 = (0.65)^n \text{ or } n = 5.3 = 6$$

Therefore it takes 6 tidal cycles for the renewal of 90% of the old water of the bay. Pillai et al. [219] have assumed that tidal water entering the bay gets uniformly mixed during the period of high tide, which is a highly favourable condition for tidal renewal of bay water. Due to the slow rate (0.28 inch per minute) of the rise in water level, the remote area of the bay tries to adjust themselves to a slowly varying hydrostatic equilibrium. Thereby the in-coming fresh volume of the tidal water pushes back a good part of the existing water in the bay. Thus water in the remote areas of the bay is not readily available for thorough mixing with tidal water and as such one would expect a poorer renewal of water than the calculations indicated. The calculation gave an upper limit of the renewal rate in the harbour.

The main objectives of the present study were to use the short-lived radium isotope as a tracer for:

1. The estimation of apparent water age in the creek ecosystem using Radium Age Model and Radium Balance Approach
2. Estimation of flushing rate of creek water
3. Comparison of Radium Age Model and Radium Balance Approach
4. Estimation of horizontal dispersion coefficient

The all four naturally occurring Ra isotopes have been used for the study of the apparent water age and various processes in the marine ecosystem. Considering the renewal rate of water (3-4 days) in the study area, short-lived radium isotopes (^{224}Ra and ^{223}Ra) were used in the present study.

4.1.2. Apparent Water Age of Creek Water using Radium Age Model

^{224}Ra and ^{223}Ra behave conservatively and their concentration at any location will depend on the initial concentration, mixing and decay. Mixing rate for ^{224}Ra and ^{223}Ra will be the same and the observed activity can be expressed as;

$${}_{obs}^{224}\text{Ra} = {}_i^{224}\text{Ra} f_{224} e^{-\lambda_{224}t} \quad \text{(Eq. 4.4)}$$

$${}_{obs}^{223}\text{Ra} = {}_i^{223}\text{Ra} f_{223} e^{-\lambda_{223}t} \quad \text{(Eq. 4.5)}$$

Where ${}_{obs}^{224}\text{Ra}$ and ${}_{obs}^{223}\text{Ra}$ are the observed activity concentrations for ^{224}Ra and ^{223}Ra respectively for a particular location, at the time of sampling; ${}_i^{224}\text{Ra}$ and ${}_i^{223}\text{Ra}$ are the initial activity concentration for ^{224}Ra and ^{223}Ra respectively; f_{224} and f_{223} are the fraction of ^{224}Ra and ^{223}Ra respectively available at sampling location; λ (days⁻¹) is the decay constant and t (days) is the time elapsed since the ^{224}Ra and ^{223}Ra were introduced in creek or apparent water age. The radium age model is based on assumptions (a) Radium input is dominated by one source with constant isotopic composition (b) No further addition of radium in the same water mass, (c) The radium isotopes are removed only by mixing and radioactive decay[241].

From equation (4.4) and (4.5) water age (t) can be calculated as (Moore, 2000b; Xu et al., 2013);

$$t = \left[\ln \left(\frac{AR_{obs}}{AR_i} \right) \right] / (\lambda_{223} - \lambda_{224}) \quad \text{(Eq. 4.6)}$$

Where, AR_{obs} refers the activity concentration ratio of the $^{224}\text{Ra}/^{223}\text{Ra}$ at specific sampling location and AR_i represents the initial activity concentration ratio of $^{224}\text{Ra}/^{223}\text{Ra}$ at the source.

The radium source defined as the point where the activity concentration ratio of $^{224}\text{Ra}/^{223}\text{Ra}$ (AR) is highest and assign the apparent water age ($t=0$) for that site [246, 247].

Moore and Jackson (Moore et al., 2006) used AR_i as the activity ratio in groundwater collected from piezometer or seepage meter. Similarly, in the present study, the activity concentration ratio of $^{224}\text{Ra}/^{223}\text{Ra}$ (AR) was analysed in the porewater collected using piezometer was considered as AR_i which corresponds to apparent water age ($t=0$).

4.1.3. Apparent Water Age of Creek Water using Radium Balance Approach

Radium age model assumed that radium added to water near the shore only which may not be true for the estuaries and salt marshes known for multiple sources. In such cases apparent age can be estimated using “Radium Balance Approach”, if the system is under steady state i.e. loss of tracer (radium) is balanced by input from sources. In the present study considering the creek in steady state, ^{224}Ra and ^{223}Ra were used to calculate the apparent water age. The addition of radium in the creek is from the river, groundwater, sediment, waste discharges and losses are due to mixing and radioactive decay. The radium balance approach equation for ^{224}Ra and ^{223}Ra can be represented as;

$$F\ ^{224}\text{Ra} = I\ ^{224}\text{Ra} (\lambda_{224} + 1/\tau) \quad \text{(Eq. 4.7)}$$

$$F\ ^{223}\text{Ra} = I\ ^{223}\text{Ra} (\lambda_{223} + 1/\tau) \quad \text{(Eq. 4.8)}$$

Where $F\ ^{224}\text{Ra}$ and $F\ ^{223}\text{Ra}$ is the total flux of ^{224}Ra and ^{223}Ra respectively to the system, $I\ ^{224}\text{Ra}$ and $I\ ^{223}\text{Ra}$ is the total inventory of ^{224}Ra and ^{223}Ra respectively in the system and τ (days) is the apparent water age of the system. Now dividing equations (4) and (5);

$$F(^{224}\text{Ra}/^{223}\text{Ra}) = I(^{224}\text{Ra}/^{223}\text{Ra}) * \frac{(\lambda_{224} + 1/\tau)}{(\lambda_{223} + 1/\tau)} \quad \text{(Eq. 4.9)}$$

Where $F(^{224}\text{Ra}/^{223}\text{Ra})$ is the activity concentration ratio of ^{224}Ra and ^{223}Ra to the system and $I(^{224}\text{Ra}/^{223}\text{Ra})$ is the activity concentration ratio of ^{224}Ra and ^{223}Ra in the system. The equation (4.9) can be solved for

$$\tau = \frac{[F(^{224}\text{Ra}/^{223}\text{Ra}) - I(^{224}\text{Ra}/^{223}\text{Ra})]}{[I(^{224}\text{Ra}/^{223}\text{Ra}) * \lambda_{224} - F(^{224}\text{Ra}/^{223}\text{Ra}) * \lambda_{223}]} \quad (\text{Eq. 4.10})$$

4.1.4. Study of Flow and Mixing of Creek Water to the offshore:

One of the objectives was to study the flow and mixing of creek water to open mouth of the bay and the Arabian Sea. The change in concentration or activity (A) with time (t) as a function of distance offshore (x) for a conservative radioactive tracer with a decay constant (λ) may be expressed as a balance of advection, dispersion, and decay as follows;

$$\frac{dA}{dt} = K_h \frac{\partial^2 A}{\partial x^2} - \omega \frac{\partial A}{\partial x} - \lambda A \quad (\text{Eq. 4.11})$$

K_h and ω are the dispersion and advection coefficient respectively. The study conducted earlier in the west coast of India on the distribution of radium provides evidence that dispersion dominates over onshore advection [248]. Thus considering $\omega=0$ and the boundary conditions ($A = A_0$ at $x=0$, $A \rightarrow 0$ as $x \rightarrow \infty$), equation (4.11) gives solution as;

$$A_x = A_0 \exp [-x\sqrt{\lambda/K_h}] \quad (\text{Eq. 4.12})$$

Where; A_x and A_0 is activity at distance x and 0 from the coast and λ = decay constant of radioactive tracer. Thus from the plot of $\ln^{223}\text{Ra}$ or $\ln^{224}\text{Ra}$ as a function of distance from the coast, K_h can be estimated from slope as;

$$m = \sqrt{\lambda/K_h} \quad (\text{Eq. 4.13})$$

4.2. Study Area and Sample Collection

The study was carried out in Mumbai Harbor Bay (MHB), located on the west coast of India (Figure 3.1). The funnel-shaped bay receives water from Panvel River, Ulhas River, Wastewater discharges and tidal waters from the Arabian Sea. As discussed in chapter 3, the

narrower, northern part of the bay, between the city of Thane and the Arabian Sea at Trombay before the Gharapuri Island called as Thane Creek (Figure 3.1). The creek receives effluents from various industries containing trace and toxic elements and acts as sinks for most of the pollutants [249]. Seawater samples were collected from different locations of MHB at the different time April 2016 (trip-1), March 2017(trip-2), May 2017(trip-3) and December 2017(trip-4) as discussed in Chapter 3 Section 3.3.1.5. The porewater (discharge through sediment pores) samples were collected during low tide near the location 14 and 16 on nearshore to find out the initial AR ($^{224}\text{Ra}/^{223}\text{Ra}$) during sampling trip-4. The samples from the open end of Bay and the Arabian Sea at equidistance of 2 km towards open sea were collected during the sampling trip-3 (Fig. 3.9C). Radium from seawater was pre-concentrated on MnO_2 fiber using in-situ sampling assembly, as discussed in section 3.6.1.1.

Fibers samples were washed with de-ionized water to remove the sea salts and particles as they may cause interference with the emanation of radon [244]. The samples were then hand squeezed and partially dried using an air blower to get water/ fiber weight ratio about 1.0. The water/ fiber weight ratio (1.0-0.3) allow achieving optimal radon emanation efficiency by having the ideal moisture content so that the maximum fraction of the produced radon enters the circulating gas stream that passes through the counting cell [188]. Adsorption efficiency of MnO_2 -fiber for radium was estimated keeping two sample holders having the identical and equal amount of MnO_2 -fiber in series [250].

4.3. Measurement of ^{224}Ra and ^{223}Ra :

Partially dried pre-concentrated Mn fiber was kept in sampler holder and He gas was flushed through the column, for carrying the gaseous radon isotopes (^{220}Rn and ^{219}Rn) produced from ^{224}Ra and ^{223}Ra to the scintillation cell. Alpha particles emitted from the decay of Radon and

its daughters Polonium (Po) were detected by scintillation cell coupled to a photomultiplier tube. The signal from PMT was routed to a total counter, Rn-219 and Rn-220 counter. The counts in both the later counters were recorded after a certain delay interval. Any interference of counts along with chance coincidence counts was subtracted as described by Moore and Arnold[251]. After initial ^{224}Ra and ^{223}Ra measurements, the Mn fiber samples were kept for around 4 weeks to allow ^{224}Ra to equilibrate with ^{228}Th adsorbed to the Mn fiber. The samples were measured to estimate the contribution from ^{228}Th . ^{224}Ra activity was corrected for ^{228}Th contribution to get excess ^{224}Ra ($^{224}\text{Ra}_{\text{exc}}$). In the present manuscript, $^{224}\text{Ra}_{\text{exc}}$ will be mentioned as ^{224}Ra only. Details of method validation, quality control of measurement and calibration of Delayed Counting system is described in Chapter 2 Section 2.31.

4.4. Result

The results of the measurement of activity concentration of ^{224}Ra and ^{223}Ra (dpm/100L), AR and apparent age of water at different locations of the creek during the sampling trips 1-4 are shown in Table 4.1-4.4. Average AR (36.09) in porewater samples was used as AR_i in equation (4.6), to calculate the apparent water age at different locations of the creek. The trip-wise results are discussed below:

4.4.1. Sampling in April 2016 (Trip-1):

During the trip-1, sampling up to location 26 was covered. The ^{224}Ra and ^{223}Ra activity concentration were found in the range of 22.88-51.46 dpm/100L and 1.03-2.26 dpm/100L with average value 35.36 ± 9.04 and 1.46 ± 0.33 dpm/100L respectively (Table 4.1). The average AR in the creek was found to be 22.84 ± 5.28 ranging from 16.28 to 29.46. Figure 4.1 shows a logarithmic variation of ^{224}Ra & ^{223}Ra activity concentration against distance and it was found

that there is no consistent trend of decreasing activity with distance in these samples, indicates there may be multiple sources of radium in the creek.

Table 4.1: Activity concentration of ^{224}Ra and ^{223}Ra (dpm/100L), AR and apparent age of water at different locations for sampling trip-1(April-2016)

Sr. No	Location No.	Activity of ^{224}Ra *	Activity of ^{223}Ra *	AR	Age** (days)
1	1	37.15	1.62	22.93	3.54
2	2	51.46	2.26	22.77	3.59
3	4	49.99	1.42	35.20	0.19
4	5	39.80	1.21	32.89	0.72
5	6	43.01	1.74	24.72	2.95
6	8	32.00	1.35	23.70	3.28
7	9	30.35	1.03	29.47	1.58
8	10	33.75	1.42	23.77	3.26
9	12	97.29	2.09	46.55	-
10	14	35.19	1.36	25.88	2.60
11	15	24.74	1.52	16.28	6.21
12	16	34.96	1.73	20.21	4.52
13	17	21.83	0.61	35.79	0.07
14	19	22.88	1.17	19.56	4.78
15	20	24.44	1.11	22.02	3.85
16	22	22.84	1.85	12.35	9.59
17	24	18.89	1.66	11.38	8.85
18	25	19.96	0.84	23.76	3.81
19	26	17.74	0.79	22.46	4.33

* The average error for ^{224}Ra and ^{223}Ra measurement is 7% and 12% respectively.

** Average error in apparent water age is 33%.

Radium activities concentrations were found lower towards the fresh water mixing zone i.e. where the rivers, a tributary to the creek ecosystem meets. This could be due to partial

depletion of radium isotopes bound to particles in the mixing zone. Higher activity concentration of ^{224}Ra was observed at locations 2, 4 and 12 compare to other locations could be due to intrusion of reused seawater from salt pan and surface water in the creek ecosystem. As we move deeper in the creek from the brink the activity concentration of radium decreases as observed at sampling locations 14, 15 and 16. This is due to dilution and decay of the radium contributed from groundwater to the creek. Compare location 9, a higher activity concentration of Ra at corresponding middle location 10 was observed indicating higher influence of intrusion of water from salt pan discharging at location 12. Higher values of AR indicate dominance the contribution of recent water in the creek ecosystem. The lower activity ratio may be attributed to aging of the water mass in creek.

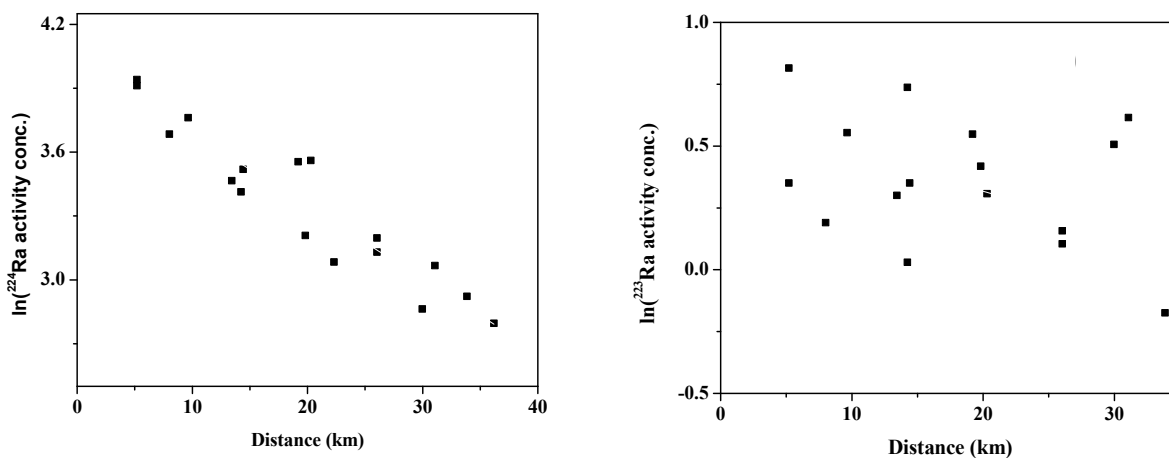


Figure 4.1: Variation of $\ln(\text{Ra activity concentration})$ as a function of distance in the creek for the sampling trip-1

4.4.2. Sampling in March 2017 (Trip-2):

The ^{224}Ra and ^{223}Ra activity concentration were found in the range of 17.58-34.22 dpm/100L and 0.83-1.49 dpm/100L with average value 25.62 ± 4.95 and 1.14 ± 0.18 dpm/100L respectively (Table 4.2).

Table 4.2: Activity concentration of ^{224}Ra and ^{223}Ra (dpm/100L), AR and apparent age of water at different locations for sampling trip-2 (March-2017)

Sr. No	Location No.	Activity of $^{224}\text{Ra}^*$	Activity of $^{223}\text{Ra}^*$	AR	Age** (days)
1	5	26.54	1.2	22.12	3.82
2	8	20.54	1.13	18.18	5.35
3	9	27.18	0.92	29.54	1.56
4	10	23.85	1.14	20.92	4.25
5	11	25.66	1.24	20.69	4.34
6	13	17.58	0.83	21.18	4.16
7	14	34.22	1.49	22.97	3.53
8	15	21.43	1.07	20.03	4.59
9	19	30.03	1.12	26.81	2.32
10	21	29.16	1.28	22.78	3.59
11	20	27.47	1.34	20.50	4.41
12	24	18.28	1.00	18.28	5.31
13	25	16.88	0.93	18.15	5.36
14	26	12.69	0.80	15.86	6.41

* The average error for ^{224}Ra and ^{223}Ra measurement is 7% and 12% respectively.

** Average error in apparent water age is 29%.

The average AR in the creek was found to be 22.52 ± 3.35 having a range from 18.18 to 29.54. There is no consistent trend of decreasing activity with distance for ^{224}Ra & ^{223}Ra in samples Figure 4.2.

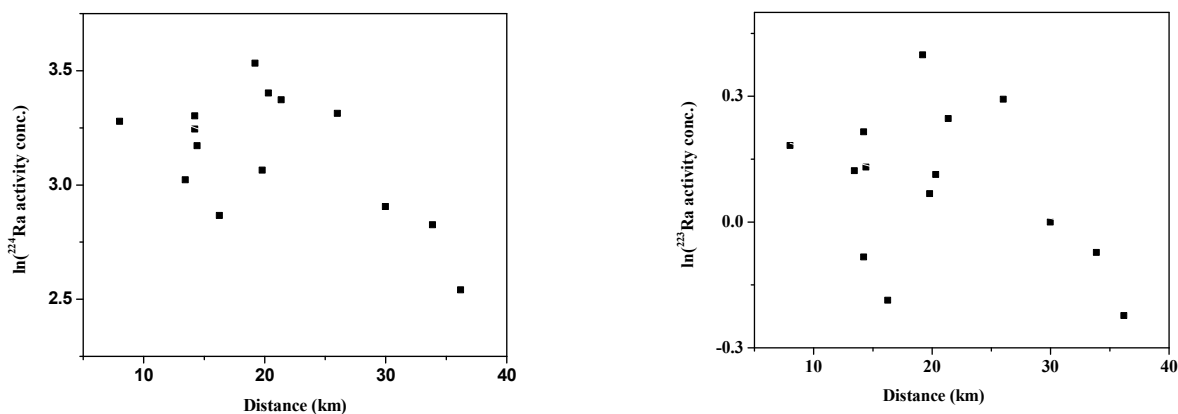


Figure 4.2: Variation of $\ln(\text{Ra activity concentration})$ as a function of distance in the creek for the sampling trip-2

4.4.3. Sampling in May 2017 (Trip-3):

Table 4.3 gives the value of activity concentration, AR and age at a different location in open end of the bay and the Arabian Sea. The age was calculated using the average activity concentration ratio of ^{224}Ra and ^{223}Ra in the creek as source value. The sampling point 18 was considered as a reference point for the measurement of distance (Table 4.3) towards the open sea. The assumption is based on maximum activity [246, 247] as beyond this points activity is gradually decreasing and there is no major source of radium towards the open sea. The ^{224}Ra and ^{223}Ra activity concentration towards the open sea were found in the range of 7.66-20.56 dpm/100L and 0.52-1.1 dpm/100L with an average value of 13.11 ± 4.73 dpm/100L and 0.77 ± 0.19 dpm/100L respectively.

Table 4.3: Activity concentration of ^{224}Ra and ^{223}Ra (dpm/100L) in seawater samples collected from the open end of the bay and the Arabian Sea for sampling trip-3

Sr. No.	Location	Activity of $^{224}\text{Ra}^*$	Activity of $^{223}\text{Ra}^*$	AR	Distance (km)	Age** (days)
1	24	20.56	1.10	18.69	6	1.23
2	25	18.42	0.89	20.70	8.5	0.43
3	26	15.22	0.80	19.03	11	1.09
4	27	12.97	0.83	15.63	20	2.62
5	28	12.43	0.63	19.73	22	0.81
6	29	8.05	0.52	15.48	24	2.70
7	30	7.66	0.57	13.45	26	3.80
8	31	9.58	0.78	12.28	28	4.51

* The average error for ^{224}Ra and ^{223}Ra measurement is 7% and 12% respectively.

** Average error in apparent water age is 34%.

4.4.4. Sampling in December 2017 (Trip-4):

The ^{224}Ra and ^{223}Ra activity concentration in porewater at location 14 were found to be 95.50 and 2.65 dpm/100L with AR value 36.02 (Table 4.4). Similarly, the ^{224}Ra and ^{223}Ra activity concentration in porewater at location 16 were found to be 131.54 and 3.64 dpm/100L with AR value 36.16. The ^{224}Ra and ^{223}Ra activity concentration in the creek was found in the range of 21.40-29.49 dpm/100L and 1.28-1.47dpm/100L with an average of 26.69 ± 3.48 and 1.38 ± 0.08 dpm/100L respectively. The average AR in the creek was found in the range of 14.56 to 23.04 with an average 20.52 ± 3.58 . There is no consistent trend of activity with distance for ^{224}Ra & ^{223}Ra in samples Figure 4.3, indicating diffused sources of radium in the creek.

Table 4.4: Activity concentration of ^{224}Ra and ^{223}Ra (dpm/100L), AR and apparent age of water at different locations for sampling trip-4 (December-2017)

Sr. No	Location No.	Activity of $^{224}\text{Ra}^*$	Activity of $^{223}\text{Ra}^*$	AR	Age** (days)
1	14	95.50	2.65	36.02	Porewater
2	16	131.54	3.64	36.16	Porewater
3	3	23.71	1.39	22.93	3.54
4	7	28.00	1.25	22.40	3.72
5	10	28.29	1.28	22.10	3.83
6	15	23.50	1.47	15.99	7.08
7	18	27.27	1.44	18.94	5.03

* The average error for ^{224}Ra and ^{223}Ra measurement is 7% and 12% respectively.

** Average error in apparent water age is 33%.

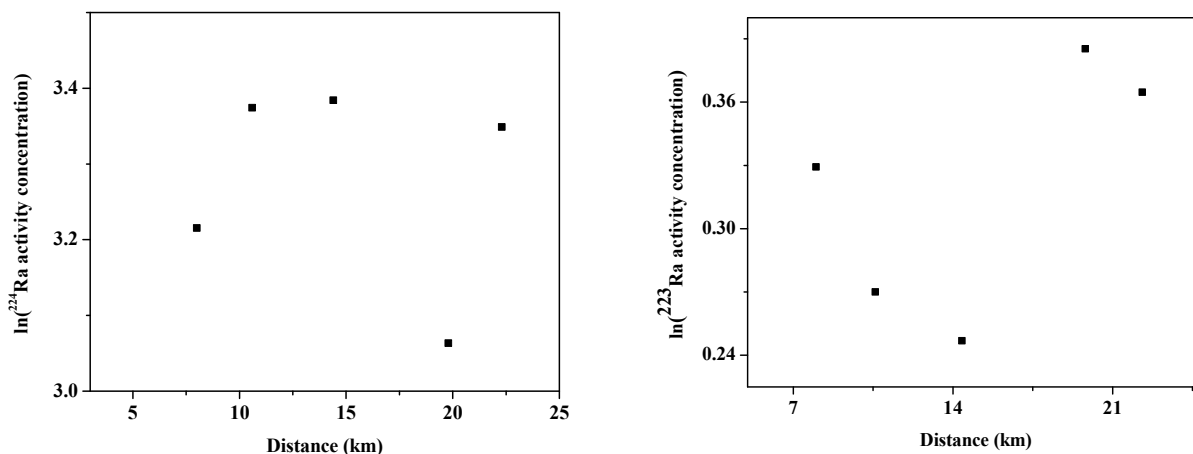


Figure 4.3: Variation of $\ln(\text{Ra activity concentration})$ as a function of distance in the creek for the sampling trip-4

4.4.5. Physico-Chemical Parameter

During sampling Physico-chemical parameters (viz. pH, Conductivity, Total Dissolved Solid (TDS) and Salinity) were measured.

Table 4.5: Physico-Chemical Parameter in Mumbai Harbour Bay

Location No.	pH	Conductivity (mS)	TDS (ppt)	Salinity (ppt)
1	7.78	36.80	31.90	26.20
2	7.66	37.10	26.80	22.40
3	7.54	38.40	28.00	21.30
4	7.69	39.40	28.00	21.80
5	7.47	39.80	28.10	23.90
6	7.39	39.20	27.80	22.70
7	7.50	39.80	28.40	24.10
8	7.35	40.40	28.30	21.30
9	7.76	39.40	27.80	21.90
10	7.29	37.20	26.50	21.60
11	7.68	39.40	28.00	21.30
12	7.58	47.20	33.50	27.50
13	7.62	37.40	26.70	21.80
14	7.67	37.90	26.90	22.00
15	7.49	41.50	29.40	24.20
16	7.64	50.48	33.02	24.73
17	7.53	49.28	32.15	24.14
18	7.42	46.18	29.81	22.59
19	7.65	39.40	27.80	22.80
20	7.76	48.20	34.10	28.30
21	7.75	52.30	37.10	31.60
22	7.73	47.50	33.70	28.00
23	7.54	48.30	33.30	27.90
24	7.42	47.90	35.60	28.60
25	7.39	49.10	34.80	29.00
26	7.50	51.40	36.40	30.50
Average	7.57±0.14	43.11±5.28	30.53±3.40	24.70±3.19

The average, conductivity, TDS and salinity in the Mumbai Harbour Bay was found to be 7.57 ± 0.14 , 43.11 ± 5.28 , 30.53 ± 3.40 and 24.70 ± 3.19 respectively Table 4.5 (Above). The average, conductivity, TDS and salinity in the Arabian Sea was found to be 7.61 ± 0.17 , 58.07 ± 4.21 , 38.58 ± 3.10 and 29.34 ± 1.00 respectively Table 4.6 (Below).

Table 4.6: Physico-Chemical Parameter in Arabian Sea

Location No.	pH	Conductivity (mS)	TDS (ppt)	Salinity (ppt)
27	7.65	51.48	33.70	29.60
28	7.71	56.72	37.58	27.79
29	7.32	61.59	41.02	30.18
30	7.74	58.99	39.33	28.97
31	7.62	61.58	41.26	30.16
Average	7.61 ± 0.17	58.07 ± 4.21	38.58 ± 3.10	29.34 ± 1.00

4.5. Discussion

4.5.1. Apparent Age by Radium Age Model:

The ^{224}Ra and ^{223}Ra activity concentration for porewater samples vary at the sampling locations but the AR value is very well in agreement at different locations, indicates similar source is contributing in the creek. Average AR value obtained in porewater samples collected using piezometer was considered as AR_i for the calculation of the apparent water age. The apparent water age at different locations for sampling trip-1, trip-2 and trip-4 were calculated using equation (4.6) and found in the range of 1.58-6.21 days, 1.56-5.35 days and 3.50-7.08 days respectively. The average apparent age of creek water for sampling trip-1, trip-2 and trip-4 were found 3.65 ± 1.22 days, 3.81 ± 1.10 days and 4.51 ± 1.51 days respectively. The relative error in individual estimate, based on error propagation was found to be about 35%. The average error in

the apparent water age based on the standard deviation of the results was found to be about 32%. The sample from location 17 shows the small value of age which reflects discharge of fresh input at this location. At location 3 and 4, obtained AR value was found comparable to that of porewater. The comparatively higher average value of activity concentration observed in samples collected from the narrow end of the creek signified the input from Ulhas River. The sampling location towards the open end of the bay showed higher apparent water age. It was observed that apparent water age increases as one move towards the open mouth of the bay (trip-4). Lower value at location 18 compared to that of location 15 may be attributed to the contribution of fresh water. The lower average AR for sampling trip-4 compare to sampling trips 1 and 2 may be attributed to the effect of the sampling site as during trip-4 samples only from the middle creek was considered.

4.5.2. Apparent Age by Radium Balance Approach:

Sampling at different time intervals indicates no temporal variation in the distribution of radium isotopes throughout the bay. Higher average activity concentration was found during sampling Trip-1 compared to other trips could be due to reduced freshwater discharge during summer. Sampling in pre-monsoon (trip-2) and post-monsoon (trip-4) of the same year showed no significant variation in the activity ratio. The small differences observed are thought to be influenced more by site location than seasonal change. This indicates the bay is in steady state i.e. loss of tracer (radium) is balanced by input from different sources. The radium mass balance approach (Eq. 4.10) was used to calculate the overall average apparent age of creek water.

The average value of AR (22.59) from sampling trips 1 and 2 was taken as $I(^{224}\text{Ra}/^{223}\text{Ra})$. Using average AR value (36.09) in porewater samples as $F(^{224}\text{Ra}/^{223}\text{Ra})$, equation (4.10) gives apparent water age as 6.51 ± 1.27 days. It was found that both the approach gives a similar

estimate of the age of the creek water. Slightly lower value of apparent water age by radium age model may be attributed to the existence of multiple radium sources in the creek. Table 4.7 shows the comparison of apparent water age of present study area with some other ecosystem of the world. The estimated apparent water age for studied bay was found comparable to Flamengo and Fortaleza Bay, Brazil and Jamaica Bay New York (Table 4.5).

Table 4.7: Comparison of Apparent Water Age from other Ecosystem of the World

S. N.	Location	Apparent water age (days)	Reference
1	Okatee Estuary, South Carolina	1.6-5 (3.4)	[238]
2	Flamengo Bay, Ubatuba, Brazil	3.5-6.5 (4.44)	[252]
3	Yangtze estuary, China	4-10	[253]
4	Jamaica Bay, NY	1.2-21 (7.5)	[80]
5	Fortaleza Bay, Ubatuba, Brazil	1.8-7.5 (4.02)	[252]
6	St. Andrew Bay, Florida	8-11	[241]
7	MHB, India (90% renewal of bay water)	3.2	[219]
8	MHB, India (radium age model)	1.56-7.53 (4.06±1.20)	Present Study
9	MHB, India (Radium Balance Approach)	6.51±2.14	Present Study

4.5.3. Tracing of Water Movement in Creek:

The average value of apparent water age from three sampling trips (1, 2 and 4) at a different location in the middle of the creek was plotted (Figure 4.4) against distance measured from location 3. It was observed that in increasing distance towards the open sea apparent age of

water mass increases which indicates the dominant source of freshwater discharge from the landlocked mass in the narrow end of the creek. Flushing rate water in creek towards the open mouth of the bay was estimated from the slope of Figure 4.4 and found as $9.09 \text{ km}\cdot\text{day}^{-1}$.

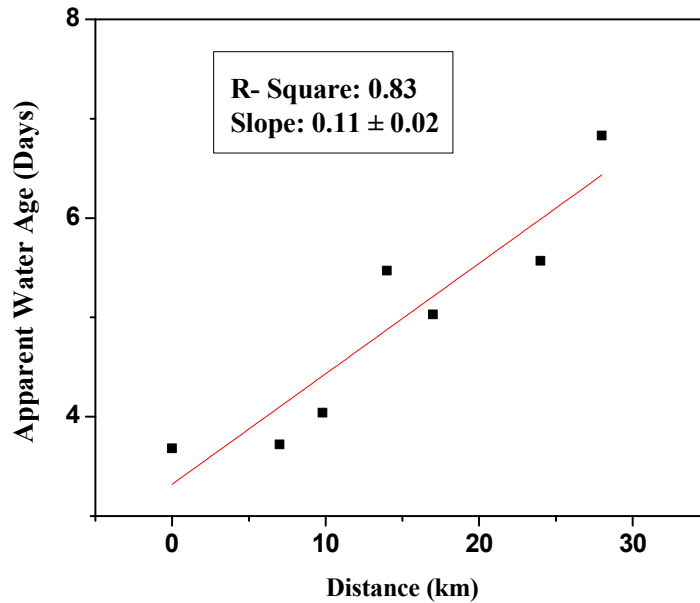


Figure 4.4: Variation of apparent water age the distance within the creek

4.5.4. Estimation of Flushing Rate of Creek Water

Figure 4.5 shows the variation of the apparent age of water mass at different locations with distance (Table 4.3) in the open mouth of the bay and the Arabian Sea. The sample from location 28 has not been considered in the estimation of the flushing rate. The linear fit gives R^2 value as 0.87 and slope as 0.15 ± 0.02 . From the slope, the flushing rate of creek water was found $6.67 \pm 0.89 \text{ km}/\text{days}$. Based on the fit the error in flushing rate was found to be 13.34%. There is a decrease in the flushing rate of water from open mouth towards offshore as compared to flushing rate of water within the creek. The decrease in the flushing rate may be attributed to widening of the bay towards the open end and also interaction with open seawater. Table 4.8

gives the comparison of flow rate value with some other bay system of the world. Moore and Oliveira [252] estimated the flushing rate for a series of small embayments near Ubatuba, Sao Paulo State, Brazil different transect of Ubatuba bay and found in the range 1.7-3.6 km.day⁻¹.

Xu et al. [245] have used the spatial and temporal distribution of naturally-occurring short-lived radium isotopes (²²⁴Ra and ²²³Ra) to study coastal water mixing dynamics of the third world largest estuary, Yangtze River Estuary (YRE). Distributions of the ²²⁴Ra/²²³Ra activity ratios within the YRE area were used to calculate apparent estuarine water ages and from age versus distance plot, they have estimated integrated water flushing rate to be 8.4 ± 0.8 km.day⁻¹.

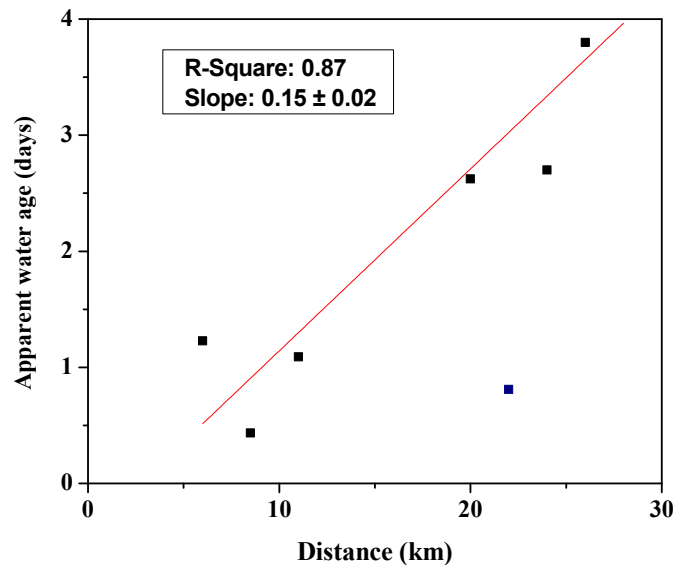


Figure 4.5: Variation of the apparent age of water mass in the open mouth of the bay and offshore location

Moore and Krest [254] have studied riverine plumes at the mouths of the Mississippi River mixing into the ocean using ²²³Ra and ²²⁴Ra as tracers in November 1993 and May 1994. During each study, water ages increased with increasing distance from the Mississippi River

mouth and the apparent velocity (flushing rate) was in the range 2.3-17 cm s⁻¹ (2.0- 14.7 km d⁻¹).

The flushing rate in the MHB was found comparable to the Yangtze estuary, China

Table 4.8: Comparison of Flushing Rate (km.day⁻¹) in the different ecosystem of the world

S. N.	Location	flushing rate (km.day ⁻¹)	Reference
1	Yangtze estuary, China	8.4 ± 0.8	[253]
2	Ubatuba, Brazil	1.7-3.6	[252]
3	Mississippi plum, USA	2.0- 14.7	[254]
4	Within Thane Creek, India	9.09 ± 1.6	Present Study
5	MHB, India (Flushing rate of creek water towards the open sea)	6.67 ± 0.89	Present Study

4.5.5. Estimation of Horizontal Dispersion Coefficient (K_h)

Figure 4.6 shows the variation of ²²³Ra activity concentration with distance measured from sampling location 18 (reference point). A linear decrease of ²²³Ra with distance (Figure 4.6) indicates dispersion is the dominant process of mixing towards the open end of the bay. This type of transport was also confirmed for the coastal area of other regions by data on conservative tracer [252]. The rate of horizontal mixing of water was estimated from the slope of ln[Ra] vs. distance plot as per equation (4.13).

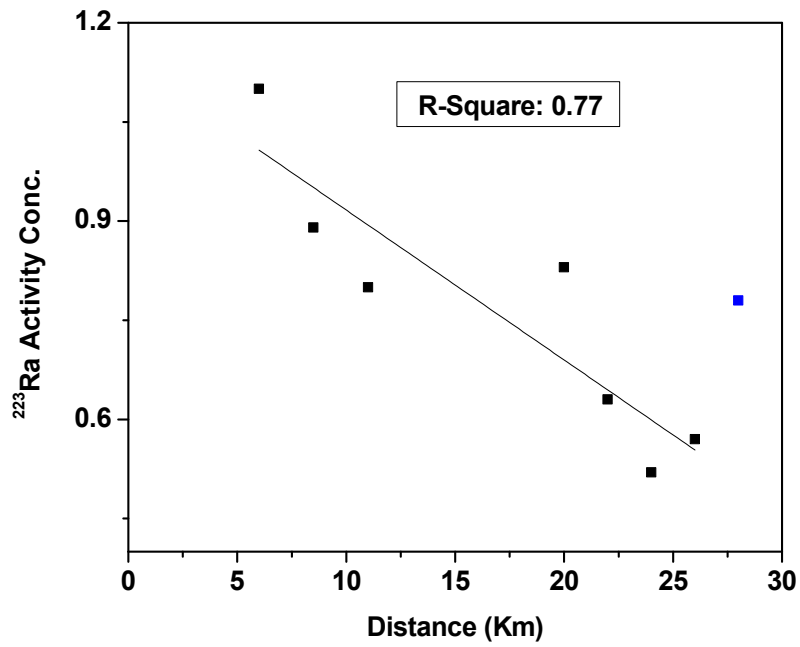


Figure 4.6: Variation of ²²³Ra activity concentration with distance

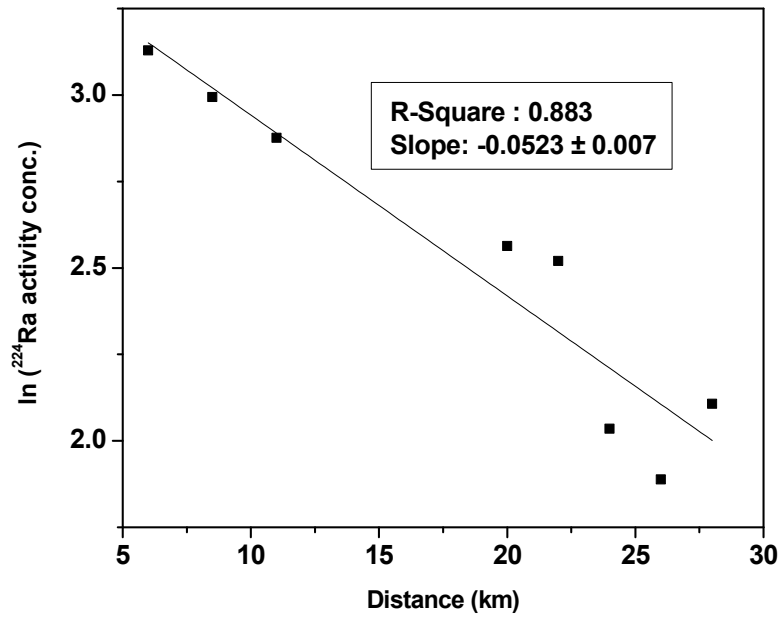


Figure 4.7: Variation of ln²²⁴Ra with distance against distance

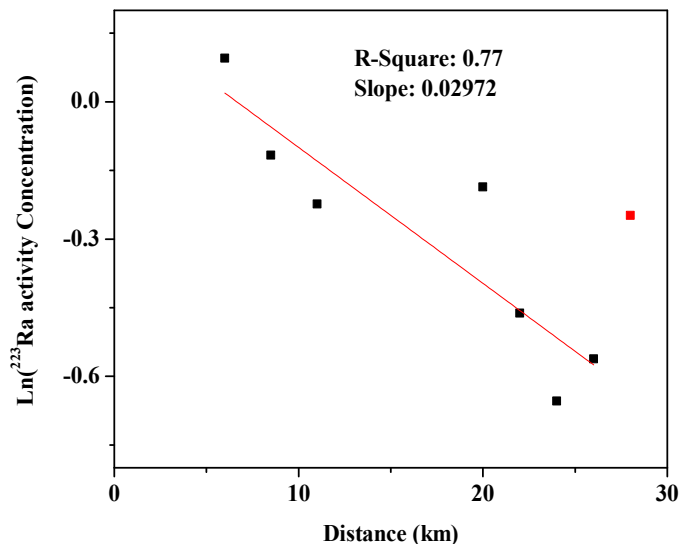


Figure 4.8: Variation of $\ln^{223}\text{Ra}$ with distance against distance

Figure 4.7 and Figure 4.8 shows the linear fit of $\ln^{224}\text{Ra}$ and $\ln^{223}\text{Ra}$ with distance respectively for the samples collected beyond the creek in MHB and offshore locations. The linear fit in Figure 4.7 gives slope value as 0.052 which results in dispersion constant as $69 \text{ km}^2\text{d}^{-1}$ ($800 \text{ m}^2\text{s}^{-1}$). The dispersion constant (K_h) $69.7 \text{ km}^2\text{d}^{-1}$ ($795 \text{ m}^2\text{s}^{-1}$) was estimated from the slope of 0.0297 obtained from the linear fit of $\ln^{223}\text{Ra}$ vs. distance (Figure 4.8). Similar K_h value from ^{223}Ra and ^{224}Ra validates our assumption that system is in steady state and dispersion is the dominant process.

Moore in 2000 [244] has studied the South Atlantic Bight and observed that offshore transects of the long-lived ^{226}Ra and ^{228}Ra indicate that eddy diffusion controls their distributions within 50km of the shore. The short-lived ^{223}Ra and ^{224}Ra distributions in this region yield an eddy diffusion coefficient of $360\text{--}420 \text{ m}^2 \text{ s}^{-1}$.

The gradient of $\ln^{224}\text{Ra}$ on the $< 30\text{km}$ section of transect had a slope of $-6.1 \times 10^{-5} \text{ m}^{-1}$ from which diffusion coefficient was calculated to be $596 \text{ m}^2 \text{ s}^{-1}$ [235]. While in the same study area at the other transect (100 to 250 km part of the transect only) had a slope of $5.9 \times 10^6 \text{ m}^{-1}$ for

$\ln^{224}\text{Ra}$ versus distance plot, resulting in an eddy diffusion coefficient K_h of $6.3 \times 10^4 \text{ m}^2 \text{ s}^{-1}$ [235]. The radium quartet (^{228}Ra , ^{226}Ra , ^{224}Ra , and ^{223}Ra) has been investigated in Loch Etive, a Scottish fjord, by Hsieh et al. [255] to study water mixing rates and inputs of Ra from sediments. Neglecting advection, the distribution of the short-lived ^{223}R and ^{224}Ra was explained by horizontal mixing rates of $6.1 \times 10^6 \text{ cm}^2 \text{ s}^{-1}$ ($610 \text{ m}^2 \text{ s}^{-1}$) and $9.1 \times 10^6 \text{ cm}^2 \text{ s}^{-1}$ ($910 \text{ m}^2 \text{ s}^{-1}$) respectively. Charkin et al. [247] studied the trends of the radionuclide behaviour after passage through the high-gradient river–coastal seawater mixing zone and estimated the exchange rate of the horizontal mixing in the Anadyr River–Bering Sea transit system. They have estimated horizontal mixing rate (K_h value) from the slope of $\ln^{224}\text{Ra}$ vs. distance to be $312\text{m}^2\text{s}^{-1}$. Table 4.9 compares the present study with some other ecosystem of the world and the K_h value for the present study area is within the reported range of other ecosystems of the world.

Table 4.9: Comparison of horizontal mixing constant (dispersion constant) from other ecosystems of the world

S. N.	Location	Horizontal mixing constant (m^2s^{-1})	Reference
1	Etive estuary, Scotland	910	[255]
2	South Atlantic Bight	420	[244]
3	Andry River-Berting Sea, Russia	312	[247]
4	Southern Ocean near the Antarctic Peninsula	596 (within 30 km)	[235]
5	Mumbai Harbour Bay, India	800	Present Study

4.6. Conclusion

The activity concentration ratio of $^{224}\text{Ra}/^{223}\text{Ra}$ in porewater samples and other surface discharge points reflects the similar source of radium in the Thane Creek. The similar average activity concentration and AR at different time intervals of sampling show the system is in steady state. The apparent water age (by radium age model) of the creek water was found to vary in the range of 1.56-7.53 days with an average of 4.06 ± 1.20 days while radium balance approach gives an average apparent age as 6.51 ± 1.27 days. Variation of AR shows the net flow of water is towards the open sea. The flushing rate in creek water towards bay was found to be 6.67 ± 0.89 km/days. Horizontal mixing constant for creek water was estimated and found to be 800 and $795 \text{m}^2 \text{s}^{-1}$ from ^{224}Ra and ^{223}Ra isotopes for our study area which validates our assumption that system is in steady state and dispersion is dominant process. The result indicated the ages do not follow an exact trend with distance offshore that may be attributed to the roughness of sea near coast and contribution from unknown sources of Ra. The information obtained could be used to help the developing management strategies for controlling the supply of terrestrial nutrients and contaminants to offshore areas and protect the environment of this area.

CHAPTER 5

ESTIMATION OF SUBMARINE GROUNDWATER DISCHARGE IN MUMBAI HARBOUR BAY

5.1. Introduction

Discharge of water from land to ocean viz. Surface water (River and streams) and groundwater flows are important pathway for material transport to the marine environment from land. The most of researcher defined groundwater as “water residing within the saturated zone of geologic material” [49, 51]. The groundwater discharges occurring as a slow diffuse flow, seepage through sediment and is characterized by substantial temporal and spatial variability [51]. Thus “submarine groundwater discharge (SGD)” is defined as any flow of water from seabed to the coastal ocean, regardless of fluid composition or driving force” [53]. Freshwater discharging directly into coastal water due to the hydraulic gradient and re-circulated seawater e.g. sediment porewater flow caused by waves and tidal pumping. The advantage of defining SGD this way is that it takes into account discharges of both: terrestrial groundwater and re-circulated seawater. The groundwater discharge into the near-shore marine ecosystem may have significant impact, as groundwater in many areas are contaminated with a variety of substances like nutrients, heavy metals, radionuclides and organic compounds [256]. McCoy and Corbett [75] showed that a large nutrient flux via SGD is the reason for not only to eutrophication but also to the occurrence of red tides in Masan Bay, Korea. Various studies indicated that SGD is generally a significant source of fluxes of trace elements and metals to the marine environment [78, 79].

Groundwater discharge to the coastal ecosystem can be estimated by a number of methods, largely falling into three categories:

1. Numerical Method
2. Physical Measurements
3. Groundwater Tracers

The most popular methods used to quantify SGD are: hydrodynamic method for calculating lateral groundwater flow [94]; methods based on investigation of the coastal drainage area [95]; methods based on investigation of the sea [95]; modeling [49, 107], direct measurements [49, 107], and tracer techniques [49, 51]. However, each technique has certain limitations because of generalized assumptions and natural variability. Typically researchers address limitations of the implemented method at particular study area or use several techniques to detect and measure SGD. The details of different method (viz. seepage meter, piezometer, natural tracers, infrared imaging, hydrologic approach, hydrograph separation techniques and mathematical models) used for the measurement of SGD were already discussed in **Chapter 1**. The isotopic measurement such as natural radioactive isotopes (^3H , ^{14}C , ^{222}Rn , ^{223}Ra , ^{224}Ra , ^{226}Ra , ^{228}Ra and ^{234}U) and stable isotopes (^2H , ^3He , ^4He , ^{13}C and ^{15}N) among available isotopes can serve as tracer of fluxes into coastal water. In the present study naturally occurring short-lived Ra isotopes (^{223}Ra and ^{224}Ra) were used for the estimation of SGD.

Ra isotopes are produced by the decay of thorium parent isotopes contained on terrigenous materials in aquifer. In freshwater Ra is highly particle reactive. However, mixing saltwater results in ion exchange transformation that causes rapid desorption of Ra from particle surfaces into solution due to reduction in the adsorption coefficient of radium with increasing salinity [257]. Thus, the sediments provide Ra isotopes to marine waters as per decay constants

of the Ra parent isotopes. The saline groundwater is enriched with Ra in order of magnitude. The high activities of ^{226}Ra in the coastal water which could not be explained by input from rivers or sediments and salty coastal well water contains high ^{226}Ra activity led to the hypothesis that SGD was responsible for the elevated activities [40].

The sources of Ra in coastal marine environment are input from SGD, surface discharges (rivers and streams), tidal water, suspended and surface sediment. The surface discharges carry Ra adsorbed on particle which undergoes exchange during mixing with seawater resulting in influx of Ra [240, 257]. Although there is some Ra initially in the dissolved phase in fresh river water, the greater portion is associated with the particulate fraction. The tidal input is the flux of Ra in the system during the high tide. Diffusion and bio-irrigation of Ra from surface sediment add a significant amount of Ra to marine system. The relative importance of these processes varies between isotopes, depending on the time scale regulating the regeneration and loss of each. The Mumbai Harbour Bay (MHB) houses a large number of industry and ports which releases various pollutants. Thus the groundwater in the present area may be heavily polluted. The surface discharge has been extensively studied [222–225], while SGD needs to be estimated to have an idea about discharges through land and also for estimation of pollutant influx via SGD. In the present study, individual Ra flux terms and the SGD using Ra mass balance approach, was estimated in Mumbai Harbour Bay.

5.2. Study Area and Sampling

The study area (Mumbai Harbour Bay) and the sampling locations, considered for the estimation of is shown in Figure 5.1. The bay is a triangular mass of brackish water which opens to the Arabian Sea in the South and the narrow end is fed by freshwater Ulhas River in the north. The Panvel River flows into the bay from the eastern mainland [219–221]. The average area of

water surface of the bay is about 215km² at high tide level and about 160km² at low tide level. The total volume of water at mean sea-level as calculated from surrounding area is 9.1x10¹¹ litres [18,19]. The average tidal volume is 4.8x10¹¹ litres [219]. The bay is subjected to wave actions and semi-diurnal tides. Seawater samples, collected from different locations of MHB is shown in Figure 5.1.

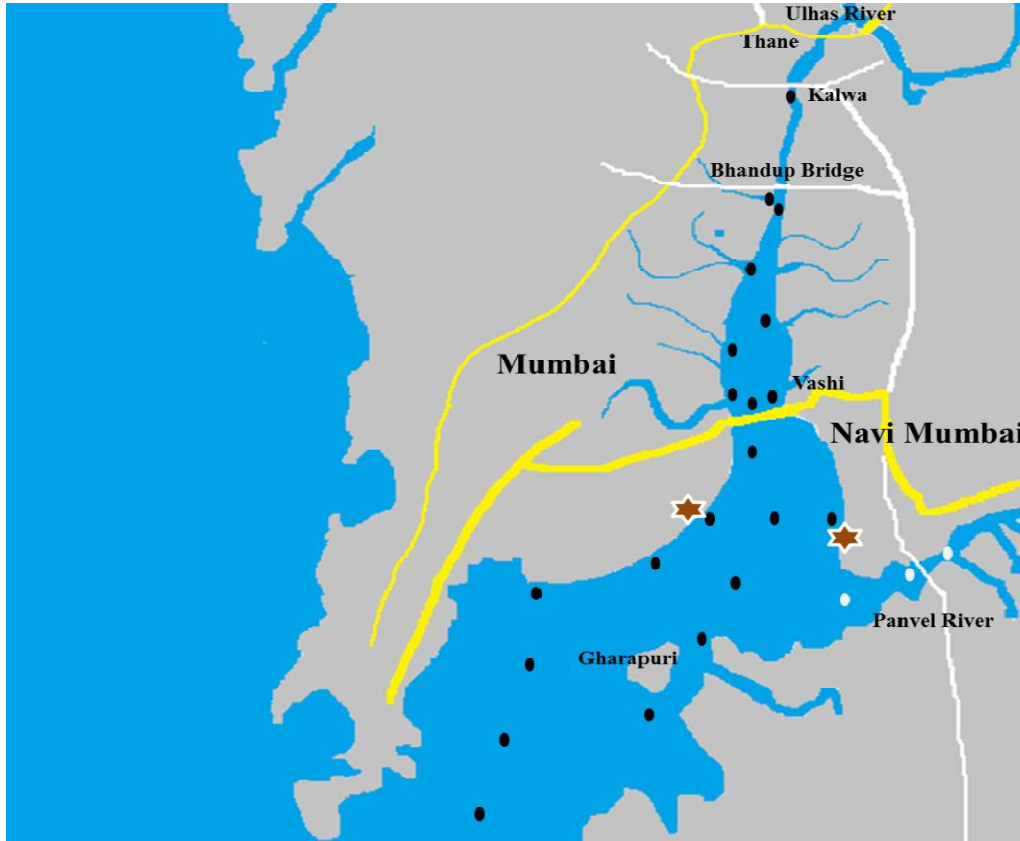


Figure 5.1: Study area (Mumbai Harbour Bay) and sampling locations. Black circles represent the locations for surface water in the bay, white circle shows sampling in Panvel River and hexagonal shape shows the location for groundwater sampling locations

The groundwater samples were taken using push point sampler (piezometer) from the 2m depth. Surface seawater from Panvel River also collected from three locations to get the input of Ra from Panvel River. Multiple samples from Kalwa (At the Northern end of bay) were collected from estimation of average input of Ra from Ulhas River. Ra from seawater was pre-

concentrated on MnO₂ fiber, processed and short-lived radium isotopes were measured using delayed coincidence counting technique [250].

5.3. Mass Balance in Mumbai Harbour Bay

The sampling at various times interval showed the system investigated under the steady state i.e. Ra loss via mixing and decay was equal to gains from different sources as discussed in Chapter 4. Thus the difference between the total Ra export from the bay via ocean exchange and decay and input from the sources described above can reasonably be ascribed to submarine groundwater discharge. A comprehensive Ra mass balance can be used to assess the magnitude of submarine groundwater discharge as;

$$A_{\text{out}} + A_{\text{decay}} = A_{\text{in}} + A_{\text{Pan}} + A_{\text{Ulh}} + A_{\text{diff}} + A_{\text{dis}} + A_{\text{susp}} + A_{\text{SGD}} \quad (\text{Eq. 5.1})$$

Where;

A_{out} = Ra export during exchange of bay water with Arabian Sea water,

A_{decay} = Ra loss via radioactive decay,

A_{in} = Flux of Ra into MHB from Arabian Sea water, i.e. tidal input

A_{Pan} = Ra input from Panvel River to MHB

A_{Ulh} = Ra input from Ulhas River to MHB

A_{diff} = Diffusive flux of Ra from surface sediments

A_{dis} = Flux of Ra associated with waste water discharge

A_{susp} = Ra desorbed from re-suspended particles, and

A_{SGD} = Ra flux from submarine groundwater discharge

Table 5.1 shows the parameters used for the calculation of different sources of Ra loss and input sources in the bay. Table 5.2 gives the estimate of different process and sources

involves in the mass balance of the Ra flux in Mumbai Harbour Bay. Figure 5.2 shows the different pathways of Ra input to bay and process of Ra loss from the bay.

Table 5.1: The parameters and values used for calculation of Ra fluxes

Description		²²³ Ra	²²⁴ Ra	Reference
Concentration of Ra isotope (dpm.100 L ⁻¹)	Avg. bay value (C _{bay})	1.41	34.36	Present Study
	Arabian Sea (C _{AS})	0.67	10.14	
	Groundwater (C _{gw})	21.85	413.89	
	Ulhas River(C _{Ulh})	1.08	25.48	
	Panvel River (C _{Pan})	1.26	34.09	
	Waste Discharge	1.75	59.64	
Diffusive flux (J _{diff}) (dpm m ⁻² h ⁻¹)		0.05	2.20	[129, 258]
Avg. Activity in Suspended Sediment (dpm.kg ⁻¹)		4.00	67.00	Present Study
Decay constant(λ) (d ⁻¹)		0.0608	0.193	[4]
Other Parameters of the bay				
Description		Values		[219]
Volume of Bay (m ³)		9.09x10 ⁸		
Tidal prism (m ³ per tide)		4.84x10 ⁸		
Tidal prism (m ³ d ⁻¹)		9.14 x10 ⁸		
Tidal range(dz) (m per cycle)		2.56		
Bay surface area(A _{Bay}) (m ²)		1.89 x10 ⁸		
Ulhas River discharge(F _{Ulh}) (m ³ d ⁻¹)		1.18 x 10 ⁵		[259]
Panvel River discharge(F _{Pan}) (m ³ d ⁻¹)		1.0 x 10 ⁵		
Waste Water Discharge (F _{dis}) (m ³ d ⁻¹)		4.4 x 10 ⁵		
Avg. Suspended Sediment (mg.L ⁻¹)		26		Present Study

5.3.1. Loss of Ra-fluxes from the bay

5.3.1.1. Radioactive Decay

The water residence time in the Mumbai harbour bay is about one week so decay of short-lived Ra isotopes will be significant. The loss of Ra flux via decay is estimated as

$$A_{\text{decay}} = V_{\text{bay}} \times C_{\text{bay}} \times \lambda_{\text{Ra}} \quad (\text{Eq. 5.2})$$

Where, C_{bay} is average activity concentration of Ra isotope in the bay, estimated from the analysis of surface water samples from various location of the bay, V_{bay} is the volume of the bay (L) and λ_{Ra} is the decay constant of the Ra isotope. From the Equation 5.2, the loss of ^{223}Ra and ^{224}Ra flux in the bay via decay was estimated and found to be $0.78 \times 10^9 \text{ dpm.d}^{-1}$ and $60.28 \times 10^9 \text{ dpm.d}^{-1}$ respectively. The radioactive decay accounts for 6% and 16% of the total ^{223}Ra and ^{224}Ra loss from the bay respectively.

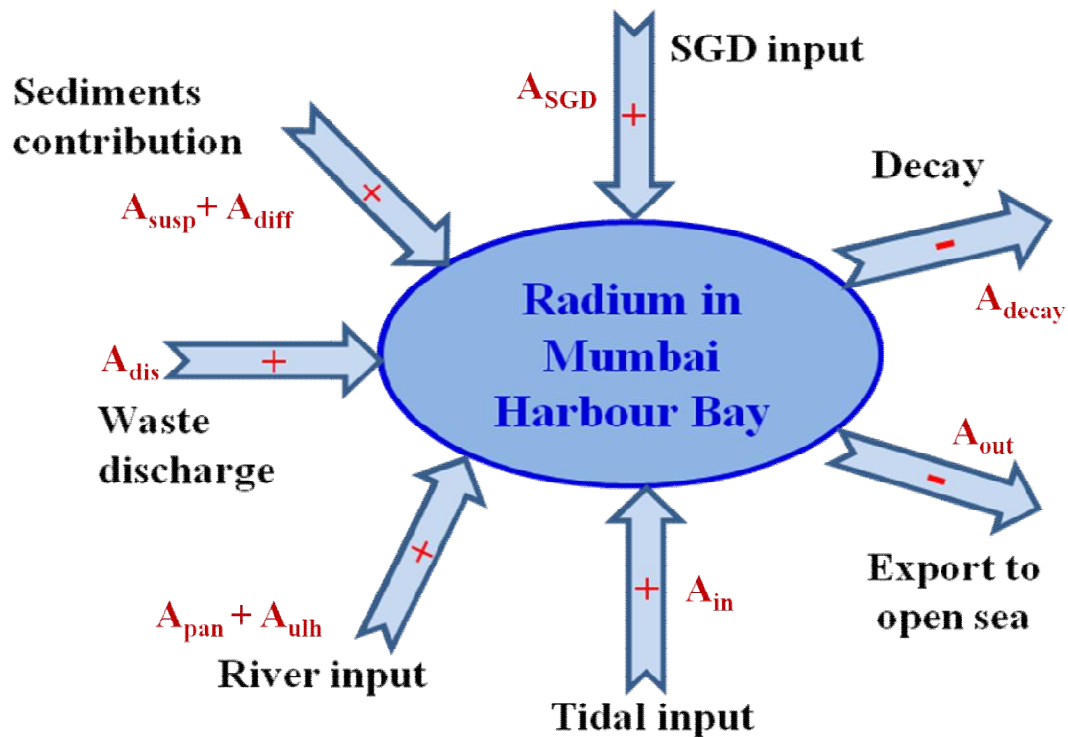


Figure 5.2: Different sources of input and loss of Ra in the Mumbai Harbour Bay

5.3.1.2. Ra export during exchange of bay water with Arabian Sea water

The bay subjected to wave actions and semi-diurnal tide which results well mixed water system in the bay. The bay receives water from rivers, streams and tidal input during the high tide. It is assumed that water in to the bay, rapidly mixed with bay water, and carries the average activity through the bay mouth to Arabian Sea during the low tide. Thus the Ra export from the bay can be estimated as;

$$A_{\text{out}} = V_{\text{out}} \times C_{\text{bay}} \times 1.89 \quad \text{(Eq. 5.3)}$$

Where V_{out} is the tidal prism volume plus average daily water discharge in the bay, C_{bay} is average activity concentration of Ra in the bay and 1.89 is number of tidal cycles per day.

From the Equation 5.3 the export of ^{223}Ra and ^{224}Ra during low tide towards Arabian Sea water was estimated to be $12.89 \times 10^9 \text{ dpm.d}^{-1}$ and $314.29 \times 10^9 \text{ dpm.d}^{-1}$ respectively. The ocean exchange contribution for loss of ^{223}Ra and ^{224}Ra is 94 % and 84 % of the total loss from the bay.

5.3.2. Input of Ra-fluxes into bay

5.3.2.1. Arabian Sea Exchange

The bay receives tidal water during the flood tides which add the Ra into the bay. The amount of Ra flux in the bay from Arabian Sea can be estimated as;

$$A_{\text{in}} = V_{\text{in}} \times C_{\text{AS}} \times 1.89 \quad \text{(Eq. 5.4)}$$

Where C_{AS} is the average activity of Ra in the Arabian Sea, near the open mouth of bay, V_{in} is the tidal prism volume and 1.89 is the number of tidal cycles per day. The sampling in the Arabian Sea was done at equidistance of 2 km towards offshore up to 10 km and average value of this was taken for calculation of Ra flux into bay. The equation 5.4 gives the contribution of ^{223}Ra and ^{224}Ra into bay as $6.04 \times 10^9 \text{ dpm.d}^{-1}$ and $94.19 \times 10^9 \text{ dpm.d}^{-1}$ respectively. As it is

discussed earlier that bay is in steady state so the total Ra export is balanced by total input. Therefore to express the percentage input from any pathways, Ra fluxes into bay from the different pathways will be compared to the total Ra loss. It was found that exchange of water at the bay inlet contribute a significant proportion of the Ra flux into the bay, and found 44 % and 25% for ^{223}Ra and ^{224}Ra respectively.

Table 5.2: Estimate of different process and sources involved in the mass balance of the Ra flux in Mumbai Harbour Bay

Sr. No.	Source	Fluxes into system (10^9 dpm.d^{-1})		% Contribution	
		^{223}Ra	^{224}Ra	^{223}Ra	^{224}Ra
1	Ulhas River	0.0013	0.03	0.01	0.01
2	Panvel River	0.0015	0.04	0.01	0.01
3	Diffusion	0.24	9.98	1.72	2.66
4	Ocean Exchange	6.04	94.19	44.13	25.15
5	Waste Discharge	0.01	0.26	0.06	0.42
6	Suspended Sediment	0.09	1.58	0.69	0.42
7	Sum Input	6.38	106.09	-	-
		Fluxes out of system (10^9 dpm.d^{-1})			
8	Decay	0.78	60.28	5.7	16.09
9	Seawater Exchange	12.90	314.29	94.3	83.91
10	Sum Output	13.68	374.57	-	-
11	Imbalance/SGD	7.30	268.48	53.38	71.68

5.3.2.2. Input from Rivers

The Panvel River is discharging water in the bay from the eastern side and the Ra flux contribution from Panvel River is estimated as;

$$A_{\text{Pan}} = F_{\text{Pan}} \times C_{\text{Pan}} \quad (\text{Eq. 5.5})$$

Where C_{Pan} is the average activity of Ra in the Panvel River and F_{Pan} is average daily water discharge from Panvel River ($L.d^{-1}$). The average activity from Panvel River was estimated from the samples collected at the mouth of the river during the low tide and receding of high tide. The flux of ^{223}Ra and ^{224}Ra via Panvel River was estimated as 1.5×10^6 dpm.d⁻¹ and 4.0×10^7 dpm.d⁻¹ respectively.

Similarly the contribution of Ra from Ulhas River was estimated using daily discharge and activity concentration in the river as;

$$A_{Ulh} = F_{Ulh} \times C_{Ulh} \quad \text{(Eq. 5.6)}$$

Where C_{Ulh} is the average activity of Ra in the Ulhas River and F_{Ulh} is the average daily water discharge from Ulhas River. The average activity at northern end of bay (Kalwa) was considered as activity in the Ulhas River. The estimated ^{223}Ra and ^{224}Ra flux was 1.5×10^6 dpm.d⁻¹ and 3.0×10^7 dpm.d⁻¹ respectively.

The activity concentration of Ra isotopes (^{223}Ra and ^{224}Ra) for river was taken near to the boundary of the bay where the rivers meets the bay. We approximate the two freshwater end-members by simply using the higher activity concentration measured near the mouth of each river. In this way all processes adding Ra to river water as it flows downstream are accounted for, even though not specifically identified. The total contribution of each ^{223}Ra and ^{224}Ra is only about 0.01% of total contribution of Ra flux in to bay. Even though we have taken upper estimate for river Ra input, mass balance is insensitive to changes in the river end-member Ra activities.

5.3.2.3. Input from Wastewater Discharge

The bay houses a number of industrial units and urban settlement and is the ultimate recipient of all the liquid discharges from these industries. The Mumbai Harbour Bay receives

260 million litres per day (MLD) domestic waste water and 180 MLD of industrial waste water. Thus about 440MLD waste water is being discharged in the bay [259]. The Ra flux in the bay via waste water discharge can be estimated as;

$$A_{\text{dis}} = F_{\text{dis}} \times C_{\text{dis}} \quad \text{(Eq. 5.7)}$$

Where C_{dis} is average activity of Ra in the wastewater discharge ($\text{dpm} \cdot 100\text{L}^{-1}$) and F_{dis} is the average daily wastewater discharge ($\text{L} \cdot \text{d}^{-1}$) in the bay. The activity at the mouth of streams was measured and average value was considered for calculation. The contribution of ^{223}Ra and ^{224}Ra via waste water discharge was found as $7.7 \times 10^6 \text{dpm} \cdot \text{d}^{-1}$ and $2.6 \times 10^8 \text{dpm} \cdot \text{d}^{-1}$ respectively. It is only about 0.06% and 0.42% of total Ra flux in the bay for ^{223}Ra and ^{224}Ra respectively.

5.3.2.4. Diffusion of Ra from bottom sediments

The estuarine surface sediment contains Ra enriched saline porewater similar to saline groundwater. The surface sediment being relatively impermeable sediments the diffusion and bio-irrigation process dominate over advection which is dominant in the case of groundwater. In the present study diffusion will refer diffusion plus bio-irrigation. The amount of Ra flux via diffusion can be estimated as;

$$A_{\text{diff}} = F_{\text{diff}} \times A_{\text{sed}} \quad \text{(Eq. 5.8)}$$

Where F_{diff} is the diffusive flux ($\text{dpm} \cdot \text{m}^{-2} \cdot \text{d}^{-1}$) of Ra from surface sediment to water and A_{sed} is the bay surface area (m^2). The diffusive fluxes of ^{224}Ra and ^{223}Ra from bottom sediments are known to be similar for different sedimentary facies e.g. muddy, sandy etc. [260]. Beck et al. has estimated diffusive flux as $0.052 \text{dpm} \cdot \text{m}^{-2} \cdot \text{h}^{-1}$ and $2.2 \text{dpm} \cdot \text{m}^{-2} \cdot \text{h}^{-1}$ in South Great Bay, NY [261] and $0.04 \text{dpm} \cdot \text{m}^{-2} \cdot \text{h}^{-1}$ and $1.17 \text{dpm} \cdot \text{m}^{-2} \cdot \text{h}^{-1}$ in Jamaica Bay, USA [80] for ^{223}Ra and ^{224}Ra respectively. Garcia et al. [262] have estimated diffusive flux for ^{223}Ra and ^{224}Ra in Venice

Lagoon, Italy as 0.046 dpm.m⁻².h⁻¹ and 1.33 dpm.m⁻².h⁻¹ respectively. The literature study also showed the similar values of the diffusive flux for ²²³Ra and ²²⁴Ra.

Thus considering the similar value of diffusive flux [260] of Ra for different facies and limitations (drawback) in the core incubation method [80] used for estimation of diffusive flux, the literature [260] value of F_{diff} for ²²³Ra and ²²⁴Ra was taken in the present study. The diffusive fluxes for ²²³Ra and ²²⁴Ra was estimated and found to be 0.24 x 10⁹dpm.d⁻¹ and 9.98 x 10⁹dpm.d⁻¹ respectively. The diffusion through sediment contributes about 2% and 3% of total Ra influx for ²²³Ra and ²²⁴Ra respectively. In the Jamaica Bay [80] the diffusion contribution was about 4–9% (²²³ Ra) and 5–11% (²²⁴ Ra) of the Ra input to the bay while in South Great Bay USA [261] diffusion contribution was 4.6% for ²²³Ra and 7.7 % for ²²⁴ Ra.

5.3.2.5. Input from suspended particles

Production of desorbable ²²³Ra and ²²⁴Ra from the particle-bound ²²⁸Th and ²²⁷Th can result in a significant inventory of Ra flux from suspended sediment. The contribution from suspended sediment can be calculates as;

$$A_{\text{susp}} = V_{\text{bay}} \times S_{\text{susp}} \times C_{\text{susp}} \times \lambda_{\text{Ra}} \quad \text{(Eq. 5.9)}$$

Where, S_{susp} is the total suspended matter in the bay (mg.L⁻¹) and C_{susp} is the activity concentration on Suspended Sediment (dpm. kg⁻¹). To determine activity concentration of 5 g of collected suspended sediment was mixed thoroughly in Ra-free seawater (seawater passed through pre-filter and MnO₂-fiber) and diluted slurry was allowed to pass through MnO₂-fiber to extract Ra. The contribution of ²²³Ra and ²²⁴Ra from suspended sediment was found to be 9.5 x 10⁷dpm.d⁻¹ and 1.58 x 10⁹ dpm.d⁻¹ respectively. Previous studies in other ecosystem also concluded that the contribution from suspended sediments is only about 1% of Ra influx in the system [80, 261].

5.3.3. Estimation of SGD

Total Ra flux going out of bay via decay and seawater exchange was found to be 13.68×10^9 dpm.d⁻¹ while total input from tidal input, diffusion, river and sediment was estimated to be 374.57×10^9 dpm.d⁻¹. Thus, there is imbalance of 7.3×10^9 dpm.d⁻¹ and 268.48×10^9 dpm.d⁻¹ for ²²³Ra and ²²⁴Ra flux in the bay respectively. The imbalance can be attributed to contribution from submarine groundwater discharge in the bay. The SGD can be estimated from the imbalance of Ra flux as:

$$\text{SGD(L. d}^{-1}\text{)} = \frac{\text{Total imbalance flux of Ra (dpm. d}^{-1}\text{)}}{\text{Activity Conc. of Ra in groundwater (dpm. l}^{-1}\text{)}} \quad \text{(Eq. 5. 10)}$$

Table 5.3: Activity concentration of ²²⁴Ra and ²²³Ra in bay, porewater and groundwater samples

Sample	Concentration (dpm.100L ⁻¹)		ln[Concentration (dpm.100L ⁻¹)]	
	²²⁴ Ra	²²³ Ra	²²⁴ Ra	²²³ Ra
Avg. Conc. in bay	35.36	1.46	0.37844	3.56558
Porewater samples	95.5	2.65	0.97456	4.55913
	131.54	3.64	1.29198	4.87931
Groundwater samples	312.35	14.85	2.698	5.74412
	515.44	28.85	3.36211	6.24502

Table 5.3 shows the average activity concentration of Ra in bay, activity concentrations at porewater samples and groundwater samples. The variation of activity concentration of ²²³Ra vs. ²²⁴Ra (figure 5.3a) and ln(²²³Ra) vs. ln(²²⁴Ra) (Figure 5.3b) suggested that the groundwater samples collected represents true representative of source water in the bay as all the activity

concentration falls on linear fit line. The ^{224}Ra and ^{223}Ra activity concentration for porewater samples vary at the sampling locations but the AR value is very well in agreement at different locations, indicates similar source is contributing in the creek. The activity concentration ratio in the groundwater samples are also found in similar range which support the similar sources of contributing in the bay. Thus average activity concentration in groundwater was taken for the calculation of SGD in Equation 5.10. The estimated SGD in the bay using ^{233}Ra and ^{224}Ra was found to be $3.34 \times 10^{10} \text{ L.d}^{-1}$ and $6.49 \times 10^{10} \text{ L.d}^{-1}$ respectively. The expected error in measurement of SGD is about 50%. The contribution of ^{233}Ra and ^{224}Ra via SGD is 53.4 % and 71.7% of total flux of radium in the Mumbai Harbour Bay.

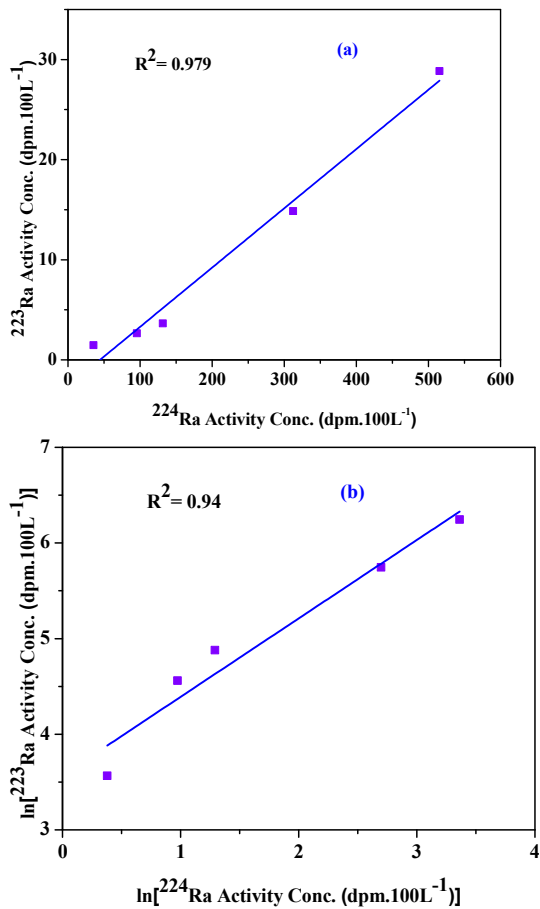


Figure 5.3: Variation of ^{223}Ra vs. ^{224}Ra (a) Activity Concentration and (b) $\ln(\text{Activity Concentration})$

5.4. Conclusion

A comprehensive mass balance has been constructed for short-lived Ra isotopes (^{223}Ra and ^{224}Ra), in Mumbai Harbour Bay and individual budget components have been evaluated separately. The different pathways of radium input sources in bay from the ocean during the high tide, river, sediment and wastewater discharge, and Ra export from bay via mixing and radioactive decay, were considered in mass balance for the estimation of SGD in bay. The total flux of ^{223}Ra and ^{224}Ra in the bay was estimated as $6.4 \times 10^9 \text{ dpm.d}^{-1}$ and $106.1 \times 10^9 \text{ dpm.d}^{-1}$ respectively. The contribution of radium flux was negligible (about 0.01% of total radium flux in the bay) from each river. The contribution from surface sediment through diffusion was found about 1.7 % and 2.7 % for ^{223}Ra and ^{224}Ra respectively. The suspended sediment contribution was found about 0.7 % and 0.4 % for ^{223}Ra and ^{224}Ra respectively. The contribution from wastewater discharge was found about 0.1 % and 0.4 % for ^{223}Ra and ^{224}Ra respectively. The tidal input for ^{223}Ra and ^{224}Ra was found as 44.1 % and 25.2 % of total radium flux respectively. Total fluxes out of the system via ocean exchange and decay was found as $7.3 \times 10^9 \text{ dpm.d}^{-1}$ and $268.5 \times 10^9 \text{ dpm.d}^{-1}$ for ^{223}Ra and ^{224}Ra respectively. The SGD in the bay was estimated based on the imbalance between input and losses contribution of radium. The volume of SGD based on ^{223}Ra and ^{224}Ra mass balance was found to be $33.4 \times 10^9 \text{ L.d}^{-1}$ and $64.9 \times 10^9 \text{ L.d}^{-1}$ respectively. The SGD contribution of ^{223}Ra and ^{224}Ra flux in the bay was found as 53.4 % and 71.7 % respectively.

CHAPTER 6

STATUS OF TRACE AND TOXIC ELEMENTS IN CREEK ECOSYSTEM USING TXRF METHOD

6.1. Introduction

The environmental balance of the marine ecosystem has been adversely affected by industrial, technological and residential development around it. The marine water bodies are continuously being loaded with large amounts of trace and toxic elements. The present study area (Thane Creek) receives effluents containing trace and toxic elements both from the mainland and from Mumbai Island in the west acts as sinks for most of the pollutants [249]. The present study was carried out to understand the status and fate of trace and heavy metals in the Thane Creek. Most of the metal present in $\mu\text{g kg}^{-1}$ to ng kg^{-1} range in the seawater hence requires analytical procedure with a detection limit in the trace to ultra-trace range. The method based on atomic absorption spectrometry (AAS) or stripping voltammetry reported either single element or simultaneous determination of four or five elements. In this area total reflection x-ray fluorescence (TXRF) spectrometry, a special variant of energy-dispersive XRF appears to be very promising [263]. The marine sediments have concentrations in the ppm-percentage range so it can be analysed without pre-concentration after digestion or slurry preparation. Even the TXRF has detection limits in the range of ppb but direct application of TXRF for the determination of trace elements in sea water is usually impeded by the high salt matrix, which hinders the detection of extremely low traces.

Thus, the separation of the trace elements from the seawater prior to measurement is needed for TXRF measurement. Also, pre-concentration during the separation of salt improves

the detection limit further. Such sample preparation steps, however, often associated with systematic errors (e.g., contamination of the sample) and so may worsen the problems of determining extremely low concentrations in seawater. A comprehensive review of the various methods available for prior enrichment in connection with water analysis by conventional XRF has recently been published [264].

6.2. Standardization of method for a simultaneous multi-element determination from seawater by TXRF

First attempts to develop a pre-concentration procedure for the determination of heavy metals by TXRF were reported in 1980 [265]. Heavy metal and trace elements in the sea-water samples were separated from the salt matrix as dithiocarbamate complexes by using the reverse-phase technique in 1982 [266]. Separation and pre-concentration of trace elements using dithiocarbamate precipitation and further digestion of precipitate in acid and analysis using SRTXRF were reported in 2005 [267].

Pre-concentration of cadmium, copper, iron, molybdenum, nickel, vanadium and zinc from sea water with ammonium tetramethylene dithiocarbamate (APDC) - diethylammonium diethyldithiocarbamate (DDDC) in chloroform and back extraction from chloroform was reported for the seawater using inductively coupled plasma emission spectrometry (ICP-ES) [266]. This pre-concentration method was standardized for TXRF analysis in the present study and double extraction of elements from seawater using APDC-DDDC has been used for the pre-concentration and separation of salt content from seawater samples.

6.2.1. Preparation and Purification of Chemicals

The method involves the determination of the very low level of concentration, it is necessary to have all chemical and glassware free of any contaminations. All the glassware used in the analysis was cleaned by heating in ultrapure nitric acid and Milli-Q water for half an hour and further keeping these in an ultrasonic cleaner for 45 min. The sample supports were first cleaned by heating in 5% ultrapure nitric acid and subsequently cleaned in ultrasonic cleaner for 45 min. De-ionised (Milli-Q) water was used as the input in the procedure and stored in pre-cleaned PTFE bottles. 16M Ultrapure nitric acid (Merck make) was used for the preparation of the 2M nitric acid solution and stored in pre-cleaned polypropylene (PP) bottles. Chloroform, APDC - DDDC solution and Ammonium acetate buffer solution used were prepared and purified as follows:

Analytical grade chloroform (400 ml; s d fine) was extracted 3-times with nitric acid (100 ml, 2 M; Merck, ultrapure) in a 500-ml separating funnel with fresh nitric acid being used for each extraction. The chloroform was next washed 3 times with high-purity water and then transferred into a PP bottle. When not in use, the PTFE bottle was placed in a black polyethylene bag and stored in a refrigerator. Usually, 2 litres of purified chloroform were prepared at one time, this solvent being stable for about 3 weeks.

Ammonium tetramethylene dithiocarbamate APDC (0.5 g, s d fine) and diethylammonium diethyldithiocarbamate DDDC (0.5 g, BDH UK) were weighed dissolved in 50 ml of water. The solution was extracted using 10 ml of purified MIBK/CHCl₃ 5 times using fresh chloroform in separating funnel. Since dithiocarbamate is only slightly soluble in MIBK/CHCl₃ whereas metal complexes are highly soluble, the reagent is easily purified in this

manner. The purified reagent was stored in a pre-cleaned 100-ml PP bottle which was stable for at least 24 h. Equal volumes (500 ml) of glacial acetic acid (s d fine, A R grade) and 25% ammonia solution (s d fine, A R grade) were mixed slowly over a 2-h period, in a polypropylene container placed in a water bath. The acetate buffer solution was then purified as follows. Purified APDC- DDDC solution (5 ml) was added to 400 ml of the buffer solution and the mixture extracted 6 times with separate 40-ml portions of purified chloroform. The purified buffer solution was stored in a pre-cleaned PP bottle.

6.2.2. Pre-concentration Procedure

About 500 g of acidified seawater (pH about 2) transferred into a 500-ml separating funnel containing 1.4 ml of acetate buffer, 2 ml of APDC - DDDC solution and 10ml of chloroform. The mixture was mechanically shaken for 3 min and then allowed to the separation of phase for 5 minutes. The organic (chloroform) layer was transferred to a 125 ml separating funnel. The aqueous phase further mixed with 10 ml of chloroform and separated the chloroform phase similarly then two chloroform extract were combined. The chloroform extract was added with 0.20ml of concentrated nitric acid, shaken for 1 min and then allowed to stand for 5 min. About 2ml of de-ionised water was added to this mixture, shaken for 1 min and then allowed to stand for 5 min for separation of phases. The chloroform layer was discarded and the aqueous layer was drained into a 4-ml PTFE beaker. The separating funnel was rinsed with about 2 ml of high-purity water and the washing was added to the PTFE beaker. The aqueous solution was evaporated to incipient dryness and the residue was dissolved in a known amount of dilute nitric acid. The pre-concentration factor 250 easily can be reached using this procedure.

6.2.3. Sample Preparation and Measurement

The sample solution was added with 500 μ L of Yttrium (Y) of 20 ppm concentration and homogenized on vertex mixture. About 10 μ L aliquots of the sample were deposited on clean and siliconised quartz sample supports and dried under IR lamp. A GNR Analytical TXRF spectrometer TX-2000 was used for TXRF measurements. Mo K α radiation produced by Mo-W dual target X-ray tube operated at 40 kV, 30 mA and monochromatized using a high reflectivity 80% (W L α /L β /Mo K α) multilayer, was used for sample excitation. A Peltier cooled Silicon Drift Detector (SDD) with an energy resolution of 139 eV at 5.9 keV (Mn K α) was used for detection of X-rays produced. The TXRF spectra were recorded for a live time of 1000s. The data acquisition and processing were performed with TXRFacq32 and SinerX computer programs provided with the instrument. The estimation of concentration in the samples was carried out using the relative sensitivity of elements as discussed in Chapter 2 Section 2.8.

6.2.4. Validation of method

Trace elements from seawater reference material (NAAS-6), was pre-concentrated using ammonium tetramethylene dithiocarbamate - diethylammonium diethyldithiocarbamate and analysed using TXRF. The acquired spectrum of the NAAS-6 is shown in figure 6.1. The result of the analysis for each element is given in Table 6.1. The average deviation of results from true value was found to be about 16%.

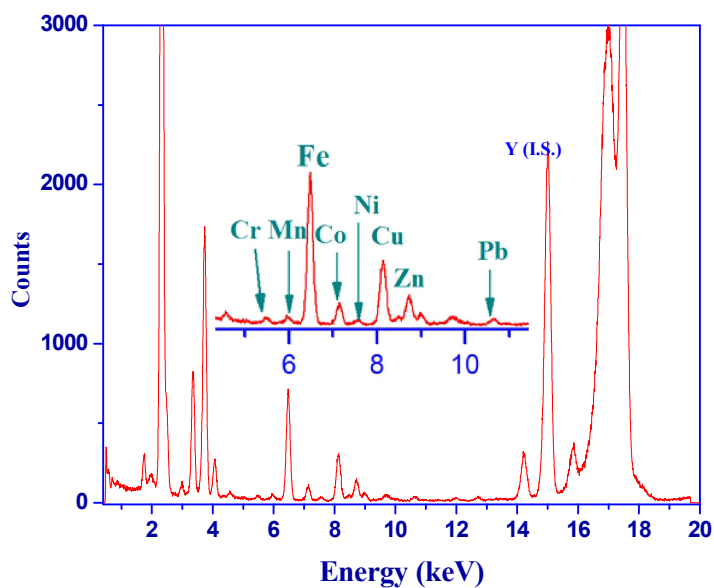


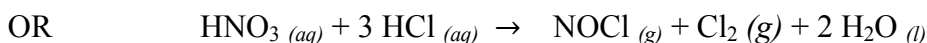
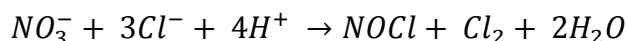
Figure 6.1: TXRF spectra of liquid phase after separation of trace elements from NAAS-6

Table 6.1: Result of analysis of seawater reference material (NAAS-6)

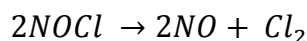
Elements	Reported Conc. (ppb)	Observed Conc. (ppb)	Detection limit (ppb)
V	1.46	1.32	0.07
Cr	0.118	0.098	0.026
Mn	0.53	0.48	0.02
Fe	0.495	0.603	0.014
Co	0.015	0.012	0.001
Ni	0.301	0.314	0.05
Cu	0.248	0.261	0.01
Zn	0.257	0.301	0.01
Pb	0.006	0.008	0.003

6.3. Development of method for removal of chloride by vapour phase decomposition from seawater sample for TXRF measurement:

Chloride is present in a very high concentration of 19000 ppm (55.04% by weight) and causes problems in the detection of lower atomic number elements in TXRF analysis. The chloride can be removed from seawater deposited on samples support by vapour phase decomposition method. A small petri dish (about 60mm diameter), containing ultrapure nitric acid was kept in the centre of a big petri dish (about 200 mm in diameter). The siliconised sample supports, deposited with 10 µl of seawater and internal standard were kept around the petri-dish containing acid as shown in Figure 6.2. The big petri dish was covered with other petri-dish of similar diameter. The chamber was heated under an infrared lamp for various time intervals (8 min, 16 min, 24 min and 32 min) in the covered state. Under the heating condition the acid present in the small petri-dish goes into vapour phase and interact with the chloride present in the sample support gives nitrosyl chloride and chlorine gas as:



Nitrosyl chloride can further decompose into nitric oxide and chlorine



The upper petri dish was removed and supports were kept under an infra-red lamp to dry the sample on support. After the sample was dried, the TXRF spectrum was recorded using WLα

excitation source for 500 seconds. Figure 6.3 shows the TXRF spectrum of untreated seawater. The intensity of Cl peak is very high compared to other elements like S, K, Ca, Fe etc. Figure 6.4 shows the TXRF Spectrum of seawater treated for 8 minutes with HNO_3 vapours, excited by WLa and counted for 500s. The scale of the spectrum was kept same to have an idea about the intensity (peak height) of the chlorine. The spectrum in the inset shows that the peak height of the chlorine has significantly decreased with respect to that of untreated seawater (Figure 6.3). The counts for the chlorine peak have reduced from 30000 to about 14000.

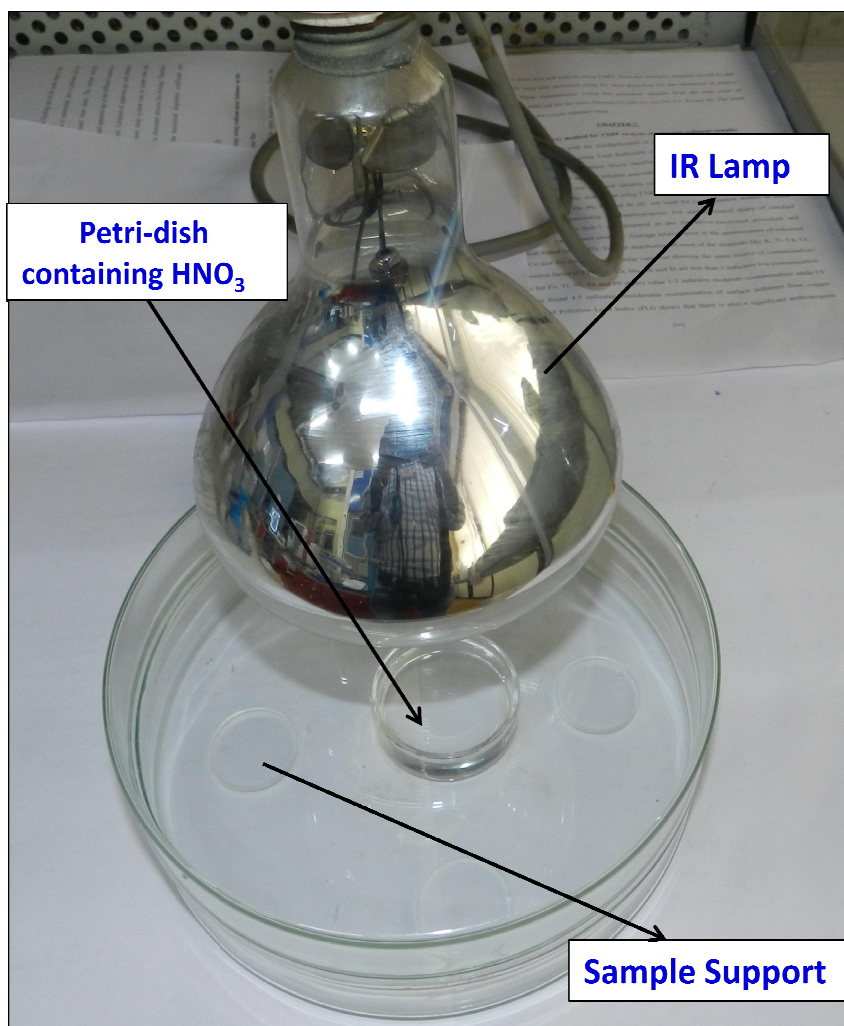


Figure 6.2: Setup for removal of chlorine from the seawater samples

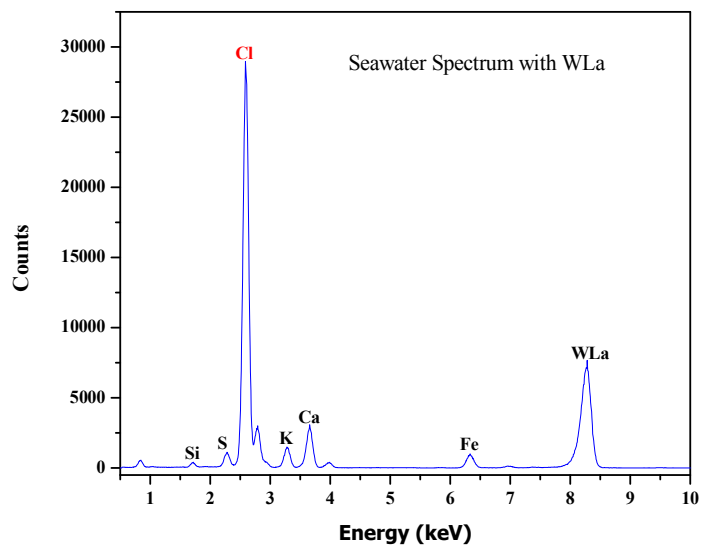


Figure 6.3: TXRF Spectrum of untreated seawater

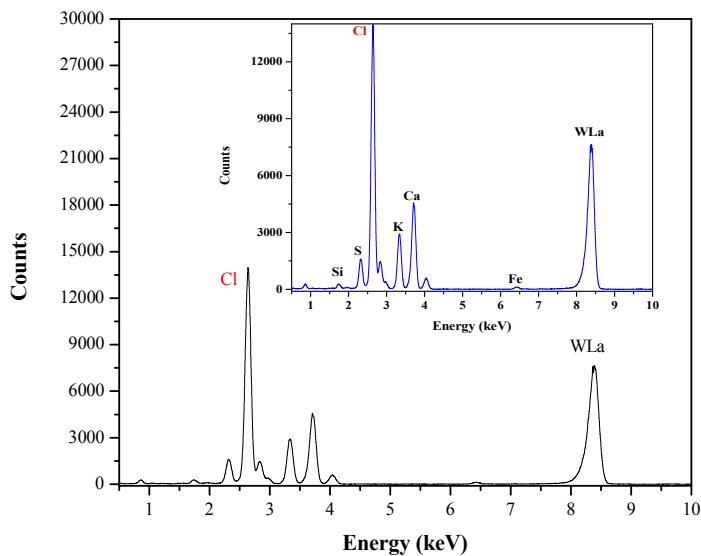


Figure 6.4: TXRF Spectrum of seawater treated for 8 minutes with HNO₃ vapour

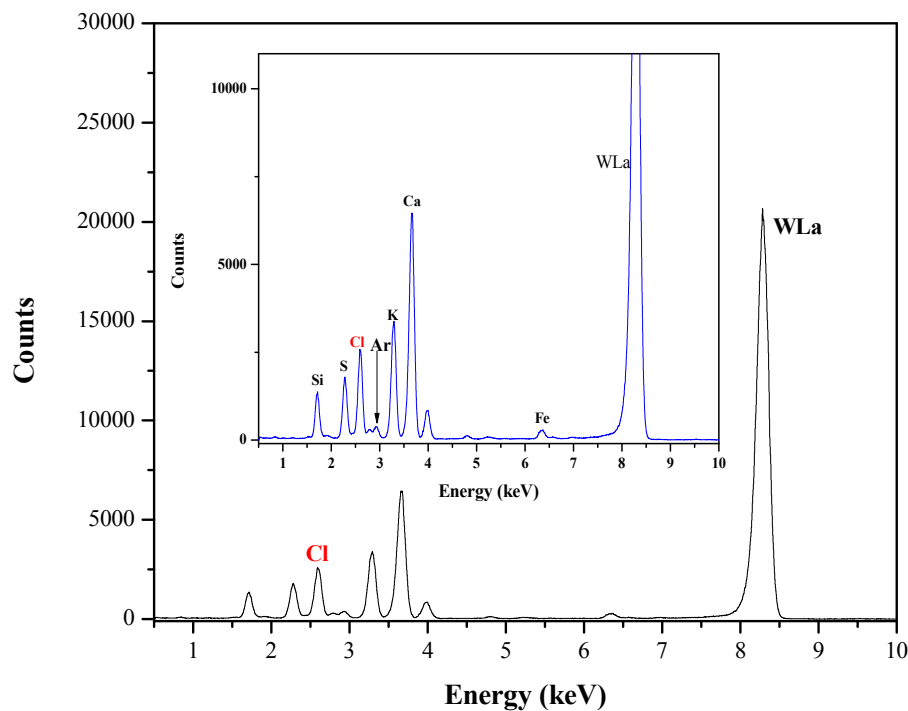


Figure 6.5: TXRF Spectrum of seawater treated for 16 minutes with HNO₃ vapour

TXRF spectrum of seawater treated with HNO₃ vapours for 16 minutes, excited by WLa and counted for 500s is shown in Figure 6.5. The height of chlorine peak has reduced further to a level of 2500 counts. It was observed that the Ar peak (energy 2.96 keV) which was not visible initially because of the intense peak of chlorine can be identified. Figure 6.6 shows the TXRF spectrum of seawater treated with HNO₃ vapours for 24, excited by WLa and counted for 500s. It is cleared that the chlorine peak has almost reduced and has count about 335 only and Ar peak can be identified easily.

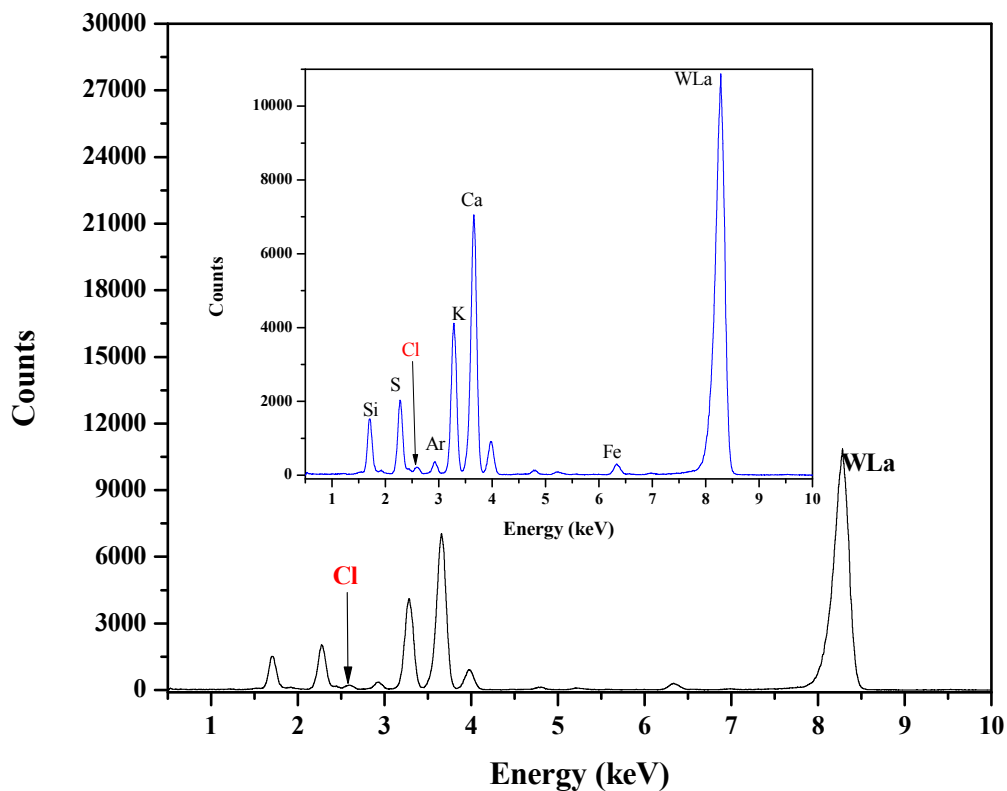


Figure 6.6: TXRF Spectrum of seawater treated for 24 minutes with HNO₃ vapour

TXRF spectrum of seawater treated with HNO₃ vapours for 32 minutes, excited by WLa and counted for 500s is shown in Figure 6.7. The chlorine peak is completely removed from the spectrum suggesting the chlorine can be removed from the sample online by vapour phase decomposition using HNO₃. The spectrum is shown up to 30000 counts to have the comparison with the untreated and treated seawater.

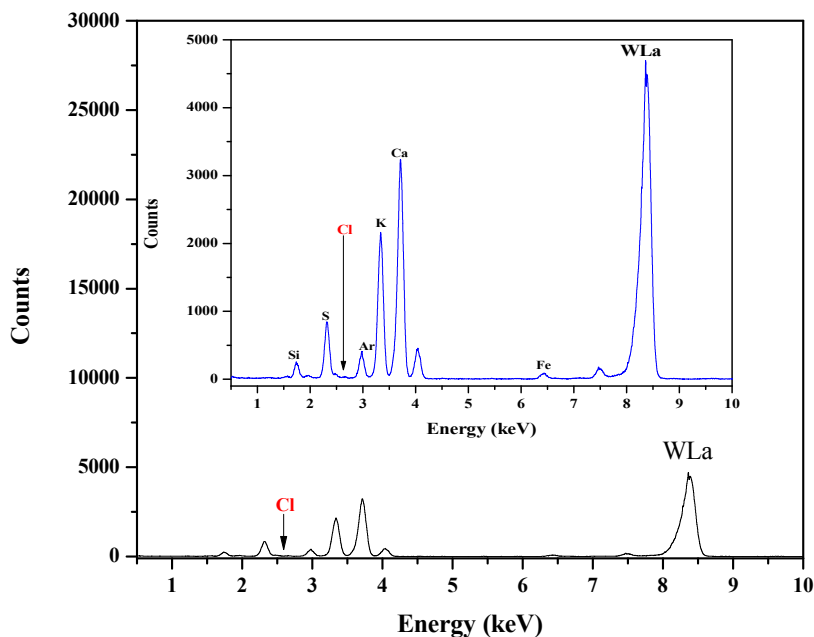


Figure 6.7: TXRF Spectrum of seawater treated for 32 minutes with HNO₃ vapours

6.4. Development of method metals detections in solid samples using TXRF coupled with slurry sampling

Generally, Analysis of samples using TXRF requires samples to be in liquid form. Therefore, analysis of sediment or any other solid samples needs to be dissolved in the liquid phase for the analysis. Normally, the analysis of sediment samples is performed by total digestion of samples but the process has some disadvantage regarding the information of the volatile component in the samples. To overcome such problem a slurry method was developed and standardized which have the following advantage over conventional digestion method.

1. No sample dissolution
2. Maximum sample information (metals, halogens and “volatile” elements)
3. Simplicity and productivity (time/cost)

The method is used for direct and simultaneous metals detection on powdered sample suspended in liquid media. Thus, the following points need to be considered for the slurry-TXRF analysis:

1. Slurry sedimentation
2. Critical mass/thickness must correspond to the TXRF conditions

6.4.1. Slurry Sedimentation:

The setting speed of particles suspended in a fluid is regulated by Stokes' law

$$v = \frac{2R^2(d_s - d_f)g}{9\eta} \quad (6.1)$$

Where:

v = setting speed,

R = Stokes radius of particles

d_s = density of the particles

d_f = density of the fluid

g = gravity constant

η = fluid viscosity

Thus for particles of different size, the setting velocity will be different and the difference between the setting velocity i.e. relative fall velocity differences can be reduced using liquid with higher fluid viscosity. In the present study, we have used 1-methyl pyrrolidone (NMP) solution for the preparation of slurry. The η NMP is greater than η H₂O, hence, reduces the grains setting speed and the relative fall velocity differences.

Figure 6.8 shows the setting velocity of quartz (SiO_2) and goethite ($\alpha\text{-FeOOH}$) in H_2O or 1-methyl pyrrolidone for different grain size of the particles using the Stokes' law. The quartz has low density of 2.6 g cm^{-3} and goethite has high density of 4.3 g cm^{-3} . Quartz and Goethite are end-members phase density minerals occurring in soils. From the figure, it is observed that the setting speed of quartz and goethite is lower in solvent compare to the aqueous phase and the relative difference between the two decreases in the solvent compared to the aqueous phase.

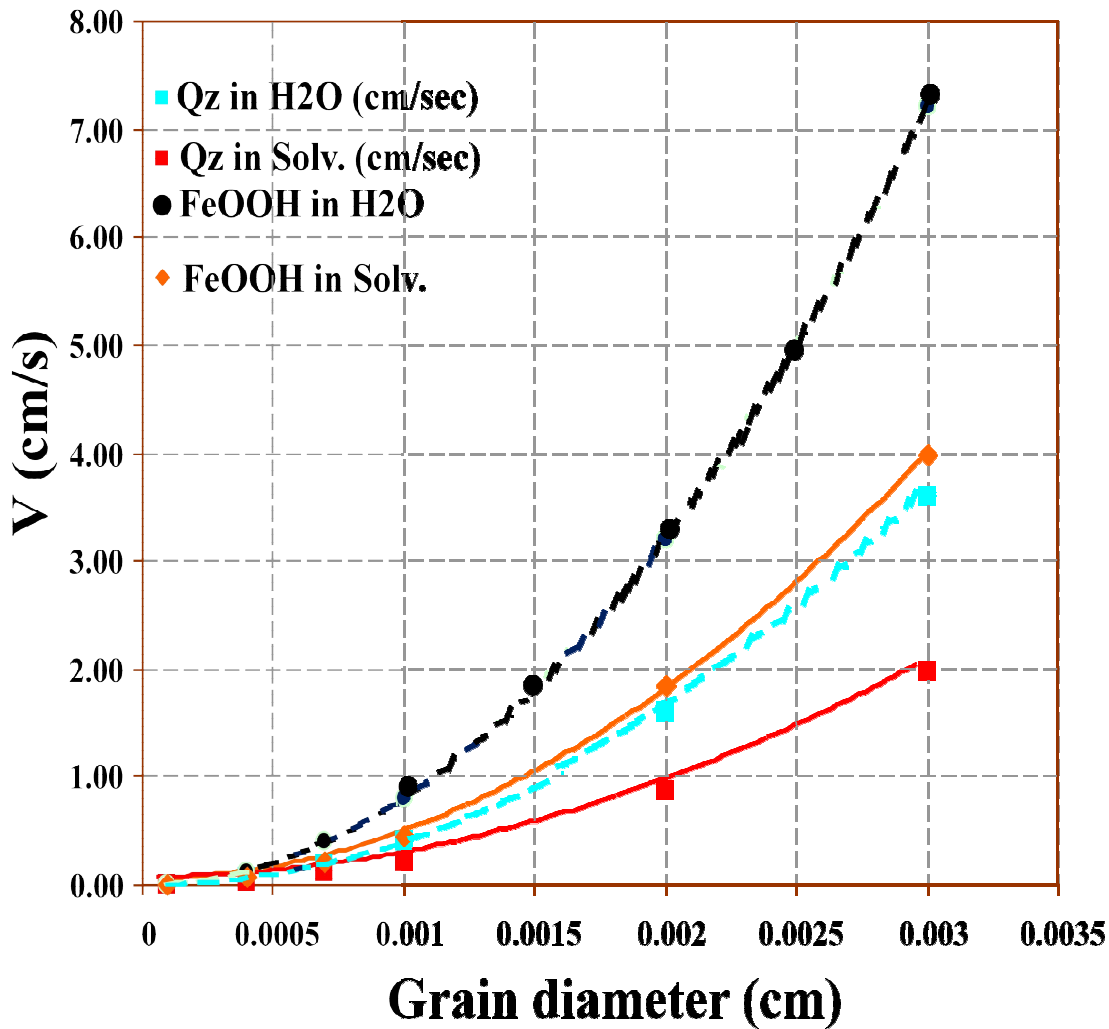


Figure 6.8: Setting velocity of quartz (SiO_2) and goethite ($\alpha\text{-FeOOH}$) in H_2O and NMP

6.4.2. Critical mass on the sample support

As it was discussed in Chapter 2 Section 2.8 that for TXRF the mass on the sample support should be less than critical mass. Therefore, the slurry was prepared such way that after drying the deposited sample, the weight of residue left on sample support should be less than 10 µg.

6.4.3. Validation of method:

To validate the slurry sampling for total reflection X-ray fluorescence (TXRF) analysis of powdered samples, about 40 mg of certified reference material IAEA-Soil-7 reference material was suspended in de-ionised (Milli-Q) water and N-Methyl-Pyrrolidone (NMP). The slurry was prepared by sonication of the suspended solution in an ultrasonic bath for 30 minutes. This slurry was added with 300ul of 100 ppm Ga as internal standard and 10 µL aliquot of this were deposited on a cleaned and siliconised quartz sample support and dried under the infra-red lamp. After drying, the TXRF spectrum was recorded for a live time of 1000 seconds using TXRFAcq32 computer programs provided with the instrument. Spectrum was analysed for K, Ca, V, Cr, Mn, Fe, Cu, Zn, Sr and Pb using SinerX computer programs provided with the instrument and average relative error in measurement was found to be 13% Table 6.2.

Table 6.2: Result of certified reference material IAEA-Soil-7 by the slurry method

Element	Certified Value (ppm)	Slurry Method (ppm)	Relative % error
K	12100	11900	-1.7
Ca	163000	159000	-2.5
Ti	3000	3500	16.7
Mn	631	610	-3.3
Fe	25700	27610	7.4
Cu	11	13.3	22.7
Cr	60	55	-8.3
Ni	26	30	15.4
Zn	104	130.3	25.3
Rb	51	58.8	15.3
Sr	108	82.5	-23.6
Pb	60	53.4	-11.0

6.5. Status of trace and toxic elements in creek ecosystem of MHB

6.5.1. Direct measurement of seawater by TXRF

Direct measurement of seawater by TXRF is not possible due to large content of dissolved solids and suspended particulates in the seawater even though the detection limit is in the range of ppb. The suspended particulates are removed by filtering the seawater with 0.45 μm syringe filter and we get dissolved metal fraction in the samples. Nearly 2g of filtered seawater

from each sample was added with internal standard Gallium (Ga) and well homogenized on cyclo mixer. Total dissolved solids in seawater were very high so whole content was diluted with Milli-Q water to reach the critical mass condition necessary for TXRF. The samples were diluted with Milli-Q water and taking salinity of seawater as 3.5% total dissolved solids on sample support after depositing 10 μ l was calculated which found to be in the range of 20 μ g. The samples were treated for chlorine removal as discussed in **Section 6.3**. For TXRF analysis, 10 μ l aliquots of the samples were deposited on clean quartz sample supports dried under IR lamp and the TXRF spectra were recorded. The concentration of K and Ca can be estimated from the spectrum using the method discussed in the **Chapter 2 Section 2.8**.

6.5.2. Pre-concentration of elements and TXRF analysis

Seawater samples collected from different locations of the study were extracted with an APDC-DDDC solution as described in the **Section 6.2.2** and analysed by TXRF for the analysis of Cr, Mn, Fe, Co, Ni, Cu, Zn and Pb. Figure 6.1 shows the TXRF spectrum of the seawater processed as per procedure discussed.

6.5.3. Results

Table 6.3 gives the result of analysis of the samples from Thane creek. The obtained value for Zn, Pb, Cu, Ni, and Co was higher with reported value in the Arabian Sea [268]. To understand the impact of discharges from city side as well as industrial side the concentration obtained from both side of the creek was divided by the concentration obtained in the middle of the creek as shown in Figure 6.9. The lower value of the concentration in water collected from mid of the creek could be due to dilution effect along with associated biological and sedimentation factor.

Table 6.3: Results of seawater analyzed by TXRF

Sr. No.	Element	Concentration ($\mu\text{g/L}$) of Element in seawater at different locations		
		Location S1	Location S2	Location S3
1	K*	599.5 \pm 3.3	583.6 \pm 3.2	677.8 \pm 3.9
2	Ca*	397.7 \pm 2.7	160.3 \pm 1.8	512.6 \pm 3.1
3	V	2.6 \pm 0.1	0.3 \pm 0.02	2.4 \pm 0.1
4	Cr	200.0 \pm 1.9	40.0 \pm 0.5	148.0 \pm 1.5
5	Mn	17.0 \pm 0.4	12.0 \pm 0.3	20.0 \pm 0.5
6	Fe	1.9 \pm 0.2	1.2 \pm 0.1	2.3 \pm 0.1
7	Co	0.2 \pm 0.05	0.2 \pm 0.04	0.4 \pm 0.05
8	Ni	12.1 \pm 0.2	2.0 \pm 0.09	10.0 \pm 0.15
9	Cu	5.0 \pm 0.2	2.0 \pm 0.09	10.0 \pm 0.16
10	Zn	46.3 \pm 0.6	29.4 \pm 0.4	71.2 \pm 0.9
11	Pb	20.0 \pm 0.3	3.6 \pm 0.1	36.0 \pm 0.4

*Concentration of these elements is given in mg/L

Comparing the concentration of the trace and toxic elements from the midstream water of the creek with the water samples collected from the industrial and domestic effluent receiving area, it was found that the concentration of K, Ca, Mn, Fe, Co, Cu, Zn and Pb were found higher in the industrial side of the creek whereas V, Cr and Ni concentration were found higher in the samples collected from the side receiving city effluent. The result for Cr, Mn and Cu was found

comparable with earlier reported range of 100–142.8, 10.4–58.7 and 2.0–178.1 µg/L respectively [269].

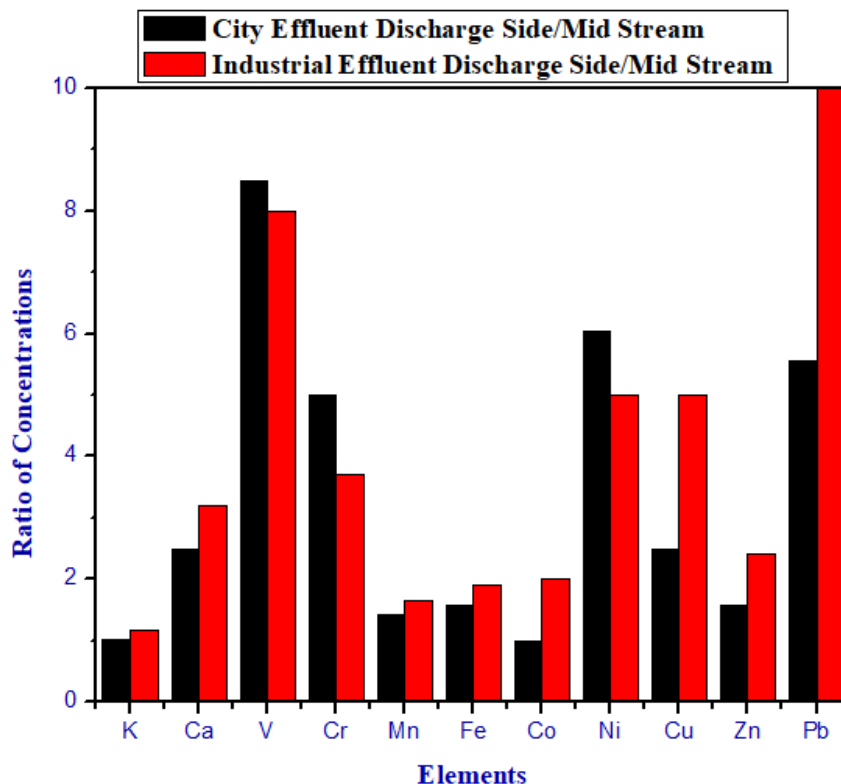


Figure 6.9: Concentration Ratio of Elements

6.6. Flux of trace and toxic elements toward the open sea

The suspended sediments, collected from 4 locations of the bay as discussed in **Chapter 3 Section 3.3.5**. The samples were dried in a laboratory oven at 110 °C, powdered using grinding machine and sieved (75 µm) to get a fine powder. The slurry of samples was prepared and measured using TXRF, as per the procedure mentioned in **Section 6.4.1.3**.

The suspended silt load at different locations is given in Table 6.4. The average suspended sediment load (26 mg/l) in the bay was taken to calculate the concentration of different elements in the seawater from suspended sediments. The total load of different trace

and toxic elements in the bay can be calculated by multiplying the average concentration in the bay by the total volume of the bay. Since the MHB is subjected to wave actions and semi-diurnal tides with a tidal period of 12 hrs of 40 minute. As discussed in the **Section 5.3.1.2**, the volume going out of the bay (V_{out}) is the tidal prism volume plus average daily water discharge in the bay, which is 9.15×10^{11} litre per day. Considering the suspended sediment thoroughly mixed in the water column the flux of elements going out of bay daily can be estimated using concentration of elements from suspended sediment in the bay and volume of water going out of the bay per day as:

$$(Flux)_i = C_i \times V_{out}$$

Where:

(Flux)_i: Flux of elements i going out per day

C_i : Concentration of element i from the suspended sediment in the bay

V_{out} : volume of water going out of the bay per day

The concentration of different elements from suspended sediments in the bay and the flux of elements going out of the bay is given in Table 6.5.

Table 6.4: Suspended sediment load (mg/l) at sampling locations

Sr. No.	Location	Suspended sediment load (mg/l)
1	L5	30.8
2	L10	30.0
3	L19	22.3
4	L23	21.0
5	Average	26.0

Table 6.5: Concentration and flux of elements from suspended sediment

Elements	Concentration of elements ($\mu\text{g/l}$) from suspended sediment at different Location(L) in the bay					Flux of Element (Kg/day)
	L5	L 10	L 19	L 23	Average	
Ca	657.80	254.80	494.00	777.40	546.00	4.99×10^5
K	241.80	236.60	288.60	273.00	260.00	2.38×10^5
Ti	236.28	133.07	258.15	239.75	216.81	1.98×10^5
V	3.86	2.19	4.15	4.25	3.61	3.3×10^3
Cr	7.13	3.96	7.27	5.09	5.86	5.36×10^3
Mn	37.40	21.45	66.67	31.69	39.30	3.59×10^4
Fe	2046.20	1164.80	2303.60	2020.20	1883.70	1.72×10^6
Ni	2.06	1.27	2.62	2.10	2.01	1.84×10^3
Cu	3.53	2.07	3.21	2.60	2.85	2.61×10^3
Zn	2.77	2.04	4.03	2.60	2.86	2.61×10^3
Pb	0.68	0.38	0.55	0.61	0.56	5.09×10^2
Rb	1.48	2.84	1.72	1.64	1.92	1.76×10^3
Sr	6.13	3.40	4.41	6.95	5.22	4.78×10^3

6.7. Analysis of core sample collected from the Thane Creek:

6.7.1. Sample Preparation and Measurement

Sediment core sample was collected from Vashi location of the creek using gravity corer.

The collected cores were extruded vertically and sliced at 6.5 cm intervals and collected in sealed

polyethene bags. Samples were dried in a laboratory oven at 110 °C. Dried samples were first crushed in Pestle and Mortar and then crushed samples were ground using grinding machine into a fine powder. These powdered samples were sieved using a 75 µm sieve to get a fine powder with grain size less than or equals to 75 µm. A slurry of about 40 mg of sediment sample was prepared and TXRF spectrum was recorded for 1000s.

6.7.2. Results

Major elements K, Ca, Fe, Ti and Mn were having concentration 10.9 ± 0.5 , 26.6 ± 2.3 , 77.4 ± 1.7 , 9.3 ± 0.5 and 1.1 ± 0.2 mg/g respectively in the core. Heavy metals Cr, Ni, Cu, Zn were found in the concentration 222.5 ± 56.9 , 71.8 ± 5.0 , 149.3 ± 22.3 and 111.6 ± 18.1 mg/kg respectively in the core. Concentrations of Pb, Rb and Sr in the given core were found to be 24.8 ± 4.8 , 58.6 ± 3.4 and 193.1 ± 29.2 mg/kg respectively. Depth profiling of different elements in the core samples is shown in Fig 1.a, Fig 1.b and Fig 1.c. The maximum concentration of K, Ti, Ca, Cr, Mn, Ni, Cu and Rb found in the 6th segment of core indicates enrichment of these elements at the depth 39 cm in the core. Zn, Pb and Sr have a maximum concentration in the 8th, 9th and 10th segment respectively of the core indicating enrichment at 52, 58.5 and 65 cm depth respectively. Enrichment factor, Concentration factor, Pollution load index and Index of geoaccumulation (Igeo) in the surface sediment core were calculated. Contamination factor (CF) For K, Ca, Mn, Rb and Sr are less than 1 indicates low contamination. CF value for Fe, Ti, Ni, Zn and Pb shows value 1-3 indicates moderate contamination while CF for Cu was found 4.5 indicates considerable contamination of surface sediment from copper.

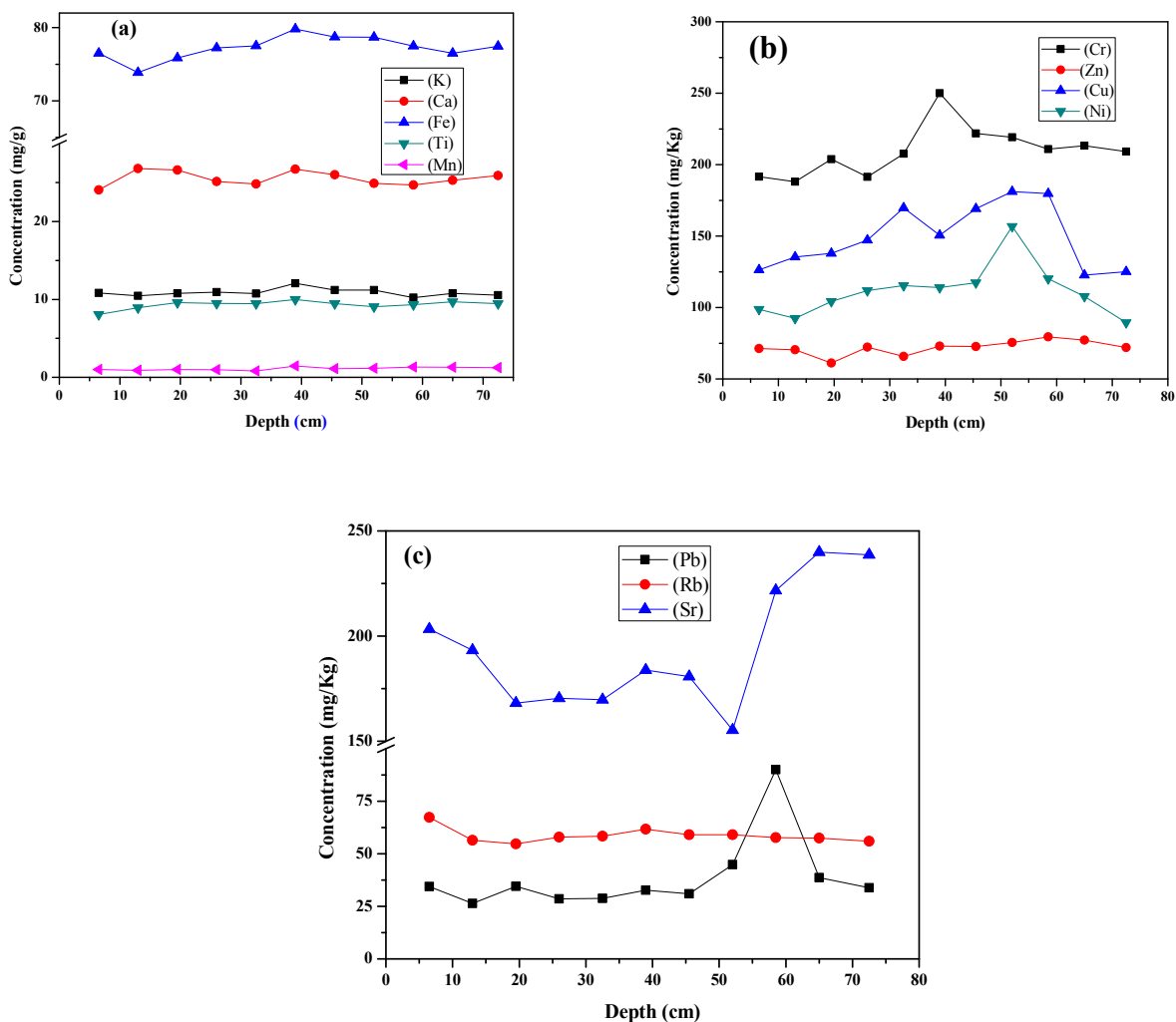


Figure 6.10 a, b and c: Depth profile of elements

Enrichment factor (EF) in the surface sediment core was calculated. K, Ca, Mn, Pb, Rb and Sr show depletion trend as their EF (<1) for surface sediment. Ti, Cr, Zn and Ni were found to be about normal or no enrichment ($EF \approx 1$). Cu was found moderately enriched as EF for this was found to be 2.31. The calculated Igeo values based on the concentration of elements in the upper continental crust was calculated. It is evident that Igeo values for K, Ca, Mn, Zn, Pb, Sr and Rb fall in class '0' at the sampling locations indicating that there is no pollution from these metals in the sampling site. The Igeo values of Ti, Cr, Ni and Fe fall in the range 0–1 (class

'2'), indicating unpolluted to moderately polluted levels in sediment core samples. Igeo values of Cu in sediment core samples found in class '3' reveal moderately polluted levels. The value of PLI greater than 1 shows that there is also a significant anthropogenic contribution to the surface sediment sample.

6.8. Conclusion

The pre-concentration of trace element using ammonium tetramethylene dithiocarbamate - diethylammonium diethyldithiocarbamate from seawater followed by TXRF measurement is suitable for analysis of trace elements in the sea water. The chlorine content from seawater deposited on sample support can be removed by treating with nitric acid vapour for the time duration of about 30 minute. The slurry preparation coupled with TXRF measurement can be used for measurement of sediment samples. The method can be used for the estimation of halogens and "volatile" elements which are not feasible by digestion of sediment and TXRF measurement. The effluent received by the creek from the city side are enriched in V, Cr and Ni whereas the effluent received from the industrial side are contributing more Mn, Fe, Cu and Zn. Comparing with earlier reported data with the present value indicates that the establishment and operationalisation of the effluents treatment plan on both sides have stopped further deterioration of the water quality of the creek water. For effective and proper management of the creek, attention should be directed towards the acquisition of long-term data on trace elements in the coastal water. The analysis of suspended sediment and estimation of flux indicates a large amount of elements is flushing out of bay daily. Vertical distribution of most of the elements like K, Ti, Ca, Cr, Mn, Ni, Cu and Rb shows nearly similar variation showing the same source of contamination. Calculation of Pollution Load Index (PLI) shows that there is also a significant anthropogenic contribution to the surface sediment sample.

CHAPTER 7

SUMMARY, CONCLUSION AND FUTURE PROSPECTS

Summary and Conclusion

Uncontrolled and rapid, industrialization and urbanization around the coastal areas have polluted the groundwater and surface water, discharging into the coastal region. These discharges carry various nutrients, heavy metals, radionuclides and organic compounds in the marine ecosystem. Distribution of the elements in any marine system depends on its physical and chemical properties and on coastal water mixing and movement towards the open sea. The status of trace and toxic elements in the study area and their mixing and transport towards the open sea needs to be studied for the better management strategies for protection of the Mumbai Harbour Bay from the land-based activities. Naturally occurring radioactive tracer can provide insight of coastal water movement and information related to Submarine Groundwater Discharge.

In the present study, the method for the estimation of tracer (^{223}Ra and ^{224}Ra) in water samples was developed and standardized. To understand the time taken by different elements (discharged in the system) to be removed from the system, the apparent water age, mixing and flushing rate was estimated. The apparent water age, flushing rate horizontal mixing coefficient of water mass in the creek was estimated using naturally occurring short-lived radium isotopes. Submarine groundwater discharge (SGD), an important pathway for the trace and toxic elements in the creek was estimated using Radium Mass Balance Model. A method based of TXRF was developed and standardized for the estimation of different trace and toxic elements in seawater

and sediment using TXRF was developed and standardized. Following are the important highlights of the present work:

Methods and Techniques

- In-situ pre-concentration sampling assembly was designed and fabricated.
- Heating bath assembly for preparation of MnO₂ coated fiber was designed and fabricated and MnO₂ was coated on acrylic fiber.
- The adsorption efficiency of Ra on MnO₂-fiber was estimated and found to be 100% for the water flow rate of 0.80 lpm.
- Estimation of efficiency for Helium, Air and Argon as carrier gas indicated higher efficiency for He compares to others.
- Variation of efficiency at a different flow rate of carrier gas showed higher efficiency in the range of 4-5 lpm flow rate.
- Study of water loss during the counting showed after 49 days decay and total 13 hrs of counting at various time interval water/fiber ratio changes from 1.0 to 0.77
- Detection limit for estimation of ²²⁴Ra and ²²³Ra was estimated to be 5.6×10^{-4} dpm 100L⁻¹ and 1.4×10^{-4} dpm 100L⁻¹ respectively.
- The efficiency of the counting system for ²²⁴Ra and ²²³Ra measurement was estimated to be 48.5% and 43.4% respectively.
- The reference material for multi-element was measured by TXRF and results compared with reference values.

Longitudinal Variation of Radium activity Concentration

- During the sampling trip-1(April 2016), the ²²⁴Ra and ²²³Ra activity concentration in the creek were found in the range of 22.88-51.46 dpm/100L and 1.03-2.26 dpm/100L with

average value 35.36 ± 9.04 and 1.46 ± 0.33 dpm/100L respectively. The average AR in the creek was found to be 22.52 ± 3.35 having a range from 16.28 to 29.46.

- During the sampling trip-2 (March 2017), the ^{224}Ra and ^{223}Ra activity concentration in the creek were found in the range of 17.58-34.22 dpm/100L and 0.83-1.49 dpm/100L with average value 25.62 ± 4.95 and 1.14 ± 0.18 dpm/100L respectively. The average AR in the creek was found to be 22.52 ± 3.35 having a range from 18.18 to 29.54.
- During the trip-3 (May 2017), the ^{224}Ra and ^{223}Ra activity concentration towards the open sea were found in the range of 7.66-20.56 dpm/100L and 0.52-1.1 dpm/100L with an average value of 13.11 ± 4.73 dpm/100L and 0.77 ± 0.19 dpm/100L respectively.
- During the trip-3 (December 2017), the ^{224}Ra and ^{223}Ra activity concentration in the creek was found in the range of 21.40-29.49 dpm/100L and 1.28-1.47 dpm/100L with an average of 26.69 ± 3.48 and 1.38 ± 0.08 dpm/100L respectively. The average AR in the creek was found in the range of 14.56 to 23.04 with an average 20.52 ± 3.58 .
- The average, conductivity, TDS and salinity in the Mumbai Harbour Bay was found to be 7.57 ± 0.14 , 43.11 ± 5.28 , 30.53 ± 3.40 and 24.70 ± 3.19 respectively.
- The average, conductivity, TDS and salinity in the Arabian Sea was found to be 7.61 ± 0.17 , 58.07 ± 4.21 , 38.58 ± 3.10 and 29.34 ± 1.00 respectively.
- Radium activities concentrations were found lower towards the fresh water mixing zone i.e. where the rivers, a tributary to the creek ecosystem meets.
- Higher activity concentration of Ra was observed at locations where reused seawater from salt pan and surface water discharge in the creek ecosystem.

- Lower activity concentration of Ra compare to shore location, was observed as we move deeper in the creek from the brink which may be due to dilution and decay of the radium contributed from the coastal area.
- A decreasing in the activity concentration of ^{224}Ra and ^{223}Ra was observed in the creek as we move towards the open sea.
- Higher activity concentration value of ^{224}Ra and ^{223}Ra in creek compared to offshore value indicates the contribution from groundwater discharge in the creek ecosystem of MHB
- The ^{224}Ra and ^{223}Ra activity concentration for porewater samples vary at the sampling locations but the AR value is very well in agreement at different locations, indicates similar source is contributing in the creek. The AR value at the discharge location of river and wastewater was also found nearly similar which support the concept of the similar source of Ra around the creek

Apparent Water Age of the creek water

- The apparent water age of the creek water for sampling trip-1, trip-2 and trip-4 were found to be in the range of 1.58-6.21days, 1.56-5.35 days and 3.50-7.08 days respectively by Radium Age Model.
- The average apparent age of creek water for sampling trip-1, trip-2 and trip-4 were found 3.65 ± 1.22 days, 3.75 ± 1.10 days and 4.51 ± 1.51 days respectively by Radium Age Model.
- It was observed that apparent water age increases as one move towards the open mouth of the bay which indicates the net water mass movement towards the open sea.
- The lower value of water age was observed at locations where the fresh water was contributing to the creek.

- The activity concentration of ^{223}Ra and ^{224}Ra in the creek was found almost similar for the different sampling trips indicating the steady state of the system. Hence, using Radium Balance Approach, the apparent water age of the creek water was estimated to be 6.51 ± 1.27 days.

Estimation of horizontal mixing and flushing rate of creek water

- A linear decrease of ^{223}Ra activity concentration from the open mouth of the bay towards the open sea shows that the dispersion is the dominant process in this part of the study area.
- The linear fit of $\ln^{224}\text{Ra}$ and $\ln^{223}\text{Ra}$ vs. distance beyond the creek in MHB and offshore locations gives the horizontal dispersion coefficient (K_h) as $800 \text{ m}^2\text{s}^{-1}$ and $795 \text{ m}^2\text{s}^{-1}$ respectively.
- A similar value of horizontal dispersion coefficient from the both ^{224}Ra and ^{223}Ra isotopes validates our assumption that system is in steady state and dispersion is dominant process in the study area.
- The flushing rate of creek water towards the open sea was estimated from the age (calculated using average AR value in the creek as source AR i.e. AR_i) vs. distance graph and found to be $6.67 \pm 0.89 \text{ km}\cdot\text{day}^{-1}$.

Estimation of SGD in Mumbai Harbour Bay

- A comprehensive mass balance has been constructed for short-lived Ra isotopes (^{223}Ra and ^{224}Ra), in Mumbai Harbour Bay and individual budget components (Input Sources: Tidal input from the ocean during the high tide, river, sediment and wastewater

discharge; Loss: Ra export from bay via mixing and radioactive decay) have been evaluated separately for the estimation SGD in the MHB

- The total flux of ^{223}Ra and ^{224}Ra in the bay was estimated and found to be 6.4×10^9 dpm.d⁻¹ and 106.1×10^9 dpm.d⁻¹ respectively
- Total fluxes out of the system via ocean exchange and decay was found as 7.3×10^9 dpm.d⁻¹ and 268.5×10^9 dpm.d⁻¹ for ^{223}Ra and ^{224}Ra respectively
- The contribution of radium flux from river, wastewater, surface sediment through diffusion, suspended sediment 0.01%, 0.1-0.4 %, 2-3% and 0.5- 0.7% of the total flux respectively.
- The tidal input, main contributor for ^{223}Ra and ^{224}Ra was estimated to be 44.1 % and 25.2 % of total radium flux respectively.
- The SGD in the bay was estimated based on the imbalance between input and losses contribution of ^{223}Ra and ^{224}Ra and found to be 33.4×10^9 L.d⁻¹ and 64.9×10^9 L.d⁻¹ respectively.
- The SGD contribution of ^{223}Ra and ^{224}Ra flux in the bay was found as 53.4 % and 71.7 % respectively.

Status of Trace and Toxic Elements in Creek Ecosystem

- The pre-concentration of trace element using ammonium tetramethylene dithiocarbamate-diethylammonium diethyldithiocarbamate from seawater followed by TXRF measurement, suitable for analysis of trace elements in the sea water was standardized. The validation of the method was carried out using reference seawater (NAAS-6) and the average deviation of results from true value was found to be about 16%. The pre-concentration factor up to 250 easily can be reached using this procedure.

- The chlorine content from seawater deposited on sample support can be removed by treating with nitric acid vapour for a time duration of about 30 minute
- The slurry preparation coupled with TXRF measurement of the sediments samples was standardized and validated using IAEA-Soil-7 reference material and the result showed average relative error in measurement was found to be 13%.
- The analysis of the trace and toxic elements in seawater was carried out to understand the status of the trace and toxic elements in the creek ecosystem. The obtained value for Zn, Pb, Cu, Ni, and Co was higher with reported value in the Arabian Sea.
- The effluents received by the creek from the city side are enriched in V, Cr and Ni whereas the effluents received from the industrial side are contributing more Mn, Fe, Cu and Zn.
- The present study indicates that the establishment and operationalisation of the effluents treatment plan on both sides have reduced further deterioration of the water quality of the creek water.
- The suspended sediment samples from the creek system were collected analysed from the different element by slurry assisted TXRF. Knowing the suspended silt load, the concentration of the elements (Ca, K, Ti, V, Cr, Mn, Fe, Ni, Cu, Zn, Pb, Rb and Sr) flux of these elements going out of the bay daily, were estimated indicates.
- Vertical distribution of most of the elements like K, Ti, Ca, Cr, Mn, Ni, Cu and Rb in sediment core sample shows nearly similar variation showing the same source of contamination.
- The estimation contamination factor showed a low level of contamination in the creek.

Future Work

Low-lying coastal areas are crucial to the development of nature and of society considered as heterogeneous domains, dynamic in space and time. 70% of cities with more than 1.6 million inhabitants settlements situated in these area comprising less than 20% of the earth's surface. Low-lying coastal areas also accounts for 90% of the global fisheries, produce about 25% of global biological productivity and major sink for sediments.

Environmental radiotracers using natural and artificial radionuclides can identify and model important particle transport processes in diverse water bodies like rivers, lakes and coastal marine environments. Many contaminants and nutrients in the water move in association with inorganic and organic particles, including plankton species and their remains. Particle-associated constituents settle through the water column to underlying sediments, where they may be mixed and re-suspended by currents or biological action, and are ultimately lost by burial in accumulating sediments. Along with such pathways, rates of particle transport often can be determined using particle-associated radionuclides. Naturally occurring Radium isotopes is used to identify the pathways and fate of environmental pollutants in the marine system. Marine water mass transport that affects the productivity of the marine waters can be studied.

India has about 7,517 km coastline and groundwater and seawater discharge is continuously taking place along the coast and within the coastal zone hydrological system. There are very few related to SGD studies reported in the Indian coastal areas. The present study will help in full filling lack of easily available and easily accessible data on the hydrological cycle in Indian coastal areas.

- The developed method can be used to study the input of different nutrients and pollutants via groundwater discharge in the other Bay, knowing the estimate of SGD.

- Natural tracers such as radium will be useful in the understanding and estimating the different component of SGD viz. freshwater discharge and re-circulated seawater which are inseparable in nature and being investigated by separate groups using different methodologies.
- Theoretical study or other technique needs to be explored for the SGD estimation in the present study area.
- Developed approach can be used to study the apparent water age, flushing rate, dispersion coefficient and submarine groundwater discharge in the other coastal area.
- The information obtained could be used to help the developing management strategies for controlling the supply of terrestrial nutrients and contaminants to offshore areas and protect the environment in the study area.

BIBLIOGRAPHY

1. Evans R, Kip A, Moberg E (1938), The radium and radon content of Pacific Ocean water, life and sediments-II. *Am. J. Sci.* 36:241–259 . doi: 10.2475/ajs.s5-36.214.241
2. Swarzenski PW, Reich C, Kroeger KD, Baskaran M (2007) Ra and Rn isotopes as natural tracers of submarine groundwater discharge in Tampa Bay, Florida. *Mar. Chem.* 104:69–84 . doi: 10.1016/j.marchem.2006.08.001
3. Convention for the protection of the marine environment of the north-east atlantic. (1992), OSPAR, Conv 35
4. The environmental behaviour of radium, IAEA-Technical Reports Series No. 310 (1990).
5. Lauria DC, Almeida RMR, Sracek O (2004) Behavior of radium, thorium and uranium in groundwater near the Buena Lagoon in the Coastal Zone of the State of Rio de Janeiro, Brazil. *Environ Geol* 47:11–19 . doi: 10.1007/s00254-004-1121-1
6. Kigoshi K (1971) Alpha-recoil thorium-234: Dissolution into water and the uranium-234/uranium-238 disequilibrium in nature. *Science* (80-) 173:47–48 . doi: 10.1126/science.173.3991.47
7. Curti E (1999) Coprecipitation of radionuclides with calcite: Estimation of partition coefficients based on a review of laboratory investigations and geochemical data. *Appl Geochemistry* 14:433–445 . doi: 10.1016/S0883-2927(98)00065-1
8. Langmuir D, Melchior D (1985) The geochemistry of Ca, Sr, Ba and Ra sulfates in some deep brines from the Palo Duro Basin, Texas. *Geochim Cosmochim Acta* 49:2423–2432 . doi: 10.1016/0016-7037(85)90242-X
9. Gonnee ME, Morris PJ, Dulaiova H, Charette MA (2008) New perspectives on radium behavior within a subterranean estuary. *Mar Chem* 109:250–267 . doi:

10.1016/j.marchem.2007.12.002

10. Kraemer TF, Reid DF (1984) The occurrence and behavior of radium in saline formation water of the U.S. Gulf Coast region. *Chem Geol* 46:153–174 . doi: 10.1016/0009-2541(84)90186-4
11. Dickson B. (1985) Radium isotopes in saline seepages, south-western Yilgarn, Western Australia. *Geochim Cosmochim Acta* 49:361–368 . doi: 10.1016/0016-7037(85)90029-8
12. Zukin JG, Hammond DE, Teh-Lung K, Elders WA (1987) Uranium-thorium series radionuclides in brines and reservoir rocks from two deep geothermal boreholes in the Salton Sea Geothermal Field, southeastern California. *Geochim Cosmochim Acta* 51:2719–2731 . doi: 10.1016/0016-7037(87)90152-9
13. Berry JA, Bond KA, Cowper MM, et al (1994) Factors influencing the diffusion of uranium, plutonium and radium through Sherwood Sandstone from Sellafield, Cumbria. *Radiochim Acta* 66–7:531–536
14. Herczeg AL, James Simpson H, Robert F, Anderson; R (1988) Uranium and radium mobility in groundwaters and brines within the Delaware basin, Southeastern New Mexico, U.S.A. *Chem Geol Isot Geosci Sect* 72:181–196 . doi: 10.1016/0168-9622(88)90066-8
15. Mahoney JJ, Langmuir D (1991) Adsorption of Sr on Kaolinite, Illite and Montmorillonite at High Ionic Strengths. *Radiochim Acta* 54:139–144 . doi: 10.1524/ract.1991.54.3.139
16. Giblin AM, Dickson BL (1984) Hydrogeochemical interpretations of apparent anomalies in base metals and radium in groundwater near Lake Maurice in the Great Victoria Desert. *J Geochemical Explor* 22:361–362
17. Langmuir D, Riese AC (1985) The thermodynamic properties of radium. *Geochim*

- Cosmochim Acta 49:1593–1601 . doi: 10.1016/0016-7037(85)90264-9
18. Gonneea ME, Morris PJ, Dulaiova H, Charette MA (2008) New perspectives on radium behavior within a subterranean estuary. *Mar Chem.* doi: 10.1016/j.marchem.2007.12.002
 19. Taylor SR (1964) Trace element abundances and the chondritic Earth model. *Geochim Cosmochim Acta* 28:1989–1998 . doi: 10.1016/0016-7037(64)90142-5
 20. UNSCEAR (2008) Sources and effects of ionizing radiation
 21. Tsai CM, Weng PS (1973) Radium-226 concentrations in Taiwan hot spring and river waters. *Health Phys* 24:429–430
 22. Moore WS, Edmond JM (1984) Radium and barium in the Amazon River system. *J Geophys Res* 89:2061 . doi: 10.1029/JC089iC02p02061
 23. Bhat SG, Krishnaswamy S (1969) Isotopes of uranium and radium in Indian rivers. *Proc Indian Acad Sci - Sect A* 70:1–17 . doi: 10.1007/BF03046931
 24. Moore WS (1967) Amazon and Mississippi river concentrations of uranium, thorium, and radium isotopes. *Earth Planet Sci Lett* 2:231–234 . doi: 10.1016/0012-821X(67)90134-3
 25. Martin P, Hancock GJ, Johnston A, Murray AS (1998) Natural-series radionuclides in traditional North Australian aboriginal foods. *J Environ Radioact* 40:37–58 . doi: 10.1016/S0265-931X(97)00065-9
 26. De Bortoli M, Gaglione P (1972) Radium-226 in environmental materials and foods. *Health Phys* 22:43–48 . doi: 10.1097/00004032-197201000-00008
 27. Conlan B, Henderson P, Walton A (1969) A simplified procedure for the assay of picocurie concentrations of radium-226 and its application to a study of the natural radioactivity in surface waters in Scotland. *Analyst* 94:15 . doi: 10.1039/an9699400015
 28. Vandenhove, H, Verrezen, F, Landa, E R, and Atwood EA (2010) Radium. In:

- Radionuclides in the Environment, ATWOOD D. Chichester, UK, pp 97–108
29. Agency EP (2000) Federal Register :: National Primary Drinking Water Regulations; Radionuclides; Final Rule
 30. Kolb W (1996) Thorium, uranium and plutonium in surface air at Vardö. *J Environ Radioact* 31:1–6 . doi: 10.1016/0265-931X(95)00046-D
 31. Langmuir D, Herman JS (1980) The mobility of thorium in natural waters at low temperatures. *Geochim Cosmochim Acta* 44:1753–1766 . doi: 10.1016/0016-7037(80)90226-4
 32. Benes P, Obdrzalek M, Cejchanov M (1982) The physicochemical forms of traces of radium in aqueous solutions containing chlorides, sulfates and carbonates. *Radiochem Radioanal Lett* 50(4):227–241
 33. Hem JD (1985) Study and interpretation of the chemical characteristics of natural water
 34. Grandia F, Merino J, Amphos JB (2008) Svensk Kärnbränslehantering AB Assessment of the radium-barium co-precipitation and its potential influence on the solubility of Ra in the near-field Assessment of the radium-barium co-precipitation and its potential influence on the solubility of Ra in the near-field. C Grup AB
 35. Epa U, of Radiation O, Air I (1999) UNDERSTANDING VARIATION IN PARTITION COEFFICIENT, K_d , VALUES Volume I: The K_d Model, Methods of Measurement, and Application of Chemical Reaction Codes
 36. Carroll D (1959) Ion exchange in clays and other minerals. *Bull Geol Soc Am* 70:749–779 . doi: 10.1130/0016-7606(1959)70[749:IEICAO]2.0.CO;2
 37. Post JE (1999) Manganese oxide minerals : Crystal structures and economic and environmental significance. *Proc. Natl. Acad Sci. USA* 96:3447–3454

38. Koulouris G (1995) Dynamic studies on sorption characteristics of ^{226}Ra on manganese dioxide. *J Radioanal Nucl Chem Artic* 193:269–279 . doi: 10.1007/BF02039884
39. Grasshoff, Klaus; Kremling, Klaus; Ehrhardt M (1999) Methods of Seawater Analysis - Chapter 10 - Nutrients. In: *Methods of Seawater Analysis*. pp 159–228
40. Moore WS (1996) Large groundwater inputs to coastal waters revealed by ^{226}Ra enrichments. *Nature* 380:612–614 . doi: 10.1038/380612a0
41. Moore WS, Shaw TJ (2008) Fluxes and behavior of radium isotopes, barium, and uranium in seven Southeastern US rivers and estuaries. *Mar Chem* 108:236–254 . doi: 10.1016/j.marchem.2007.03.004
42. Dowdall M, Selnaes G, Gwynn JP, Davids C (2004) Simultaneous determination of ^{226}Ra and ^{238}U in soil and environmental materials by gamma-spectrometry in the absence of radium progeny equilibrium. *J Radioanal Nucl Chem* 261:513–521 . doi: 10.1023/B:JRNC.0000037091.19952.d3
43. Murray AS, Marten R, Johnston A, Martin P (1987) Analysis for naturally occurring radionuclides at environmental concentrations by gamma spectrometry. *J Radioanal Nucl Chem Artic* 115:263–288 . doi: 10.1007/BF02037443
44. Johnston A, Martin P (1997) Rapid analysis of ^{226}Ra in waters by gamma-ray spectrometry. *Appl Radiat Isot* 48:631–638 . doi: 10.1016/S0969-8043(97)00009-2
45. Salonen L (1993) A rapid method for monitoring of uranium and radium in drinking water. *Sci Total Environ* 130–131:23–35 . doi: 10.1016/0048-9697(93)90056-C
46. Cohen AS, O’Nions RK (1991) Precise determination of femtogram quantities of radium by thermal ionization mass spectrometry. *Anal Chem* 63:2705–2708 . doi: 10.1021/ac00023a008

47. Roos P (2008) Analysis of radionuclides using ICP-MS. *Radioact. Environ.* 11:295–330
48. Tims SG, Hancock GJ, Wacker L, Fifield LK (2004) Measurements of Pu and Ra isotopes in soils and sediments by AMS. In: *Nuclear Instruments and Methods in Physics Research, Section B: Beam Interactions with Materials and Atoms.* pp 796–801
49. Moore WS (2010) The Effect of Submarine Groundwater Discharge on the Ocean. *Annu Rev Mar Sci* 2:59–88 . doi: 10.1146/annurev-marine-120308-081019
50. LAROCHE J, NUZZI R, WATERS R, et al (1997) Brown Tide blooms in Long Island’s coastal waters linked to interannual variability in groundwater flow. *Glob Chang Biol* 3:397–410 . doi: 10.1046/j.1365-2486.1997.00117.x
51. Burnett WC, Dulaiova H (2006) Radon as a tracer of submarine groundwater discharge into a boat basin in Donnalucata, Sicily. *Cont Shelf Res* 26:862–873 . doi: 10.1016/j.csr.2005.12.003
52. Taniguchi M, Burnett WC, Cable JE, Turner J V. (2002) Investigation of submarine groundwater discharge. *Hydrol Process* 16:2115–2129 . doi: 10.1002/hyp.1145
53. Burnett WC, Dulaiova H (2003) Estimating the dynamics of groundwater input into the coastal zone via continuous radon-222 measurements. In: *Journal of Environmental Radioactivity.* pp 21–35
54. . Massel S, Przyborska A, Przyborski M (2005) Attenuation of wave-induced groundwater pressure in shallow water. Part 2 Theory. *Oceanologia* 47:232-291 - Google Search. <https://www.google.co.in/search?ei=wLKCWpKfE8rRvgTcz7Fg&q=.Massel+S%2C+Przyborska+A%2C+Przyborski+M+%282005%29+Attenuation+of+wave-induced+groundwater+pressure+in+shallow+water.+Part+2+Theory.+Oceanologia+47%3A232-291&oq=.Massel+S%2C+Przyborska+A%2C+Przyb>. Accessed 13 Feb 2018

55. Michael HA, Mulligan AE, Harvey CF (2005) Seasonal oscillations in water exchange between aquifers and the coastal ocean. *Nature* 436:1145–1148 . doi: 10.1038/nature03935
56. Piekarek-Jankowska H (1996) Hydrochemical effects of submarine groundwater discharge to the Puck Bay (southern Baltic Sea, Poland). *Geogr Pol* 67:103–119
57. Johannes R (1980) The Ecological Significance of the Submarine Discharge of Groundwater . *Mar Ecol Prog Ser* 3:365–373 . doi: 10.3354/meps003365
58. Fanning KA, Byrne RH, Breland JA, et al (1981) Geothermal springs of the West Florida continental shelf: Evidence for dolomitization and radionuclide enrichment. *Earth Planet Sci Lett* 52:345–354 . doi: 10.1016/0012-821X(81)90188-6
59. Church TM (1996) An underground route for the water cycle. *Nature* 380:579–580
60. Li L, Barry DA, Stagnitti F, Parlange JY (1999) Submarine groundwater discharge and associated chemical input to a coastal sea. *Water Resour Res* 35:3253–3259 . doi: 10.1029/1999WR900189
61. Hussain N, Church TM, Kim G (1999) Use of ^{222}Rn and ^{226}Ra to trace groundwater discharge into the Chesapeake Bay. *Mar Chem* 65:127–134 . doi: 10.1016/S0304-4203(99)00015-8
62. Kim G, Hwang D-W (2002) Tidal pumping of groundwater into the coastal ocean revealed from submarine ^{222}Rn and CH_4 monitoring. *Geophys Res Lett* 29:23-1-23–4 . doi: 10.1029/2002GL015093
63. Charette MA, Sholkovitz ER (2002) Oxidative precipitation of groundwater-derived ferrous iron in the subterranean estuary of a coastal bay. *Geophys Res Lett* 29:85-1-85–4 . doi: 10.1029/2001GL014512

64. Valiela I, Teal JM, Volkman S, et al (1978) Nutrient and particulate fluxes in a salt marsh ecosystem: Tidal exchanges and inputs by precipitation and groundwater 1. *Limnol Oceanogr* 23:798–812 . doi: 10.4319/lo.1978.23.4.0798
65. Valiela I, Foreman K, LaMontagne M, et al (1992) Couplings of Watersheds and Coastal Waters: Sources and Consequences of Nutrient Enrichment in Waquoit Bay, Massachusetts. *Estuaries* 15:443 . doi: 10.2307/1352389
66. Valiela I, Bowen JL, Kroeger KD (2002) Assessment of models for estimation of land-derived nitrogen loads to shallow estuaries. *Appl Geochemistry* 17:935–953 . doi: 10.1016/S0883-2927(02)00073-2
67. Corbett DR, Chanton J, Burnett W, et al (1999) Patterns of groundwater discharge into Florida Bay. *Limnol Oceanogr* 44:1045–1055 . doi: 10.4319/lo.1999.44.4.1045
68. Corbett DR, Dillon K, Burnett W, Chanton J (2000) Estimating the groundwater contribution into Florida Bay via natural tracers, ^{222}Rn and CH_4 . *Limnol Oceanogr* 45:1546–1557 . doi: 10.4319/lo.2000.45.7.1546
69. Bokuniewicz H (1980) Groundwater seepage into Great South Bay, New York. *Estuar Coast Mar Sci* 10:437–444 . doi: 10.1016/S0302-3524(80)80122-8
70. Bokuniewicz H, Pavlik B (1990) Groundwater seepage along a Barrier Island. *Biogeochemistry* 10:257–276 . doi: 10.1007/BF00003147
71. Krest JM, Moore WS, Gardner LR, Morris JT (2000) Marsh nutrient export supplied by groundwater discharge: Evidence from radium measurements. *Global Biogeochem Cycles* 14:167–176 . doi: 10.1029/1999GB001197
72. Lapointe BE, O’Connell JD, Garrett GS (1990) Nutrient couplings between on-site sewage disposal systems, groundwaters, and nearshore surface waters of the Florida Keys.

- Biogeochemistry 10:289–307 . doi: 10.1007/BF00003149
73. Lapointe BE, O’Connell J (1989) Nutrient-enhanced growth of *Cladophora prolifera* in harrington sound, bermuda: Eutrophication of a confined, phosphorus-limited marine ecosystem. *Estuar Coast Shelf Sci* 28:347–360 . doi: 10.1016/0272-7714(89)90084-X
74. Hwang DW, Kim G, Lee YW, Yang HS (2005) Estimating submarine inputs of groundwater and nutrients to a coastal bay using radium isotopes. *Mar Chem*. doi: 10.1016/j.marchem.2004.11.002
75. McCoy CA, Corbett DR (2009) Review of submarine groundwater discharge (SGD) in coastal zones of the Southeast and Gulf Coast regions of the United States with management implications. *J Environ Manage* 90:644–651 . doi: 10.1016/j.jenvman.2008.03.002
76. Moore WS (1997) High fluxes of radium and barium from the mouth of the Ganges-Brahmaputra River during low river discharge suggest a large groundwater source. *Earth Planet Sci Lett* 150:141–150 . doi: 10.1016/S0012-821X(97)00083-6
77. Shaw TJ, Moore WS, Kloepfer J, Sochaski MA (1998) The flux of barium to the coastal waters of the southeastern USA: The importance of submarine groundwater discharge. *Geochim Cosmochim Acta* 62:3047–3054 . doi: 10.1016/S0016-7037(98)00218-X
78. Santos IR, Burnett WC, Dittmar T, et al (2009) Tidal pumping drives nutrient and dissolved organic matter dynamics in a Gulf of Mexico subterranean estuary. *Geochim Cosmochim Acta* 73:1325–1339 . doi: 10.1016/j.gca.2008.11.029
79. Basu AR, Jacobsen SB, Poreda RJ, et al (2001) Large groundwater strontium flux to the oceans from the bengal basin and the marine strontium isotope record. *Science* (80-) 293:1470–1473 . doi: 10.1126/science.1060524

80. Beck AJ, Rapaglia JP, Cochran JK, Bokuniewicz HJ (2007) Radium mass-balance in Jamaica Bay, NY: Evidence for a substantial flux of submarine groundwater. *Mar Chem* 106:419–441 . doi: 10.1016/j.marchem.2007.03.008
81. Windom HL, Moore WS, Niencheski LFH, Jahnke RA (2006) Submarine groundwater discharge: A large, previously unrecognized source of dissolved iron to the South Atlantic Ocean. *Mar Chem* 102:252–266 . doi: 10.1016/j.marchem.2006.06.016
82. Baumann T, Fruhstorfer P, Klein T, Niessner R (2006) Colloid and heavy metal transport at landfill sites in direct contact with groundwater. *Water Res* 40:2776–2786 . doi: 10.1016/j.watres.2006.04.049
83. Beck AJ, Cochran JK, Sañudo-Wilhelmy SA (2010) The distribution and speciation of dissolved trace metals in a shallow subterranean estuary. *Mar Chem* 121:145–146 . doi: 10.1016/j.marchem.2010.04.003
84. Laurier FJG, Cossa D, Beucher C, Brévière E (2007) Reprint of “The impact of groundwater discharges on mercury partitioning, speciation and bioavailability to mussels in a coastal zone.” *Mar Chem* 106:352–364 . doi: 10.1016/j.marchem.2007.06.007
85. Bone SE, Charette MA, Lamborg CH, Gonnee ME (2007) Has submarine groundwater discharge been overlooked as a source of mercury to coastal waters? *Environ Sci Technol* 41:3090–3095 . doi: 10.1021/es0622453
86. Black FJ, Paytan A, Knee KL, et al (2009) Submarine Groundwater Discharge of Total Mercury and Methylmercury to Central California Coastal Waters. *Environ Sci Technol* 43:5652–5659 . doi: 10.1021/es900539c
87. Lee Y, Rahman MM, Kim G, Han S (2011) Mass Balance of Total Mercury and Methylmercury in Coastal Embayments of a Volcanic Island: Significance of

- Submarine Groundwater Discharge. *Environ Sci Technol* 45:9891–9900 . doi:
10.1021/es202093z
88. Ganguli PM, Conaway CH, Swarzenski PW, et al (2012) Mercury speciation and transport via submarine groundwater discharge at a southern California coastal lagoon system. *Environ Sci Technol* 46:1480–1488 . doi: 10.1021/es202783u
89. Rahman MDM, Lee YG, Kim G, et al (2013) Significance of submarine groundwater discharge in the coastal fluxes of mercury in Hampyeong Bay, Yellow Sea. *Chemosphere* 91:320–327 . doi: 10.1016/j.chemosphere.2012.11.052
90. Cai W-J, Wang Y, Krest J, Moore WS The geochemistry of dissolved inorganic carbon in a surficial groundwater aquifer in North Inlet, South Carolina, and the carbon fluxes to the coastal ocean. doi: 10.1016/S0016-7037(02)01167-5
91. Goni MA, Gardner LR (2003) Seasonal dynamics in dissolved organic carbon concentrations in a coastal water-table aquifer at the forest-marsh interface. *Aquat Geochemistry* 9:209–232 . doi: 10.1023/B:AQUA.0000022955.82700.ed
92. Moore WS (2003) Sources and fluxes of submarine groundwater discharge delineated by radium isotopes. *Biogeochemistry* 66:75–93 . doi:
10.1023/B:BIOG.0000006065.77764.a0
93. Kim G, Kim J-S, Hwang D-W (2011) Submarine groundwater discharge from oceanic islands standing in oligotrophic oceans: Implications for global biological production and organic carbon fluxes. *Limnol Oceanogr* 56:673–682 . doi: 10.4319/lo.2011.56.2.0673
94. Zektser IS, Dzyuba A V. (2014) Submarine discharge into the Barents and White Seas. *Environ Earth Sci* 71:723–729 . doi: 10.1007/s12665-013-2474-0
95. Peltonen K, Nordisk Ministerråd, Nordisk Råd (2002) Direct groundwater inflow to the

Baltic Sea. Nordisk Ministerråd, Copenhagen

96. Israelsen OW, Reeve RC (1944) Bulletin No . 313 - Canal Lining Experiments in the Delta Area , Utah Canal Lining Experiments · the Delta Area , Utah
97. Lee DR (1977) A device for measuring seepage flux in lakes and estuaries1. *Limnol Oceanogr* 22:140–147 . doi: 10.4319/lo.1977.22.1.0140
98. Szymczycha B, Vogler S, Pempkowiak J (2012) Nutrient fluxes via submarine groundwater discharge to the Bay of Puck, southern Baltic Sea. *Sci Total Environ* 438:86–93 . doi: 10.1016/j.scitotenv.2012.08.058
99. Taniguchi M, Burnett WC, Dulaiova H, et al (2006) Submarine groundwater discharge measured by seepage meters in sicilian coastal waters. *Cont Shelf Res* 26:835–842 . doi: 10.1016/J.CSR.2005.12.002
100. Shaw RD, Prepas EE (1990) Groundwater-lake interactions: I. Accuracy of seepage meter estimates of lake seepage. *J Hydrol* 119:105–120 . doi: 10.1016/0022-1694(90)90037-X
101. Shaw RD, Prepas EE (1990) Groundwater-lake interactions: II. Nearshore seepage patterns and the contribution of ground water to lakes in central Alberta. *J Hydrol* 119:121–136 . doi: 10.1016/0022-1694(90)90038-Y
102. Fellows CR, Brezonik PL (1980) SEEPAGE FLOW INTO FLORIDA LAKES. *JAWRA J Am Water Resour Assoc* 16:635–641 . doi: 10.1111/j.1752-1688.1980.tb02442.x
103. Shaw RD, Prepas EE (1989) Anomalous, short-term influx of water into seepage meters. *Limnol. Oceanogr.* 34:1343–1351
104. Belanger T V., Montgomery MT (1992) Seepage meter errors. *Limnol. Oceanogr.* 37:1787–1795
105. Libelo EL, MacIntyre WG (1994) Effects Of Surface-Water Movement On Seepage-

- Meter Measurements Of Flow Through The Sediment-Water Interface. *Appl Hydrogeol* 2:49–54 . doi: 10.1007/s100400050047
106. Shinn EA, Reich CD, Hickey TD (2002) Seepage meters and Bernoulli's revenge. *Estuaries* 25:126–132 . doi: 10.1007/BF02696056
107. Burnett WC, Aggarwal PK, Aureli A, et al (2006) Quantifying submarine groundwater discharge in the coastal zone via multiple methods. *Sci. Total Environ.* 367:498–543
108. Boyle DR (1994) Design of a seepage meter for measuring groundwater fluxes in the nonlittoral zones of lakes-Evaluation in a boreal forest lake. *Limnol Oceanogr* 39:670–681 . doi: 10.4319/lo.1994.39.3.0670
109. Sayles FL, Dickinson WH (1991) The Seep Meter: a benthic chamber for the sampling and analysis of low velocity hydrothermal vents. *Deep Sea Res Part A, Oceanogr Res Pap* 38:129–141 . doi: 10.1016/0198-0149(91)90058-N
110. Paulsen RJ, Smith CF, O'Rourke D, Wong TF (2001) Development and evaluation of an ultrasonic ground water seepage meter. *Ground Water* 39:904–911 . doi: 10.1111/j.1745-6584.2001.tb02478.x
111. Krupa SL, Belanger T V, Heck HH, et al (1998) Krupaseep - the next generation seepage meter. In: International coastal symposium (ICS 1998).
112. Taniguchi M, Fukuo Y (1993) Continuous Measurements of Ground Water Seepage Using an Automatic Seepage Meter. *Groundwater* 31:675–679 . doi: 10.1111/j.1745-6584.1993.tb00601.x
113. Sholkovitz ER, Herbold CW, Charette M a. (2003) An automated dye-dilution based seepage meter for the time-series measurement of submarine groundwater discharge. *Limnol Oceanogr Methods* 1:16–28 . doi: 10.4319/lom.2011.1.16

114. Huettel M, Ziebis W, Forster S (1996) Flow-induced uptake of particulate matter in permeable sediments. *Limnol Oceanogr* 41:309–322 . doi: 10.4319/lo.1996.41.2.0309
115. Freeze RA, Cherry JA (1979) *Groundwater*
116. Povinec PP, Bokuniewicz H, Burnett WC, et al (2008) Isotope tracing of submarine groundwater discharge offshore Ubatuba, Brazil: results of the IAEA-UNESCO SGD project. *J Environ Radioact* 99:1596–1610 . doi: 10.1016/j.jenvrad.2008.06.010
117. Barwell VK, Lee DR (1981) Determination of horizontal to vertical hydraulic conductivity ratios from seepage measurements on lake beds. *Water Resour Res* 17:565–570 . doi: 10.1029/WR017i003p00565
118. Taniguchi M (1995) Change in Groundwater Seepage Rate into Lake Biwa, Japan. *Japanese J Limnol* 56: . doi: 10.3739/rikusui.56.261
119. Cable JE, Bugna GC, Burnett WC, Chanton JP (1996) Application of ²²²Rn and CH₄ for assessment of groundwater discharge to the coastal ocean. *Limnol Oceanogr* 41:1347–1353 . doi: 10.4319/lo.1996.41.6.1347
120. Cable JE, Burnett WC, Chanton JP, Weatherly GL (1996) Estimating groundwater discharge into the northeastern Gulf of Mexico using radon-222. *Earth Planet Sci Lett* 144:591–604 . doi: 10.1016/S0012-821X(96)00173-2
121. Porcelli D, Swarzenski PW (2003) The Behavior of U- and Th-series Nuclides in Groundwater. *Rev Mineral Geochemistry* 52:317–361 . doi: 10.2113/0520317
122. Cornett RJ, Risto BA, Lee DR (1989) Measuring groundwater transport through lake sediments by advection and diffusion. *Water Resour Res* 25:1815–1823 . doi: 10.1029/WR025i008p01815
123. Vanek V (1993) Groundwater regime of a tidally influenced coastal pond. *J Hydrol*

- 151:317–342 . doi: 10.1016/0022-1694(93)90241-Z
124. Burnett WC, Cowart JB, Deetae S (1990) Radium in the Suwannee River and estuary: Spring and river input to the Gulf of Mexico. *Biogeochemistry* 10:237–255 . doi: 10.1007/BF00003146
125. Rama, Moore WS (1996) Using the radium quartet for evaluating groundwater input and water exchange in salt marshes. *Geochim Cosmochim Acta* 60:4645–4652 . doi: 10.1016/S0016-7037(96)00289-X
126. Cable JE, Martin JB, Swarzenski PW, et al (2004) Advection within shallow pore waters of a coastal Lagoon, Florida. *Ground Water* 42:1011–1020 . doi: 10.1111/j.1745-6584.2004.tb02640.x
127. Moore WS, Shaw TJ (1998) Chemical signals from submarine fluid advection onto the continental shelf. *J Geophys Res Ocean* 103:21543–21552 . doi: 10.1029/98JC02232
128. Moore WS (2000) Ages of continental shelf waters determined from ^{223}Ra and ^{224}Ra . *J Geophys Res Ocean* 105:22117–22122 . doi: 10.1029/1999JC000289
129. Charette MA, Buesseler KO, Andrews JE (2001) Utility of radium isotopes for evaluating the input and transport of groundwater-derived nitrogen to a Cape Cod estuary. *Limnol Oceanogr* 46:465–470 . doi: 10.4319/lo.2001.46.2.0465
130. Kelly RP, Moran SB (2002) Seasonal changes in groundwater input to a well-mixed estuary estimated using radium isotopes and implications for coastal nutrient budgets. *Limnol Oceanogr* 47:1796–1807 . doi: 10.4319/lo.2002.47.6.1796
131. Burnett B, Chanton J, Christoff J, et al (2002) Assessing methodologies for measuring groundwater discharge to the ocean. *Eos, Trans Am Geophys Union* 83:117 . doi: 10.1029/2002EO000069

132. Garrison GH, Glenn CR, McMurtry GM (2003) Measurement of submarine groundwater discharge in Kahana Bay, O'ahu, Hawai'i. *Limnol Oceanogr* 48:920–928 . doi: 10.4319/lo.2003.48.2.0920
133. Krest JM, Harvey JW (2003) Using natural distributions of short-lived radium isotopes to quantify groundwater discharge and recharge. *Limnol Oceanogr* 48:290–298 . doi: 10.4319/lo.2003.48.1.0290
134. Crotwell AM, Moore WS (2003) Nutrient and radium fluxes from submarine groundwater discharge to Port Royal Sound, South Carolina. *Aquat Geochemistry* 9:191–208 . doi: 10.1023/B:AQUA.0000022954.89019.c9
135. Moore WS, Wilson AM (2005) Advective flow through the upper continental shelf driven by storms, buoyancy, and submarine groundwater discharge. *Earth Planet Sci Lett* 235:564–576 . doi: 10.1016/j.epsl.2005.04.043
136. Luo X, Jiao JJ, Moore WS, Lee CM (2014) Submarine groundwater discharge estimation in an urbanized embayment in Hong Kong via short-lived radium isotopes and its implication of nutrient loadings and primary production. *Mar Pollut Bull* 82:144–154 . doi: 10.1016/J.MARPOLBUL.2014.03.005
137. Burnett WC, Cable JE, Corbett DR (2003) Radon Tracing of Submarine Groundwater Discharge in Coastal Environments. In: *Land and Marine Hydrogeology*. pp 25–43
138. Rahaman W, Singh SK (2012) Sr and $^{87}\text{Sr}/^{86}\text{Sr}$ in estuaries of western India: Impact of submarine groundwater discharge. *Geochim Cosmochim Acta* 85:275–288 . doi: 10.1016/j.gca.2012.02.025
139. Martin JB, Cable JE, Jaeger J, et al (2006) Thermal and chemical evidence for rapid water exchange across the sediment-water interface by bioirrigation in the Indian River Lagoon,

- Florida. *Limnol Oceanogr* 51:1332–1341 . doi: 10.4319/lo.2006.51.3.1332
140. Fischer WA, Moxham RM, Polcyn F, Landis GH (1964) Infrared surveys of Hawaiian volcanoes. *Science* (80-) 146:733–742
141. Roxburgh IS (1985) Thermal infrared detection of submarine springs associated with the plymouth limestone. *Hydrol Sci J* 30:185 . doi: 10.1080/02626668509490983
142. Banks WSL, Paylor RL, Hughes WB (1996) Using Thermal-Infrared Imagery to Delineate Ground-Water Discharged. *Ground Water* 34:434–443 . doi: 10.1111/j.1745-6584.1996.tb02024.x
143. Zektzer IS, Ivanov VA, Meskheteli A V. (1973) The problem of direct groundwater discharge to the seas. *J Hydrol* 20:1–36 . doi: 10.1016/0022-1694(73)90042-5
144. Muir KS (1968) Ground-water reconnaissance of the Santa Barbara-Montecito area, Santa Barbara County, California. *Water Supply Pap*
145. Pluhowski EJ, Kantrowitz IH (1964) Hydrology of the Babylon-Islip Area Suffolk County Long Island , New York
146. Sekulic B (1996) Balance of Average Annual Fresh Water Inflow into the Adriatic Sea. *Int J Water Resour Dev* 12:89–98 . doi: 10.1080/713672198
147. Zektzer IS, Dzhamalov RG (1981) Groundwater discharge to the Pacific Ocean. *Hydrol Sci* 26:271–280 . doi: 10.1080/02626668109490886org/10.1080/02626668109490886
148. Williams JB, Pinder JE (1990) GROUND WATER FLOW AND RUNOFF IN A COASTAL PLAIN STREAM. *JAWRA J Am Water Resour Assoc* 26:343–352 . doi: 10.1111/j.1752-1688.1990.tb01377.x
149. Kohout FA (1966) Submarine springs: a neglected phenomenon of coastal hydrology. *Hydrology* 26:391–413

150. Williams M. (1946) Bahrain: port of pearls and petroleum. *Natl Geogr* 194–210
151. Zektser IS (1996) Groundwater discharge into the seas and oceans: state of the art. In: *Groundwater Discharge in the Coastal Zone*, Buddemeier. Russian Academy of Sciences, Texel, Netherlands/Moscow, pp 122–123
152. Valiela I DC (1990) Groundwater inputs to coastal waters. *Biogeochemistry* 10:328
153. Veizer J, Mackenzie FT (2014) Evolution of Sedimentary Rocks. In: *Treatise on Geochemistry (Second Edition)*, 1st ed. New York : Norton, 1971., pp 399–435
154. Alle (1987) Report of the second conference on scientific ocean drilling COSOD II. *Second Conf. Sci. Ocean Drill. COSOD II*
155. Kitheka JU (1998) Groundwater outflow and its linkage to coastal circulation in a mangrove-fringed creek in Kenya. *Estuar Coast Shelf Sci* 47:63–75 . doi: 10.1006/ecss.1998.0325
156. Zektser IS, Loaiciga HA (1993) Groundwater fluxes in the global hydrologic cycle: past, present and future. *J Hydrol* 144:405–427 . doi: 10.1016/0022-1694(93)90182-9
157. Lvovich MI (1979) World water resources, present and future. *GeoJournal* 3:423–433 . doi: 10.1007/BF00455981
158. Bokuniewicz H (1980) Groundwater seepage into Great South Bay, New York. *Estuar Coast Mar Sci* 10:437–444 . doi: 10.1016/S0302-3524(80)80122-8
159. Sekulic B (1996) Balance of Average Annual Fresh Water Inflow into the Adriatic Sea. *Int J Water Resour Dev* 12:89–98 . doi: 10.1080/713672198
160. Valiela I, Costa JE (1988) Eutrophication of Buttermilk Bay, a cape cod coastal embayment: Concentrations of nutrients and watershed nutrient budgets. *Environ Manage* 12:539–553 . doi: 10.1007/BF01873266

161. Church TM (1996) An underground route for the water cycle. *Nature* 380:579–580
162. Charette MA, Splivallo R, Herbold C, et al (2003) Salt marsh submarine groundwater discharge as traced by radium isotopes. *Mar Chem* 84:113–121 . doi: 10.1016/j.marchem.2003.07.001
163. Valiela I, Teal JM, Volkmann SB, et al (1980) On the measurement of tidal exchanges and groundwater flow in salt marshes1. *Limnol Oceanogr* 25:187–192 . doi: 10.4319/lo.1980.25.1.0187
164. Lee DR (1980) Groundwater-solute influx. *Limnol Oceanogr* 25:183–186 . doi: 10.4319/lo.1980.25.1.0183
165. Hemond HF, Fifield JL (1982) Subsurface flow in salt marsh peat: A model and field study1. *Limnol Oceanogr* 27:126–136 . doi: 10.4319/lo.1982.27.1.0126
166. Verma S, Phansalkar SJ (2007) India’s water future 2050: potential deviations from “business-as-usual”
167. Mukherjee A, Fryar AE, Howell PD (2007) Regional hydrostratigraphy and groundwater flow modeling in the arsenic-affected areas of the western Bengal basin, West Bengal, India. *Hydrogeol J* 15:1397–1418 . doi: 10.1007/s10040-007-0208-7
168. L CS and RA (2008) Comparison of subsurface ground water discharge in east and west coast of India , DST- ILTP project Progress report 2007–2008, Govt of India
169. Jacob N, Suresh Babu DS, Shivanna K (2009) Radon as an indicator of submarine groundwater discharge in coastal regions. *Curr Sci* 97:1313–1320 . doi: 10.2307/24109725
170. Chawla D, Jacob N, Mohokar H V. (2014) Identification of groundwater discharge in Cuddalore coast, Tamil Nadu using radium isotopes. *J Radioanal Nucl Chem.* doi:

10.1007/s10967-014-3004-6

171. Debnath P, Mukherjee A, Rokade P, Joshi G, Rao S KG (2015) Stable isotopes and major ion chemistry of discharging groundwater to the Bay of Bengal: implications to strontium flux. In: Goldschmidt Conference. Prague, Czech Republic
172. Debnath P, Mukherjee A (2016) Quantification of tidally-influenced seasonal groundwater discharge to the Bay of Bengal by seepage meter study. *J Hydrol* 537:106–116 . doi: 10.1016/J.JHYDROL.2016.03.010
173. Ravindran AA, Ramanujam N (2014) Detection of submarine groundwater discharge to coastal zone study using 2d electrical resistivity imaging study at Manapad, Tuticorin , India
174. Krishan G, Rao MS, Kumar CP, et al (2015) A Study on Identification of Submarine Groundwater Discharge in Northern East Coast of India. *Aquat Procedia* 4:3–10 . doi: 10.1016/j.aqpro.2015.02.002
175. Rengarajan R, Sarma VVSS (2015) Submarine groundwater discharge and nutrient addition to the coastal zone of the Godavari estuary. *Mar Chem* 172:57–69 . doi: 10.1016/j.marchem.2015.03.008
176. Prakash R, Srinivasamoorthy K, Gopinath S, et al (2018) Radon isotope assessment of submarine groundwater discharge (SGD) in Coleroon River Estuary, Tamil Nadu, India. *J Radioanal Nucl Chem* 317:25–36 . doi: 10.1007/s10967-018-5877-2
177. Sackett WM, Potratz HA, Goldberg ED (1958) Thorium Content of Ocean Water. *Science* 128:204–5 . doi: 10.1126/science.128.3317.204
178. Sackett WM (1960) Protactinium-231 Content of Ocean Water and Sediments. *Science* (80-) 132:1761–1762 . doi: 10.1126/science.132.3441.1761-a

179. Rosholt JN (1957) Quantitative Radiochemical Methods for Determination of Sources of Natural Radioactivity. *Anal Chem* 29:1398–1408 . doi: 10.1021/ac60130a002
180. Rosholt JN, Emiliani C, Geiss J, et al (1961) Absolute Dating of Deep-Sea Cores by the Pa²³¹ /Th²³⁰ Method. *J Geol* 69:162–185 . doi: 10.1086/jg.69.2.30057142
181. Giffin C, Kaufman A, Broecker W (1963) Delayed Coincidence Counter for the Assay of Actinon and Thoron. *J Geophys Res* 68:1749–1757 . doi: 10.1029/JZ068i006p01749
182. Moore WS, Arnold R (1996) Measurement of²²³Ra and²²⁴Ra in coastal waters using a delayed coincidence counter. *J Geophys Res C Ocean* 101:1321–1329 . doi: 10.1029/95JC03139
183. Garcia-Solsona E, Garcia-Orellana J, Masqué P, Dulaiova H (2008) Uncertainties associated with²²³Ra and²²⁴Ra measurements in water via a Delayed Coincidence Counter (RaDeCC). *Mar Chem* 109:198–219 . doi: 10.1016/j.marchem.2007.11.006
184. Moore WS, Reid DF (1973) Extraction of Radium from Natural Waters Using Manganese-Impregnated Acrylic Fibers. *J Geophys Res* 78:8880–8886 . doi: 10.1029/JC078i036p08880
185. Colbert SL (2004) Ra Isotopes in San Pedro Bay, CA: Constraint on Inputs and Use of Nearshore Distribution to Compute Horizontal Eddy Diffusion Rates. University of Southern California
186. Hancock G., Webster I., Ford P., Moore W. (2000) Using Ra isotopes to examine transport processes controlling benthic fluxes into a shallow estuarine lagoon. *Geochim Cosmochim Acta* 64:3685–3699 . doi: 10.1016/S0016-7037(00)00469-5
187. Moore WS (2008) Fifteen years experience in measuring²²⁴Ra and²²³Ra by delayed-coincidence counting. *Mar Chem* 109:188–197 . doi: 10.1016/j.marchem.2007.06.015

188. Sun Y, Torgersen T (1998) The effects of water content and Mn-fiber surface conditions on ^{224}Ra measurement by ^{220}Rn emanation. *Mar Chem* 62:299–306
189. Smith KL, Robison BH, Helly JJ, et al (2007) Free-Drifting Icebergs: Hot Spots of Chemical and Biological Enrichment in the Weddell Sea. *Science* (80-) 317:478–482 . doi: 10.1126/science.1142834
190. Scholten JC, Pham MK, Blinova O, et al (2010) Preparation of Mn-fiber standards for the efficiency calibration of the delayed coincidence counting system (RaDeCC). *Mar Chem.* doi: 10.1016/j.marchem.2010.04.009
191. Moore WS, Cai P (2013) Calibration of RaDeCC systems for ^{223}Ra measurements. *Mar Chem* 156:130–137 . doi: 10.1016/j.marchem.2013.03.002
192. Lucas HF (1957) Improved Low Level Alpha Scintillation Counter for Radon. *Rev Sci Instrum* 28:680–683 . doi: 10.1063/1.1715975
193. Key RM, Brewer RL, Stockwell JH, et al (1979) Some improved techniques for measuring radon and radium in marine sediments and in seawater. *Mar Chem* 7:251–264 . doi: 10.1016/0304-4203(79)90042-2
194. Semkow TM, Parekh PP, Schwenker CD, et al (1994) Efficiency of the Lucas scintillation cell. *Nucl Inst Methods Phys Res A* 353:515–518 . doi: 10.1016/0168-9002(94)91712-4
195. Röntgen WC (1896) ON A NEW KIND OF RAYS. *Science* 3:227–31 . doi: 10.1126/science.3.59.227
196. Bertin EP (1975) Principles and Practice of X-Ray Spectrometric Analysis. Springer US
197. Jenkins R (2006) X-Ray Techniques: Overview. In: *Encyclopedia of Analytical Chemistry*. pp 13269–13288
198. Lifshin E, Wiley InterScience (Online service) (1999) X-ray characterization of materials.

Wiley-VCH

199. Canepari S, Perrino C, Astolfi ML, et al (2009) Determination of soluble ions and elements in ambient air suspended particulate matter: Inter-technique comparison of XRF, IC and ICP for sample-by-sample quality control. *Talanta* 77:1821–1829 . doi: 10.1016/J.TALANTA.2008.10.029
200. Hida M, Mitsui T, Minami Y (1997) Forensic investigation of counterfeit coins. *Forensic Sci Int* 89:21–26 . doi: 10.1016/S0379-0738(97)00070-4
201. Hutton JT, Elliott SM (1980) An accurate XRF method for the analysis of geochemical exploration samples for major and trace elements using one glass disc. *Chem Geol* 29:1–11 . doi: 10.1016/0009-2541(80)90002-9
202. Kalnicky DJ, Singhvi R (2001) Field portable XRF analysis of environmental samples. *J Hazard Mater* 83:93–122 . doi: 10.1016/S0304-3894(00)00330-7
203. Compton AH (1923) *The total reflexion of X-rays*. London, Edinburgh, Dublin Philos Mag J Sci 45:1121–1131 . doi: 10.1080/14786442308634208
204. Yoneda Y, Horiuchi T (1971) Optical Flats for Use in X-Ray Spectrochemical Microanalysis. *Rev Sci Instrum* 42:1069–1070 . doi: 10.1063/1.1685282
205. Knoth J, Prange A, Reus U, Schwenke H (1999) Formula for the background in TXRF as a function of the incidence angle and substrate material. *Spectrochim acta, Part B At Spectrosc* 54:1513–1515 . doi: 10.1016/S0584-8547(99)00104-4
206. Valkovic V, Markowicz A, Haselberger N (1993) Review of recent applications of radioisotope excited x-ray fluorescence. *X-Ray Spectrom* 22:199–207 . doi: 10.1002/xrs.1300220407
207. Iida A, Sakurai K, Matsushita T, Gohshi Y (1985) Energy dispersive X-ray fluorescence

- analysis with synchrotron radiation. Nucl Instruments Methods Phys Res Sect A Accel Spectrometers, Detect Assoc Equip 228:556–563 . doi: 10.1016/0168-9002(85)90304-3
208. D Coolidge BW Second Series December, JgJ3 A POWERFUL RONTGEN RAY TUBE WITH A PURE ELECTRON DISCHARGE
209. Beatty RT (1913) The Energy of Rontgen Rays. Proc R Soc A Math Phys Eng Sci 89:314–327 . doi: 10.1098/rspa.1913.0086
210. Esaka F, Watanabe K, Onodera T, et al (2003) The use of Si carriers for aerosol particle collection and subsequent elemental analysis by total-reflection X-ray fluorescence spectrometry. Spectrochim Acta Part B At Spectrosc 58:2145–2155 . doi: 10.1016/S0584-8547(03)00189-7
211. Prange A, Kramer K, Reus U (1993) Boron nitride sample carriers for total-reflection X-ray fluorescence. Spectrochim Acta Part B At Spectrosc 48:153–161 . doi: 10.1016/0584-8547(93)80019-Q
212. Theisen M, Niessner R (1999) Sapphire sample carriers for silicon determination by total-reflection X-ray fluorescence analysis. Spectrochim Acta Part B At Spectrosc 54:1839–1848 . doi: 10.1016/S0584-8547(99)00125-1
213. Murty VRK, Devan KRS (2001) On the suitability of Peltier cooled Si-PIN detectors in transmission experiments. Radiat Phys Chem 61:495–496 . doi: 10.1016/S0969-806X(01)00312-7
214. Streltsov C, Wobrauschek P, Schraik I (2004) Comparison of SiLi detector and silicon drift detector for the determination of low Z elements in total reflection X-ray fluorescence. Spectrochim Acta Part B At Spectrosc 59:1211–1213 . doi: 10.1016/j.sab.2004.01.018
215. Klockenkämper R, von bohlen A (1989) Determination of the critical thickness and the

- sensitivity for thin-film analysis by total reflection X-ray fluorescence spectrometry. *Spectrochim. Acta Part B At. Spectrosc.* 44:461–469
216. Rastegar B, Jundt F, Gallmann A, et al (1986) Sample homogeneity in energy-dispersive XRF trace metal analysis. *X-Ray Spectrom* 15:83–86 . doi: 10.1002/xrs.1300150203
217. Subramanian V (2015) *Surface and Sub-surface Water in Asia : Issues and Perspectives.* IOS Press
218. (2001) *Mumbai Metropolitan Region Development Authority Report: Basic Statistics.* Mumbai
219. Pillai, K C S and GKC (1958) Tidal movement and water renewal rate in Bombay Harbour Bay, AEET/HP/RWD/2. Mumbai
220. Ganguly AK (1983) Tracing the radionuclides in a tropical near – shore environment. In: *Commemoration symposium*
221. Desai, M.V.M., Kulkarni, V.V, Dey, N.N., Rao, S.R., Borker, M.D., More, A.K. S, Kumar, Chhapgar, B.F. and Pillai KC (1985) Role of sediments in accumulation and transport of radionuclides in waterways
222. Zingde MD, Desai BN (1981) Mercury in Thana Creek, Bombay Harbour. *Mar Pollut Bull* 12:237–241 . doi: 10.1016/0025-326X(81)90363-5
223. Jha SK, Chavan SB, Pandit GG, Sadasivan S (2003) Geochronology of Pb and Hg pollution in a coastal marine environment using global fallout¹³⁷Cs. In: *Journal of Environmental Radioactivity.* Elsevier, pp 145–157
224. Bhosale U, Sahu KC (1991) Heavy metal pollution around the island city of Bombay, India. Part II: distribution of heavy metals between water, suspended particles and sediments in a polluted aquatic regime. *Chem Geol* 90:285–305 . doi: 10.1016/0009-

2541(91)90105-Z

225. Sharma P, Borole D V., Zingde MD (1994) ^{210}Pb based trace element fluxes in the nearshore and estuarine sediments off Bombay, India. *Mar Chem* 47:227–241 . doi: 10.1016/0304-4203(94)90022-1
226. Menetrez, M. DA and ES (1989) *Manganese Dioxide Coated Filters for Removing Radium from Drinking Water*. Washington, D.C.
227. Kinniburgh DG, Jackson ML (1981) Cation adsorption by hydrous metal oxides and clay. *Adsorpt Inorganics Solid/Liquid Interfaces* (edited by M A Anderson A J Rubin) Ann Arbor Sci Publ Inc 23:23–160
228. Davranche M, Bollinger JC (2000) Heavy metals desorption from synthesized and natural iron and manganese oxyhydroxides: Effect of reductive conditions. *J Colloid Interface Sci* 227:531–539 . doi: 10.1006/jcis.2000.6904
229. Tripathy SS, Kanungo SB, Mishra SK (2001) The Electrical Double Layer at Hydrous Manganese Dioxide/Electrolyte Interface. *J Colloid Interface Sci* 241:112–119 . doi: 10.1006/JCIS.2001.7722
230. Dong D, Liu L, Hua X, Lu Y (2007) Comparison of lead, cadmium, copper and cobalt adsorption onto metal oxides and organic materials in natural surface coatings. *Microchem J* 85:270–275 . doi: 10.1016/J.MICROC.2006.06.015
231. Al-Sewailem M., Khaled E., Mashhady A. (1999) Retention of copper by desert sands coated with ferric hydroxides. *Geoderma* 89:249–258 . doi: 10.1016/S0016-7061(98)00082-2
232. McKenzie RM (1989) Manganese oxides and hydroxides. *Miner Soil Environ* 439–461 . doi: 10.2136/sssabookser1.2ed.c9

233. Burns RG and VMB (1978) Mineralogy. Marine Manganese Depositso
234. Ingenieurwissenschaften DDER, Calder C (2010) Synthesis and application of manganese dioxide coated magnetite for removal of metal ions from aqueous solutions
235. Dulaiova H, Ardelan M V., Henderson PB, Charette MA (2009) Shelf-derived iron inputs drive biological productivity in the southern Drake Passage. *Global Biogeochem Cycles* 23:1–14 . doi: 10.1029/2008GB003406
236. American Public Health Association (1985) Standard Methods for the Examination of Water and Wastewater: including bottom sediments and sludges, 16th ed. American Public Health Association
237. R. H. Pillay, S. S. Gothankar, S. J. Sartande*, S. K. Jha RMT (2017) Enrichment Factor of major and trace elements in suspended particulate matter of MHB. In: Symposium on Nuclear and Radiochemistry
238. Moore WS, Blanton JO, Joye SB (2006) Estimates of flushing times, submarine groundwater discharge, and nutrient fluxes to Okatee Estuary, South Carolina. *J Geophys Res Ocean* 111: . doi: 10.1029/2005JC003041
239. Li YH, Ku TL, Mathieu GG, Wolgemuth K (1973) Barium in the Antarctic Ocean and implications regarding the marine geochemistry of Ba and ²²⁶Ra. *Earth Planet Sci Lett* 19:352–358 . doi: 10.1016/0012-821X(73)90085-X
240. Webster IT, Hancock GJ, Murray AS (1995) Modelling the effect of salinity on radium desorption from sediments. *Geochim Cosmochim Acta* 59:2469–2476 . doi: 10.1016/0016-7037(95)00141-7
241. Eller KT, Burnett WC, Fitzhugh LM, Chanton JP (2014) Radium Sampling Methods and Residence Times in St. Andrew Bay, Florida. *Estuaries and Coasts* 37:94–103 . doi:

- 10.1007/s12237-013-9661-9
242. Dulaiova H, Burnett WC (2008) Evaluation of the flushing rates of Apalachicola Bay, Florida via natural geochemical tracers. *Mar Chem* 109:395–408 . doi: 10.1016/j.marchem.2007.09.001
243. Dulaiova H, Burnett WC, Wattayakorn G, Sojisuporn P (2006) Are groundwater inputs into river-dominated areas important? The Chao Phraya River - Gulf of Thailand. *Limnol Oceanogr* 51:2232–2247 . doi: 10.4319/lo.2006.51.5.2232
244. Moore WS (2000) Determining coastal mixing rates using radium isotopes. *Cont Shelf Res* 20:1993–2007 . doi: 10.1016/S0278-4343(00)00054-6
245. Xu BC, Dimova NT, Zhao L, et al (2013) Determination of water ages and flushing rates using short-lived radium isotopes in large estuarine system, the Yangtze River Estuary, China. *Estuar Coast Shelf Sci* 121–122:61–68 . doi: 10.1016/j.ecss.2013.02.005
246. Peterson RN, Burnett WC, Taniguchi M, et al (2008) Determination of transport rates in the Yellow River-Bohai Sea mixing zone via natural geochemical tracers. *Cont Shelf Res* 28:2700–2707 . doi: 10.1016/j.csr.2008.09.002
247. Charkin AN, Dudarev O V., Salyuk AN, et al (2017) Short-lived ^{224}Ra and ^{223}Ra isotopes in the Anadyr River–Bering Sea system. *Dokl Chem* 476:211–214 . doi: 10.1134/S0012500817090026
248. Sartandel SJ, Jha SK, Bara S V., Tripathi RM (2014) Assessment of ^{226}Ra and ^{228}Ra activity concentration in west coast of India. *J Radioanal Nucl Chem* 300:873–877 . doi: 10.1007/s10967-014-3037-x
249. Jha SK, Chavan SB, Pandit GG, et al (2002) Behaviour and fluxes of trace and toxic elements in creek sediment near Mumbai, India. *Environ Monit Assess* 76:249–262 . doi:

10.1023/A:1015579913509

250. Yadav VB, Sartandel SJ, Jha SK, Tripathi RM (2017) Measurement of ^{224}Ra and ^{223}Ra activity using MnO_2 based in situ pre-concentration technique coupled with delayed coincidence counting in creek ecosystem of Mumbai Harbour Bay. *J Radioanal Nucl Chem* 311:565–570 . doi: 10.1007/s10967-016-5103-z
251. Moore WS, Arnold R (1996) Measurement of ^{223}Ra and ^{224}Ra in coastal waters using a delayed coincidence counter. *J Geophys Res Ocean* 101:1321–1329 . doi: 10.1029/95JC03139
252. Moore WS, de Oliveira J (2008) Determination of residence time and mixing processes of the Ubatuba, Brazil, inner shelf waters using natural Ra isotopes. *Estuar Coast Shelf Sci* 76:512–521 . doi: 10.1016/j.ecss.2007.07.042
253. Qi D-M, Shen H-T, Zhu J-R (2003) Flushing time of the Yangtze estuary by discharge: A model study. *J Hydrodyn* 15:63–71
254. Moore WS, Krest J (2004) Distribution of ^{223}Ra and ^{224}Ra in the plumes of the Mississippi and Atchafalaya Rivers and the Gulf of Mexico. *Mar Chem* 86:105–119 . doi: 10.1016/j.marchem.2003.10.001
255. Hsieh Y Te, Geibert W, Van-Beek P, et al (2013) Using the radium quartet (^{228}Ra , ^{226}Ra , ^{224}Ra , and ^{223}Ra) to estimate water mixing and radium inputs in Loch Etive, Scotland. *Limnol Oceanogr* 58:1089–1102 . doi: 10.4319/lo.2013.58.3.1089
256. LAROCHE J, NUZZI R, WATERS R, et al (1997) Brown Tide blooms in Long Island's coastal waters linked to interannual variability in groundwater flow. *Glob Chang Biol* 3:397–410 . doi: 10.1046/j.1365-2486.1997.00117.x
257. Li Y-H, Mathieu G, Biscaye P, Simpson HJ (1977) The flux of ^{226}Ra from estuarine and

- continental shelf sediments. *Earth Planet Sci Lett* 37:237–241 . doi: 10.1016/0012-821X(77)90168-6
258. Krest JM, Moore WS, Rama (1999) 226 Ra and 228 Ra in the mixing zones of the Mississippi and Atchafalaya Rivers: indicators of groundwater input. *Mar Chem* 64:129–152 . doi: 10.1016/S0304-4203(98)00070-X
259. (2007) Water Quality Status of Water Bodies of Maharashtra with Recourse to Analytical/Statistical Tools
260. Ford PW, Bird FL, Hancock GJ (1999) Effect of burrowing macrobenthos on the flux of dissolved substances across the water–sediment interface. *Mar Freshw Res* 50:523 . doi: 10.1071/MF98059
261. Beck AJ, Rapaglia JP, Cochran JK, et al (2008) Submarine groundwater discharge to Great South Bay, NY, estimated using Ra isotopes. *Mar Chem* 109:279–291 . doi: 10.1016/j.marchem.2007.07.011
262. Garcia-Solsona E, Masqué P, Garcia-Orellana J, et al (2008) Estimating submarine groundwater discharge around Isola La Cura, northern Venice Lagoon (Italy), by using the radium quartet. *Mar Chem*. doi: 10.1016/j.marchem.2008.02.007
263. Klockenkämper R (1997) Total-reflection X-ray fluorescence analysis. Wiley
264. Marguí E, Van Grieken R, Fonta'S C, et al (2010) Preconcentration methods for the analysis of liquid samples by X-ray fluorescence techniques. *Appl Spectrosc Rev* 45:179–205 . doi: 10.1080/05704920903584198
265. Knöchel A, Prange A (1980) Analysis of Trace Elements in Seawater. Part II Determination of Heavy Metal Traces in Sea Water by X-Ray Fluorescence Analysis with Totally Reflecting Sample Holders. *Mikrochim Acta* 74:395–408 . doi:

10.1007/BF01197607

266. McLeod CW, Otsuki A, Okamoto K, et al (1981) Simultaneous determination of trace metals in sea water using dithiocarbamate pre-concentration and inductively coupled plasma emission spectrometry. *Analyst* 106:419 . doi: 10.1039/AN9810600419
267. Costa ACM, Anjos MJ, Lopes RT, et al (2005) Multi-element analysis of sea water from Sepetiba Bay, Brazil, by total reflection x-ray fluorescence spectrometry using synchrotron radiation. *X-Ray Spectrom* 34:183–188 . doi: 10.1002/xrs.779
268. Report of COMAPS Department of Ocean Development 1988– 1993
269. Krishnamurthy TM, Sastry VN TR (1999) Marine environmental investigation in the trans Thane Creek area industries impact study. In: Eighth national symposium on environment. Kalpakkam, pp 33–35